

The Development of Ru(II) and Fe(II) Complexes for C–H and H₂ Bond Activation

Kathleen Hall Taylor
Pasadena, CA

Bachelor of Science Chemistry, Meredith College, 2010

A Dissertation presented to the Graduate Faculty
of the University of Virginia in Candidacy for the Degree of
Doctor of Philosophy

Department of Chemistry

University of Virginia
August, 2016

ABSTRACT

TAYLOR, KATHLEEN H. The Development of Ru(II) and Fe(II) Complexes for C–H and H₂ Bond Activation. (Under the direction of Professor T. Brent Gunnoe).

Hydrocarbons serve as the feedstocks for numerous commodity chemicals. Industrial methods to functionalize hydrocarbons in order to convert them into higher value chemicals often involve cost and energy intensive processes. Furthermore, these processes often do not provide high selectivity for the desired products. Thus, the development of a catalytic method to functionalize hydrocarbons with high selectivity and under mild reaction conditions is highly attractive. C–H bond activation, the breaking of a substrate's C–H bond, is a vital step in hydrocarbon functionalization. The work described in this thesis involves the development and study of octahedral Ru(II) complexes for C–H and H₂ bond activation and octahedral Fe(II) complexes for C–H activation and furyl ring-opening.

The Ru(II) complexes of the type $\{[\text{HC}(\text{pz}^5)_3]\text{Ru}[\text{P}(\text{OCH}_2)_3\text{CEt}](\text{py})(\text{NHAr})\}[\text{BAr}'_4]$ ($\text{HC}(\text{pz}^5)_3$ = tris(5-methyl)pyrazolylmethane, $\text{P}(\text{OCH}_2)_3\text{CEt}$ = 2,6,7-trioxa-1-phospha-bicyclo[2,2,1]octane, py = pyridine, Ar = 4-isopropylphenyl, 4-methylphenyl, phenyl, 4-chlorophenyl, 4-fluorophenyl, BAr'_4 = tetrakis[3,5-bis(trifluoromethyl)phenyl]borate) have been demonstrated to activate H₂. Complexes with less basic anilido ligands tend to have faster reaction rates with H₂.

The Fe(II) complex $\text{Cp}^*\text{Fe}[\text{P}(\text{OCH}_2)_3\text{CEt}]_2\text{Ph}$ (Cp^* = 1,2,3,4,5-pentamethylcyclopentadienyl) is capable of C–H activation of furan and 2-methylfuran via a non-radical mechanism under photolytic conditions to produce $\text{Cp}^*\text{Fe}[\text{P}(\text{OCH}_2)_3\text{CEt}]_2(2\text{-furyl})$ and $\text{Cp}^*\text{Fe}[\text{P}(\text{OCH}_2)_3\text{CEt}]_2[2\text{-(5-methylfuryl)}]$. Under photolytic conditions, both $\text{Cp}^*\text{Fe}[\text{P}(\text{OCH}_2)_3\text{CEt}]_2(2\text{-furyl})$ and $\text{Cp}^*\text{Fe}[\text{P}(\text{OCH}_2)_3\text{CEt}]_2[2\text{-(5-methylfuryl)}]$ react with 2-butyne to form the ring-opened complexes $\text{Cp}^*\text{Fe}[\eta^5\text{-C}_5\text{Me}_4(\text{CH}=\text{CHCHO})]$ and $\text{Cp}^*\text{Fe}[\eta^5\text{-C}_5\text{Me}_4(\text{CH}=\text{CHCOCH}_3)]$, respectively. $\text{Cp}^*\text{Fe}[\text{P}(\text{OCH}_2)_3\text{CEt}]_2(2\text{-furyl})$ has been shown to react

with several other internal alkynes to form the corresponding furyl ring-opened sandwich complexes.

TABLE OF CONTENTS

LIST OF SCHEMES.....	VI
LIST OF FIGURES.....	IX
LIST OF TABLES.....	XII
1. Introduction.....	1
1.1 Overview: Hydrocarbons as Chemical Feedstocks.....	1
1.2 Chemicals from Natural Gas and Petroleum.....	2
1.3 Methane to Methanol and Partial Oxidation of Other Light Alkanes.....	3
1.4 Current Methods of Converting Methane to Methanol: Heterogeneous Catalysis..	5
1.5 Homogeneous Catalysis in Industry.....	6
1.6 Transition Metal-Mediated Partial Oxidation of Hydrocarbons via C–H Activation..	8
1.7 Types of Transition Metal-Mediated C–H Activation.....	11
1.8 Examples of 1,2-CH-Addition.....	15
1.8.1 Early Transition Metal Complexes for 1,2-CH-Addition.....	15
1.8.2 Late Transition Metal Complexes for 1,2-CH-Addition.....	19
1.9 Examples of H ₂ Activation by 1,2-Addition to Late Transition Metal Complexes..	23
1.10 1,2-CH-Addition and Proposed Catalytic Cycle for Hydrocarbon Functionalization.....	25
1.11 Functionalization of Hydrocarbons: Oxygen Atom Insertion.....	27
1.12 Thesis Aims.....	31
References.....	35
2. Design and Synthesis of Cationic Ru(II) Complexes for C–H and H₂ Bond Activation Using the Tetra(pyrazolyl)methane Ligand.....	41
2.1 Introduction.....	41
2.2 General Synthetic Details.....	43
2.3 Synthesis of $\{[C(pz)_4]Ru[P(OCH_2)_3Ct](4\text{-chloroanilido})(L)\}^n$ (L = OTf or THF, n = 0 or +1).....	49
2.3.1 Initial Halide Abstraction Followed by Deprotonation.....	50
2.3.2 Initial Deprotonation Followed by Halide Abstraction.....	51
2.4 Attempted <i>in situ</i> 1,2-Addition Experiments with C–H and H ₂ Bonds.....	54
2.5 Conclusions.....	58
2.6 Experimental Section.....	60
References.....	64
3. Synthesis of Neutral and Cationic Ru(II) Precursors for C–H or H₂ Bond Activation Using Tris(5-methyl-pyrazolyl)methane (HC(pz⁵)₃).....	66
3.1 Introduction.....	66
3.2 Synthesis of [HC(pz ⁵) ₃]Ru Complexes.....	67
3.3 Reactivity of $\{[HC(pz^5)_3]Ru[P(OCH_2)_3Ct](NH_2Ph)(Cl)\}[OTf]$ (4).....	73
3.4 Reactivity of $[HC(pz^5)_3]Ru[P(OCH_2)_3Ct](Cl)_2$ (2).....	80
3.4.1 Attempted Synthesis of a Ru–OMe or Ru–OH Species.....	80
3.4.2 Attempts to Synthesize Ru–OTf or Ru–Solvento Species.....	81

3.5 Ligand Substitution Reactions with $\{[\text{HC}(\text{pz}^5)_3]\text{Ru}[\text{P}(\text{OCH}_2)_3\text{CEt}](\text{THF})(\text{OTf})\}[\text{OTf}]$ (11).....	86
3.6 Reactivity of $\{[\text{HC}(\text{pz}^5)_3]\text{Ru}[\text{P}(\text{OCH}_2)_3\text{CEt}](\text{py})(\text{OTf})\}[\text{OTf}]$ (16).....	90
3.7 Initial Experiments Exploring the Reactivity of $\{[\text{HC}(\text{pz}^5)_3]\text{Ru}[\text{P}(\text{OCH}_2)_3\text{CEt}](\text{py})(\text{X})\}^+$ (X = NPh, OMe).....	98
3.8 Attempted Methylation of the $\text{HC}(\text{pz}^5)_3$ Backbone.....	99
3.9 Conclusions.....	100
3.10 Experimental Section.....	102
References.....	112
4. Dihydrogen Activation by $\{[\text{HC}(\text{pz}^5)_3]\text{Ru}[\text{P}(\text{OCH}_2)_3\text{CEt}](\text{py})(\text{NHAr})\}[\text{BAr}'_4]$ Complexes.....	113
4.1 Introduction.....	113
4.2 Nature of $\{[\text{HC}(\text{pz}^5)_3]\text{Ru}[\text{P}(\text{OCH}_2)_3\text{CEt}](\text{py})(\text{NHPH})\}[\text{BAr}'_4]$ (1).....	114
4.3 H_2 Activation by $\{[\text{HC}(\text{pz}^5)_3]\text{Ru}[\text{P}(\text{OCH}_2)_3\text{CEt}](\text{py})(\text{NHPH})\}[\text{BAr}'_4]$ (1).....	117
4.4 Analysis of Hydride Species Formed During H_2 Activation by $\{[\text{HC}(\text{pz}^5)_3]\text{Ru}[\text{P}(\text{OCH}_2)_3\text{CEt}](\text{py})(\text{NHPH})\}[\text{BAr}'_4]$ (1).....	124
4.4.1 Synthesis of $\{[\text{HC}(\text{pz}^5)_3]\text{Ru}[\text{P}(\text{OCH}_2)_3\text{CEt}](\text{py})(\text{H})\}^+$ (3).....	126
4.4.2 Synthesis of $\{[\text{HC}(\text{pz}^5)_3]\text{Ru}[\text{P}(\text{OCH}_2)_3\text{CEt}](\text{NH}_2\text{Ph})(\text{H})\}^+$ (2).....	127
4.4.3 Attempted synthesis of $\{[\text{HC}(\text{pz}^5)_3]\text{Ru}[\text{P}(\text{OCH}_2)_3\text{CEt}](\text{THF})(\text{H})\}^+$ (4).....	129
4.5 Proposed Mechanism for H_2 Activation and Formation of Hydride Complexes...132	
4.6 Kinetic and Mechanistic Studies of H_2 Activation by $\{[\text{HC}(\text{pz}^5)_3]\text{Ru}[\text{P}(\text{OCH}_2)_3\text{CEt}](\text{py})(\text{NHPH})\}[\text{BAr}'_4]$ (1).....	133
4.6.1 Control Experiments.....	133
4.6.2 General Reaction Setup for Kinetic Studies involving $\{[\text{HC}(\text{pz}^5)_3]\text{Ru}[\text{P}(\text{OCH}_2)_3\text{CEt}](\text{py})(\text{NHPH})\}[\text{BAr}'_4]$ (1).....	134
4.6.3 H_2 Pressure Dependence Studies.....	135
4.6.4 D_2 Activation by Complex 1.....	142
4.6.5 Pyridine Dependence Studies.....	142
4.6.6 Degenerative Pyridine Exchange Studies.....	143
4.7 H_2 activation by $\{[\text{HC}(\text{pz}^5)_3]\text{Ru}[\text{P}(\text{OCH}_2)_3\text{CEt}](\text{py})(\text{NHAr})\}[\text{BAr}'_4]$ (Ar = 4-isopropylphenyl, 4-methylphenyl, 4-chlorophenyl, 4-fluorophenyl).....	145
4.8 Conclusions.....	150
4.9 Experimental Section.....	150
References.....	160
5. Combined Furan C–H Activation and Furyl Ring-Opening by an Iron(II) Complex...161	
5.1 Introduction.....	161
5.2 Furyl C–H activation by $\text{Cp}^*\text{Fe}[\text{P}(\text{OCH}_2)_3\text{CEt}]_2\text{Ph}$	162
5.3 Photolytic reactions of $\text{Cp}^*\text{Fe}[\text{P}(\text{OCH}_2)_3\text{CEt}]_2(2\text{-furyl})$ (1) and $\text{Cp}^*\text{Fe}[\text{P}(\text{OCH}_2)_3\text{CEt}]_2[2\text{-(5-methylfuryl)}]$ (2) with 2-butyne.....	165
5.4 Substrate scope study of reaction of $\text{Cp}^*\text{Fe}[\text{P}(\text{OCH}_2)_3\text{CEt}]_2(2\text{-furyl})$ (1) with alkynes.....	169
5.5 Mechanistic and kinetic studies of the reaction of $\text{Cp}^*\text{Fe}[\text{P}(\text{OCH}_2)_3\text{CEt}]_2(2\text{-furyl})$ (1) with 2-butyne.....	172
5.5.1 Intermediates and products formed from the reaction of $\text{Cp}^*\text{Fe}[\text{P}(\text{OCH}_2)_3\text{CEt}]_2(2\text{-furyl})$ (1) with 2-butyne.....	172
5.5.2 Dependence of free $\text{P}(\text{OCH}_2)_3\text{CEt}$ on the reaction of $\text{Cp}^*\text{Fe}[\text{P}(\text{OCH}_2)_3\text{CEt}]_2(2\text{-furyl})$ (1) with 2-butyne.....	174

5.5.3 Dependence of 2-butyne on the reaction of 1 with 2-butyne.....	176
5.6 Proposed rate law for the reaction of 1 with 2-butyne.....	177
5.7 Conclusions.....	179
5.8 Experimental Section.....	180
References.....	186

LIST OF SCHEMES

CHAPTER 1

Scheme 1. Wacker process for production of aldehydes.....	7
Scheme 2. Monsanto acetic acid process.....	7
Scheme 3. Cobalt-catalyzed hydroformylation.....	8
Scheme 4. Shilov cycle for functionalization of methane.....	9
Scheme 5. Periana's Hg(II) (left) and (bpym)PtCl ₂ (right) catalyzed reactions for methane functionalization.....	11
Scheme 6. Types of transition metal-mediated C–H activation.....	12
Scheme 7. 1,2-CH-Addition of C ₆ D ₆ by (^t Bu ₃ SiNH) ₃ Zr(CH ₃).....	16
Scheme 8. Formation of (Cp) ₂ Zr(N ^t Bu) followed by 1,2-addition of benzene.....	16
Scheme 9. Formation of [(^t Bu) ₃ SiO] ₂ Ti[NSi(^t Bu) ₃] followed by 1,2-addition of benzene.....	17
Scheme 10. 1,2-CH-Addition of a pyridine C–H bond to a Sc(III) complex.....	18
Scheme 11. Cyclometallation and release of ammonia by (PCP)Ru(CO)(NH ₂) (PCP = 2,6-(CH ₂ P ^t Bu ₂) ₂ C ₆ H ₃).....	20
Scheme 12. 1,2-CH-Addition of C ₆ H ₆ to (acac) ₂ Ir(OMe)(py).....	20
Scheme 13. 1,2-Addition of C ₆ D ₆ to (PNP)Rh(OH) (PNP = 2,6-(di- <i>tert</i> -butylphosphinomethyl)pyridine).....	21
Scheme 14. H/D Exchange between C ₆ D ₆ and OH or NPh via 1,2-addition of C ₆ D ₆ with TpRu(PMe ₃) ₂ (XH) (X = O, NPh).....	22
Scheme 15. 1,2-HH-Addition to Ru(Cl)(PPh ₃)[κ ³ -N-(SiMe ₂ CH ₂ PPh ₂) ₂].....	23
Scheme 16. H ₂ activation by (PCP)Ru(CO)(NH ₂) (PCP = 2,6-(CH ₂ P ^t Bu ₂) ₂ C ₆ H ₃).....	24
Scheme 17. 1,2-Addition of H ₂ to [(^t bpy) ₂ Rh(OMe)(MeOH)] ²⁺	25
Scheme 18. Proposed catalytic cycles for hydrocarbon partial oxidation.....	27
Scheme 19. Organometallic Baeyer-Villiger reaction involving methyltrioxorhenium and a generic oxidant (YO = OIPh, IO ₄ ⁻ , IO ₃ ⁻ , H ₂ O ₂ , pyridine-N-oxide).....	29
Scheme 20. Reaction of (PMe ₃) ₂ Ni(κ ² -C,C-CH ₂ CMe ₂ - <i>o</i> -C ₆ H ₄) with N ₂ O proceeding through OMBV transition state.....	29
Scheme 21. Reaction of Cp [*] W(O) ₂ (CH ₂ SiMe ₃) with IO ₄ ⁻ via an OMBV pathway.....	30
Scheme 22. Thermal reaction of Cp [*] Fe(CO)(NCMe)(Ph) with oxidants to yield benzoic acid.....	31
Scheme 23. Photolytic reaction of Cp [*] Fe[P(OCH ₂) ₃ CET] ₂ (Ph) with Me ₃ NO to yield phenol.....	31
Scheme 24. General synthetic strategy for electrophilic Ru(II)-heteroatom complexes and 1,2-addition of C–H or H–H bonds.....	32
Scheme 25. H ₂ activation by {[HC(pz ⁵) ₃]Ru[P(OCH ₂) ₃ CET](py)(NHPh)}[BAR' ₄].....	34
Scheme 26. C–H activation and furyl ring-opening by Fe(II) complexes.....	34

CHAPTER 2

Scheme 1. 1,2-Addition of C ₆ D ₆ to TpRu(PMe ₃) ₂ (XH) (X = O, NPh).....	41
Scheme 2. Synthetic strategy for electrophilic [C(pz) ₄]Ru(II)-amido complexes and 1,2-addition of C–H or H–H bonds.....	43
Scheme 3. Synthesis of [C(pz) ₄]Ru(PPh ₃)(Cl) ₂ (1) and [C(pz) ₄]Ru[P(OCH ₂) ₃ CET](Cl) ₂ (2).....	44
Scheme 4. Synthesis of {[C(pz) ₄]Ru[P(OCH ₂) ₃ CET](Cl)} ₂ [OTf] ₂ (3) and {[C(pz) ₄]Ru[P(OCH ₂) ₃ CET](Cl)(NH ₂ Ar)}[OTf] (Ar = 2,6-di(isopropyl)phenyl, 3,5-di(<i>tert</i> -butyl)phenyl, 4-chlorophenyl, 4-nitrophenyl).....	47
Scheme 5. Strategies for synthesis of {[C(pz) ₄]Ru[P(OCH ₂) ₃ CET](4-chloroanilido)(L)} ⁿ (n = +1, X = THF or n = 0, X = OTf; Y = Na, Ag, Tl, TMS).....	50
Scheme 6. Synthesis of [C(pz) ₄]Ru[P(OCH ₂) ₃ CET](Cl)(4-chloroanilido) (7).....	52
Scheme 7. Putative reaction of PMe ₃ with Ru–Cl–NaBAR' ₄ adduct.....	54

Scheme 8. Attempted reactions of $C(pz)_4Ru[P(OCH_2)_3CEt](Cl)(4\text{-chloroanilido})$ (7) with halide abstractors and C_6D_6	55
Scheme 9. Attempted reaction of $[C(pz)_4]Ru[P(OCH_2)_3CEt](Cl)(4\text{-chloroanilido})$ (7) with halide abstractors and phenylacetylene.....	56
Scheme 10. Attempted reaction of $[C(pz)_4]Ru[P(OCH_2)_3CEt](Cl)(4\text{-chloroanilido})$ (7) with halide abstractors and H_2	57
Scheme 11. Intramolecular C–H activation of the 5-position of a pyrazolyl ring.....	59

CHAPTER 3

Scheme 1. Tris(5-methyl-pyrazolyl)methane-ligated Ru target complexes.....	66
Scheme 2. Synthesis of $[HC(pz^5)_3]Ru[PPh_3](Cl)_2$ (1).....	67
Scheme 3. Synthesis of $[HC(pz^5)_3]Ru[P(OCH_2)_3CEt](Cl)_2$ (2).....	69
Scheme 4. Synthesis of $\{[HC(pz^5)_3]Ru[P(OCH_2)_3CEt](\mu\text{-Cl})_2[OTf]_2$ (3) and $\{[HC(pz^5)_3]Ru[P(OCH_2)_3CEt](NH_2Ph)(Cl)[OTf]$ (4).....	72
Scheme 5. Reaction of $\{[HC(pz^5)_3]Ru[P(OCH_2)_3CEt](NH_2Ph)(Cl)[OTf]$ (4) with NaH.....	76
Scheme 6. Synthesis of $\{[HC(pz^5)_3]Ru[P(OCH_2)_3CEt](NH_2Ph)(OTf)[OTf]$ (6).....	77
Scheme 7. Reaction of $\{[HC(pz^5)_3]Ru[P(OCH_2)_3CEt](NH_2Ph)(OTf)[OTf]$ (6) with NCMe and subsequent deprotonation.....	80
Scheme 8. Target Ru–OR, Ru–OH, and Ru–NHR complexes synthesized by chloride exchange from $[HC(pz^5)_3]Ru[P(OCH_2)_3CEt](Cl)_2$ (2).....	80
Scheme 9. Reaction of $[HC(pz^5)_3]Ru[P(OCH_2)_3CEt](Cl)_2$ (2) with NaOH or NaOMe.....	81
Scheme 10. Reactivity of $[HC(pz^5)_3]Ru[P(OCH_2)_3CEt](Cl)_2$ (2) with triflate sources.....	82
Scheme 11. Reactivity of $[HC(pz^5)_3]Ru[P(OCH_2)_3CEt](Cl)_2$ (2) with $NaBAR'_4$, TlOTf and KOTf in THF.....	83
Scheme 12. Reaction of $[HC(pz^5)_3]Ru[P(OCH_2)_3CEt](Cl)_2$ (2) with triflate salts in CD_3CN	83
Scheme 13. Synthesis of $\{[HC(pz^5)_3]Ru[P(OCH_2)_3CEt](THF)(OTf)[OTf]$ (11).....	84
Scheme 14. Reactivity of $\{[HC(pz^5)_3]Ru[P(OCH_2)_3CEt](THF)(OTf)[OTf]$ (11) to form dicationic complexes 12-14	87
Scheme 15. Synthesis of $\{[HC(pz^5)_3]Ru[P(OCH_2)_3CEt](py)(OTf)[OTf]$ (16).....	88
Scheme 16. Synthesis of $\{[HC(pz^5)_3]Ru[P(OCH_2)_3CEt](py)(MeOH)[OTf]_2$ (18) and $\{[HC(pz^5)_3]Ru[P(OCH_2)_3CEt](py)(OMe)[OTf]$ (19).....	90
Scheme 17. Synthesis of $\{[HC(pz^5)_3]Ru[P(OCH_2)_3CEt](py)(NH_2Ph)[OTf]_2$ (20) and $\{[HC(pz^5)_3]Ru[P(OCH_2)_3CEt](py)(NHPh)[OTf]$ (24).....	92
Scheme 18. Synthesis of $\{[HC(pz^5)_3]Ru[P(OCH_2)_3CEt](py)(OTf)[BAR'_4]$ (21), $\{[HC(pz^5)_3]Ru[P(OCH_2)_3CEt](py)(NH_2Ph)[OTf][BAR'_4]$ (22), and $\{[HC(pz^5)_3]Ru[P(OCH_2)_3CEt](py)(NHPh)[BAR'_4]$ (25).....	94
Scheme 19. Initial 1,2-CH and HH-addition experiments with $\{[HC(pz^5)_3]Ru[P(OCH_2)_3CEt](py)(X)^+$ ($X = NHPh, OMe$).....	99
Scheme 20. Attempted methylation of the $HC(pz^5)_3$ backbone.....	100
Scheme 21. Overall synthetic procedure for $\{[HC(pz^5)_3]Ru[P(OCH_2)_3CEt](py)(NHPh)[BAR'_4]$ (25).....	102

CHAPTER 4

Scheme 1. Alternate synthetic pathways to $\{[HC(pz^5)_3]Ru[P(OCH_2)_3CEt](py)(NHPh)[BAR'_4]$ (1) and $\{[:C(pz^5)_3]Ru[P(OCH_2)_3CEt](py)(NH_2Ph)[BAR'_4]$ (1').....	117
Scheme 2. H_2 activation by $\{[HC(pz^5)_3]Ru[P(OCH_2)_3CEt](py)(NHPh)[BAR'_4]$ (1).....	118
Scheme 3. Formation of $\{[:C(pz^5)_3]Ru[P(OCH_2)_3CEt](py)_2\}[BAR'_4]$ (5).....	124
Scheme 4. H_2 activation by $\{[HC(pz^5)_3]Ru[P(OCH_2)_3CEt](py)(NHPh)[BAR'_4]$ (1) with intermediate $\{[HC(pz^5)_3]Ru[P(OCH_2)_3CEt](NH_2Ph)(H)[BAR'_4]$ (2).....	125

Scheme 5. Synthesis of $\{[\text{HC}(\text{pz}^5)_3]\text{Ru}[\text{P}(\text{OCH}_2)_3\text{CEt}](\text{py})(\text{H})\}[\text{OTf}]$ (3).....	127
Scheme 6. Synthesis of $\{[\text{HC}(\text{pz}^5)_3]\text{Ru}[\text{P}(\text{OCH}_2)_3\text{CEt}](\text{NH}_2\text{Ph})(\text{H})\}[\text{OTf}]$ (2).....	128
Scheme 7. Proposed mechanism of H_2 activation by $\{[\text{HC}(\text{pz}^5)_3]\text{Ru}[\text{P}(\text{OCH}_2)_3\text{CEt}](\text{py})(\text{NHPh})\}[\text{BAr}'_4]$ (1) with formation of $\{[\text{HC}(\text{pz}^5)_3]\text{Ru}[\text{P}(\text{OCH}_2)_3\text{CEt}](\text{THF})(\text{H})\}^+$ (4) in THF.....	133
Scheme 8. Reaction of $\{[\text{HC}(\text{pz}^5)_3]\text{Ru}[\text{P}(\text{OCH}_2)_3\text{CEt}](\text{py})(\text{NH}_2\text{Ph})\}[\text{OTf}][\text{BAr}'_4]$ with H_2	134
Scheme 9. Reaction of $\{[\text{HC}(\text{pz}^5)_3]\text{Ru}[\text{P}(\text{OCH}_2)_3\text{CEt}](\text{py})(\text{NHPh})\}[\text{BAr}'_4]$ (1) under N_2	134
Scheme 10. Dissociation of pyridine from 1 to allow coordination of H_2 (top) and dissociation of pyridine from 1 to allow exchange with pyridine- d_5 (bottom).....	144
Scheme 11. H_2 activation by $\{[\text{HC}(\text{pz}^5)_3]\text{Ru}[\text{P}(\text{OCH}_2)_3\text{CEt}](\text{py})(\text{NHAr})\}[\text{BAr}'_4]$	147

CHAPTER 5

Scheme 1. Reaction of $\text{Cp}^*\text{Fe}[\text{P}(\text{OCH}_2)_3\text{CEt}]_2\text{Ph}$ with furan and 2-methylfuran.....	163
Scheme 2. Reaction of $\text{Cp}^*\text{Fe}[\text{P}(\text{OCH}_2)_3\text{CEt}]_2(2\text{-furyl})$ (1) with 2-butyne.....	166
Scheme 3. Reaction of $\text{Cp}^*\text{Fe}[\text{P}(\text{OCH}_2)_3\text{CEt}]_2[2\text{-}(5\text{-methylfuryl})]$ (2) with 2-butyne.....	169
Scheme 4. Reaction of intermediate 1a with HCl	174
Scheme 5. Proposed reaction mechanism of $\text{Cp}^*\text{Fe}[\text{P}(\text{OCH}_2)_3\text{CEt}]_2(2\text{-furyl})$ (1) with 2-butyne under photolytic conditions.....	179

LIST OF FIGURES

CHAPTER 1

Figure 1. 1,2-Addition reaction coordinate.....	14
Figure 2. Comparison of metal-C–H and metal-H–H bonding.....	23
Figure 3. <i>Para</i> -substituted anilido ligands.....	33

CHAPTER 2

Figure 1. A poly(pyrazolyl)alkane ligand, demonstrating facial coordination to a generic metal center.....	43
Figure 2. ¹ H NMR (300 MHz, CDCl ₃) spectrum of [C(pz) ₄]Ru(PPh ₃)(Cl) ₂ (1).....	45
Figure 3. ¹ H NMR (500 MHz, CD ₂ Cl ₂) spectrum of [C(pz) ₄]Ru[P(OCH ₂) ₃ CEt](Cl) ₂ (2).....	46
Figure 4. ¹ H NMR (500 MHz, CD ₂ Cl ₂) spectrum of {[C(pz) ₄]Ru[P(OCH ₂) ₃ CEt](μ-Cl) ₂ }[OTf] ₂ (3).....	48
Figure 5. ¹ H NMR (300 MHz, CD ₂ Cl ₂) spectrum of {[C(pz) ₄]Ru[P(OCH ₂) ₃ CEt](4-chloroaniline)(Cl)}[OTf] (4).....	49
Figure 6. ¹ H NMR (500 MHz) spectrum of [C(pz) ₄]Ru[P(OCH ₂) ₃ CEt](4-chloroanilido)(Cl) (7) in THF- <i>d</i> ₈	52
Figure 7. ¹ H NMR (300 MHz) spectra of the downfield region of 7 + NaBAR' ₄ in THF- <i>d</i> ₈	58

CHAPTER 3

Figure 1. ¹ H NMR spectrum (300 MHz, CDCl ₃) of [HC(pz ⁵) ₃]Ru(PPh ₃)(Cl) ₂ (1).....	68
Figure 2. ¹ H NMR spectrum (300 MHz, CD ₂ Cl ₂) of [HC(pz ⁵) ₃]Ru[P(OCH ₂) ₃ CEt](Cl) ₂ (2).....	70
Figure 3. ORTEP of [HC(pz ⁵) ₃]Ru[P(OCH ₂) ₃ CEt](Cl) ₂ (2) (50% probability with H atoms omitted).....	71
Figure 4. ¹ H NMR spectrum (300 MHz, CD ₂ Cl ₂) of {[HC(pz ⁵) ₃]Ru[P(OCH ₂) ₃ CEt](μ-Cl) ₂ }[OTf] ₂ (3).....	72
Figure 5. ¹ H NMR spectrum (300 MHz, CD ₂ Cl ₂) of {[HC(pz ⁵) ₃]Ru[P(OCH ₂) ₃ CEt](NH ₂ Ph)(Cl)}[OTf] (4).....	73
Figure 6. ¹ H NMR spectra (THF- <i>d</i> ₈ , 300 MHz) of {[HC(pz ⁵) ₃]Ru[P(OCH ₂) ₃ CEt](NH ₂ Ph)(Cl)}[OTf] (4) (bottom) and {[:C(pz ⁵) ₃]Ru[P(OCH ₂) ₃ CEt](Cl)(NHPh)}[Na] (5) (top).....	74
Figure 7. Downfield region of the ¹ H NMR spectra (300 MHz, THF- <i>d</i> ₈) of 4 (bottom) and aniline complex formed from adding AgOTf to 5 (top).....	75
Figure 8. ¹ H NMR spectra (300 MHz, THF- <i>d</i> ₈) of {[HC(pz ⁵) ₃]Ru[P(OCH ₂) ₃ CEt](NH ₂ Ph)(Cl)}[OTf] (4) (bottom) and {[HC(pz ⁵) ₃]Ru[P(OCH ₂) ₃ CEt](NH ₂ Ph)(OTf)}[OTf] (6) (top).....	77
Figure 9. ¹ H NMR spectrum (300 MHz, THF- <i>d</i> ₈) of {[HC(pz ⁵) ₃]Ru[P(OCH ₂) ₃ CEt](NH ₂ Ph)(NCMe)}[OTf] ₂ (7).....	78
Figure 10. ¹ H NMR spectrum (300 MHz, THF- <i>d</i> ₈) of {[HC(pz ⁵) ₃]Ru[P(OCH ₂) ₃ CEt](NHPh)(NCMe)}[OTf] or {[HC(pz ⁵) ₃]Ru[P(OCH ₂) ₃ CEt][N(H)C(Me)N(Ph)]}[OTf] (8).....	79
Figure 11. ¹ H NMR spectrum (600 MHz, THF- <i>d</i> ₈) of {[HC(pz ⁵) ₃]Ru[P(OCH ₂) ₃ CEt](THF)(OTf)}[OTf] (11).....	85
Figure 12. ORTEP of {[HC(pz ⁵) ₃]Ru[P(OCH ₂) ₃ CEt](THF)(OTf)}[OTf] (11) (50% probability with H atoms and uncoordinated OTf omitted).....	85
Figure 13. ¹ H NMR spectrum (300 MHz, THF- <i>d</i> ₈) of {[HC(pz ⁵) ₃]Ru[P(OCH ₂) ₃ CEt](py)(OTf)}[OTf] (16).....	89

Figure 14. Preliminary crystal structure of $\{[\text{HC}(\text{pz}^5)_3]\text{Ru}[\text{P}(\text{OCH}_2)_3\text{CEt}](\text{py})(\text{OTf})\}[\text{OTf}]$ (16).....	89
Figure 15. ^1H NMR (300 MHz, THF- d_8) spectra of $\{[\text{HC}(\text{pz}^5)_3]\text{Ru}[\text{P}(\text{OCH}_2)_3\text{CEt}](\text{py})(\text{MeOH})\}[\text{OTf}]_2$ (18) (bottom) and $\{[\text{HC}(\text{pz}^5)_3]\text{Ru}[\text{P}(\text{OCH}_2)_3\text{CEt}](\text{py})(\text{OMe})\}[\text{OTf}]$ (19) (top).....	91
Figure 16. ^1H NMR spectrum (300 MHz, THF- d_8) of $\{[\text{HC}(\text{pz}^5)_3]\text{Ru}[\text{P}(\text{OCH}_2)_3\text{CEt}](\text{py})(\text{NH}_2\text{Ph})\}[\text{OTf}]_2$ (20).....	92
Figure 17. ^1H NMR spectrum (600 MHz, CD_2Cl_2) of $\{[\text{HC}(\text{pz}^5)_3]\text{Ru}[\text{P}(\text{OCH}_2)_3\text{CEt}](\text{py})(\text{NH}_2\text{Ph})\}[\text{OTf}][\text{BAR}'_4]$ (22). Inset: Non-first order splitting pattern of $\text{P}(\text{OCH}_2)_3\text{CEt}$ diastereotopic methylene groups.....	95
Figure 18. ORTEP of $\{[\text{HC}(\text{pz}^5)_3]\text{Ru}[\text{P}(\text{OCH}_2)_3\text{CEt}](\text{py})(\text{NH}_2\text{Ph})\}[\text{OTf}][\text{BAR}'_4]$ (22) (50% probability ellipsoids with H atoms and counterions omitted).....	96

CHAPTER 4

Figure 1. $\{[\text{HC}(\text{pz}^5)_3]\text{Ru}[\text{P}(\text{OCH}_2)_3\text{CEt}](\text{py})(\text{NHAr})\}[\text{BAR}'_4]$ targets for this study.....	114
Figure 2. Portion of ^1H NMR (500 MHz, THF- d_8) spectrum of $\{[\text{HC}(\text{pz}^5)_3]\text{Ru}[\text{P}(\text{OCH}_2)_3\text{CEt}](\text{py})(^{15}\text{NHPH})\}[\text{BAR}'_4]$ showing ^{15}NH doublet partially obscured by $\text{P}(\text{OCH}_2)_3\text{CEt}$ resonance.....	115
Figure 3. ^1H - ^{15}N correlation NMR spectrum of $\{[\text{HC}(\text{pz}^5)_3]\text{Ru}[\text{P}(\text{OCH}_2)_3\text{CEt}](\text{py})(^{15}\text{NHPH})\}[\text{BAR}'_4]$	116
Figure 4. Hydride region of the ^1H NMR spectra (600 MHz, THF- d_8) during the reaction of $\{[\text{HC}(\text{pz}^5)_3]\text{Ru}[\text{P}(\text{OCH}_2)_3\text{CEt}](\text{py})(\text{NHPh})\}[\text{BAR}'_4]$ (1) with 25 psi H_2 at 90 °C.....	118
Figure 5. Example of concentration of complexes 1-5 over the course of H_2 activation by 1 at 110 °C and 55 psig H_2	119
Figure 6. ^1H NMR spectrum (500 MHz, THF- d_8) of complex 5	120
Figure 7. ^1H NMR spectra (500 MHz, THF- d_8) of complex 5 before addition of HCl (bottom) and after addition of HCl (top).....	122
Figure 8. ORTEP of $\{[\text{HC}(\text{pz}^5)_3]\text{Ru}[\text{P}(\text{OCH}_2)_3\text{CEt}](\text{py})_2\}[\text{BAR}'_4]$ (50% probability with H atoms and BAR'_4 omitted).....	123
Figure 9. ^1H NMR spectrum (500 MHz, THF- d_8) at the end of the reaction between $\{[\text{HC}(\text{pz}^5)_3]\text{Ru}[\text{P}(\text{OCH}_2)_3\text{CEt}](\text{py})(\text{NHPh})\}[\text{BAR}'_4]$ (1) and H_2	126
Figure 10. ^1H NMR spectrum (500 MHz, THF- d_8) of $\{[\text{HC}(\text{pz}^5)_3]\text{Ru}[\text{P}(\text{OCH}_2)_3\text{CEt}](\text{py})(\text{H})\}[\text{OTf}]$ (2).....	127
Figure 11. ^1H NMR spectrum (500 MHz, THF- d_8) of $\{[\text{HC}(\text{pz}^5)_3]\text{Ru}[\text{P}(\text{OCH}_2)_3\text{CEt}](\text{NH}_2\text{Ph})(\text{H})\}[\text{OTf}]$ (3).....	129
Figure 12. Proposed identity of complex 4	131
Figure 13. ^{31}P NMR spectra (500 MHz, THF- d_8) of the H_2 activation reaction by $\{[\text{HC}(\text{pz}^5)_3]\text{Ru}[\text{P}(\text{OCH}_2)_3\text{CEt}](\text{py})(\text{NHPh})\}[\text{BAR}'_4]$ (1) in progress (top) and the product of the reaction of $\{[\text{HC}(\text{pz}^5)_3]\text{Ru}[\text{P}(\text{OCH}_2)_3\text{CEt}](\mu\text{-Cl})_2\}[\text{OTf}]_2$ with LiAlH_4 (bottom).....	132
Figure 14. Plot of $\ln[\mathbf{1}]$ vs time (s) for the reactions of 1 (0.0528 M) with H_2 at 35 (a.), 45 (b.), 55 (c.), 65 (d.) psig at 90 °C.....	137
Figure 15. Concentration of H_2 in solution over reaction time.....	138
Figure 16. Three plots of k_{obs} vs H_2 pressure (35, 45, 55, 65 psig) obtained by performing H_2 activation experiments in triplicate.....	138-139
Figure 17. Three plots of k_{obs} vs initial $[\text{H}_2]$ for 35, 45, 55 and 65 psig H_2 obtained by performing H_2 activation experiments in triplicate.....	140-141
Figure 18. Plot of $\ln[\text{sum of } \mathbf{2}, \mathbf{3}, \text{ and } \mathbf{4}]$ vs time (s) for the reactions of 1 (0.0528 M) with H_2 at 35 (a.), 45 (b.), 55 (c.), 65 (d.) psig at 90 °C.....	141
Figure 19. Plot of $\ln[\mathbf{1}]$ vs time (s) for the reactions of 1 (0.0528 M) with added pyridine (0, 0.3, 0.5, 1.0 eq) and 55 psig H_2 at 90 °C.....	143

Figure 20. Plot of the $\ln[1]$ vs time (s) for the degenerative exchange of pyridine- d_5 with 1 at 50 psi N_2 , 90 °C.....	145
Figure 21. Hammett plot of $\log(k_{\text{substituent}}/k_H)$ vs σ_p^+	148
Figure 22. 1,2-Addition reaction coordinate.....	149

CHAPTER 5

Figure 1. ORTEP of $Cp^*Fe[P(OCH_2)_3CEt]_2(2\text{-furyl})$ (1) (30% probability ellipsoids; H atoms omitted).....	163
Figure 2. 1H NMR spectrum for $Cp^*Fe[P(OCH_2)_3CEt]_2(2\text{-furyl})$ (1) in C_6D_6	164
Figure 3. 1H NMR spectrum of $Cp^*Fe[P(OCH_2)_3CEt]_2[2\text{-}(5\text{-methylfuryl})]$ (2) in C_6D_6	165
Figure 4. ORTEP of $Cp^*Fe[\eta^5\text{-}C_5Me_4(CH=CHCHO)]$ (3-trans) (50% probability ellipsoids; H atoms omitted).....	167
Figure 5. 1H NMR spectrum of $Cp^*Fe[\eta^5\text{-}C_5Me_4(CH=CHCOH)]$ (3) in C_6D_6	168
Figure 6. 1H NMR spectrum of $Cp^*Fe[C_5Me_4(CH=CHOMe)]$ (4) in C_6D_6	169
Figure 7. 1H NMR spectra of the downfield region for the reaction between 1 and 2-butyne in C_6D_6 under photolytic conditions.....	173
Figure 8. Concentration (M) of 1 vs time for the reaction of 1 with 2-butyne as a function of added $P(OCH_2)_3CEt$	175
Figure 9. Plot of $\log(k_{\text{obs}})$ vs $\log[P(OCH_2)_3CEt]$ for the reaction of 1 (0.069 M) with 2-butyne (0.141 M) in the presence of varying amounts of added $P(OCH_2)_3CEt$ (slope = -0.94, $R^2 = 0.90$).....	175
Figure 10. Concentration (M) of 1 vs. time as a function of 2-butyne concentration.....	176
Figure 11. Plot of $\log k_{\text{obs}}$ vs $\log [2\text{-butyne}]$ for the reaction of 1 (0.069 M) with varying amounts of 2-butyne ($R^2 = 0.99$).....	177
Figure 12. Plot of $\log k_{\text{obs}}$ vs $\log [2\text{-butyne}]$ for the reaction of 1 (0.069 M) with varying amounts of 2-butyne in the presence of 0.5 equiv of $P(OCH_2)_3CEt$ (relative to 1) (slope = 0.9, $R^2 = 0.8$).....	177

LIST OF TABLES

CHAPTER 4

Table 1. H ₂ pressure dependence on experimental rates of H ₂ activation.....	137
Table 2. Concentration of pyridine dependence on experimental rates for H ₂ activation.....	143
Table 3. % Yield of complex 5 as a function of added pyridine.....	145
Table 4. Experimental K _{eq} values of the equilibrium between {[HC(pz ⁵) ₃]Ru[P(OCH ₂) ₃ CEt](py)(NHAr)}[BAr' ₄] and {[:C(pz ⁵) ₃]Ru[P(OCH ₂) ₃ CEt](py)(NHAr)}.....	146
Table 5. Experimental k _{obs} (s ⁻¹) values for H ₂ activation by {[HC(pz ⁵) ₃]Ru[P(OCH ₂) ₃ CEt](py)(NHAr)}[BAr' ₄] complexes at 90 °C and 55 psig H ₂	148

CHAPTER 5

Table 1. Alkyne substrate scope and percent yield of corresponding furyl ring-opening product.....	171
--	-----

1 Introduction

1.1 Overview: Hydrocarbons as Chemical Feedstocks

Hydrocarbons derived from natural gas and petroleum are vital resources for the chemical industry and serve as feedstocks for the production of many commodity chemicals, including ethylene, propylene, methanol, ethanol, ethylene glycol, isopropanol, and propylene glycol.¹ Starting from basic hydrocarbon building blocks, ~90% of organic chemicals can be produced.² For example, the catalytic reforming of naphtha, the C5-C9 aliphatic and cycloaliphatic fraction of petroleum which produces benzene, toluene, and xylenes (also known as the BTX series), serves as the major source for aromatic chemicals in the United States.² Nevertheless, the growing concern over the depletion of petroleum reserves has served as the driving force to develop alternative energy sources and identify new chemical feedstocks. The conversion of light alkanes from natural gas to aromatics has been identified as a possible replacement for naphtha-based feedstocks.²⁻⁵ The demand for natural gas has been growing steadily since 1986,⁶ and it is projected that global natural gas consumption will continue to increase by 1.4-1.6% per year through 2035.⁷ Despite the growth of natural gas upgrading industry, difficulties remain with regard to the transportation of natural gas from the source (often remote) to the marketplace. Given the expense of current cryogenic natural gas liquefaction strategies (a liquefied natural gas plant can cost in the billions of dollars⁸), the chemical conversion of methane (the major component of natural gas) into a more easily transportable liquid under ambient conditions (e.g., methanol) is highly desirable. Chemical conversion of natural gas into methanol fundamentally involves net oxygen atom insertion—the cleavage of a C–H bond (C–H activation) followed by the insertion of an oxygen atom to form a new C–O bond (functionalization). While these two fundamental reaction steps (i.e., C–H bond breaking and C–O bond formation) are known and have been successfully employed in many other processes, the functionalization of simple hydrocarbons is unusually challenging due to the chemically inert nature of the hydrocarbon C–H

bond, and often involves costly and harsh reaction conditions. Transition metal complexes that are capable of catalytic hydrocarbon functionalization could revolutionize both the chemical manufacturing and energy sectors if economically competitive catalysts could be developed.

1.2 Chemicals from Natural Gas and Petroleum

Currently, the primary hydrocarbon feedstocks for petrochemicals are light alkanes (from natural gas and petroleum) and aromatics (from petroleum). While aromatic feedstocks are used to produce a substantial portion of petrochemicals (plastics, paints, adhesives, pharmaceuticals, cosmetics, textiles, epoxy resins, and rubber goods)⁹, the vast majority of petroleum is used to generate energy; in fact, petroleum serves as the United States' largest energy source.¹⁰ Only about 5% of petroleum is used as feedstock for petrochemicals.¹¹ Given the global depletion of petroleum resources, a rational decision would be to conserve these hydrocarbons for the manufacture of petrochemical products in lieu of burning them for fuel.^{12,13} An attractive alternative energy source is natural gas, as burning natural gas produces less pollutants and less CO₂ than does burning petroleum.⁷ Natural gas is also appealing due to the United States' substantial domestic reserves; as of 2013, these reserves contained ~2,276 trillion cubic feet of natural gas.¹⁴ For perspective, the United States consumed ~27 trillion cubic feet of natural gas in 2014.¹⁵ However, sources of natural gas are often situated in remote locations such as the Bakken oil field in North Dakota where there is no adequate natural gas transportation infrastructure,¹⁶ making it difficult and expensive to move natural gas to places where it can be used.² Pipelines provide the means to exploit some of this natural gas but have not been utilized to their fullest potential due to the great expense (between \$30,000 and \$100,000 per inch-mile—for example, a 24 inch diameter pipeline at \$100,000 per inch-mile costs \$2,400,000 per mile—between 1993 and 2007¹⁷) and frequent public opposition resulting from environmental and safety concerns.

Liquefied natural gas (LNG) is one potential route for transportation. The physical liquefaction of natural gas to make LNG involves cooling the gas to cryogenic temperatures while applying high pressures to force a phase change to the liquid state. Once liquefied, LNG needs to be kept at low temperatures (-160 to -162 °C) to prevent it from converting back into a gas.^{7,18} The physical liquefaction process is also expensive and capital intensive due to the need for costly compressors, heat exchangers, and for the overall energy consumed to operate the refrigeration systems.⁷ In fact, the liquefaction step makes up 41% of the cost of the entire process of supplying consumers with natural gas via the LNG method.⁷ Transport of liquefied natural gas is also expensive, as an LNG ship can cost around \$200 million to build.¹⁹ Due to the prohibitively high cost of building effective infrastructure for natural gas transportation, money and resources are lost as companies often choose to flare natural gas.² In the United States, an estimated 2.9 million cubic feet of natural gas is vented or flared per year.²⁰ Methane loss to the atmosphere brings a further problem in that methane is an even worse greenhouse gas than CO₂.^{16,21} The United States is currently a net importer of natural gas,²² but reduction of flaring may aid in the country's predicted transition to exporter of natural gas in 2017 as the industry continues to grow.²³

1.3 Methane to Methanol and Partial Oxidation of Other Light Alkanes

One possible solution for increasing the use of natural gas as an energy resource is to convert methane, the primary component of natural gas, to methanol. As a liquid at room temperature, methanol is easier to transport using current infrastructure. Methanol itself is used as a feedstock for formaldehyde, acetic acid, acetic anhydride, and methyl *tert*-butyl ether, and is also used as an additive to gasoline, which could further increase natural gas's usefulness to the chemical industry.^{24,25} In fact, in 2002, 90% of methanol was already produced from methane; 75% of this methanol was used to make other chemicals and 25% of it was used in fuels.² Considering the vast domestic natural gas resources, the potential economic benefit of using

natural gas as a liquid fuel for transportation is substantial. However, converting methane to methanol, while thermodynamically favorable (eq 1), is kinetically challenging—involving activation of an inert C–H bond of methane (104 kcal/mol), a process that is by no means trivial.^{24,26}

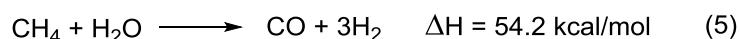
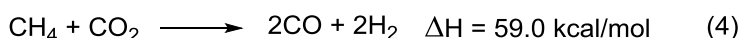
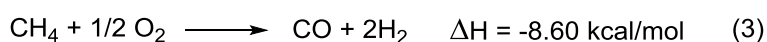
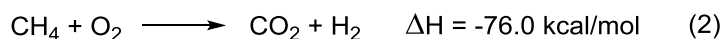


Similarly, the catalytic direct partial oxidation of ethane and propane to ethanol and propanol could prove an extremely valuable replacement for current methods of production (for example, ethanol is produced by first cracking ethane to ethylene, which is subsequently reacted with water at 300 °C and 70 bar in the presence of a H₃PO₄ catalyst and SiO₂ to form the desired product).² However, partial oxidation of ethane and propane would be important not only as a source for ethanol and propanol, but also as a potential route to ethylene and propylene, two of the most important petrochemicals.² Ethylene and propylene are olefins essential in the production of numerous polymers (polyethylene, polypropylene, etc.) and other important chemicals (ethylene glycol, acetaldehyde, acrylonitrile, propylene oxide, cumene, etc.).² A current route of producing ethylene and propylene is by steam cracking ethane and propane, respectively. Steam cracking is the process in which feedstocks such as ethane, propane, butane, cycloalkanes are converted to olefins at high temperatures (650-900 °C) in the presence of steam (no catalyst is used in steam cracking); steam is employed to dilute the hydrocarbon mixtures (a precaution against potential explosions) and reduce coking.² Cracked gases must be cooled by ~900 °C before further processing, adding yet another layer of expense to this industrial process through the use of heat exchangers and refrigeration equipment.² Ethylene and propylene can be produced by the dehydration of ethanol and isopropanol, respectively. If a process can be developed to partially oxidize ethane and propane to ethanol and propanol, the energy intensive cracking process can be avoided by dehydrating the alcohols to their corresponding olefins. Additionally, the partial oxidation of benzene to produce phenol would be desirable, as phenol is

used as a precursor to such chemicals as bisphenol A (used to make epoxy resins and polycarbonates) and phenolic resins (an important component of adhesives).²

1.4 Current Methods of Converting Methane to Methanol: Heterogeneous Catalysis

Current industrial methods of transforming methane to methanol start by the reforming of methane to produce synthesis gas (syn gas), a mixture of CO and H₂, which is subsequently reacted to give the final product, methanol. The reforming step can be conducted in one of two ways: 1) methane is first desulfurized at 360-400 °C to prevent catalyst poisoning,² then methane is combined with H₂O (steam reforming) in an endothermic reaction to produce a mixture of CO and H₂ at 800 °C and 35 bar ($\Delta H = 54$ kcal/mol) over a nickel/alumina or nickel/potassium oxide catalyst (in some cases, excess CO₂ is added to the mixture to react with excess H₂, depending on the ratio of syn gas components and the desired composition)² or 2) through the burning of methane in a flame at 1300-1400 °C and 60-80 bar with a residence time of 2-5 seconds to initiate the following reactions (eq 2-5) to produce a syn gas mixture.²



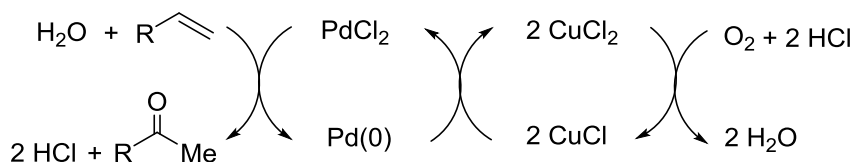
Once formed, the syn gas is then reacted to form methanol over a heterogeneous catalyst such as CuO/ZnO/Cr₂O₃; temperatures and pressures for this step can range from 240-380 °C and from 50-340 bar, respectively.² There are 144 operating syn gas plants in the world, 18 of which are in the United States.²⁷ A large amount of capital is necessary to build and maintain plants capable of sustaining the reaction conditions for making syn gas (and ultimately methanol) from methane;²⁴ thus, it is desirable to develop an economically competitive process for the direct partial oxidation of methane to methanol using air or O₂ as the oxidant (either directly or indirectly).

1.5 Homogeneous Catalysis in Industry

The functionalization of hydrocarbons is challenging because hydrocarbon C–H bonds are typically chemically inert (C–H bond dissociation energies (BDEs) are often 95-110 kcal/mol) and the over-functionalization of hydrocarbons to undesired products is a common problem; once a C–H bond is replaced with a carbon–functional group bond, the products tend to be more reactive than the starting material, making it difficult to achieve the desired selectivity to mono-functionalized products.^{25,28} For methane, over-oxidation to CO₂ is an issue. Homogeneous transition metal catalysts for hydrocarbon functionalization are particularly appealing in that they can perform chemical transformations directly with better selectivity and under milder reaction conditions.^{29,30} While heterogeneous catalysts are central to many industrial reactions, mechanistic and kinetic studies are generally easier to perform for homogeneous catalysts than for traditional heterogeneous systems, making it more straightforward to study ways to improve catalytic performance.² Furthermore, it is more facile to modulate electronic and steric properties of a homogeneous catalyst active site by ligand tuning. Homogeneous transition metal complexes can be tailored to selectively activate stronger C–H bonds such as terminal C–H bonds of C₃ and greater alkanes as well as arene C–H bonds in the presence of weaker benzylic C–H bonds.^{26,31,32} This is an attractive trait when hydrocarbons functionalized at primary carbons are the desired products.^{26,32} However, an industrially viable catalyst for hydrocarbon functionalization would have to exhibit desired reactivity at ~200 °C and have a turn over frequency (TOF) of approximately one turn over (TO) per second.^{33,34}

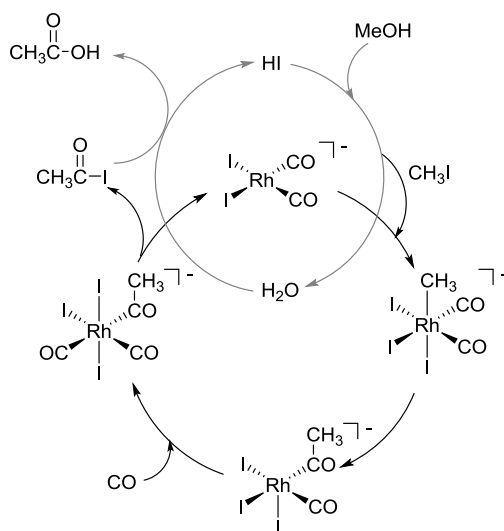
There are several examples of homogeneous transition metal catalysts that have been implemented on an industrial scale, including use in the Wacker process, the Monsanto acetic acid process, and hydroformylation.^{35,36} The Wacker process uses PdCl₂ salts to oxidize alkenes to aldehydes on a 4 million tons per year scale (Scheme 1).³⁵ To recycle palladium, the resulting Pd(0) is oxidized by CuCl₂, and CuCl in turn is re-oxidized to CuCl₂ by air in the presence of

HCl.³⁵ The use of atmospheric oxygen as the ultimate oxidant makes the Wacker process a cost effective method of producing aldehydes.



Scheme 1. Wacker process for production of aldehydes.

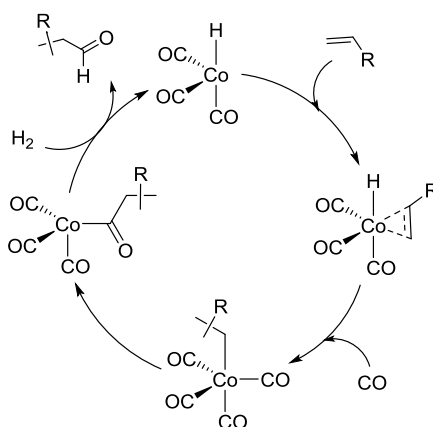
The Monsanto acetic acid process uses $[\text{RhI}_2(\text{CO})_2]^-$ to convert methanol and CO to acetic acid at 180 °C and 30 atm in over two million tons a year with >99% selectivity (Scheme 2).³⁵ In this process, HI is added to produce an equilibrium between methanol and methyl iodide; the methyl iodide oxidatively adds to $[\text{RhI}_2(\text{CO})_2]^-$ to form an octahedral $[\text{Rh}(\text{Me})(\text{I})_3(\text{CO})_2]^-$ complex. CO inserts into the Rh–Me bond, after which the Rh(III) intermediate reductively acyl iodide. Finally, the acyl iodide is converted to acetic acid upon reaction with water.³⁵



Scheme 2. Monsanto acetic acid process.

Hydroformylation is the process in which an olefin is converted to an aldehyde.³⁵ Hydroformylation was originally performed industrially by a cobalt-catalyzed process developed

by Otto Roelen in 1938 (Scheme 3).³⁶ This process operated at 150-180 °C and 200-350 bar and involved a $\text{HCo}(\text{CO})_4$ catalyst from which a CO would dissociate and an olefin would coordinate. Olefin insertion into the Co–H bond occurs, followed by CO insertion into the Co–hydrocarbyl bond. Addition of H_2 releases the product and regenerates the active catalyst.³⁶ Co-catalyzed hydroformylation has been improved upon and largely replaced by Rh-catalyzed hydroformylation that operates with better chemo- and regioselectivity.³⁶ In the Co-catalyzed process, 1° or 2° aldehydes are produced from olefins such as propene because the products are determined by the rate at which 1° vs 2° coordinated alkyls migrate to CO.³⁵ For complexes such as $\text{HRh}(\text{CO})(\text{PPh}_3)_3$, developed at Union Carbide, selectivity for the desired 1° aldehydes is enhanced because the steric bulk of the phosphine ligand promotes formation of the less sterically hindered 1° alkyl ligand.^{32,35}

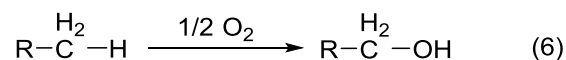


Scheme 3. Cobalt-catalyzed hydroformylation.

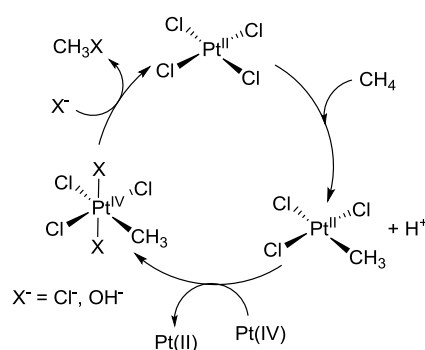
1.6 Transition Metal-Mediated Partial Oxidation of Hydrocarbons via C–H Activation

Transition metal-mediated partial oxidation of hydrocarbons can be thought of in two steps: C–H activation and insertion of oxygen into the C–H bond (functionalization) (eq 6). Direct transition metal-mediated partial oxidation of hydrocarbons has yet to be implemented industrially due to challenges associated with developing a suitable catalyst. The engineering and

scientific communities agree that minimal requirements to make a process which converts methane to methanol economically viable include $\geq 85\%$ selectivity for methanol, $\geq 30\%$ conversion, and the oxidant must be oxygen.^{37,38}



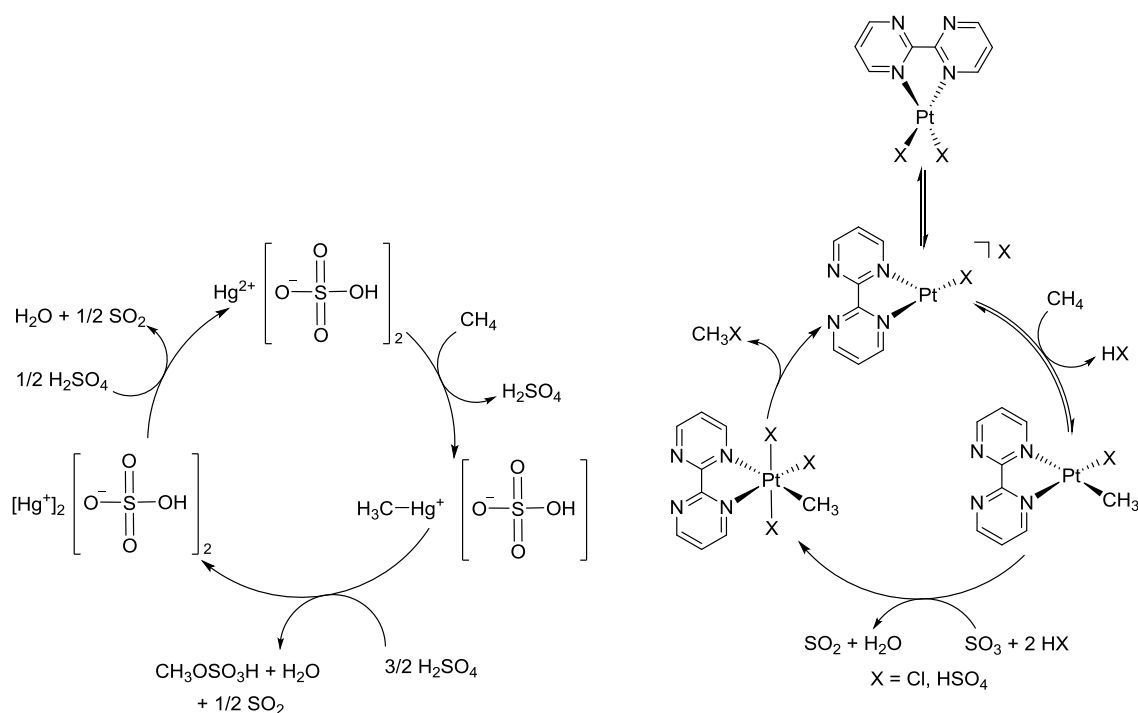
Designing a catalyst to meet these requirements continues to be an insurmountable goal, though significant progress has been made. In the 1970s, Shilov and co-workers developed a system using water soluble Pt^{II} salts to C–H activate and functionalize alkanes (Scheme 4);^{35,38-40} for example, this system can transform methane to methanol and chloromethane under mild conditions. This process involves methane coordination to a $[\text{Pt}(\text{Cl})_4]^{2-}$ salt followed by C–H activation to result in a Pt–Me species. This species is then oxidized to Pt(IV), after which X^- (OH^- or Cl^-) would perform nucleophilic attack to release functionalized product (MeX).^{24,35} A major drawback to the Shilov system is the use of Pt(IV) as a stoichiometric oxidant; the expense and lack of recyclability of the Pt(IV) oxidant ensures that the Shilov system is not industrially viable.



Scheme 4. Shilov cycle for functionalization of methane.

Periana and co-workers developed a system in which $\text{Hg}(\text{II})$ salts in H_2SO_4 convert methane to methyl bisulfate at $180\text{ }^\circ\text{C}$ (Scheme 5).^{35,37} This process benefits from the solvent

serving as an oxidant, and the bisulfate group deactivates the methyl bisulfate product towards undesired over-oxidation due to the electron withdrawing nature of bisulfate—that is, there is less electron density at the methyl group of $\text{CH}_3\text{OSO}_3\text{H}$ than that for methane, making electrophilic C–H activation of methane more favorable than for methyl bisulfate.^{26,41} This system was able to achieve methane conversions of 50% with 85% selectivity for $\text{CH}_3\text{OSO}_3\text{H}$ with turnover frequencies of $\sim 10^{-3} \text{ s}^{-1}$ at $180 \text{ }^\circ\text{C}$.^{37,41} However, major drawbacks include the inability to separate the products from the reaction mixture (methyl bisulfate must be hydrolyzed to methanol and distilled from sulfuric acid, after which sulfuric acid must be reconcentrated), the corrosive nature of sulfuric acid, and the toxicity of Hg.^{37,41} The (bpym)PtCl₂ (bpym = 2,2'-bipyrimidine) system designed by Periana and co-workers also catalyzes the conversion of methane to methyl bisulfate in oleum with observed turnover frequencies of 10^{-2} s^{-1} at $180\text{-}220 \text{ }^\circ\text{C}$ and $\sim 500 \text{ psi}$ CH_4 , faster than for the Hg(II) catalyst (Scheme 5).^{24,25} While a 72% yield of methyl bisulfate from methane was achieved,⁴¹ drawbacks to this system are TOFs too low to be economically competitive (two orders of magnitude lower than desired) and the continued difficulty and expense of separating methanol from concentrated sulfuric acid.⁴² Sen and co-workers developed a bimetallic system for the selective conversion of methane to methanol involving 5% Pd on carbon and Cu(II) salts in 3:1 mixture of trifluoroacetic acid and water under O_2 and CO pressure; while the reaction operates at $140\text{-}150 \text{ }^\circ\text{C}$, a very high pressure of $\sim 1000 \text{ psi}$ (total pressure of CH_4 , CO, and O_2) was required for the result of $65 \times 10^{-4} \text{ M/min}$ conversion of methane to methanol.²⁹ With each of these systems having significant drawbacks, more research is needed for the development of economically feasible transition metal-mediated hydrocarbon partial oxidation catalysis.

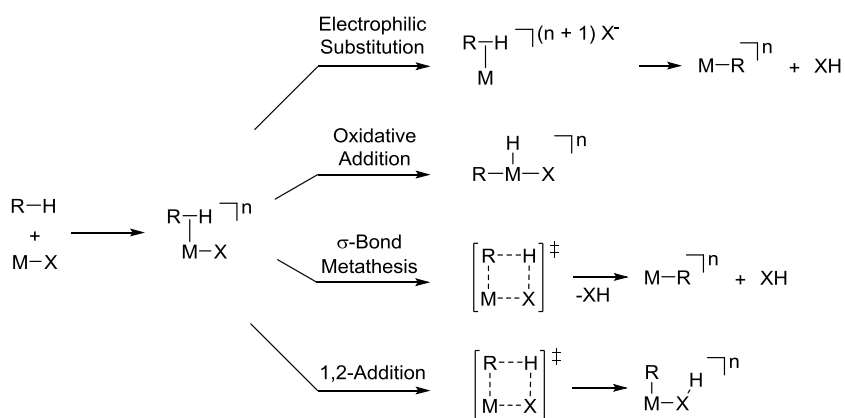


Scheme 5. Periana's Hg(II) (left) and (bpym)PtCl₂ (right) catalyzed reactions for methane functionalization.

1.7 Types of Transition Metal-Mediated C–H Activation

Transition metal-mediated C–H activation is the coordination of a C–H bond to a metal center followed by breakage of the C–H bond.³¹ There are four classical mechanisms for transition metal-mediated C–H activation: oxidative addition, electrophilic substitution, σ -bond metathesis, and 1,2-addition across metal–heteroatom bonds (Scheme 6).³¹ Oxidative addition involves the insertion of a metal into a C–H bond to give a metal–hydrocarbyl and a metal–hydride bond, increasing the metal coordination number by 2 and the metal oxidation state by +2. In electrophilic substitution, H^+ is transferred to an external (i.e., non-ligated) base to result in a metal–hydrocarbyl bond. σ -Bond metathesis is a concerted four-centered, four-electron process in which a metal activates a C–H bond to transfer a H atom to another ligand. Similar to σ -bond metathesis, 1,2-CH-addition is a concerted reaction that involves a kite-shaped four-membered

transition state in which a C–H bond adds across a metal–ligand bond to result in a metal–hydrocarbyl and metal–protonated ligand bond; six electrons are involved in the transition state, with the extra two electrons coming from the lone pair of the ligand receiving the activated proton.



Scheme 6. Types of transition metal-mediated C–H activation.

Transition metal complexes with filled $d\pi$ orbitals can promote 1,2-CH-addition since electron density is localized on the heteroatom, as opposed to being donated into an empty metal $d\pi$ orbital.⁴³ The electron lone pair of the heteroatom ligand is thought to directly interact with the proton of the C–H bond being activated, and one might expect that the more basic the heteroatom ligand is, the lower the energy barrier for bond activation and more favorable C–H activation will be. However, the extent to which the basicity of the lone pair is important in C–H activation is still a point in question, as experimental and computational evidence suggest that greater basicity may inhibit 1,2-CH-addition.⁴⁴ Computational work by Ess and co-workers probed the energetics of bond activation by 1,2-CH-addition through studying models of actual octahedral d^6 metal complexes experimentally shown to perform 1,2-CH-addition, including $(\text{acac})_2\text{Ir}(\text{X})$ and $\text{TpRu}(\text{CO})(\text{X})$ (acac = acetylacetonate, Tp = hydrido(trispyrazolyl)borate, X = OH, OMe, NH_2 , NMe_2).⁴⁴ Methane was used as a model substrate.⁴⁴ 1,2-CH-Addition is calculated to proceed through several steps on the reaction energy profile (Figure 1): ligand loss,

C–H coordination, and C–H cleavage. In an octahedral d^6 complex, a ligand would first dissociate to form a five-coordinate trigonal bipyramidal or square pyramidal intermediate (ΔE_{lig}), opening a coordination site. Trigonal bipyramidal geometry stabilizes the intermediate by positioning the lone electron pair in the heteroatom p-orbital for favorable overlap with the metal $d\pi$ orbitals to form a multiple bond between the metal center and the heteroatom.⁴⁴ Then, a hydrocarbon would fill the 6th coordination site by the η^2 -binding of a C–H bond (ΔE_{coord}).⁴⁴ Afterwards, 1,2-CH-addition would occur to give the product, an octahedral complex with a metal–hydrocarbyl and a metal–protonated heteroatom ligand bond. Important values in this computational study include $\Delta E_{\text{act}}^\ddagger$, the difference in energy between the five-coordinate intermediate and the C–H activation transition state; $\Delta E_{\text{clv}}^\ddagger$, the difference in energy between the metal– η^2 -C–H complex and the C–H activation transition state; and $\Delta E_{\text{tot}}^\ddagger$, the energy difference between the initial octahedral complex and the C–H activation transition state.

For the five-coordinate $(\text{acac})_2\text{Ir}(\text{X})$ ($\text{X} = \text{OH}, \text{OMe}, \text{NH}_2, \text{NMe}_2$) species, the geometry is predicted to be trigonal bipyramidal, as calculations indicate an increase in the HOMO-LUMO gap upon removal of pyridine (the ligand in the 6th coordination site); this geometry in turn affects bond activation energies due to the metal fragment's need to return to octahedral geometry for substrate coordination.⁴⁴ In contrast, the methyl ligand of five-coordinate $(\text{acac})_2\text{Ir}(\text{Me})$ cannot π -donate into the metal d-orbitals, and $(\text{acac})_2\text{Ir}(\text{Me})$ is predicted to have square pyramidal geometry (octahedral with an empty 6th coordination site). It was found that the $\Delta E_{\text{clv}}^\ddagger$ was lower for $(\text{acac})_2\text{Ir}(\text{Me})$ (8.7 kcal/mol) than for $(\text{acac})_2\text{Ir}(\text{OH})$ and $(\text{acac})_2\text{Ir}(\text{OMe})$ (11.7 and 11.6 kcal/mol, respectively); in fact, $\Delta E_{\text{act}}^\ddagger$ was calculated to follow the trend of $\text{CH}_3 < \text{OH} \approx \text{OMe}, \text{NH}_2, \text{NMe}_2$.⁴⁴ The lowest $\Delta E_{\text{act}}^\ddagger$ barrier for $(\text{acac})_2\text{Ir}(\text{Me})$ is likely a result of the square pyramidal geometry of the complex allowing for a more facile return to octahedral geometry. Accounting for a strongly coordinating donor ligand on the metal center is another important factor that affects energy barriers, particularly ΔE_{lig} and ΔE_{coord} . For example, pyridine (py) is

calculated to bind more strongly in $(\text{acac})_2\text{Ir}(\text{X})(\text{py})$ when $\text{X} = \text{Me}$ than when $\text{X} = \text{OH}$ or NH_2 . Furthermore, the calculated ΔE_{coord} for C–H activation is lower for $(\text{acac})_2\text{Ir}(\text{Me})$ compared to $(\text{acac})_2\text{Ir}(\text{NH}_2)$ and $(\text{acac})_2\text{Ir}(\text{OH})$ because Me (with no electrons available to π -donate to the metal center) allows for a more electrophilic vacant coordination site (that is, coordination of a C–H bond is more favorable).⁴⁴

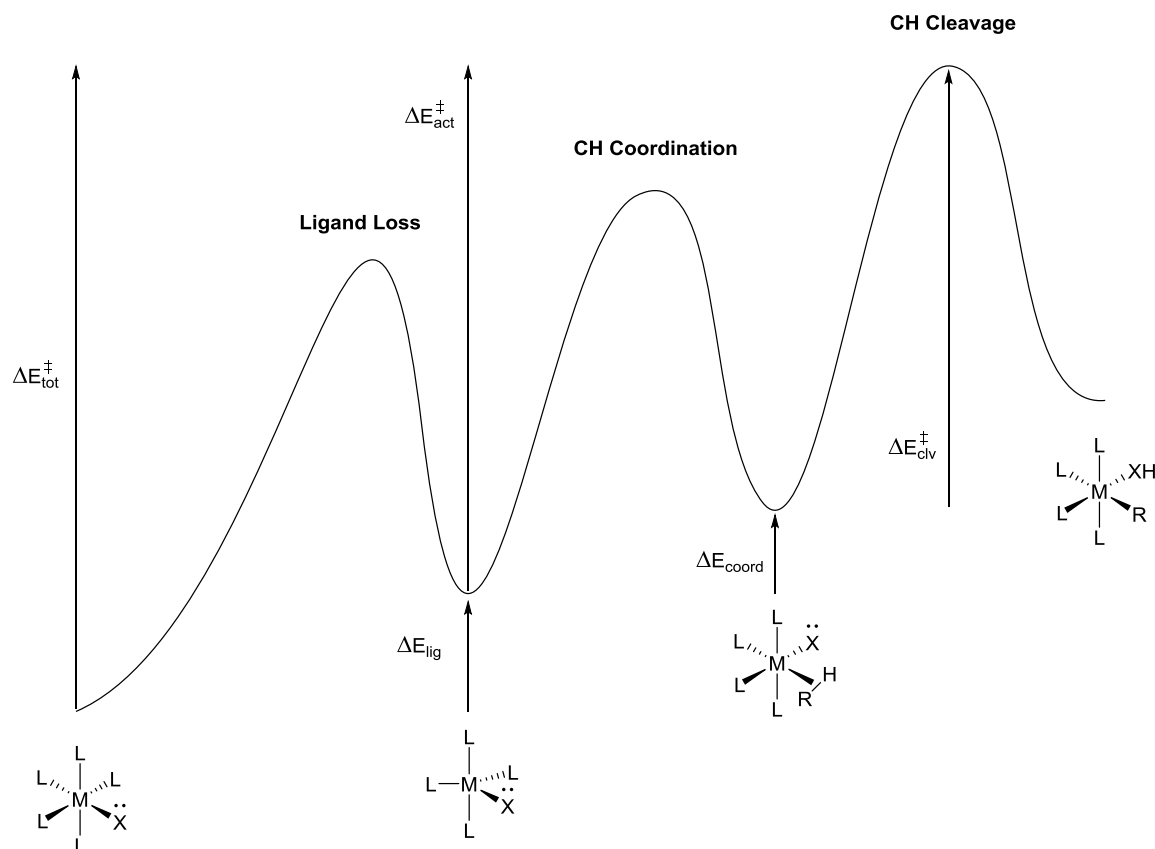


Figure 1. 1,2-Addition reaction coordinate.⁴⁴

Similarly, the geometry of five coordinate $\text{TpRu}(\text{CO})(\text{X})$ ($\text{X} = \text{OH}$, OMe , NH_2) is distorted from octahedral geometry towards a more trigonal bipyramidal arrangement, while $\text{TpRu}(\text{CO})(\text{CH}_3)$ retains an square pyramidal configuration. Interestingly, the $\Delta E_{\text{clv}}^\ddagger$ cleavage for $\text{TpRu}(\text{CO})(\text{CH}_3)$ and $\text{TpRu}(\text{CO})(\text{OH})$ is 19.3 kcal/mol and 16.9 kcal/mol, respectively; the $\Delta E_{\text{act}}^\ddagger$ predicts energy barriers from smallest to largest as follows: $\text{X} = \text{OH} < \text{CH}_3 \approx \text{OMe} \approx \text{NMe}_2 \approx$

NH₂. In this case, the largest $\Delta E_{\text{act}}^{\ddagger}$ values for the amido groups are due to their donor ability. More basic heteroatom lone pairs lower the 1,2-CH-addition transition state energy, as one would expect, but also stabilize the trigonal bipyramidal intermediate.⁴⁴ If the trigonal bipyramidal intermediate is stabilized to a greater extent than the transition state for C–H activation, greater lone pair basicity could actually increase the overall energy activation barrier, making 1,2-CH-addition less favorable.

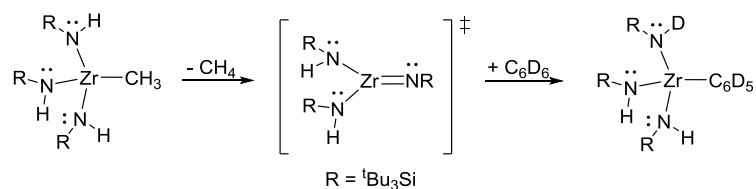
The amount of orbital stabilization in a trigonal bipyramidal arrangement also depends on the energy of both the metal orbitals and the lone pair.⁴⁴ The return to an octahedral arrangement involves an energetic penalty. Five-coordinate metal–alkyl complexes, which remain square pyramidal, do not experience the penalty unlike five-coordinate heteroatom complexes with lone pairs to donate to the metal d orbitals. Thus, (acac)₂Ir(X) and TpRu(CO)(X) differ by the energy expended to attain octahedral geometry for the transition state.⁴⁴ The octahedral geometry for the transition state for C–H activation implies that facially coordinating scaffold ligands would promote 1,2-addition because they tend to enforce octahedral geometry.

1.8 Examples of 1,2-CH-Addition

Examples of transition metal complexes capable of 1,2-CH-addition fall into two main categories—early d⁰ transition metal complexes with imido ligands, and late transition metal complexes with amido, aryloxo, hydroxo, etc. ligands.^{43,45}

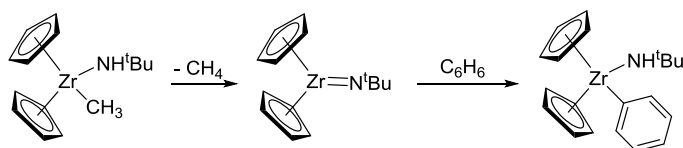
1.8.1 Early Transition Metal Complexes for 1,2-CH-Addition

Wolczanski and co-workers found that a transient (^tBu₃SiNH)₂Zr=NSi^tBu₃ complex is capable of benzene and methane C–H activation (Scheme 7).⁴⁶ Labeling experiments showed that an amido proton from the starting complex (^tBu₃SiNH)₃ZrR (R = Me, Ph, Cy) was abstracted by the coordinated methyl group to release methane, after which a benzene or methane C–H bond added across a Zr=NR bond.⁴⁶



Scheme 7. 1,2-CH-Addition of C₆D₆ by (^tBu₃SiNH)₃Zr(CH₃).

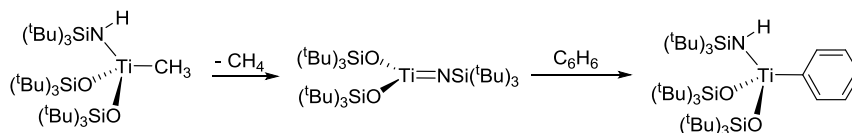
Similarly, Bergman and co-workers found that transient Cp₂Zr=NR (Cp = η⁵-cyclopentadienyl) complexes could C–H activate benzene to form a Cp₂Zr(NHR)(Ph) complex.⁴⁷ In this work, Cp₂Zr(CH₃)(NH^tBu) eliminates methane to form Cp₂Zr=N^tBu, which then activates a benzene C–H bond to form the resulting phenyl complex (Scheme 8).⁴⁵ A study of the Kohn-Sham HOMO-1 (Zr–N π bond parallel to the equatorial girdle of the Cp₂Zr complex) and HOMO (Zr–N π bond perpendicular to the equatorial girdle of the Cp₂Zr complex) of the Cp₂Zr(NR)(η²-CH-benzene) transition state demonstrates that HOMO-1 is more polarized.⁴⁵ As HOMO-1 is positioned to interact with the C–H bond of coordinated benzene, the higher amount of electron density in this orbital indicates the presence of an electron lone pair on N due to a Zr=N–R resonance structure; it is believed the electron lone pair aids in C–H activation.⁴⁵



Scheme 8. Formation of (Cp)₂Zr(N^tBu) followed by 1,2-addition of benzene.

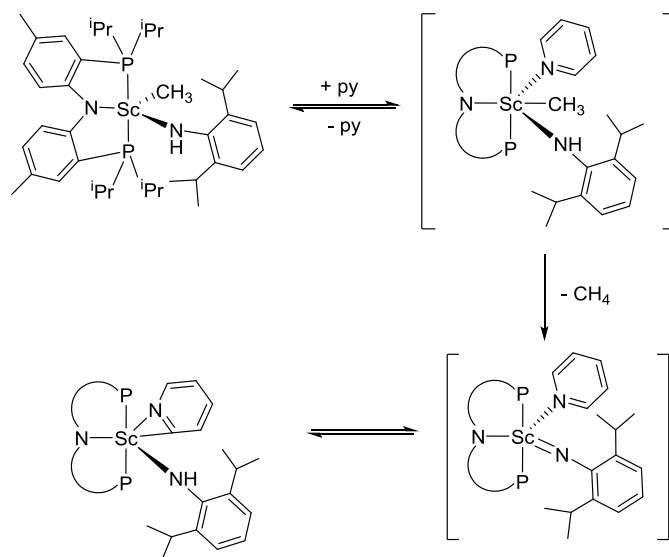
Wolczanski and coworkers also observed C–H activation of RH (R = H, CH₂CH₃, *c*-C₃H₅, *c*-C₅H₉, C₆H₄Me, CH₂C₆H₅, C₆H₅) by d⁰ (silox)₂Ti=NSi^tBu₃ (silox = ^tBu₃SiO[−]) complexes to form (silox)₂(^tBu₃SiNH)Ti(R) (Scheme 9).⁴⁸ Computational results support the idea of formation of an alkane adduct in these reactions,⁴⁹ and mechanistic studies show that the C–H bond is activated in a single step; both observations support bond activation via 1,2-CH-addition.³¹ The observed kinetic selectivity for activating stronger C–H bonds (e.g., benzene 1,2-

CH-addition was favored over methane 1,2-CH-addition) results from the fact that the Ti–C bonds formed are stronger than the C–H bonds that are selectively broken.^{31,48} Ta, V and W–imido complexes also exhibit reactivity towards 1,2-CH-addition.^{48,49}



Scheme 9. Formation of $[(\text{tBu})_3\text{SiO}]_2\text{Ti}[\text{NSi}(\text{tBu})_3]$ followed by 1,2-addition of benzene.

An in-depth study of a rare-earth metal complex capable of 1,2-CH-addition involved a Sc(III) system developed by Mindiola and co-workers.⁵⁰ In the presence of pyridine, $(\text{PNP})\text{Sc}(\text{NH}[\text{DIPP}])(\text{CH}_3)$ (PNP = bis(2-diisopropylphosphino-4-tolyl)amide, DIPP = 2,6-diisopropylphenyl) releases methane at 50 °C to form $(\text{PNP})\text{Sc}=\text{N}[\text{DIPP}](\text{py})$ (Scheme 10). This imido complex then activates a C–H bond in the 2,6-position of coordinated pyridine via 1,2-CH-addition to form $(\text{PNP})\text{Sc}(\text{NH}[\text{DIPP}])(\eta^2\text{-NC}_5\text{H}_4)$. The authors propose that pyridine helps to facilitate the elimination of methane from $(\text{PNP})\text{Sc}(\text{NH}[\text{DIPP}])(\text{CH}_3)$ by lowering the proton transfer energy barrier, that is, the coordination of pyridine prior to methane release pushes the methyl and amide ligands closer together. The observed exchange of pyridine-*d*₅ with $(\text{PNP})\text{Sc}(\text{NH}[\text{DIPP}])(\eta^2\text{-NC}_5\text{H}_4)$ indicates that formation of $(\text{PNP})\text{Sc}=\text{N}[\text{DIPP}](\text{py})$ is reversible.



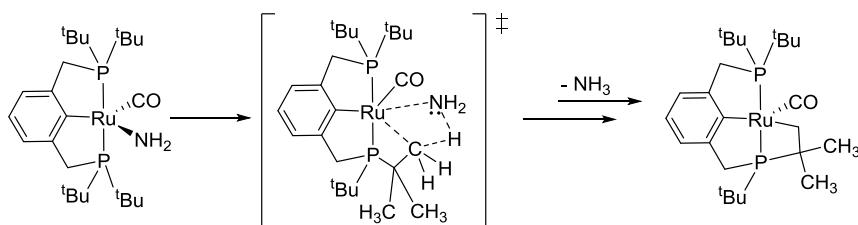
Scheme 10. 1,2-CH-Addition of a pyridine C–H bond to a Sc(III) complex.

One explanation for the ability of several early transition metal–imido complexes to activate C–H bonds via 1,2-CH-addition is because they possess multiple other π -donor ligands.⁴⁵ This creates a condition known as “ π -loading,” in which the lone pairs from ligands interact in a competing fashion with $d\pi$ orbitals of the metal center, allowing the lone pair on the reactive imido ligand to be localized on the heteroatom instead of being donated to the metal center.⁴⁵ Computational studies of H_2 activation by $(H_2N)_2Zr=NH$ as a model reaction, by both Mulliken Population Analysis and *ab initio* (Hartree Fock theory) calculations, support the hypothesis that negative charge is localized on the heteroatom of the imido ligand.⁴⁵ While $(t\text{-Bu}_3\text{SiNH})_2\text{Zr}=\text{NSi}^t\text{Bu}_3$ and other early metal complexes can activate methane C–H bonds, these early transition metals are apparently incapable of reductively eliminating a C–N bond to release functionalized product; early transition metals are electropositive, and the activation barriers for reducing the metal are prohibitively high, making catalytic hydrocarbon functionalization by these early transition metal complexes unfeasible.⁴⁵

1.8.2 Late Transition Metal Complexes for 1,2-CH-Addition

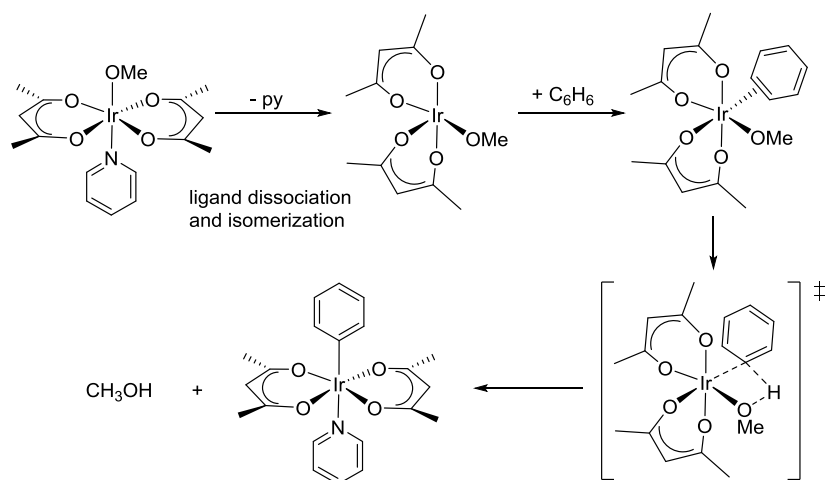
The other class of transition metal complexes capable of performing 1,2-addition of C–H or H₂ bonds are d⁶ octahedral or d⁸ late transition metal complexes with amido, aryloxo, or hydroxo ligands.⁴⁵ This category of complexes is potentially more attractive for catalytic hydrocarbon functionalization since later transition metals are often more “redox flexible” than early transition metals,⁴⁵ and they can often undergo reductive elimination to release functionalized product. Transition metal–heteroatom ligand bonding involves both σ and π interactions; thus, if a metal center has empty d π orbitals, a multiple bond can occur between the metal and the heteroatom and subsequently delocalizing electron density.⁴³ Late transition metals tend to favor low oxidation states, and in turn, more electrons in the metal d orbitals; a higher metal d electron count promotes the localization of the ligand lone pair of electrons on the heteroatom, thus making the lone pair available for participation in 1,2-addition of C–H or H₂.⁴³

1,2-CH-Addition by late transition metal complexes can occur inter- or intramolecularly.⁴⁵ For the complex (PCP)Ru(CO)(NH₂) (PCP = 2,6-(CH₂P^tBu₂)₂C₆H₃), a C–H bond on one of the *tert*-butyl groups of the PCP ligand was activated for addition across the Ru–NH₂ bond.^{45,51} This reaction results in the release of ammonia (NH₃) to form a cyclometalated complex (Scheme 11).⁵¹ (PCP)Ru(CO)(Me) (PCP = 2,6-(CH₂P^tBu₂)₂C₆H₃) also intramolecularly C–H activates a *tert*-butyl group of the ligand to release methane and form the cyclometalated complex.⁵¹ Interestingly, the reaction of (PCP)Ru(CO)(Me) to release methane is roughly five times faster ($k_{\text{obs}} = 3.2(1) \times 10^{-4} \text{ s}^{-1}$) than the corresponding reaction of (PCP)Ru(CO)(NH₂) to release ammonia ($k_{\text{obs}} = 6.0(3) \times 10^{-5} \text{ s}^{-1}$) at 50 °C in benzene, most likely due to the fact that the ΔS^\ddagger for the release of methane (–18(4)) is ~5 entropy units more favorable than that for the release of ammonia (–23(4)).⁵¹



Scheme 11. Cyclometallation and release of ammonia by $(\text{PCP})\text{Ru}(\text{CO})(\text{NH}_2)$ ($\text{PCP} = 2,6\text{-}(\text{CH}_2\text{P}^t\text{Bu}_2)_2\text{C}_6\text{H}_3$).

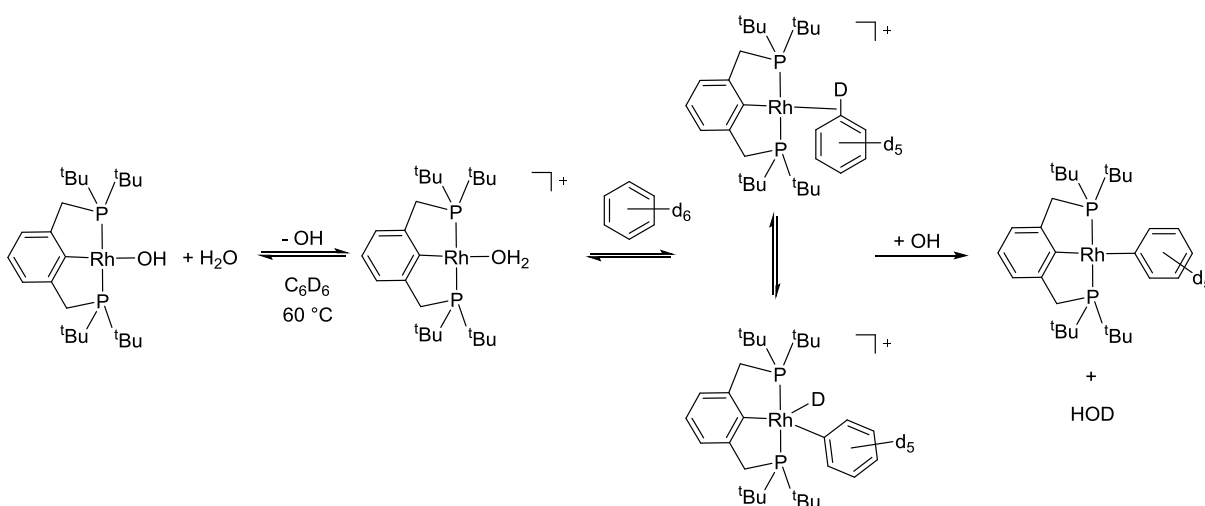
Periana, Goddard and co-workers found that $\text{Ir}(\text{acac})_2(\text{py})(\text{OH})$ ($\text{acac} = \text{acetylacetonate}$, $\text{py} = \text{pyridine}$) is capable of activating benzene to release H_2O .⁵² A similar transformation is possible with the methoxy version of the Ir complex (Scheme 12).⁵³ For $(\text{acac})_2\text{Ir}(\text{OMe})(\text{py})$, pyridine must first dissociate to provide an open coordination site.⁴⁵ The Ir complex then isomerizes to form a complex in which the acac ligands are in a facial arrangement, after which benzene coordinates and 1,2-addition of a benzene C–H bond across the Ir–OMe bond occurs.⁴⁵



Scheme 12. 1,2-CH-Addition of C_6H_6 to $(\text{acac})_2\text{Ir}(\text{OMe})(\text{py})$.

Goldberg and co-workers found that $\text{Rh}(\text{I})$ phenoxide and acetate complexes can perform H/D exchange between arenes and water via 1,2-addition.⁵⁴ Goldberg and coworkers were also able to observe stoichiometric 1,2-CH-addition with d^8 $\text{Rh}(\text{I})$ complexes $(\text{PNP})\text{Rh}(\text{X})$ where $\text{PNP} = 2,6\text{-}(\text{di-}t\text{-butylphosphinomethyl})\text{pyridine}$ and $\text{X} = \text{OH}, \text{OCH}_2\text{CF}_3$ (Scheme 13).^{45,55} For these

complexes, heterolytic dissociation of OH or OCH₂CF₃ from Rh is proposed, followed by coordination of the arene.⁴⁵ C–H activation of the arene occurs at the metal center in which the Rh-η²-CH-arene is in equilibrium with a Rh-hydrocarbyl/hydride species that transfers the H to the outer sphere OH or OCH₂CF₃.⁴⁵

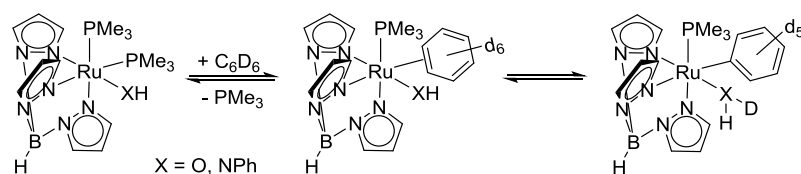


Scheme 13. 1,2-Addition of C₆D₆ to (PNP)Rh(OH) (PNP = 2,6-(di-*tert*-butylphosphinomethyl)pyridine).

Periana and coworkers have observed catalytic H/D exchange between hydrocarbons and strongly basic solvents using the complex (IPI)Ru(II)(OH)_n(H₂O)_m (IPI = 2,6-diimidazolylpyridine).⁵⁶ This provides an example of base-accelerated nucleophilic C–H activation of a d⁶ Ru(II) complex with a protic polydentate ligand, as rates of H/D exchange are faster in the presence of base than in the solvent alone. H/D exchange catalyzed by (IPI)Ru(II)(OH)_n(H₂O)_m was studied for water soluble aromatic and aliphatic substrates at 90 and 160 °C, respectively, in the presence of aqueous KOH.⁵⁶

We have been able to observe H/D exchange via 1,2-addition of C₆D₆ with TpRu(PMe₃)₂(X) (Tp = hydrido(trispyrazolyl)borate, X = OH, NHR) at 80-130 °C (Scheme 14).^{45,57,58} For TpRu(PMe₃)₂(OH), the H/D exchange $k_{\text{obs}} = 8.0(2) \times 10^{-5} \text{ s}^{-1}$ at 80 °C, and was

found to be first order in $\text{TpRu}(\text{PMe}_3)_2(\text{OH})$.⁴⁵ For $\text{TpRu}(\text{PMe}_3)_2(\text{NHPh})$, the $k_{\text{obs}} = 1.4(2) \times 10^{-5} \text{ s}^{-1}$ at $130 \text{ }^\circ\text{C}$.⁴⁵ H/D exchange was inhibited upon addition of 1 equivalent of PMe_3 to the reaction mixture.⁴⁵ The proposed mechanism for this reaction involves the dissociation of PMe_3 to open up a coordination site at the metal center. Coordination of benzene, followed by 1,2-addition of C–D across the Ru–X bond results in formation of bound HOD or NHDR, respectively. Computational studies were done on a model complex, $(\text{Tab})\text{Ru}(\text{PH}_3)_2(\text{X})$ where $\text{X} = \text{Me}, \text{OH},$ or NH_2 ; Tab (tris(azo)borate) and PH_3 served as models for Tp and PMe_3 , respectively.⁴⁵ For $\text{X} = \text{OH}$, a ΔG of $+2.8 \text{ kcal/mol}$ was predicted for the first step, dissociation of PH_3 .⁵⁷ Next, benzene was predicted to coordinate to the five-coordinate $(\text{Tab})\text{Ru}(\text{PH}_3)(\text{OH})$ to form $(\text{Tab})\text{Ru}(\text{PH}_3)(\eta^2\text{-C}_6\text{H}_6)(\text{OH})$ with a ΔG of $+11.2 \text{ kcal/mol}$; the overall reaction has a predicted ΔG of $+18.4 \text{ kcal/mol}$.⁵⁷ The calculated $\Delta\text{G}^\ddagger = 17.6 \text{ kcal/mol}$ for C–H activation by $(\text{Tab})\text{Ru}(\text{PH}_3)(\text{OH})(\eta^2\text{-C}_6\text{H}_6)$.⁴⁵ Thus, the 1,2-CH-addition of benzene to $\text{TpRu}(\text{PMe}_3)_2(\text{OH})$ is shown to be endergonic, indicating that the lack of observing $\text{TpRu}(\text{PMe}_3)(\text{Ph})(\text{OH}_2)$ experimentally is due to unfavorable thermodynamics.⁵⁷ These computational studies also showed that C–H activation occurs via a σ -bond-metathesis-type of interaction, with four-centered kite shaped transition states.⁴⁵ Interestingly, the predicted transition states for 1,2-CH-addition of benzene show shorter Ru– C_{phenyl} and Ru–H distances when $\text{X} = \text{Me}$, indicating that the metal center formal oxidation state could be closer to +4; when $\text{X} = \text{OH}$ or NH_2 , these calculated distances are longer as a result of the heteroatom electron lone pair, indicating a Ru formal oxidation state of +2.⁴⁵



Scheme 14. H/D Exchange between C_6D_6 and OH or NHPh via 1,2-addition of C_6D_6 with $\text{TpRu}(\text{PMe}_3)_2(\text{XH})$ ($\text{X} = \text{O}, \text{NPh}$).

1.9 Examples of H₂ Activation by 1,2-Addition to Late Transition Metal Complexes

H₂ activation is often used as a model for C–H activation due to its similar BDE (~104 kcal/mol) and polarity.^{26,45,59} H₂ is also an attractive substrate in that one can observe reactivity while avoiding the steric bulk of some hydrocarbon ligands. H₂ binds to transition metals in the same way that C–H bonds bind—through the electrons in the sigma bond; that is, the σ -bond electrons are donated into an empty orbital on the metal.⁵⁹ However, H₂ tends to be a more reactive substrate than C–H bonds due to better orbital overlap with metal d orbitals (that is, the spherical σ orbital (s orbitals) of H₂ provides for a more even overlap with a d orbital than the dumbbell shaped σ orbital (sp³ and s orbital) of C–H), making H₂ complexes more stable than alkane complexes (Figure 2).⁵⁹ Back bonding of electron density from the metal into the σ^* H₂ orbital helps elongate and therefore activate H₂.⁵⁹

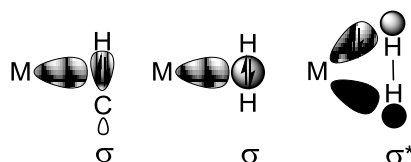
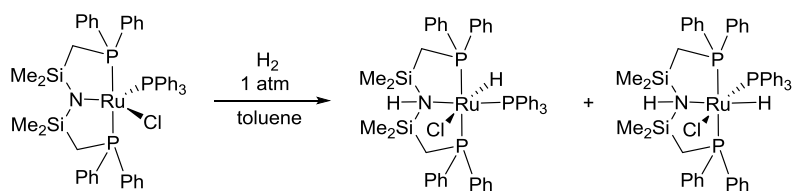


Figure 2. Comparison of metal-C–H and metal-H–H bonding.

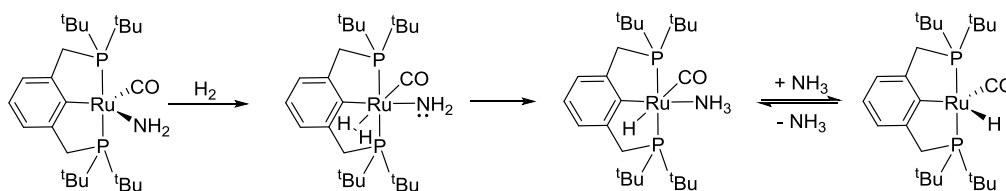


Scheme 15. 1,2-HH-Addition to Ru(Cl)(PPh₃)[κ^3 -N-(SiMe₂CH₂PPh₂)₂].

Breaking H–H bonds is useful in hydrogenation reactions, fine chemical and pharmaceutical synthesis, and in the conversion of lignocellulosic biomass into fuel.⁶⁰ There are several examples of 1,2-HH-addition by d⁶ and d⁸ hydroxide and amido complexes.⁴⁵ The

complex $\text{Ru}(\text{Cl})(\text{PPh}_3)[\kappa^3\text{-N}-(\text{SiMe}_2\text{CH}_2\text{PPh}_2)_2]$ is able to activate H_2 to produce two isomers of $\text{Ru}(\text{Cl})(\text{PPh}_3)(\text{H})[\kappa^3\text{-NH}-(\text{SiMe}_2\text{CH}_2\text{PPh}_2)_2]$ (Scheme 15).^{45,61}

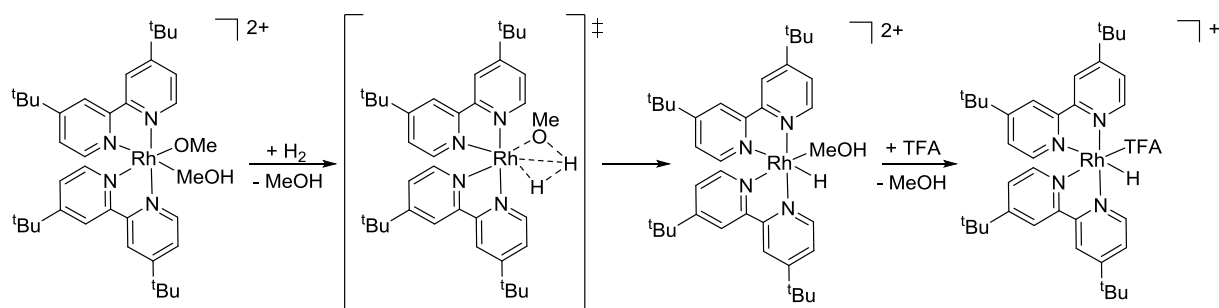
At room temperature, H_2 is activated by $(\text{PCP})\text{Ru}(\text{CO})(\text{NH}_2)$ ($\text{PCP} = 2,6-(\text{CH}_2\text{P}^t\text{Bu}_2)_2\text{C}_6\text{H}_3$) via an $\eta^2\text{-H}_2$ intermediate. Dihydrogen activation results in formation of free ammonia and the complex $(\text{PCP})\text{Ru}(\text{CO})(\text{H})$ (Scheme 16).^{45,51} While $(\text{PCP})\text{Ru}(\text{CO})(\text{NH}_2)$ is capable of H_2 activation and intramolecular CH activation of the PCP ligand, it is unable to perform intermolecular C–H activation. To elucidate reasons for this reactivity, DFT calculations were performed on $(\text{PCP}')\text{Ru}(\text{CO})(\text{NH}_2)$, with PCP' being the simplified model ligand $2,6-(\text{CH}_2\text{PH}_2)_2\text{C}_6\text{H}_3$. The bond activation reactions of $(\text{PCP}')\text{Ru}(\text{CO})(\text{NH}_2)$ with H_2 and CH_4 were studied. H_2 activation was found to be exothermic ($\Delta\text{H} = -16.9$ kcal/mol) and exergonic ($\Delta\text{G} = 8.9$ kcal/mol). On the other hand, the C–H activation of methane was calculated to be endothermic ($\Delta\text{H} = 3.7$ kcal/mol) and endergonic ($\Delta\text{G} = 13.6$ kcal/mol). The endothermicity of methane C–H activation is a result of the enthalpic penalty caused by conversion of the nondative amido, NH_2 , to the less-strongly coordinating dative amine, NH_3 , upon bond activation. That is, the calculated BDE of $\text{Ru-NH}_2 = 52.5$ kcal/mol while the calculated BDE of $\text{Ru-NH}_3 = 12.6$ kcal/mol. Therefore, the ΔBDE of 39.9 kcal/mol is significant enough to outweigh the enthalpic gain (~ 32 kcal/mol) from activation of the methane C–H bond and formation of the N–H and Ru–C bonds in the product $(\text{PCP})\text{Ru}(\text{CO})(\text{Me})(\text{NH}_3)$.



Scheme 16. H_2 activation by $(\text{PCP})\text{Ru}(\text{CO})(\text{NH}_2)$ ($\text{PCP} = 2,6-(\text{CH}_2\text{P}^t\text{Bu}_2)_2\text{C}_6\text{H}_3$).

Goldberg and co-workers found that $(\text{PCP})\text{Pd}(\text{OR})$ where $\text{PCP} = 2,6-(\text{CH}_2\text{P}^t\text{Bu}_2)_2\text{C}_6\text{H}_3$ and $\text{R} = \text{H}$ or CH_3 performs 1,2-HH-addition to release water or methanol, respectively; the final

transition metal product formed is the hydride species (PCP)Pd(H).^{45,62,63} Furthermore, we have shown 1,2-addition of dihydrogen occurs across a Rh(III)–OMe bond.⁶⁰ The complex $[(^t\text{bpy})_2\text{Rh}(\text{OMe})(\text{MeOH})][\text{TFA}][\text{OTf}]$ (^tbpy = 4,4'-di-*tert*-butylbipyridyl, TFA = trifluoroacetate, OTf = trifluoromethanesulfonate) is proposed to activate H_2 via the pathway in Scheme 17. Methanol first dissociates from the complex, after which H_2 binds to the metal center in an η^2 fashion. 1,2-Addition of the dihydrogen ligand occurs across the Rh–OMe bond to produce a rhodium hydride/methanol species. Methanol dissociates, and TFA binds to the empty coordination site, giving the final product $[(^t\text{bpy})_2\text{Rh}(\text{TFA})(\text{H})][\text{OTf}]$.⁶⁰ Kinetic data revealed that the reaction exhibits a dependence on H_2 concentration between zero and first order.⁶⁰

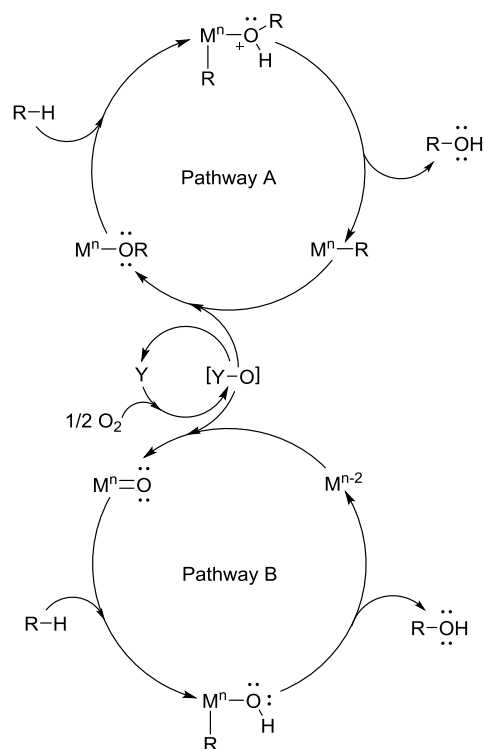


Scheme 17. 1,2-Addition of H_2 to $[(^t\text{bpy})_2\text{Rh}(\text{OMe})(\text{MeOH})]^{2+}$.

1.10 1,2-CH-Addition and Proposed Catalytic Cycle for Hydrocarbon Functionalization

1,2-CH-Addition of a C–H bond features in proposed catalytic cycles for the partial oxidation of hydrocarbons (Scheme 18).²⁴ In pathway A, a hydrocarbon C–H bond would add across a M–OR bond to give coordinated ROH, which would then dissociate to release the functionalized product. The M–OR species would be regenerated through the reaction of the M–hydrocarbyl species with oxidant. In cycle B (Scheme 18), a hydrocarbon C–H bond would add across a M–oxo bond, followed by reductive elimination of the hydroxyl and hydrocarbyl ligands to release functionalized product. Reaction of the reduced metal center with oxidant would

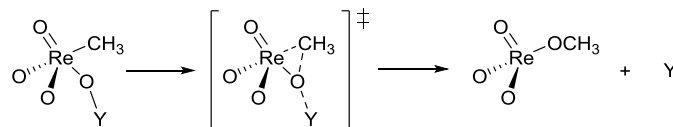
regenerate M=O. Ideally, the oxidant (YO) can be recycled from oxygen. Similarly, one can envision catalytic cycles involving nitrene sources to produce amines. A metal center suitable for this type of catalysis would need to be capable of C–H activation via 1,2-CH-addition while being tolerant towards heteroatom functional groups; while there are examples of C–H activation (including C–H activation of methane) by early transition metal complexes such as Zr, Ti, and Sc–imido complexes, early metals tend to be less tolerant toward functional groups.^{24,46,48,50} Thus, later transition metals, particularly electrophilic metal systems, would appear to be better candidates for the proposed catalytic cycles due to their compatibility with heteroatoms.^{24,38} Furthermore, the capacity of the metal center to access both low and high oxidation states is necessary, as bond activation is favorable at low oxidation states and both functionalization and metal center reduction to release functionalized product is favorable at high oxidation states.²⁴ A notable example of a late transition metal system capable of C–H activation and the access of necessary oxidation states would be Pt(II)/(IV).²⁴



Scheme 18. Proposed catalytic cycles for hydrocarbon partial oxidation.

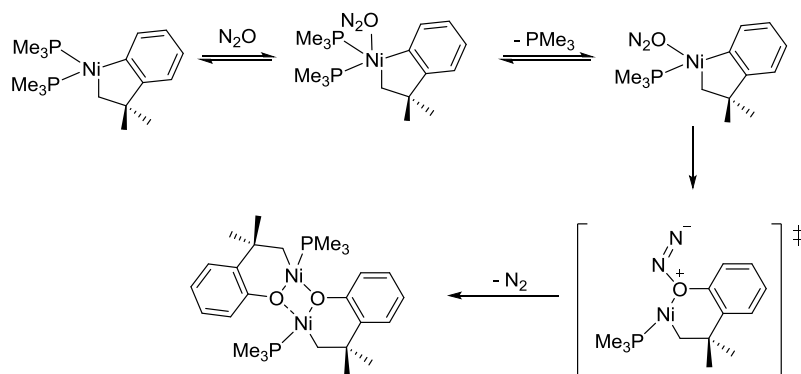
1.11 Functionalization of Hydrocarbons: Oxygen Atom Insertion

A vital part of transition metal-mediated oxy-functionalization of hydrocarbons via the strategy employed in the catalytic cycles for hydrocarbon partial oxidation (Scheme 7) is the ability of a catalyst to insert an oxygen atom (or N) into a metal–hydrocarbyl bond. Unfortunately, transition metal systems that can perform such net oxygen-atom insertions are rare, one reason being that the polar nature of metal–oxo and metal–hydrocarbyl bonds results in the oxo and hydrocarbyl being nucleophilic.³⁸ This aspect is influenced by the LUMO of the metal complex, which tends to be metal-based instead of carbon-based (of the hydrocarbyl ligand) in metal-oxo complexes; thus, the electrophilicity of the oxo ligand would need to be increased (perhaps by oxo to metal π -donation, for example) in order for migration to a hydrocarbyl ligand to occur.^{38,64} In one possible method of oxygen atom insertion into a metal–hydrocarbyl bond, an oxidant “OY” coordinates to a metal center and dissociates “Y” to produce



Scheme 19. Organometallic Baeyer-Villiger reaction involving methyltrioxorhenium and a generic oxidant (YO = OIPh, IO_4^- , IO_3^- , H_2O_2 , pyridine-N-oxide).

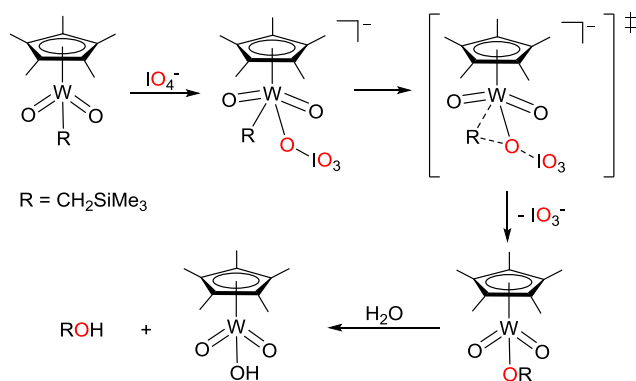
Oxygen atom transfer has been demonstrated with a square planar Ni(II) complex, $(\text{PMe}_3)_2\text{Ni}(\kappa^2\text{-C,C-CH}_2\text{CMe}_2\text{-}o\text{-C}_6\text{H}_4)$ (Scheme 20).⁶⁶ The reaction of $(\text{PMe}_3)_2\text{Ni}(\kappa^2\text{-C,C-CH}_2\text{CMe}_2\text{-}o\text{-C}_6\text{H}_4)$ with N_2O in benzene involves dissociation of a PMe_3 to allow coordination of N_2O to Ni. The oxygen atom of N_2O then inserts regioselectively into the Ni–aryl bond indicating the formation of a heterocumulene as opposed to a direct oxygen-atom transfer; one of the proposed transition states is that for an organometallic Baeyer-Villiger transformation. The resulting product is the dimer $[(\text{PMe}_3)_2\text{Ni}(\kappa^2\text{-O,C-O-}o\text{-C}_6\text{H}_4\text{CMe}_2\text{-CH}_2)]_2$.⁶⁶



Scheme 20. Reaction of $(\text{PMe}_3)_2\text{Ni}(\kappa^2\text{-C,C-CH}_2\text{CMe}_2\text{-}o\text{-C}_6\text{H}_4)$ with N_2O proceeding through OMBV transition state.

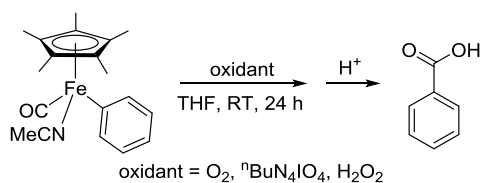
Our group has observed oxygen-atom insertion into a $\text{W-CH}_2\text{SiMe}_3$ bond of both the $\text{Cp}^*\text{W}(\text{O})_2(\text{CH}_2\text{SiMe}_3)$ and $\text{Cp}^*\text{W}(\text{O})(\eta^2\text{-O}_2)(\text{CH}_2\text{SiMe}_3)$ ($\text{Cp}^* = 1,2,3,4,5\text{-pentamethylcyclopentadienyl}$) complexes.⁶⁷ $\text{Cp}^*\text{W}(\text{O})_2(\text{CH}_2\text{SiMe}_3)$ reacts with oxidants such as H_2O_2 , PhIO, and IO_4^- in THF/water to release $\text{HOCH}_2\text{SiMe}_3$. The reaction of $\text{Cp}^*\text{W}(\text{O})_2(\text{CH}_2\text{SiMe}_3)$ with IO_4^- is reported to involve the OMBV pathway, in which IO_4^-

coordinates followed by O-atom insertion and dissociation of IO_3^- (“Y”) (Scheme 21). It was determined that the inserted oxygen atom originates from the oxidant IO_4^- , instead of one of the oxygens of the tungsten complex, by the use of isotopically labeled $\text{NaI}^{18}\text{O}_4^-$. Protonolysis by water releases the alcohol product. Alternately, the reaction of $\text{Cp}^*\text{W}(\text{O})_2(\text{CH}_2\text{SiMe}_3)$ with H_2O_2 forms the complex $\text{Cp}^*\text{W}(\text{O})(\eta^2\text{-O}_2)(\text{CH}_2\text{SiMe}_3)$, which subsequently releases $\text{HOCH}_2\text{SiMe}_3$ in the presence of HCl or NaOH .

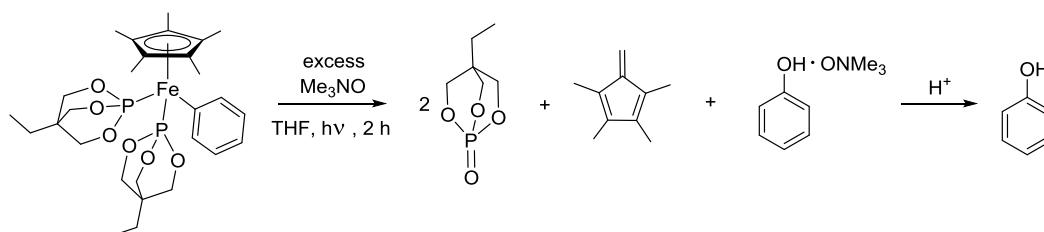


Scheme 21. Reaction of $\text{Cp}^*\text{W}(\text{O})_2(\text{CH}_2\text{SiMe}_3)$ with IO_4^- via an OMBV pathway.

Oxygen atom insertion has also been proposed for $\text{Fe}(\text{II})$ –phenyl and –methyl bonds.⁶⁸ $\text{Cp}^*\text{Fe}(\text{CO})(\text{NCMe})(\text{Ph})$ is known to activate C–H bonds of several aromatic substrates;⁶⁹ it was also demonstrated to produce benzoic acid upon reacting with the oxidants O_2 , $[\text{nBuN}_4][\text{IO}_4]$ and H_2O_2 at room temperature (Scheme 22).⁶⁸ Also, $\text{Cp}^*\text{Fe}[\text{P}(\text{OCH}_2)_3\text{CEt}]_2(\text{Ph})$ was demonstrated to react with excess Me_3NO to produce $\text{PhOH}\cdot\text{ONMe}_3$ (hydrolyzed to phenol) under both ambient light and photolytic conditions (Scheme 23). Unfortunately, the reaction also sacrifices the complex, as Cp^* and $\text{P}(\text{OCH}_2)_3\text{CEt}$ are oxidized to 1,2,3,4-tetramethylfulvene and $\text{O}=\text{P}(\text{OCH}_2)_3\text{CEt}$, respectively.



Scheme 22. Thermal reaction of Cp*Fe(CO)(NCMe)(Ph) with oxidants to yield benzoic acid.



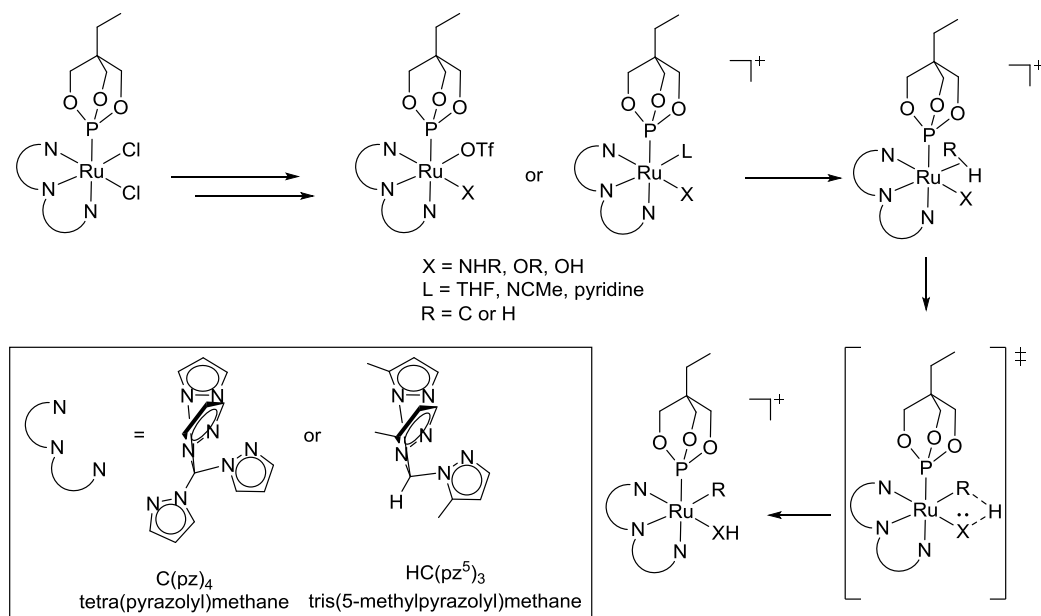
Scheme 23. Photolytic reaction of Cp*Fe[P(OCH₂)₃CEt]₂(Ph) with Me₃NO to yield phenol.

Unfortunately, no current transition metal system capable of OMBV chemistry has also been capable of activating C–H bonds to initiate catalysis, perhaps due the oxygen ligands often found in these systems pulling electron density away from the metal d orbitals; thus the design of a catalyst that is electron rich enough to activate C–H bonds (that is, having the electron density available to donate into the C–H σ^* orbital, thus elongating and cleaving the bond) while being capable of performing an OMBV transformation is desirable.^{31,38}

1.12 Thesis Aims

The goal of this project was to design an octahedral Ru(II) complex for 1,2-addition of H–H and C–H bonds across Ru–X bonds that would improve upon and circumvent the drawbacks of our previously reported TpRu(PMe₃)₂(X) system. We proposed that a more electrophilic metal center would help facilitate hydrocarbon coordination, and the design of a complex that is less electron-rich than TpRu(PMe₃)₂(X) was desired. Thus, the work discussed herein involves the use of polypyrazolylalkanes as scaffold ligands (Scheme 24). Polypyrazolylalkanes are charge neutral (enhancing metal center electrophilicity compared to Tp

ligands), and the facial binding mode of these scorpionate ligands would ensure an octahedral geometry with the coordination sites of the heteroatom ligand and the substrate being *cis* to each other. The two polypyrazolylalkane ligands chosen for this study were tetrapyrazolylmethane ($C(pz)_4$) and tris(5-methyl)pyrazolylmethane ($HC(pz^5)_3$).



Scheme 24. General synthetic strategy for electrophilic Ru(II)-heteroatom complexes and 1,2-addition of C–H or H–H bonds.

Tetra(pyrazolyl)methane was selected for the possibility that the four pyrazolyl rings would enhance solubility compared to tris(pyrazolyl)methane; nevertheless, this ligand has been observed to undergo intramolecular C–H activation of the 5-position on the pyrazolyl ring.⁷⁰ This reactivity could potentially interfere with the study of the desired 1,2-addition of substrates. Thus, tris(5-methyl)pyrazolylmethane was used in the synthesis of Ru complexes because the methyl groups in the 5-position of the pyrazolyl rings would prevent intramolecular C–H activation of the pyrazolyl rings. The methyl groups also provide a convenient spectroscopic handle to determine its symmetry. $P(OCH_2)_3\text{CEt}$ was chosen as an ancillary ligand because it is

less π -donating than PMe_3 and would result in less electron-rich complexes; also, the tied-back geometry of the phosphite prevents any intramolecular C–H activation.

Once a Ru–X (X = NHPH, OH, OR, SR) target complex could be synthesized, the focus of this work would involve conducting H_2 and C–H bond activation studies. Investigating the role the heteroatom lone pair plays in bond activation is also a major goal of this work; we hoped to accomplish this study by modulating basicity using electron-withdrawing and electron-donating groups on a heteroatom ligand such as anilido (NHPH). NHPH is a particularly attractive ligand for a basicity study in that a wide range of functional groups can be installed at the para-position of the phenyl ring, thus influencing the electronics of the ligand (Figure 3).

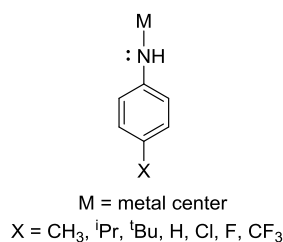
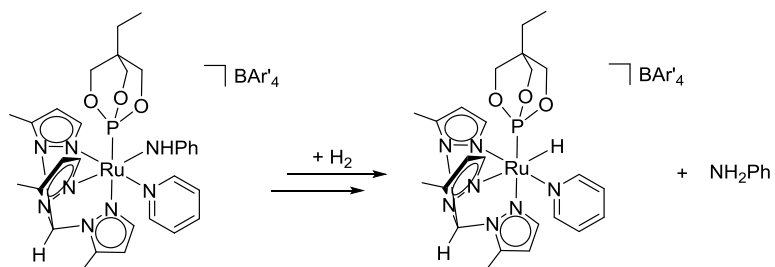
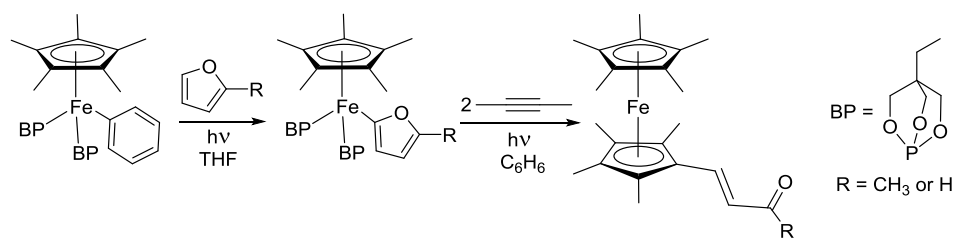


Figure 3. *Para*-substituted anilido ligands.

An outline of the chapters follows: Chapter 2 discusses the synthesis and reactivity of several $\text{C}(\text{pz})_4\text{Ru}$ complexes. Chapter 3 describes the design and synthesis of many $(\text{HC}(\text{pz}^5)_3)\text{Ru}$ complexes, including the synthesis of a series of $(\text{HC}(\text{pz}^5)_3)\text{Ru}$ -anilido complexes. Chapter 4 presents work on H_2 activation by $\{[\text{HC}(\text{pz}^5)_3]\text{Ru}[\text{P}(\text{OCH}_2)_3\text{CET}](\text{py})(\text{NHAr})\}[\text{BAR}'_4]$ complexes, including the discussion of reaction intermediates and reporting kinetic and mechanistic studies (Scheme 25). Chapter 5 deviates somewhat from the main focus of this thesis to present results on kinetic and mechanistic studies performed on the reaction of Cp^*Fe -furyl complexes with alkynes to produce furyl ring-opened sandwich complexes under photolytic conditions (Scheme 26).



Scheme 25. H₂ activation by $\{[\text{HC}(\text{pz}^5)_3\text{Ru}[\text{P}(\text{OCH}_2)_3\text{CEt}](\text{py})(\text{NHPh})]\}[\text{BAR}'_4]$.



Scheme 26. C–H activation and furyl ring-opening by Fe(II) complexes.

References

- (1) Hashiguchi, B. G.; Konnick, M. M.; Bischof, S. M.; Gustafson, S. J.; Devarajan, D.; Gunsalus, N.; Ess, D. H.; Periana, R. A. *Science* **2014**, *343*, 1232.
- (2) Wittcoff, H. A. R., B. G.; Plotkin, J. S. *Industrial Organic Chemicals*; 2nd ed.; Wiley-Interscience: Hoboken, N. J., 2004.
- (3) Guo, X. G.; Fang, G. Z.; Li, G.; Ma, H.; Fan, H. J.; Yu, L.; Ma, C.; Wu, X.; Deng, D. H.; Wei, M. M.; Tan, D. L.; Si, R.; Zhang, S.; Li, J. Q.; Sun, L. T.; Tang, Z. C.; Pan, X. L.; Bao, X. H. *Science* **2014**, *344*, 616.
- (4) Xue, J.; Chen, Y.; Wei, Y. Y.; Feldhoff, A.; Wang, H. H.; Caro, J. *ACS Catal.* **2016**, *6*, 2448.
- (5) Niziolek, A. M.; Onel, O.; Floudas, C. A. *Aiche J.* **2016**, *62*, 1531.
- (6) *Annual Energy Outlook 2001: With Projections to 2020*, Energy Information Administration Office of Integrated Analysis and Forecasting U.S. Department of Energy, 2000.
- (7) Lim, W.; Choi, K.; Moon, I. *Industrial & Engineering Chemistry Research* **2013**, *52*, 3065.
- (8) Songhurst, B. *LNG Plant Cost Escalation*, The Oxford Institute for Energy Studies, 2014.
- (9) Manufacturers, A. F. P. Petrochemicals. [Online Early Access]. Published Online: 2015. <https://www.afpm.org/policy-positions-petrochemicals/>
- (10) Administration, U. S. E. I. Oil: Crude and Petroleum Products Explained Use of Oil. [Online Early Access]. Published Online: 2016. http://www.eia.gov/energyexplained/index.cfm?page=oil_use (accessed February 2, 2016).
- (11) Cobb, K. Oil is too Precious to be Used as Transportation Fuel. [Online Early Access]. Published Online: 2012. <http://oilprice.com/Energy/Crude-Oil/Oil-is-too-Precious-to-be-Used-as-Transportation-Fuel.html>.

- (12) Cobb, K. U. S. Needs to Stop Burning Oil and Electrify Transportation. [Online Early Access]. Published Online: 2012. <http://www.econmatters.com/2012/11/us-needs-to-stop-burning-oil-and.html>.
- (13) Olah, G. A. a. M., Arpad *Hydrocarbon Chemistry*; John Wiley & Sons, Inc.: New York, 1995.
- (14) Administration, U. S. E. I. How much natural gas does the United States have, and how long will it last? *Frequently Asked Questions* [Online Early Access]. Published Online: 2015. <http://www.eia.gov/tools/faqs/faq.cfm?id=58&t=8> (accessed November 18, 2015).
- (15) Beta, U. S. E. I. A. Total Energy. [Online Early Access]. Published Online: 2015. <http://www.eia.gov/beta/MER/?tbl=T01.01#/?f=A&start=1949&end=2014&charted=4-6-7-14>.
- (16) Johnson, J. *Chemical & Engineering News Archive* **2014**, 92, 10.
- (17) Tubb, R. *Pipeline & Gas Journal* **2009**, 236.
- (18) Dobrota, D. L., Branko; Komar, Ivan *Transactions on Maritime Science* **2013**, 2, 91.
- (19) Chen, X. Y. A guide to liquefied natural gas carriers and key shipping costs. [Online Early Access]. Published Online: 2014. <http://marketrealist.com/2014/05/expensive-lng-carriers-results-in-dividends/>.
- (20) Administration, U. S. E. I. Natural Gas Gross Withdrawals and Production. [Online Early Access]. Published Online: 2016. http://www.eia.gov/dnav/ng/ng_prod_sum_a_epg0_vgv_mmcf_a.htm (accessed 5/31/2016).
- (21) Allen, D. *Accounts Chem. Res.* **2016**.
- (22) Administration, U. S. E. I. U.S. energy imports and exports to come into balance for first time since 1950s. *Today in Energy* [Online Early Access]. Published Online: 2015. <http://www.eia.gov/todayinenergy/detail.cfm?id=20812>.

- (23) Administration, U. S. E. I. Projections show U.S. becoming a net exporter of natural gas. *Today in Energy* [Online Early Access]. Published Online: 2015. <http://www.eia.gov/todayinenergy/detail.cfm?id=20992>.
- (24) Webb, J. R.; Bolano, T.; Gunnoe, T. B. *ChemSusChem* **2011**, *4*, 37.
- (25) Periana, R. A.; Taube, D. J.; Gamble, S.; Taube, H.; Satoh, T.; Fujii, H. *Science* **1998**, *280*, 560.
- (26) Sen, A. *Accounts Chem. Res.* **1998**, *31*, 550.
- (27) Laboratory, N. E. T. 2016.
- (28) Ahlquist, M.; Nielsen, R. J.; Periana, R. A.; Goddard Iii, W. A. *J. Am. Chem. Soc.* **2009**, *131*, 17110.
- (29) Lin, M.; Hogan, T.; Sen, A. *J. Am. Chem. Soc.* **1997**, *119*, 6048.
- (30) Lin, M.; Hogan, T. E.; Sen, A. *J. Am. Chem. Soc.* **1996**, *118*, 4574.
- (31) Gunnoe, T. B. In *Physical Inorganic Chemistry: Reactions, Processes, and Applications*; Bakac, A., Ed.; John Wiley and Sons: Hoboken, NJ, 2010, p 495.
- (32) Hartwig, J. F. *Organotransition Metal Chemistry From Bonding to Catalysis*; University Science Books: Mill Valley, CA, 2010.
- (33) Hashiguchi, B. G.; Bischof, S. M.; Konnick, M. M.; Periana, R. A. *Accounts Chem. Res.* **2012**, *45*, 885.
- (34) Conley, B. L.; Tenn, W. J.; Young, K. J. H.; Ganesh, S. K.; Meier, S. K.; Ziatdinov, V. R.; Mironov, O.; Oxgaard, J.; Gonzales, J.; Goddard, W. A.; Periana, R. A. *J. Mol. Catal. A-Chem.* **2006**, *251*, 8.
- (35) Crabtree, R. H. *The Organometallic Chemistry of the Transition Metals*; 4th ed.; John Wiley and Sons: Hoboken, NJ, 2005.
- (36) Pospech, J.; Fleischer, I.; Franke, R.; Buchholz, S.; Beller, M. *Angew. Chem.-Int. Edit.* **2013**, *52*, 2852.

- (37) Periana, R. A.; Taube, D. J.; Evitt, E. R.; Löffler, D. G.; Wentreck, P. R.; Voss, G.; Masuda, T. *Science* **1993**, *259*, 340.
- (38) Figg, T. M.; Webb, J. R.; Cundari, T. R.; Gunnoe, T. B. *J. Am. Chem. Soc.* **2012**, *134*, 2332.
- (39) Lin, M.; Shen, C.; Garcia-Zayas, E. A.; Sen, A. *J. Am. Chem. Soc.* **2001**, *123*, 1000.
- (40) Siegbahn, P. E. M.; Crabtree, R. H. *J. Am. Chem. Soc.* **1996**, *118*, 4442.
- (41) Tijm, P. J. A.; Waller, F. J.; Brown, D. M. *Appl. Catal. A-Gen.* **2001**, *221*, 275.
- (42) Golisz, S. R.; Gunnoe, T. B.; Goddard, W. A.; Groves, J. T.; Periana, R. A. *Catal. Lett.* **2011**, *141*, 213.
- (43) Gunnoe, T. B. *Eur. J. Inorg. Chem.* **2007**, 1185.
- (44) Ess, D. H.; Gunnoe, T. B.; Cundari, T. R.; Goddard, W. A.; Periana, R. A. *Organometallics* **2010**, *29*, 6801.
- (45) Webb, J. R.; Burgess, S. A.; Cundari, T. R.; Gunnoe, T. B. *Dalton Trans.* **2013**, *42*, 16646.
- (46) Cummins, C. C.; Baxter, S. M.; Wolczanski, P. T. *J. Am. Chem. Soc.* **1988**, *110*, 8731.
- (47) Walsh, P. J.; Hollander, F. J.; Bergman, R. G. *J. Am. Chem. Soc.* **1988**, *110*, 8729.
- (48) Bennett, J. L.; Wolczanski, P. T. *J. Am. Chem. Soc.* **1994**, *116*, 2179.
- (49) Cundari, T. R.; Klinckman, T. R.; Wolczanski, P. T. *J. Am. Chem. Soc.* **2002**, *124*, 1481.
- (50) Wicker, B. F.; Fan, H.; Hickey, A. K.; Crestani, M. G.; Scott, J.; Pink, M.; Mindiola, D. J. *J. Am. Chem. Soc.* **2012**, *134*, 20081.
- (51) Conner, D.; Jayaprakash, K. N.; Cundari, T. R.; Gunnoe, T. B. *Organometallics* **2004**, *23*, 2724.

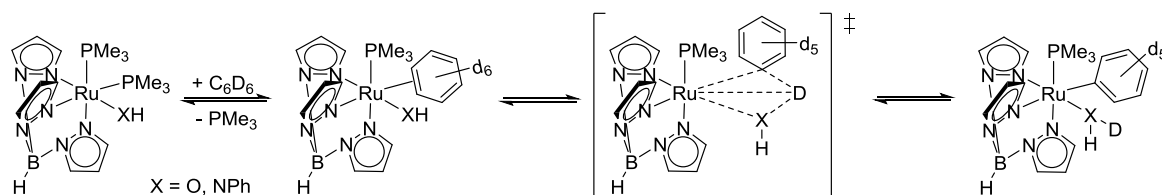
- (52) Tenn, W. J.; Young, K. J. H.; Oxgaard, J.; Nielsen, R. J.; Goddard, W. A.; Periana, R. A. *Organometallics* **2006**, *25*, 5173.
- (53) Tenn, W. J.; Young, K. J. H.; Bhalla, G.; Oxgaard, J.; Goddard, W. A.; Periana, R. A. *J. Am. Chem. Soc.* **2005**, *127*, 14172.
- (54) Hanson, S. K.; Heinekey, D. M.; Goldberg, K. I. *Organometallics* **2008**, *27*, 1454.
- (55) Kloek, S. M.; Heinekey, D. M.; Goldberg, K. L. *Angew. Chem.-Int. Edit.* **2007**, *46*, 4736.
- (56) Hashiguchi, B. G.; Young, K. J. H.; Yousufuddin, M.; Goddard, W. A.; Periana, R. A. *J. Am. Chem. Soc.* **2010**, *132*, 12542.
- (57) Feng, Y. L., M.; Barakat, K. A.; Cundari, T. R.; Gunnoe, T. B.; Petersen, J. L. *J. Am. Chem. Soc.* **2005**, *127*, 14174.
- (58) Feng, Y. L., M.; Foley, N. A.; Gunnoe, T. B.; Barakat, K. A.; Cundari, T. R.; Petersen, J. L. *J. Am. Chem. Soc.* **2006**, *128*, 7982.
- (59) Kubas, G. J. *Metal Dihydrogen and sigma-Bond Complexes Structure, Theory, and Reactivity*; Kluwer Academic/Plenum Publishers: New York, 2001.
- (60) Burgess, S. A.; Devarajan, D.; Bolano, T.; Ess, D. H.; Gunnoe, T. B.; Sabat, M.; Myers, W. H. *Inorg. Chem.* **2014**, *53*, 5328.
- (61) Fryzuk, M. D.; Montgomery, C. D.; Rettig, S. J. *Organometallics* **1991**, *10*, 467.
- (62) Fulmer, G. R.; Muller, R. P.; Kemp, R. A.; Goldberg, K. I. *J. Am. Chem. Soc.* **2009**, *131*, 1346.
- (63) Fulmer, G. R.; Herndon, A. N.; Kaminsky, W.; Kemp, R. A.; Goldberg, K. I. *J. Am. Chem. Soc.* **2011**, *133*, 17713.
- (64) Brown, S. N.; Mayer, J. M. *J. Am. Chem. Soc.* **1996**, *118*, 12119.
- (65) Carey, F. A. *Organic Chemistry*; 7th ed.; McGraw Hill: Boston, 2008.
- (66) Koo, K. H., G. L.; Rheingold, A. L. *Organometallics* **1995**, *14*, 456.

- (67) Mei, J. J.; Carsch, K. M.; Freitag, C. R.; Gunnoe, T. B.; Cundari, T. R. *J. Am. Chem. Soc.* **2013**, *135*, 424.
- (68) Mei, J. J.; Pardue, D. B.; Kalman, S. E.; Gunnoe, T. B.; Cundari, T. R.; Sabat, M. *Organometallics* **2014**, *33*, 5597.
- (69) Kalman, S. E.; Petit, A.; Gunnoe, T. B.; Ess, D. H.; Cundari, T. R.; Sabat, M. *Organometallics* **2013**, *32*, 1797.
- (70) Joslin, E. E.; Quillian, B.; Gunnoe, T. B.; Cundari, T. R.; Sabat, M.; Myers, W. *H. Inorg. Chem.* **2014**, *53*, 6270.

2 Design and Synthesis of Cationic Ru(II) Complexes for C–H and H₂ Bond Activation Using the Tetra(pyrazolyl)methane Ligand

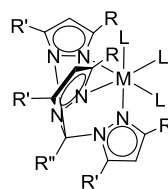
2.1 Introduction

A successful homogeneous transition metal catalyst for hydrocarbon functionalization must be able to activate C–H bonds. While there are several methods of transition metal-mediated C–H activation, 1,2-CH-addition—herein defined as the addition of a C–H bond across a metal-heteroatom bond—is the focus on the work described herein. As discussed in Chapter 1, our group has observed the 1,2-addition of C₆D₆ with the complex TpRu(PMe₃)₂(X) (Tp = hydrido(trispyrazolyl)borate, X = OH or NPh) between 80 °C and 130 °C (Scheme 1).¹ Both the dissociation of PMe₃ from TpRu(PMe₃)₂(OH) and the C–H activation step are calculated to be thermodynamically unfavorable. Thus, the design of a Ru(II) complex with features overcoming these drawbacks was desired. By replacing a halide ligand with a non-coordinating anion to give a five-coordinate cationic Ru(II) complex or six-coordinate Ru(II) with a labile ligand, it was hypothesized that 1,2-CH-addition would be more favorable, especially as a cationic Ru(II) species might facilitate C–H coordination and activation toward intramolecular H⁺ transfer to a heteroatom ligand, X, by making the metal center more electrophilic. That is, an electrophilic metal center would draw electron density away from the coordinated C–H σ-bond, giving H a partial positive charge and making it easier for the electron lone pair on the heteroatom to abstract the proton.



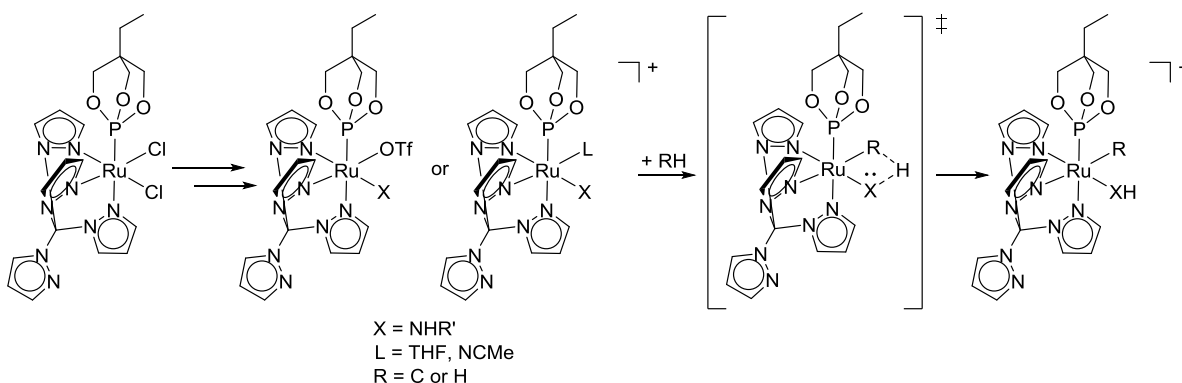
Scheme 1. 1,2-Addition of C₆D₆ to TpRu(PMe₃)₂(XH) (X = O, NPh).¹

Tris- and tetra(pyrazolyl)alkanes often coordinate in κ^3 mode by binding facially to the metal center.² Although they are both nearly isosteric and isoelectronic with formally anionic poly(pyrazolyl)borates, such as Tp,^{3,4} poly(pyrazolyl)alkanes are charge neutral and therefore less donating than corresponding poly(pyrazolyl)borates.⁵ Thus, use of this ligand class could afford a metal complex that exhibits a greater disposition toward performing C–H activation by enhancing metal center electrophilicity, in turn promoting binding of hydrocarbon substrates to the metal and activating η^2 -coordinated C–H bonds toward 1,2-CH-addition across a metal–X bond.^{2,5} In addition, these ligands are capable of being substituted at the 3- and 5-positions of the pyrazolyl rings with substituents such as methyl, phenyl, isopropyl, and *tert*-butyl groups,^{4,6-8} enabling steric and electronic modification of the scorpionate ligand and examination of the subsequent effect on C–H activation (Figure 1). The backbone carbon of tris(pyrazolyl)alkanes can also be functionalized in some cases with alcohol, aldehyde, ester,^{4,6,7} methyl, ether, silyl,⁹ and sulfonate (SO_3^-) groups (Figure 1).¹⁰ Also, a metal-coordinated tris(pyrazolyl)alkane has even been observed with a naked carbanion backbone.¹¹ The study of poly(pyrazolyl)alkanes as ligands is not as well developed as for the poly(pyrazolyl)borate variants due in part to synthetic challenges (including moderate to low yields and multi-step isolation procedures); nevertheless, progress is being made towards greater use of this class of ligand,^{3,6,9} particularly for their use in the synthesis of Cu(II)-selective membrane electrodes,¹² Re complexes for diagnostic purposes,⁷ and as scaffold ligands for successful Ru(II) ethylene hydrophenylation catalysts.¹³ In fact, the use of tris(5-methylpyrazolyl)methane ($\text{HC}(\text{pz}^5)_3$) in $\{[\text{HC}(\text{pz}^5)_3]\text{Ru}[\text{P}(\text{OCH}_2)_3\text{CEt}](\text{NCMe})(\text{Ph})\}[\text{BAr}'_4]$ ($\text{BAr}'_4 = \text{tetrakis}[3,5\text{-bis}(\text{trifluoromethyl})\text{phenyl}]\text{borate}$) for ethylene hydrophenylation exhibits greater longevity and thermal stability compared to the Tp variant of the catalyst.¹³ Given the success of poly(pyrazolyl)alkane-ligated metal complexes in the areas discussed above, these complexes were targeted for 1,2-CH-addition across metal–heteroatom bonds (Scheme 2).



R and R' = alkyl or aryl
 R'' = alkyl, alcohol,
 aldehyde, ester, ether,
 silyl, SO_3^-

Figure 1. A poly(pyrazolyl)alkane ligand, demonstrating facial coordination to a generic metal center.



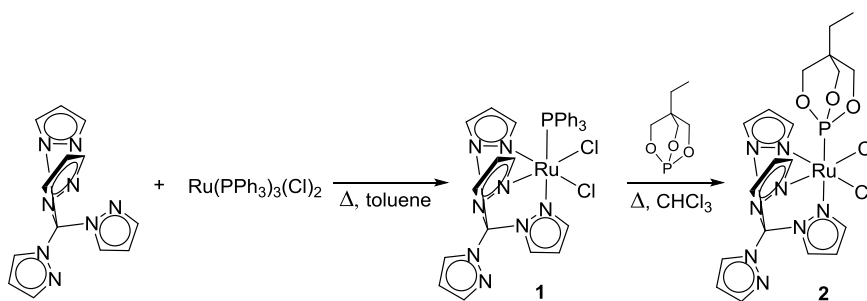
Scheme 2. Synthetic strategy for electrophilic $[\text{C}(\text{pz})_4]\text{Ru}(\text{II})$ -amido complexes and 1,2-addition of C–H or H–H bonds.

2.2 General Synthetic Details

Initial synthetic efforts focused on the use of tetra(pyrazolyl)methane ($\text{C}(\text{pz})_4$) to prepare Ru(II) complexes for 1,2-CH-addition (Scheme 2). The use of various bases (NaH, LiNHPh, etc.) features in the synthetic strategies towards a Ru–heteroatom complex (discussed below); the fourth pyrazolyl group on the quaternary carbon acts as a potential “protecting group” for the ligand, as we hypothesized that an acidic C–H bond (e.g., the methine proton of tris(pyrazolyl)methane) could be incompatible; additionally, the fourth pyrazolyl ring was also thought to possibly promote solubility in common organic solvents.

The synthesis of $[\text{C}(\text{pz})_4]\text{Ru}(\text{PPh}_3)(\text{Cl})_2$ (**1**) (82% yield) had been optimized previously and involved refluxing $\text{C}(\text{pz})_4$ and $\text{Ru}(\text{PPh}_3)_3(\text{Cl})_2$ in toluene (Scheme 3).⁵ In the ^1H NMR

spectrum in CDCl₃, nine pyrazolyl resonances are observed along with a phenyl resonance (triplet) for PPh₃ (7.82 ppm) with coincidental overlap with the CDCl₃ solvent peak partially obscuring the other phenyl resonances (Figure 2). Although there are twelve protons on C(pz)₄, only nine resonances are observed by ¹H NMR spectroscopy due to the C_s symmetry of complex **1**, making the protons in the 3-, 4-, and 5-positions of the pyrazolyl rings *trans* to the chlorides equivalent. Ligand exchange of P(OCH₂)₃CEt (4-ethyl-2,6,7-trioxa-1-phosphabicyclo[2.2.2]octane) for the PPh₃ ligand of complex **1** afforded [C(pz)₄Ru[P(OCH₂)₃CEt](Cl)₂] (**2**) in 88% yield (Scheme 3).⁵ For complex **2**, nine pyrazolyl resonances are visible by ¹H NMR spectroscopy in DCM-*d*₂ and resonances for P(OCH₂)₃CEt are observed at 4.38 ppm (d, ³J_{PH} = 5 Hz, methylene protons), 1.28 ppm (q, ³J_{HH} = 8 Hz, -CH₂CH₃) and 0.86 ppm (t, ³J_{HH} = 8 Hz, -CH₂CH₃) (Figure 3).



Scheme 3. Synthesis of [C(pz)₄Ru(PPh₃)(Cl)₂] (**1**) and [C(pz)₄Ru[P(OCH₂)₃CEt](Cl)₂] (**2**).

P(OCH₂)₃CEt was chosen as an ancillary ligand because, as a phosphite, it is less electron donating than a phosphine, contributing to the overall electrophilicity of the metal center. Also, the “tied-back” geometry of the phosphite should inhibit intramolecular C–H activation; for example, PPh₃ bound to coordinatively unsaturated Ru(Cl)₂(PPh₃)₃ is known to undergo an intramolecular agostic interaction between an *ortho* C–H bond of a phenyl ring and the metal center.¹⁴

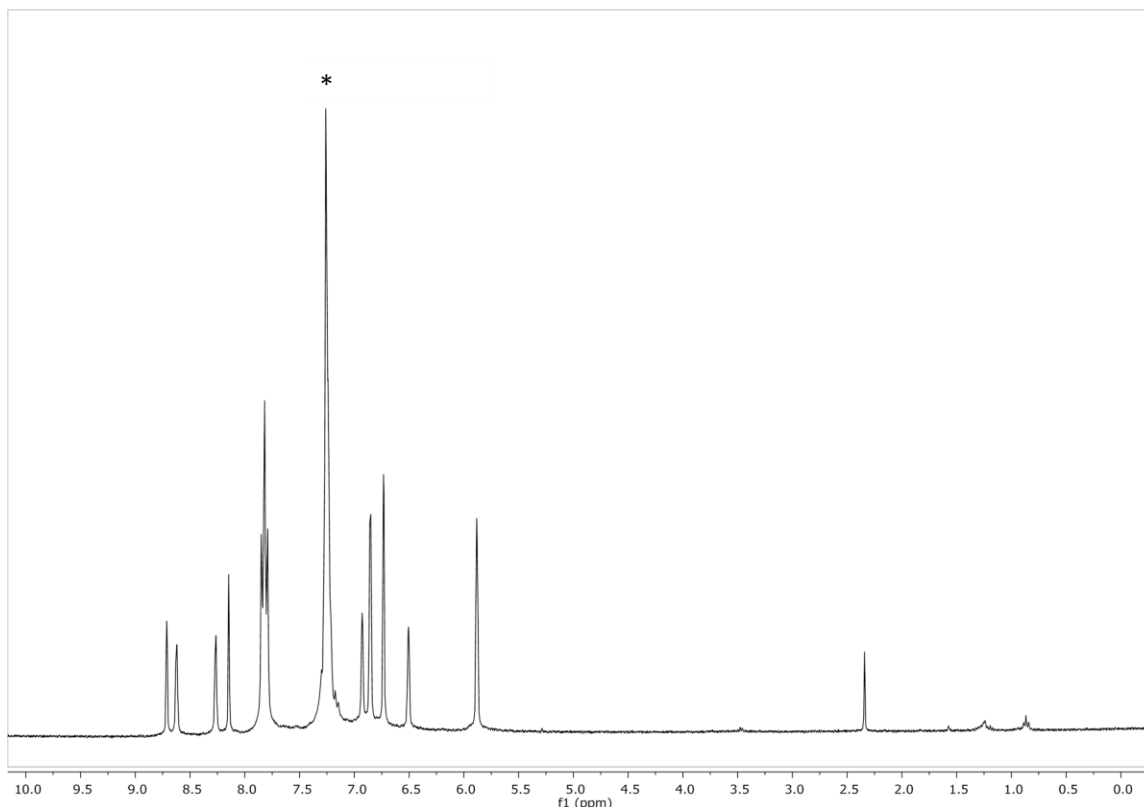


Figure 2. ^1H NMR (300 MHz, CDCl_3) spectrum of $[\text{C}(\text{pz})_4]\text{Ru}(\text{PPh}_3)(\text{Cl})_2$ (**1**). Solvent resonance denoted by *.

Upon reaction of **2** with TlOTf (OTf = trifluoromethanesulfonate, triflate) in dichloromethane (DCM)/MeOH, the dimer $\{[\text{C}(\text{pz})_4]\text{Ru}[\text{P}(\text{OCH}_2)_3\text{CEt}](\mu\text{-Cl})_2\}[\text{OTf}]_2$ (**3**) is formed in 64% isolated yield (Scheme 4); nine pyrazolyl resonances are observed by ^1H NMR spectroscopy with resonances due to $\text{P}(\text{OCH}_2)_3\text{CEt}$ at 4.53 ppm (d, $^3J_{\text{PH}} = 4$ Hz), 1.37 ppm (q, $^3J_{\text{HH}} = 8$ Hz), and 0.91 ppm (t, $^3J_{\text{HH}} = 8$ Hz) by in $\text{DCM}-d_2$ (Figure 4). While complexes **2** and **3** share common spectral features (nine pyrazolyl resonances and $\text{P}(\text{OCH}_2)_3\text{CEt}$ resonances), there is a distinct difference in chemical shift of the pyrazolyl resonances of **2** and **3**; furthermore, the ^{31}P NMR spectra of the two complexes are different (127.6 ppm for **2** and 128.9 ppm for **3**). Previous work has demonstrated that the addition of trimethylphosphine to a DCM solution of **3** results in a complex with coordinated phosphite and phosphine ligands, as evidenced by two doublets ($^2J_{\text{PP}} = 594$ Hz) in the ^{31}P NMR spectrum; this observation indicates that complex **3** is a

dimer in equilibrium with its monomer.⁵ The addition of various anilines to a suspension of complex **3** in THF at 90 °C produces complexes of the type $\{[C(pz)_4]Ru[P(OCH_2)_3CEt](Cl)(NH_2Ar)][OTf]\}$ (Ar = 2,6-di(isopropyl)phenyl, 3,5-di(*tert*-butyl)phenyl, 4-chlorophenyl, 4-nitrophenyl) (Scheme 4).⁵

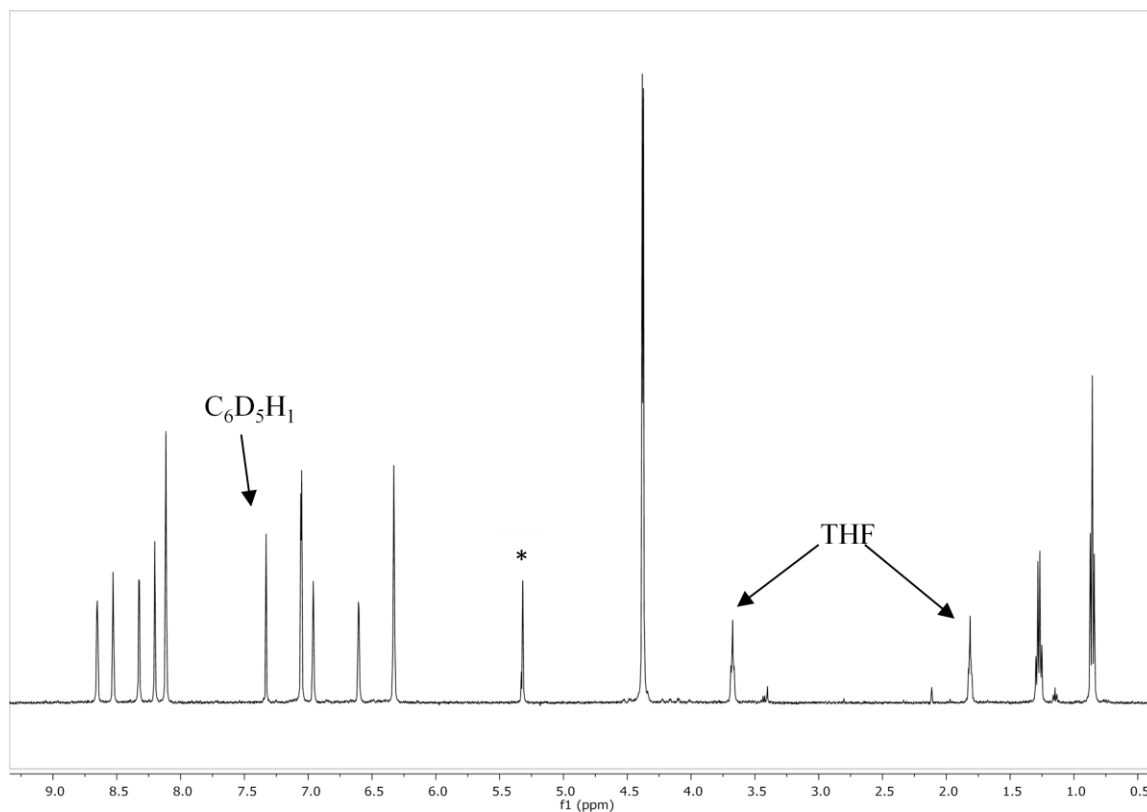
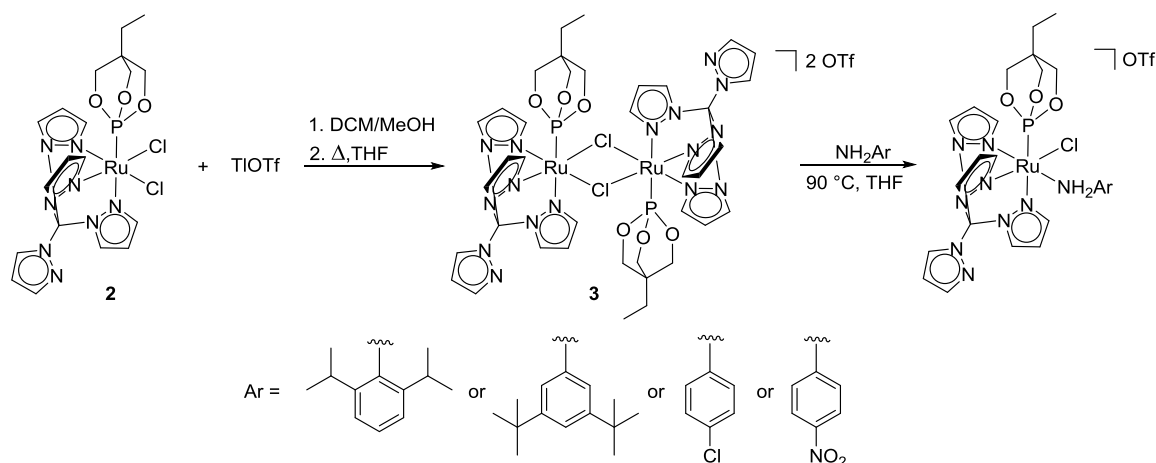


Figure 3. 1H NMR (500 MHz, CD_2Cl_2) spectrum of $[C(pz)_4]Ru[P(OCH_2)_3CEt](Cl)_2$ (**2**). Solvent resonance denoted by *.



Scheme 4. Synthesis of $\{[C(pz)_4]Ru[P(OCH_2)_3CEt](Cl)]_2[OTf]_2$ (**3**) and $\{[C(pz)_4]Ru[P(OCH_2)_3CEt](Cl)(NH_2Ar)]\}[OTf]$ (Ar = 2,6-di(isopropyl)phenyl, 3,5-di(*tert*-butyl)phenyl, 4-chlorophenyl, 4-nitrophenyl).

Two challenges remained before the desired $\{[C(pz)_4]Ru[P(OCH_2)_3CEt](L)(NHAr)]^+$ or $[C(pz)_4]Ru[P(OCH_2)_3CEt](OTf)(NHAr)$ complexes could be obtained: 1) deprotonation of the aniline ligand and 2) exchange of the chloride for a more labile ligand. Previous work suggested that deprotonation of the complex $\{[C(pz)_4]Ru[P(OCH_2)_3CEt](NH_2Ph)(Cl)]\}[OTf]$ led to an unstable species, presumably $[C(pz)_4]Ru[P(OCH_2)_3CEt](NHPH)(Cl)$.⁵ Thus, we hypothesized that substituted aniline ligands may improve the stability of the desired Ru–anilido complexes (produced by the same synthetic route as the parent complex) by modulating the ligand's (and thus the complex's) electronic properties. Previous work had shown that the putative complex $[C(pz)_4]Ru[P(OCH_2)_3CEt](NHPH)(Cl)$ underwent facile protonation from undesired (and unidentified) sources (e.g., *not* by 1,2-CH-addition of a substrate) to revert to $\{[C(pz)_4]Ru[P(OCH_2)_3CEt](NH_2Ph)(Cl)]\}^+$.⁵ Thus, installing a more electron-withdrawing group on the anilido ligand, such as chloride, was hypothesized to decrease the basicity of the nitrogen lone pair and subsequently discourage facile re-protonation.

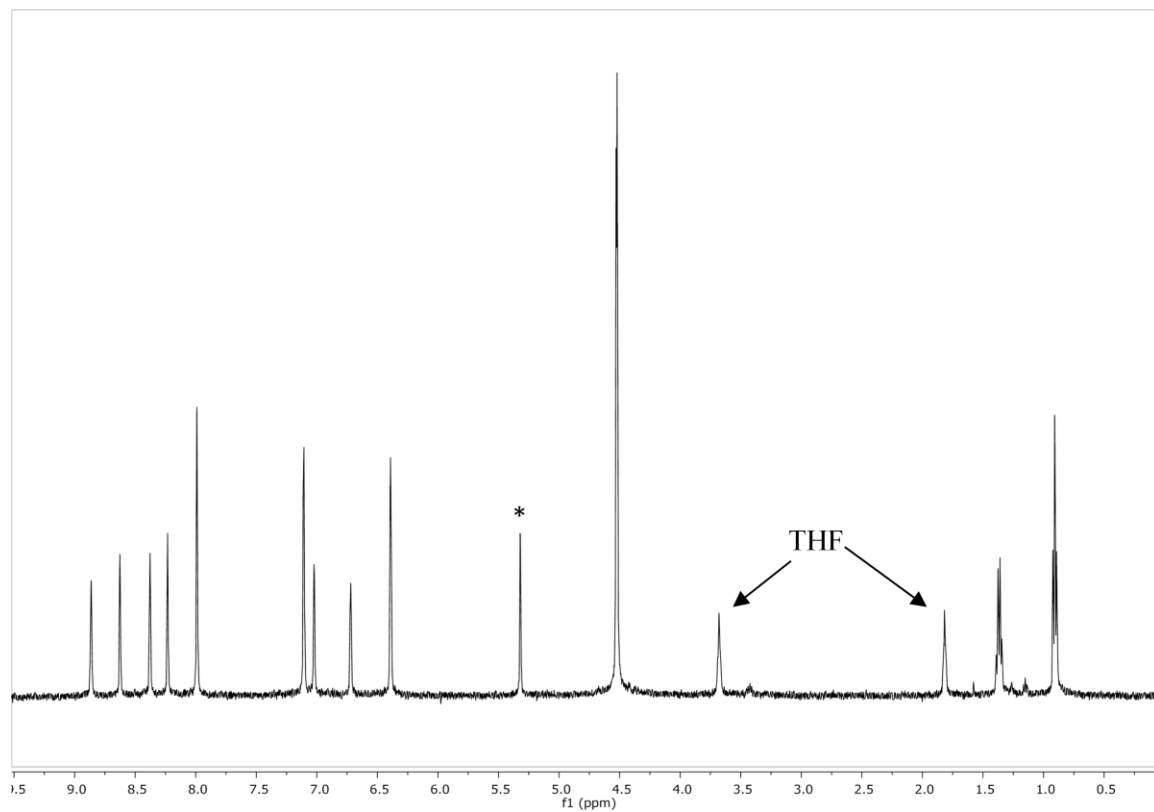


Figure 4. ^1H NMR (500 MHz, CD_2Cl_2) spectrum of $\{[\text{C}(\text{pz})_4\text{Ru}[\text{P}(\text{OCH}_2)_3\text{CEt}](\mu\text{-Cl})_2][\text{OTf}]_2\}$ (**3**). Solvent resonance denoted by *.

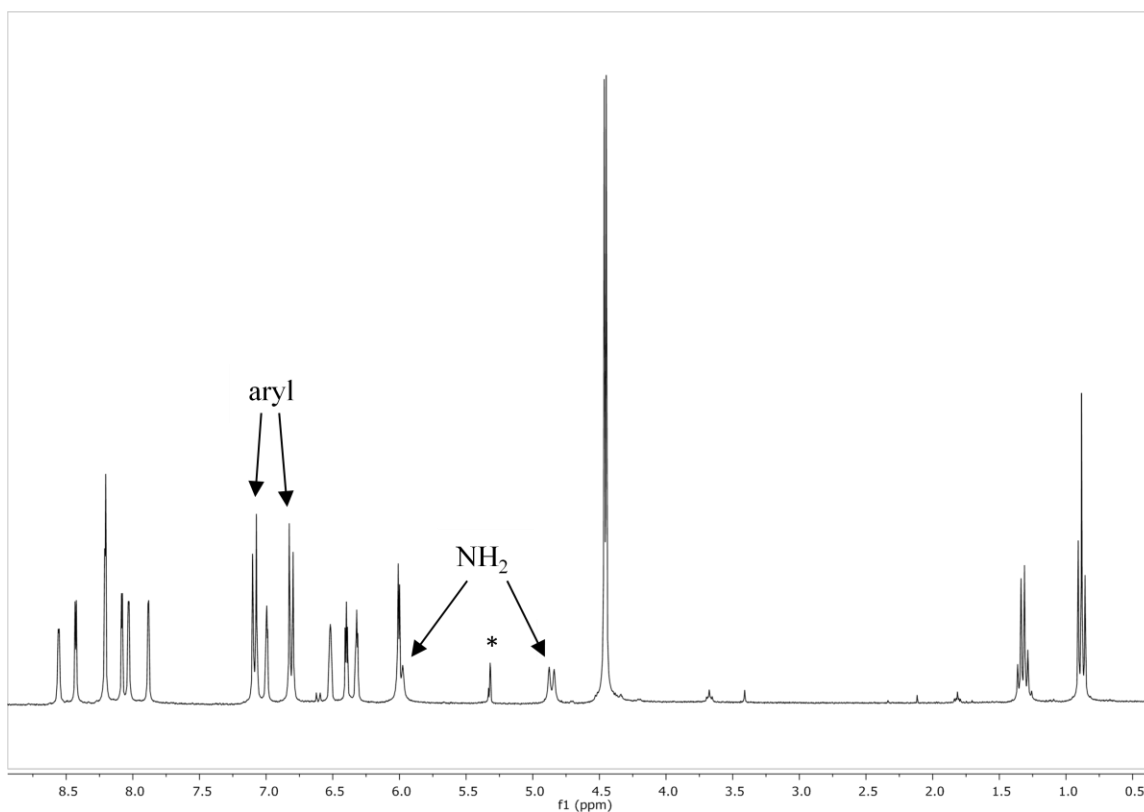


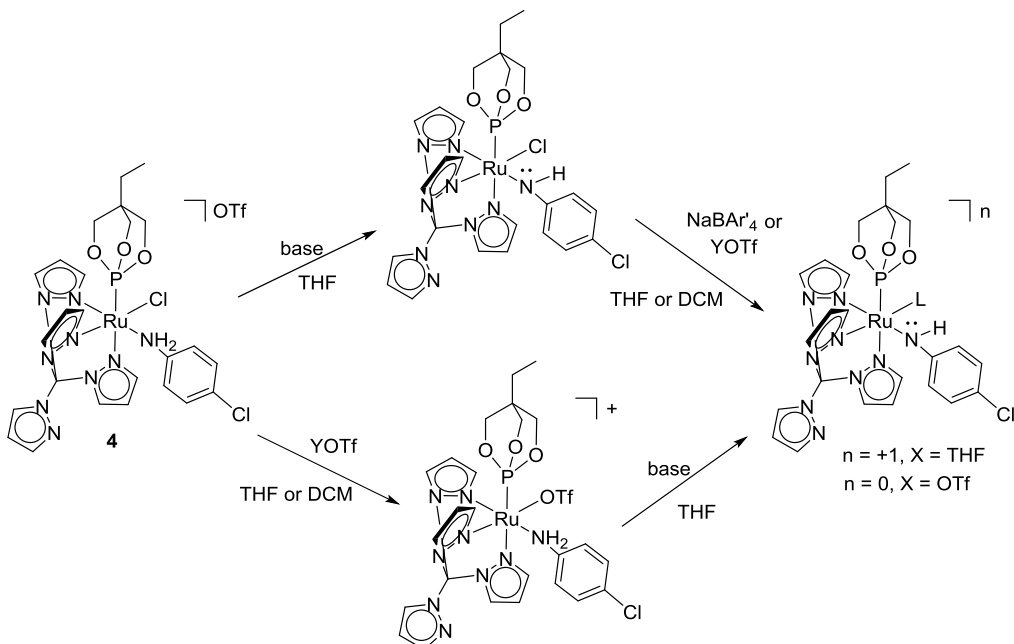
Figure 5. ^1H NMR (300 MHz, CD_2Cl_2) spectrum of $\{[\text{C}(\text{pz})_4]\text{Ru}[\text{P}(\text{OCH}_2)_3\text{CEt}](4\text{-chloroaniline})(\text{Cl})\}[\text{OTf}]$ (**4**). Solvent resonance denoted by *.

2.3 Synthesis of $\{[\text{C}(\text{pz})_4]\text{Ru}[\text{P}(\text{OCH}_2)_3\text{CEt}](4\text{-chloroanilido})(\text{L})\}^n$ ($\text{L} = \text{OTf}$ or THF , $n = 0$ or $+1$)

The complex $\{[\text{C}(\text{pz})_4]\text{Ru}[\text{P}(\text{OCH}_2)_3\text{CEt}](4\text{-chloroaniline})(\text{Cl})\}[\text{OTf}]$ (**4**) was synthesized in 67% isolated yield by the route described in Section 2.2 for Ru–aniline complexes; twelve pyrazolyl resonances, consistent with an asymmetric complex, are observed by ^1H NMR spectroscopy in CD_2Cl_2 (Figure 5). Phenyl resonances for coordinated 4-chloroaniline are observed at 7.09 and 6.81 ppm (doublets, protons *meta* and *ortho* to the NH_2); NH_2 resonances were observed at 5.98 (d, overlapping with pyrazolyl resonance at 6.00 ppm) and 4.86 ppm (d, $^2J_{\text{HH}} = 11$ Hz).

Multiple attempts were made to synthesize precursors to $\{[\text{C}(\text{pz})_4]\text{Ru}[\text{P}(\text{OCH}_2)_3\text{CEt}](4\text{-chloroanilido})(\text{L})\}^n$ ($\text{L} = \text{labile ligand}$, $n = 0$ or $+1$). Two general strategies were employed

(Scheme 5): 1) abstraction of the chloride and subsequent coordination of a labile ligand followed by deprotonation of the anilido, and 2) deprotonation of the anilido ligand followed by coordination of a labile ligand.



Scheme 5. Strategies for synthesis of $\{[C(pz)_4]Ru[P(OCH_2)_3Cet](4\text{-chloroanilido})(L)\}^n$ ($n = +1$, $X = THF$ or $n = 0$, $X = OTf$; $Y = Na, Ag, Tl, TMS$).

2.3.1 Initial Halide Abstraction Followed by Deprotonation

Reactions were performed to abstract chloride from **4** to produce $\{[C(pz)_4]Ru[P(OCH_2)_3Cet](4\text{-chloroanilino})(OTf)\}[OTf]$ (**5**). While the reaction of **4** with TlOTf in THF was not successful (no reaction occurred) even upon heating from 70-90 °C, AgCl precipitate was visible in the reaction of **4** with AgOTf in THF upon heating at 70 °C. Conversion to desired product occurred after ~18 h at 70 °C. The reaction of **4** with TMSOTf in DCM at 70 °C after ~5 h also gave the desired product, as evidenced by conversion to a new complex and formation of TMSCl, both observed by 1H NMR spectroscopy. The BAR'_4 variants of these complexes could also be made as follows: a counterion exchange was performed with **4** and $NaBAR'_4$ in DCM to produce $\{[C(pz)_4]Ru[P(OCH_2)_3Cet](4\text{-chloroanilino})(Cl)\}[BAR'_4]$ (**4'**).

Complex **4'** was reacted with AgOTf in THF; heating at 70 °C produced a white precipitate (AgCl). The desired product, $[[C(pz)_4]Ru[P(OCH_2)_3CEt](4\text{-chloroaniline})(OTf)][Bar'_4]$ (**5'**), was formed after ~18 h at 70 °C, although a small amount of unidentified side product was also formed. The reaction of **4'** with TMSOTf in DCM at 70 °C ~18 h also produced **5'**; this appeared to be a cleaner reaction than that of **4'** with AgOTf, as no obvious side product was formed. Unfortunately, attempting to make $[C(pz)_4]Ru[P(OCH_2)_3CEt](4\text{-chloroanilido})(OTf)$ (**6**) by deprotonating **5** with either NaH or NaHMDS led to decomposition; as this most likely would also have occurred with **5'**, deprotonation of **5'** was not attempted. Thus, synthesizing $[C(pz)_4]Ru[P(OCH_2)_3CEt](4\text{-chloroanilido})(OTf)$ via this route was deemed unsuccessful.

2.3.2 Initial Deprotonation Followed by Halide Abstraction

Deprotonation of **4** was attempted using NaHMDS (sodium hexamethyldisilazide) ($pK_a = 26$) in THF- d_8 at -78 °C; the reaction resulted in two products in roughly 2:1 ratio, and after ~24 h decomposition was evident as free 4-chloroaniline was observed in solution by 1H NMR spectroscopy.¹⁵ Although it appeared that the major product from the deprotonation of **4** with NaHMDS was putative $[C(pz)_4]Ru[P(OCH_2)_3CEt](Cl)(4\text{-chloroanilido})$ (**7**), the minor product was not identified. The reaction of **4** with LDA (lithium di(isopropyl)amide) (di(isopropyl)amine $pK_a = 40$)¹⁶ in THF- d_8 at -78 °C was performed; this reaction resulted in one new complex, the putative complex **7**, that converted to a different complex overnight that was not identified or isolated. Deprotonation of **4** with NaH ($pK_a = 35$)¹⁷ in THF- d_8 at room temperature resulted in the same initial product as the deprotonation of **4** with LDA and converted to the same unidentified complex overnight as the reaction with LDA (Scheme 6). The reaction of **4** with NaH gave **7** in 96% yield by 1H NMR spectroscopy; twelve pyrazolyl resonances were visible in THF- d_8 (Figure 6). Phenyl resonances for the anilido ligand appeared as doublets at 6.26 ppm ($^3J_{HH} = 9$ Hz) and 5.65 ppm ($^3J_{HH} = 8$ Hz); the NH resonance was observed at 2.42 ppm (br s, integrating for 1 H).

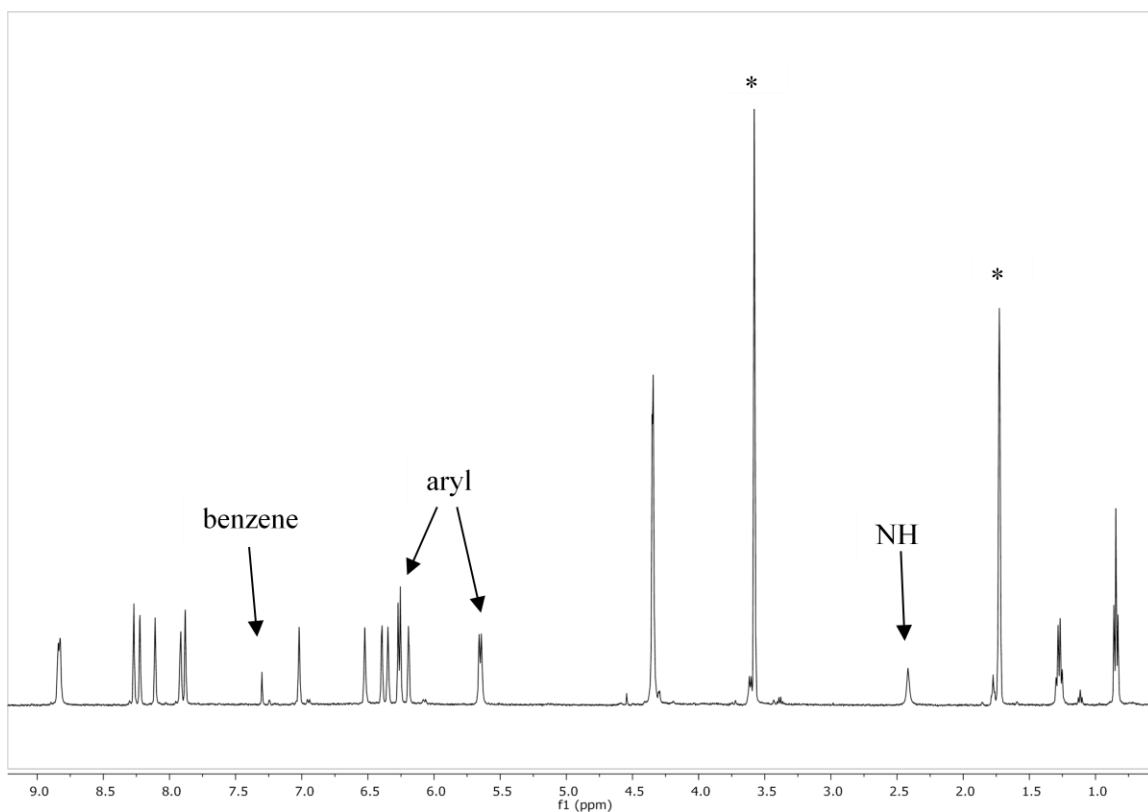
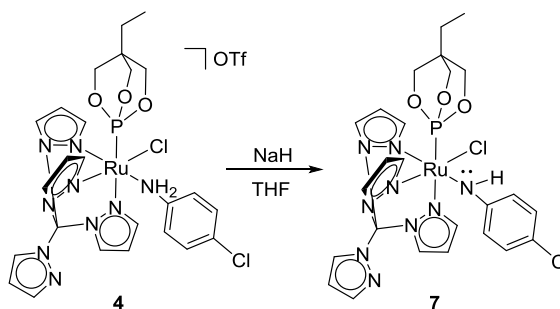


Figure 6. ^1H NMR (500 MHz) spectrum of $[\text{C}(\text{pz})_4]\text{Ru}[\text{P}(\text{OCH}_2)_3\text{CEt}](4\text{-chloroanilido})(\text{Cl})$ (**7**) in $\text{THF-}d_8$. Solvent resonances denoted by *.

It would appear from these results that stronger bases such as LDA and NaH are necessary for clean deprotonation of **4**. Moving forward, complex **7** was synthesized using NaH due to the ease of removing excess insoluble NaH from the reaction mixture versus attempting to remove homogeneous impurities introduced by LDA.

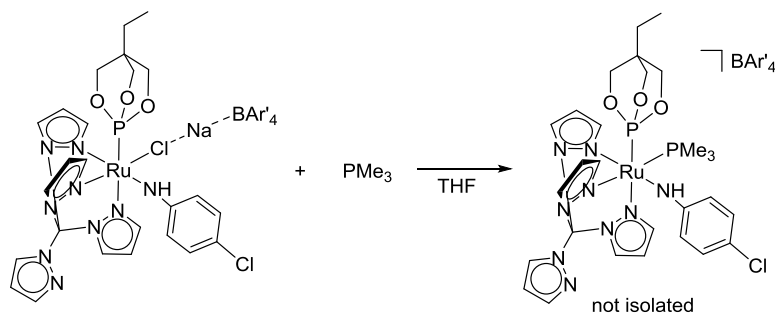


Scheme 6. Synthesis of $[\text{C}(\text{pz})_4]\text{Ru}[\text{P}(\text{OCH}_2)_3\text{CEt}](\text{Cl})(4\text{-chloroanilido})$ (**7**).

Once synthesized, efforts were made to abstract the chloride from **7** using NaBAR'₄, NaOTf, AgOTf, and TlOTf in THF, and TMSOTf (TMS = trimethylsilyl) in DCM. Reactions of **7** with NaBAR'₄ and the various metal triflate reagents at room temperature produced dramatic color changes; while **7** is red in solution, addition of TMSOTf and TlOTf turned the reaction solution yellow, adding AgOTf turned it blue, NaOTf turned it orange, and NaBAR'₄ turned the solution a golden yellow. The color changes perhaps resulted from some sort of interaction between the cations of the salts and **7**, and from protonation of the anilido ligand in the case of TMSOTf ($\{[C(pz_4)]Ru[P(OCH_2)_3CEt](X)(4\text{-chloroaniline})\}^+$ complexes are typically yellow). The reactions involving TMSOTf and AgOTf unfortunately protonated the anilido ligand to form coordinated 4-chloroaniline at room temperature as evident by NH₂ resonances observed by ¹H NMR spectroscopy. Heating the reactions involving NaBAR'₄, NaOTf and TlOTf at 70-90 °C to initiate halide abstraction also resulted in protonation to form the 4-chloroaniline ligand. There was evidence for halide abstraction at room temperature in the reaction of **7** with TlOTf, due to formation of a white precipitate (presumably TlCl), and in the reaction of **7** with TMSOTf at room temperature, as TMSCl was observed by ¹H NMR spectroscopy. NaBAR'₄, NaOTf and AgOTf did not produce noticeable precipitates, indicating the possibility that adducts between the Ru-Cl and the respective salts were forming rather than the complexes undergoing the desired chloride abstraction.

Despite the initially unsuccessful attempts to synthesize $[C(pz_4)]Ru[P(OCH_2)_3CEt](4\text{-chloroanilido})(OTf)$ (with the apparent exception of the reaction with TlOTf, to be discussed in Section 2.4), the reaction of **7** with NaBAR'₄ in THF was analyzed further. It was hypothesized that adding a reactive substrate such as a phosphine to the solution might drive a putative $\{[C(pz_4)]Ru[P(OCH_2)_3CEt](Cl)(4\text{-chloroanilido})\}\text{-NaBAR}'_4$ adduct to precipitate NaCl at room temperature and allow coordination of the phosphine (Scheme 7). After the addition of NaBAR'₄ to **7** at room temperature, ~1 equivalent of PMe₃ (relative to Ru) was added in an attempt to make $\{[C(pz_4)]Ru[P(OCH_2)_3CEt](PMe_3)(4\text{-chloroanilido})\}[BAR'_4]$ —a reaction *did* occur to produce

eight new resonances in the ^{31}P NMR spectrum—121.6, 118.0, 116.7, and 113.4 ppm in the phosphite region and -0.05, -1.90, -4.91, -6.46 ppm in the phosphine region. PMe_3 was added to a room temperature solution of **7** and NaOTf ; this reaction resulted in ^{31}P NMR resonances at 117.3, 112.7, -0.55, and -5.09 ppm. Some decomposition was also evident in this reaction, as free 4-chloroaniline was observed by ^1H NMR spectroscopy. Thus, the reactions with PMe_3 did not appear to give the desired result of producing $\{[\text{C}(\text{pz})_4]\text{Ru}[\text{P}(\text{OCH}_2)_3\text{CEt}](\text{PMe}_3)(4\text{-chloroanilido})\}[\text{BAr}'_4]$ and NaCl . Reactions involving proligands other than PMe_3 gave varying results. The reaction of the complex **7** with NaBAr'_4 in $\text{THF-}d_8$ with $^t\text{BuNC}$ at room temperature and reactions with pyridine and $\text{P}(\text{OCH}_2)_3\text{CEt}$ at 70°C resulted in several intractable products. However, dissolving **7** in CH_3CN with NaBAr'_4 resulted in the formation of two species in a 3:1 ratio, with the major species appearing to possibly be $\{[\text{C}(\text{pz})_4]\text{Ru}[\text{P}(\text{OCH}_2)_3\text{CEt}](\text{NCMe})(4\text{-chloroanilido})\}[\text{BAr}'_4]$, as a coordinated acetonitrile resonance at 2.45 ppm was observed by ^1H NMR spectroscopy in $\text{THF-}d_8$.



Scheme 7. Putative reaction of PMe_3 with $\text{Ru-Cl-NaBAr}'_4$ adduct.

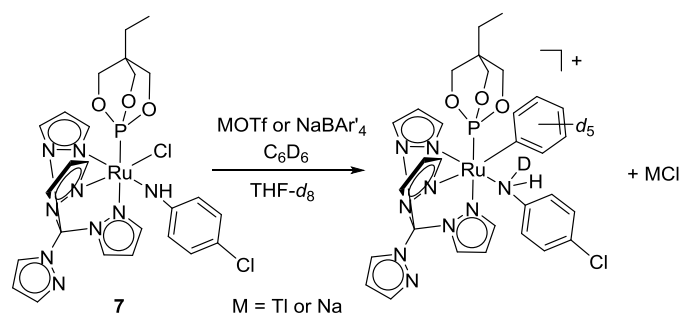
The reactions involving **7**, NaBAr'_4 , and acetonitrile, $^t\text{BuNC}$ or PMe_3 appear to support the hypothesis that an empty coordination site on complex **7** could be generated *in situ* in the presence of a halide abstractor and proligand.

2.4 Attempted *in situ* 1,2-Addition Experiments with C–H and H₂ Bonds

As the isolation of $[\text{C}(\text{pz})_4]\text{Ru}[\text{P}(\text{OCH}_2)_3\text{CEt}](\text{X})(4\text{-chloroanilido})$ complexes appeared to be difficult due to the ease of protonating the 4-chloroanilido ligand, *in situ* 1,2-addition

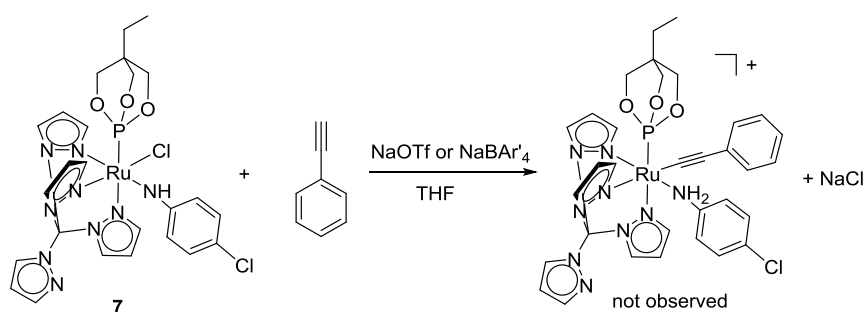
experiments were attempted. Deuterated benzene (C_6D_6) was added to the reaction of TlOTf with **7** and heated at 50 and 70 °C, resulting in the appearance of coordinated aniline NH_2 resonances by 1H NMR spectroscopy (Scheme 8). Nevertheless, deuterium incorporation was not evident (suggesting that there was no reaction between the putative $[C(pz)_4]Ru[P(OCH_2)_3CEt](OTf)(4\text{-chloroanilido})$ and C_6D_6), and there was no change in chemical shift for any of the pyrazolyl resonances before and after heating.

NaOTf was added to a solution of complex **7** in the presence of deuterated benzene in THF- d_8 in an attempt to promote a 1,2-addition reaction of C_6D_6 with putative $[C(pz)_4]Ru[P(OCH_2)_3CEt](OTf)(4\text{-chloroanilido})$ (see discussion in Section 2.3.1) (Scheme 8). Observing the reaction mixture over time at 70 °C by 1H NMR spectroscopy revealed an aniline NH_2 doublet growing in (the second NH_2 doublet was obscured by coincidental overlap); however, no change in chemical shift was observed for any of the other resonances, and the expected products of 1,2-CH-addition— $[C(pz)_4]Ru[P(OCH_2)_3CEt](OTf)(Ph-d_5)$ and 4-chloroaniline- d_1 were not observed by 1H NMR spectroscopy. The reaction with protio-benzene was similarly unsuccessful. Adding $NaBAR'_4$ to **7** in THF- d_8 and then adding C_6D_6 and heating at 70 °C revealed aniline NH_2 doublets growing in by 1H NMR spectroscopy (Scheme 8); however, as with the reaction involving NaOTf, none of the other resonances changed, and no deuterium incorporation was observed (indicating that no reaction occurred between putative $\{[C(pz)_4]Ru[P(OCH_2)_3CEt](THF)(4\text{-chloroanilido})\}[BAR'_4]$ and C_6D_6).



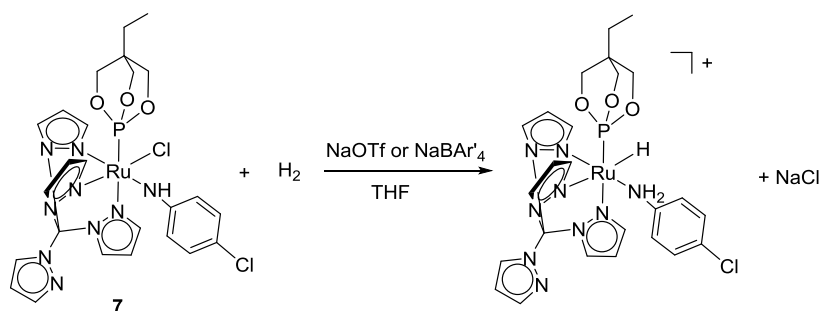
Scheme 8. Attempted reactions of $C(pz)_4Ru[P(OCH_2)_3CEt](Cl)(4\text{-chloroanilido})$ (**7**) with halide abstractors and C_6D_6 .

Phenylacetylene was then chosen as an alternate substrate for 1,2-CH-addition; although the terminal alkyne C–H has a BDE of 125 kcal/mol, the acidity of this bond ($\text{pK}_a = 25$)¹⁸ was thought to make activation more facile than for the C–H bonds of benzene (112 kcal/mol, $\text{pK}_a = 43$).^{16,18} Adding phenylacetylene to **7** in the presence of NaOTf and heating at 70 °C resulted in the appearance of 4-chloroaniline NH₂ doublets in the ¹H NMR spectrum, but once again, no changes to any of the other resonances were observed (Scheme 9). Repeating the reaction using NaBAR₄' instead of NaOTf gave identical results.



Scheme 9. Attempted reaction of [C(pz)₄]Ru[P(OCH₂)₃CET](Cl)(4-chloroanilido) (**7**) with halide abstractors and phenylacetylene.

A THF-*d*₈ solution of **7** and NaOTf was pressurized with 25 psi H₂ (Scheme 10). After heating at 70 °C, aniline NH₂ doublets grew in the ¹H NMR spectrum, but there did not appear to be any reaction with hydrogen (no hydride resonances were observed). NaBAR₄' was added to a THF-*d*₈ solution of **7** and pressurized with H₂ (this time at 45 psi); this reaction mixture exhibited the same reactivity as observed for the experiment with NaOTf.



Scheme 10. Attempted reaction of $[C(pz)_4]Ru[P(OCH_2)_3CEt](Cl)(4\text{-chloroanilido})$ (**7**) with halide abstractors and H_2 .

The following control reaction was performed to confirm that the NH_2 resonances observed from the previous reactions were a result of the $Ru(II)$ complex gaining a proton from a source other than added substrates. Complex **7** was combined with $NaBAR'_4$ in THF and benzene was added to the reaction mixture to force the apparent precipitation of $NaCl$. It was subsequently filtered through Celite that had been freshly dried in a vacuum oven. The product was isolated and then reconstituted in $THF-d_8$ that had been dried by distillation over $Na/benzophenone$ in the glovebox and stored over 4\AA molecular sieves. The 1H NMR spectrum of the isolated complex showed a broad peak at 5.73 ppm, originally thought to be the NH resonance of 4-chloroanilido (Figure 7). Heating this complex at $70\text{ }^\circ C$ for ~ 30 minutes resolved the broad peak into two NH_2 doublets (Figure 7). All twelve pyrazolyl resonances were unchanged after heating. The NMR tube used for this sample had been silylated with a 1:10 solution of $TMSCl:CHCl_3$ to prevent the complex from abstracting protons from the glass surface of the tube. Thus, the proton source was not obvious.

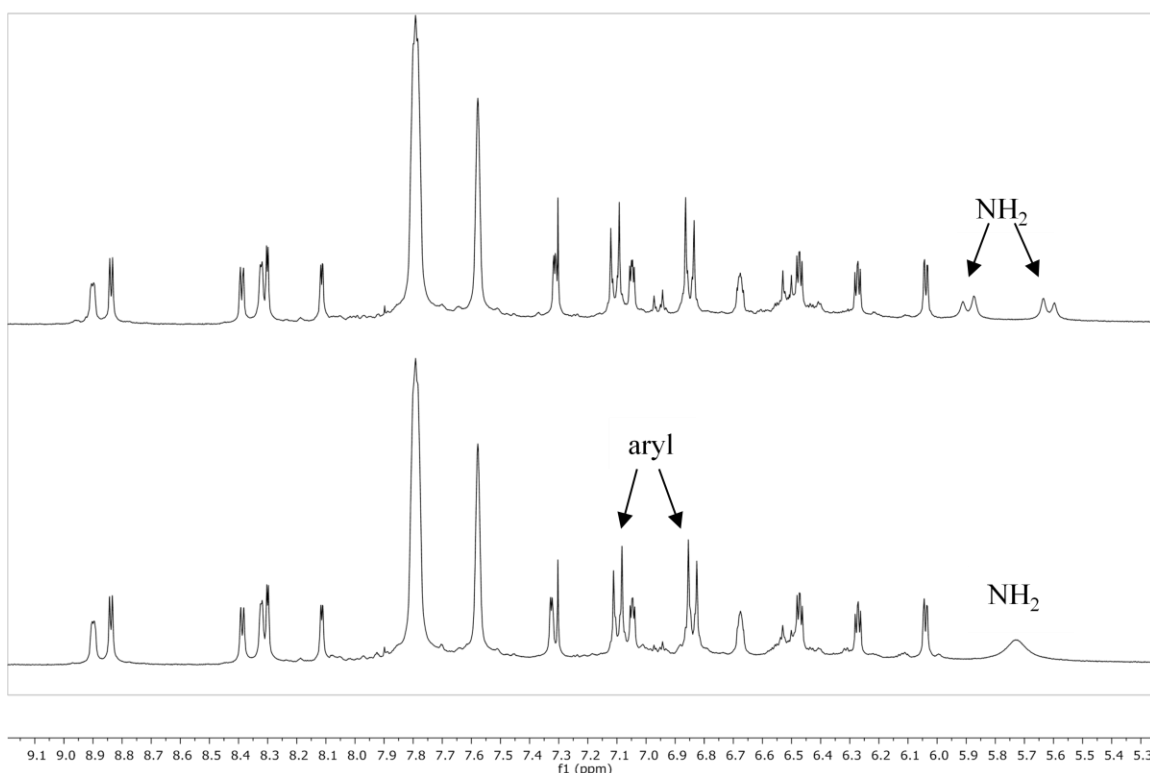
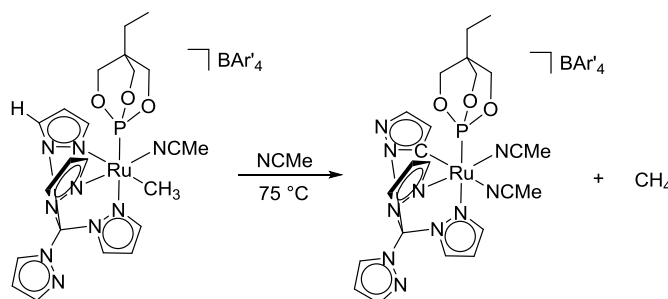


Figure 7. ^1H NMR (300 MHz) spectra of the downfield region of **7** + NaBAR'_4 in $\text{THF-}d_8$ (bottom, room temperature; top, heating at $70\text{ }^\circ\text{C}$ for 30 min).

2.5 Conclusions

Attempts to abstract a chloride from $[\text{C}(\text{pz})_4]\text{Ru}[\text{P}(\text{OCH}_2)_3\text{CEt}](\text{Cl})(4\text{-chloroanilido})$ (**7**) resulted in species that did not appear to perform C–H or H_2 activation chemistry. The deprotonation of $\{[\text{C}(\text{pz})_4]\text{Ru}[\text{P}(\text{OCH}_2)_3\text{CEt}](\text{OTf})(4\text{-chloroaniline})\}^+$ led to decomposition. Attempted *in situ* 1,2-addition experiments with **7** and a halide abstractor (TfOTf, NaOTf, NaBAR'_4) did not show any desired 1,2-CH, CD, or HH-addition with C_6H_6 , C_6D_6 , phenylacetylene, or H_2 . Instead, ^1H NMR spectra of these experiments revealed the growth of aniline NH_2 doublets without any other change to the complex, indicating that **7** is abstracting a proton from some source other than the desired substrates—perhaps from impurities in the halide abstractors (TfOTf, NaOTf, NaBAR'_4)—with the NH_2 resonances appearing upon heating. AgOTf ,¹⁹ TMSOTf ,²⁰ and Lewis acidic triflate salts such as $\text{Bi}(\text{OTf})_3$ ²¹ have been demonstrated or

proposed to generate triflic acid (HOTf) *in situ*. Triflic acid has been shown to be produced by the reaction of AgOTf with 1,2-dichloroethane (DCE) or with *tert*-butylchloride in benzene or chloroform.¹⁹ ¹H NMR data indicates triflic acid is generated from TMSOTf in the production of peracetyl oxazolines from peracetyl saccharides.²⁰ Bi(OTf)₃·*n*H₂O is proposed to generate triflic acid via hydrolysis.²¹ However, *in situ* generated HOTf does not appear to be a likely proton source as **7** is protonated in the presence of NaOTf (to our knowledge, this metal triflate salt has not been shown to generate triflic acid) and NaBAR'₄. Poly(pyrazolyl)alkanes can have smaller activation barriers for the metal–nitrogen cleavage of a pyrazolyl ring than Tp does,¹³ allowing for a greater possibility for intramolecular C–H activation to occur. Thus, formation of the coordinated 4-chloroaniline ligand could occur by C–H activation of a pyrazolyl ring. Although intramolecular C–H activation of pyrazolyl rings have been reported (Scheme 11),²² there is no evidence of this type of reaction occurring for **7** with TiOTf, NaOTf, or NaBAR'₄ and C₆H₆, C₆D₆, phenylacetylene, or H₂, as all twelve pyrazolyl resonances were accounted for in the ¹H NMR spectrum of the reaction mixture. With the overall difficulty in synthesizing a stable target complex and the lack of success with preliminary 1,2-addition experiments, C(pz)₄ was concluded to be an unsuccessful ligand for designing a Ru(II) complex suitable for the study of H₂ and C–H activation.



Scheme 11. Intramolecular C–H activation of the 5-position of a pyrazolyl ring.²²

2.6 Experimental Section

General Considerations. Unless otherwise noted, all synthetic procedures were performed under anaerobic conditions in a nitrogen-filled glovebox or by using standard Schlenk techniques. Glovebox purity was maintained by periodic nitrogen purges and was monitored by an oxygen analyzer ($O_2 < 15$ ppm for all reactions). Tetrahydrofuran and *n*-pentane were dried by distillation from sodium/benzophenone and P_2O_5 , respectively. Diethyl ether and acetonitrile was distilled over CaH_2 . Benzene, methylene chloride, and hexanes were purified by passage through a column of activated alumina. Benzene- d_6 , acetone- d_6 , CD_3CN , CD_2Cl_2 , and $CDCl_3$ were used as received and stored under a N_2 atmosphere over 4Å molecular sieves. THF- d_8 was distilled over sodium/benzophenone and stored over 4Å molecular sieves. 1H NMR spectra were recorded on a Varian 300 MHz, Varian 500 MHz or a Bruker 600 MHz or 800 MHz spectrometer, and $^{13}C\{^1H\}$ NMR spectra were recorded on a Bruker 600 MHz (operating frequency = 150 MHz) or a Bruker 800 MHz (operating frequency = 201 MHz). All 1H and ^{13}C spectra are referenced against residual proton signals (1H NMR) or ^{13}C resonances (^{13}C NMR) of the deuterated solvents. $^{31}P\{^1H\}$ NMR spectra were obtained on a Varian 300 MHz (operating frequency = 121 MHz), Varian 500 MHz (operating frequency = 201 MHz) or Varian 600 MHz (operating frequency = 243 MHz) spectrometer and referenced against an external standard of H_3PO_4 ($\delta = 0$). $^{19}F\{^1H\}$ NMR spectra were obtained on a Varian 300 MHz (operating frequency = 282 MHz) or a Varian 600 MHz (operating frequency = 565 MHz). Tetra(pyrazolyl)methane was synthesized according to a previously reported procedure.²² All other reagents were used as received from the manufacturers.

$[C(pz)_4]Ru(PPh_3)(Cl)_2$ (1). Tetra(pyrazolyl)methane (0.1880 g, 0.0671 mmol) was added to a solution of $Ru(PPh_3)_3(Cl)_2$ (0.7084 g, 0.7388 mmol) in ~20 mL of toluene. The reaction mixture was refluxed for 18 h, after which it was cooled. Hexanes were added to further precipitate the yellow solid that had formed; solid was collected on a fine porosity frit and washed with toluene, followed by washing with pentane to yield **1** in 82% yield (0.4315 g). 1H NMR

(CDCl₃, 300 MHz): δ = 8.71 (1H, s, pz 3 or 5 position), 8.62 (1H, s, pz 3 or 5 position), 8.26 (1H, s, pz 3 or 5 position), 8.15 (1H, s, pz 3 or 5 position), 7.82, 7.25 (overlaps with residual CDCl₃ solvent resonance) (15H total, each a m, PPh₃), 6.98 (1H, s, pz 4 position), 6.85 (2H, d, $^3J_{\text{HH}} = 3$ Hz, coordinated pz 3 or 5 position), 6.73 (2H, s, coordinated pz 3 or 5 position), 6.50 (1H, s pz 4 position), and 5.88 (2H, s, coordinated pz 4 position). ^{31}P NMR (CD₂Cl₂, 243 MHz): δ = 51.4 ppm. ^{13}C NMR (CD₂Cl₂, 201 MHz): δ = 151.5, 148.4, 145.3, 136.8, 135.1, 134.1 (each a s, pz 3 or 5 position) 135.4 (d, $^2J_{\text{PC}} = 9$ Hz, phenyl ipso), 133.2, 129.5 (each a s, phenyl meta and para), 128.0 (d, $^2J_{\text{PC}} = 9$ Hz, phenyl ortho), 111.9, 109.3 (2 C, coincidental overlap) (each a s, pz 4 position), 94.7 (C(pz)₄). Attempts to obtain favorable elemental analysis results were not successful.

[C(pz)₄]Ru[P(OCH₂)₃CEt](Cl)₂ (2). P(OCH₂)₃CEt (0.3047 g, 1.879 mmol) was added to a solution of [C(pz)₄]Ru(PPh₃)(Cl)₂ (**1**) (0.3006 g, 0.4207 mmol) in ~20 mL CHCl₃ and refluxed for 18 h. The reaction mixture was then allowed to cool. The yellow-green solid was collected on a fine porosity frit and washed with hexanes to remove excess P(OCH₂)₃CEt. The filtrate was reduced to ~5 mL under vacuum; hexanes were added to precipitate more of the solid, which was then collected via vacuum filtration and washed with hexanes to remove excess P(OCH₂)₃CEt. also. The solid was returned to the reaction vessel and dissolved in fresh CHCl₃; the mixture was allowed to reflux for an additional 6 h to convert all Ru species to the desired product. The reaction mixture was cooled, hexanes were added to yield a precipitate, and the yellow solid was collected on a frit, and washed with pentane to afford **2** in 88% yield (0.2265 g). ^1H NMR (CD₂Cl₂, 500 MHz): δ = 8.65 (1H, s, pz 3 or 5 position), 8.53 (1H, s, pz 3 or 5 position), 8.33 (1H, d, $^3J_{\text{HH}} = 3$ Hz, pz 3 or 5 position), 8.20 (1H, d $^3J_{\text{HH}} = 1$ Hz, pz 3 or 5 position), 8.12 (2H, m, coordinated pz 3 or 5 position), 7.05 (2H, d, $^3J_{\text{HH}} = 3$ Hz, coordinated pz 3 or 5 position), 6.96 (1H, dd, $^3J_{\text{HH}} = 3$ Hz, pz 4 position), 6.61 (1H, bs, pz 4 position) and 6.33 (2H, m, coordinated pz 4 position), 4.38 (6H, d, $^3J_{\text{PH}} = 5$ Hz, P(OCH₂)₃CEt), 1.28 (2H, q, $^3J_{\text{HH}} = 8$ Hz, -CH₂CH₃) and 0.86 (3H, t, $^3J_{\text{HH}} = 8$ Hz, -CH₂CH₃). ^{31}P NMR (CD₂Cl₂, 201 MHz): δ = 127.6 ppm.

^{13}C NMR (CD_2Cl_2 , 201 MHz): $\delta = 151.4, 148.1, 145.5, 136.8, 133.8, 132.9$ (each a s, pz 3 or 5 position), 112.1, 109.6, 109.1 (each a s, pz 4 position), 94.5 ($\text{C}(\text{pz})_4$), 74.7 (d, $^2J_{\text{PC}} = 6\text{Hz}$, $-(\text{OCH}_2)_3$), 35.8 (d, $^3J_{\text{PC}} = 31\text{Hz}$, $-(\text{OCH}_2)_3\text{C}-$), 23.9 (s, $-\text{CH}_2\text{CH}_3$), 7.39 (s, $-\text{CH}_2\text{CH}_3$). Attempts to obtain favorable elemental analysis results were not successful.

$\{[\text{C}(\text{pz})_4]\text{Ru}[\text{P}(\text{OCH}_2)_3\text{CEt}](\mu\text{-Cl})_2\}[\text{OTf}]_2$ (3). $[\text{C}(\text{pz})_4]\text{Ru}[\text{P}(\text{OCH}_2)_3\text{CEt}](\text{Cl})_2$ (2) (0.0664 g, 0.1081 mmol) was dissolved in ~30 mL of DCM. TiOTf (0.0478 g, 0.1352 mmol) was dissolved in a minimal amount of methanol and added to the solution of **2** in DCM. The reaction mixture was allowed to stir for 4 h at room temperature, after which the reaction mixture was filtered to remove a dark gray precipitate. The orange filtrate was reduced to dryness, then reconstituted in THF and refluxed for 3 h. The cream-beige product was collected via vacuum filtration. Product was washed with THF and pentane to give **3** in 64% yield (0.0503 g). ^1H NMR (CD_2Cl_2 , 500 MHz): $\delta = 8.86$ (1H, s, pz 3 or 5 position), 8.63 (1H, s, pz 3 or 5 position), 8.38 (1H, d, $^3J_{\text{HH}} = 3\text{Hz}$, pz 3 or 5 position), 8.23 (1H, bs, pz 3 or 5 position), 7.99 (2H, bs, coordinated pz 3 or 5 position), 7.11 (2H, d, $^3J_{\text{HH}} = 3\text{Hz}$, coordinated pz 3 or 5 position), 7.02 (1H, dd, $^3J_{\text{HH}} = 3\text{Hz}$, pz 4 position), 6.72 (1H, bs, pz 4 position), 6.39 (2H, m, coordinated pz 4 position), 4.53 (6H, d $^3J_{\text{PH}} = 4\text{Hz}$, $\text{P}(\text{OCH}_2)_3\text{CEt}$), 1.37 (2H, q, $^3J_{\text{HH}} = 8\text{Hz}$, $-\text{CH}_2\text{CH}_3$), and 0.91 (3H, t, $^3J_{\text{HH}} = 8\text{Hz}$, $-\text{CH}_2\text{CH}_3$) ppm. ^{31}P NMR (CD_2Cl_2 , 201 MHz): $\delta = 128.9$ ppm. ^{19}F NMR (CD_2Cl_2 , 565 MHz): $\delta = -79.3$ ppm. ^{13}C NMR (CD_2Cl_2 , 201 MHz): $\delta = 151.3, 147.7, 145.8, 137.0, 134.8, 133.8$ (each a s, pz 3 or 5 position), 112.6, 109.6, 109.4 (pz 4 positions), 94.3 ($\text{C}(\text{pz})_4$), 75.3 (d, $^2J_{\text{PC}} = 7\text{Hz}$, $-(\text{OCH}_2)_3$), 23.7 (s, $-\text{CH}_2\text{CH}_3$), 7.28 (s, $-\text{CH}_2\text{CH}_3$).

$\{[\text{C}(\text{pz})_4]\text{Ru}[\text{P}(\text{OCH}_2)_3\text{CEt}](\text{Cl})(4\text{-chloroaniline})\}[\text{OTf}]$ (4). A suspension of $\{[\text{C}(\text{pz})_4]\text{Ru}[\text{P}(\text{OCH}_2)_3\text{CEt}](\mu\text{-Cl})_2\}[\text{OTf}]_2$ (**3**) (0.1135 g, 0.0780 mmol) was made in ~10 mL of THF in a pressure tube equipped with a stir bar. 4-Chloroaniline (0.0523 g, 0.4100 mmol) was added to the reaction mixture. The tube was sealed and set in a 90 °C oil bath for ~18 h, during which time the solution turned yellow and a white precipitate formed. In the glovebox, the reaction mixture was filtered to remove the white precipitate; Et_2O was then added to the yellow

filtrate to precipitate the product. The beige-white product was collected via vacuum filtration and washed with Et₂O and pentane to give **4** in 67% yield (0.0890 g). ¹H NMR (CD₂Cl₂, 300 MHz): δ = 8.56 (1H, dd, ³J_{HH} = 3 Hz, pz 3 or 5 position), 8.43 (1H, d, ³J_{HH} = 3 Hz, pz 3 or 5 position), 8.21 (1H, m, pz 3 or 5 position), 8.20 (1H, s, pz 3 or 5 position), 8.08 (1H, d, ³J_{HH} = 2 Hz, pz 3 or 5 position), 8.03 (1H, d, ³J_{HH} = 2 Hz, pz 3 or 5 position), 7.88 (1H, d, ³J_{HH} = 2 Hz, pz 3 or 5 position), 7.00 (1H, dd, ³J_{HH} = 3 Hz, pz 3 or 5 position), 6.52 (1H, m, pz 4 position), 6.40 (1H, dd, ³J_{HH} = 3 Hz, pz 4 position), 6.32 (1H, dd, ³J_{HH} = 3 Hz, pz 4 position), and 6.00 (1H, d, ³J_{HH} = 3 Hz, pz 4 position), 7.09 (2H, d, ³J_{HH} = 9 Hz, phenyl resonance meta to –CNH₂), 6.81 (2H, d, ³J_{HH} = 9 Hz, phenyl resonance ortho to –CNH₂), 5.98 (1H, d, overlapping with pyrazolyl resonance at 6.00, NH₂), 4.86 ppm (d, ²J_{HH} = 11 Hz, NH₂), 4.46 (6H, d, ³J_{PH} = 5 Hz, P(OCH₂)₃CEt), 1.32 (2H, q, ³J_{HH} = 8 Hz, –CH₂CH₃), 0.88 (3H, t, ³J_{HH} = 8 Hz, –CH₂CH₃). ³¹P NMR (THF-*d*₈, 243 MHz): δ = 129.8 ppm. ¹⁹F NMR (THF-*d*₈, 565 MHz): δ = -79.2 ppm. ¹³C NMR (THF-*d*₈, 201 MHz): δ = 152.5, 152.0, 149.2, 146.3, 145.1, 139.1, 136.4, 133.6, (pz 3 or 5 position) 130.0 (s, phenyl ipso), 129.5, 124.4, (phenyl ortho, meta, para), 112.6, 109.7, 109.5, 109.4, (pz 4 position), 95.2 (s, C(pz)₄), 75.4 (d, ²J_{PC} = 6 Hz, –(OCH₂)₃), 36.6 (d, ³J_{PC} = 31.7 Hz –(OCH₂)₃C–), 24.1 (s, –CH₂CH₃), 7.62 (s, –CH₂CH₃).

[C(pz)₄]Ru[P(OCH₂)₃CEt](Cl)(4-chloroanilido) (7).

{[C(pz)₄]Ru[P(OCH₂)₃CEt](Cl)(4-chloroaniline)}[OTf] (**4**) (0.0123 g, 0.0174 mmol) was dissolved in THF-*d*₈. A small amount of NaH (0.0023 g, 0.0958 mmol) was added to the solution, resulting in H₂ effervescence and turning the yellow solution to red, affording **7** in 96% yield as determined by ¹H NMR spectroscopy using hexamethyldisilane (HMDS) as an internal standard. ¹H NMR (THF-*d*₈, 500 MHz): δ = 8.84 (1H, s, pz 3 or 5 position), 8.83 (1H, s, pz 3 or 5 position), 8.27 (1H, s, pz 3 or 5 position), 8.22 (1H, s, pz 3 or 5 position), 8.11 (1H, s, pz 3 or 5 position), 7.91 (1H, d, ³J_{HH} = 3 Hz, pz 3 or 5 position), 7.88 (1H, d, ³J_{HH} = 1 Hz, pz 3 or 5 position), 7.02 (1H, s, pz 3 or 5 position), 6.52 (1H, s, pz 4 position), 6.39 (1H, d, ³J_{HH} = 2 Hz, pz 4 position), 6.35 (1H, dd, ³J_{HH} = 3 Hz, pz 4 position), 6.19 (1H, dd, ³J_{HH} = 3 Hz, pz 4 position), 6.26 (2H, d,

$^3J_{\text{HH}} = 9$ Hz, phenyl resonance meta to $-\text{CNH}_2$), 5.65 (2H, d, $^3J_{\text{HH}} = 8$ Hz, phenyl resonance ortho to $-\text{CNH}_2$), 2.42 (1H, bs, NH). ^{31}P NMR (THF- d_8 , 243 MHz): $\delta = 129.1$ ppm. ^{13}C NMR (THF- d_8 , 201 MHz): $\delta = 162.4, 152.0, 151.4, 148.1, 145.9, 138.9, 135.1, 134.1$ (pz 3 or 5), 133.0 (s, phenyl ipso), 128.0, 117.7 (phenyl ortho, meta, para), 112.2, 109.3, 109.1, 108.6 (pz 4 position), 95.5 (s, $\text{C}(\text{pz})_4$), 75.0 (d, $^2J_{\text{PC}} = 6$ Hz, $-(\text{OCH}_2)_3$), 36.3 (d, $^3J_{\text{PC}} = 30$ Hz, $-(\text{OCH}_2)_3\text{C}-$), 24.3 (s, $-\text{CH}_2\text{CH}_3$), 7.62 (s, $-\text{CH}_2\text{CH}_3$).

References

- (1) Webb, J. R.; Burgess, S. A.; Cundari, T. R.; Gunnoe, T. B. *Dalton Trans.* **2013**, 42, 16646.
- (2) Trofimenko, S. *J. Am. Chem. Soc.* **1970**, 92, 5118.
- (3) Benisvy, L.; Wanke, R.; Kuznetsov, M. L.; da Silva, M.; Pombeiro, A. J. L. *Tetrahedron* **2009**, 65, 9218.
- (4) Pettinari, C.; Pettinari, R. *Coord. Chem. Rev.* **2005**, 249, 525.
- (5) Wang, C. Master's, University of Virginia, 2012.
- (6) Reger, D. L.; Grattan, T. C.; Brown, K. J.; Little, C. A.; Lamba, J. J. S.; Rheingold, A. L.; Sommer, R. D. *J. Organomet. Chem.* **2000**, 607, 120.
- (7) Kunz, P. C.; Berghahn, M.; Bruckmann, N. E.; Dickmeis, M.; Kettel, M.; Spingler, B. *Z. Anorg. Allg. Chem.* **2009**, 635, 471.
- (8) Zhao, D. W.; Xie, Y. F.; Song, H. B.; Tang, L. F. *J. Organomet. Chem.* **2012**, 718, 89.
- (9) Reger, D. L.; Grattan, T. C. *Synthesis* **2003**, 350.
- (10) Miguel, S.; Diez, J.; Gamasa, M. P.; Lastra, M. E. *Eur. J. Inorg. Chem.* **2011**, 4745.

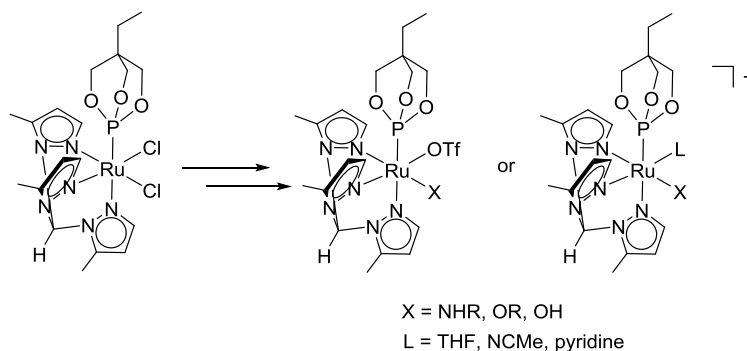
- (11) Lawrence, S. C.; Skinner, M. E. G.; Green, J. C.; Mountford, P. *Chemical Communications* **2001**, 705.
- (12) Yoshimoto, S.; Mukai, H.; Kitano, T.; Sohrin, Y. *Anal. Chim. Acta* **2003**, 494, 207.
- (13) McKeown, B. A.; Lee, J. P.; Mei, J.; Cundari, T. R.; Gunnoe, T. B. *Eur. J. Inorg. Chem.* **2016**, 2016, 2296.
- (14) Gunnoe, T. B. In *Physical Inorganic Chemistry: Reactions, Processes, and Applications*; Bakac, A., Ed.; John Wiley and Sons: Hoboken, NJ, 2010, p 495.
- (15) Fraser, R. R.; Mansour, T. S.; Savard, S. *The Journal of Organic Chemistry* **1985**, 50, 3232.
- (16) pKa Values for Organic and Inorganic Bronsted Acids at 25 °C. [Online Early Access]. <https://owl.oit.umass.edu/departments/OrganicChemistry/appendix/pKaTable.html>.
- (17) pKa Table: Effect of Electronegativity and Resonance. [Online Early Access]. <http://www.nku.edu/~russellk/courses/chm310/ho/pKa-short.pdf>.
- (18) Feng, Y.; Gunnoe, T. B.; Grimes, T. V.; Cundari, T. R. *Organometallics* **2006**, 25, 5456.
- (19) Dang, T. T.; Boeck, F.; Hintermann, L. *The Journal of Organic Chemistry* **2011**, 76, 9353.
- (20) Warren, C. D. J., R. W.; Nakabayashi, S.; C08B 37/00, C07H 17/00, 15/00 C07H 17/02 ed.; World Intellectual Property Organization, I. B., Ed. USA, 1988, p 31.
- (21) Mathia, F.; Szolcsanyi, P. *Organic & Biomolecular Chemistry* **2012**, 10, 2830.
- (22) Joslin, E. E.; Quillian, B.; Gunnoe, T. B.; Cundari, T. R.; Sabat, M.; Myers, W. H. *Inorg. Chem.* **2014**, 53, 6270.

3 Synthesis of Neutral and Cationic Ru(II) Precursors for C–H or H₂ Bond Activation Using

Tris(5-methyl-pyrazolyl)methane (HC(pz⁵)₃)

3.1 Introduction

While tetra(pyrazolyl)methane (C(pz)₄) ligated Ru(II) complexes did not prove suitable for the 1,2-addition of C–H or H₂ bonds across Ru–N bonds (see Chapter 2), it was hypothesized that complexes with other poly(pyrazolyl)alkane ligands could be capable of successful bond activation. For example, attempts to use $\{[C(pz)_4]Ru[P(OCH_2)_3CEt](NCMe)(Me)\}^+$ for catalytic ethylene hydrophenylation were unsuccessful due to the intramolecular C–H activation of a pyrazolyl ring to release methane and form $\{[(\kappa^3-N,C^5,N)C(pz)_4]Ru[P(OCH_2)_3CEt](NCMe)_2\}^+$.¹ However, the use of tris(5-methyl-pyrazolyl)methane (HC(pz⁵)₃) in the complex $\{[HC(pz^5)_3]Ru[P(OCH_2)_3CEt](NCMe)(Ph)\}^+$ gave 565 turnovers of ethylbenzene under 15 psi ethylene at 90 °C in benzene (after 131 h), a 28-fold improvement in turnovers compared to catalysis using TpRu[P(OCH₂)₃CEt](NCMe)(Ph).^{2,3} Thus, HC(pz⁵)₃-ligated Ru complexes were subsequently targeted for 1,2-addition of C–H bonds or H₂ across Ru–X bonds (X = OR, NHR). Tris(5-methyl-pyrazolyl)methane, a charge neutral proligand, is substituted with methyl groups on the 5-position of the pyrazolyl rings in an effort to prevent intramolecular activation of a pyrazolyl C–H bond (Scheme 1).

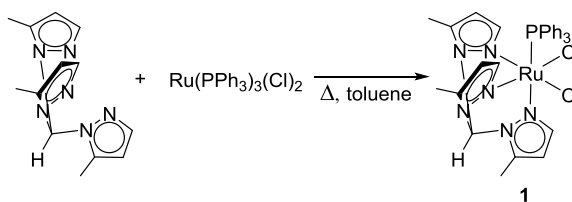


Scheme 1. Tris(5-methyl-pyrazolyl)methane-ligated Ru target complexes.

3.2 Synthesis of $[\text{HC}(\text{pz}^5)_3]\text{Ru}$ Complexes

The desired target complexes for this project included $[\text{HC}(\text{pz}^5)_3]\text{Ru}[\text{P}(\text{OCH}_2)_3\text{CEt}](\text{OTf})(\text{X})$ or cationic $\{[\text{HC}(\text{pz}^5)_3]\text{Ru}[\text{P}(\text{OCH}_2)_3\text{CEt}](\text{L})(\text{X})\}^+$ in which X is an amido, alkoxo or hydroxo ligand and L is a labile solvent molecule such as tetrahydrofuran (THF), acetonitrile (NCMe) or pyridine (py). $\text{P}(\text{OCH}_2)_3\text{CEt}$ was chosen as an ancillary ligand for its tied-back geometry, preventing intramolecular C–H activation of the phosphite. Initial efforts focused on synthesizing $[\text{HC}(\text{pz}^5)_3]\text{Ru}[\text{P}(\text{OCH}_2)_3\text{CEt}](\text{Cl})_2$, as this bis(chloride) complex was thought to be a useful precursor for the synthesis of the target complexes via exchange of chlorides for other ligands.

As a precursor to $[\text{HC}(\text{pz}^5)_3]\text{Ru}[\text{P}(\text{OCH}_2)_3\text{CEt}](\text{Cl})_2$, $[\text{HC}(\text{pz}^5)_3]\text{Ru}(\text{PPh}_3)(\text{Cl})_2$ (**1**) was synthesized in 99% yield by refluxing $\text{HC}(\text{pz}^5)_3$ and $\text{Ru}(\text{PPh}_3)_3(\text{Cl})_2$ in toluene (Scheme 2). The ^1H NMR spectrum of **1** (Figure 1) shows the expected 2:1 pattern for the methyl groups of the $\text{HC}(\text{pz}^5)_3$ ligand, indicating a C_s symmetric complex. A single resonance for coordinated PPh_3 is observed at 51.9 ppm in the ^{31}P NMR spectrum.



Scheme 2. Synthesis of $[\text{HC}(\text{pz}^5)_3]\text{Ru}(\text{PPh}_3)(\text{Cl})_2$ (**1**).

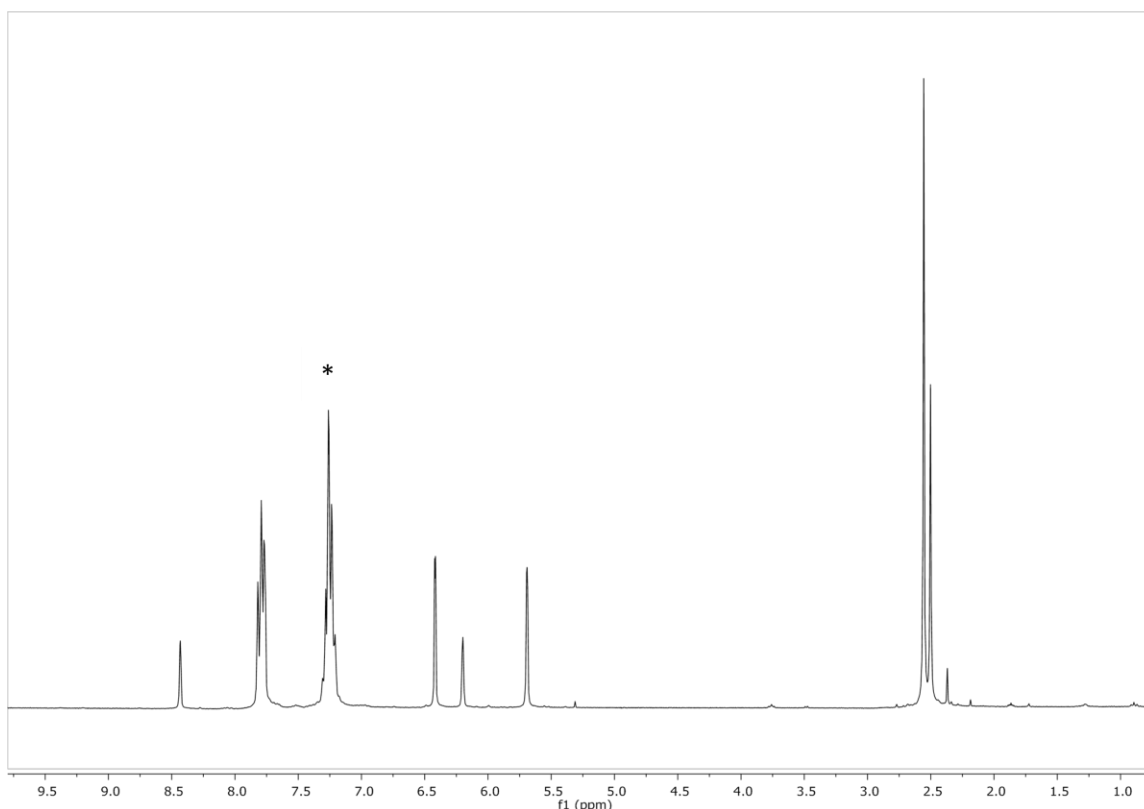
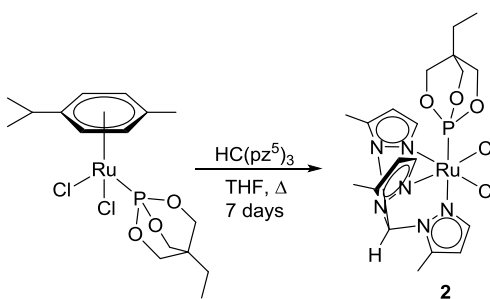


Figure 1. ^1H NMR spectrum (300 MHz, CDCl_3) of $[\text{HC}(\text{pz}^5)_3]\text{Ru}(\text{PPh}_3)(\text{Cl})_2$ (**1**). Solvent resonance denoted by *, which is referenced against DCM present in the solvent.

Refluxing $\text{P}(\text{OCH}_2)_3\text{CEt}$ and complex **1** in CHCl_3 did not result in the formation of $[\text{HC}(\text{pz}^5)_3]\text{Ru}[\text{P}(\text{OCH}_2)_3\text{CEt}](\text{Cl})_2$ (**2**), instead affording a mixed phosphine/phosphite species, presumably $[[\text{HC}(\text{pz}^5)_3]\text{Ru}(\text{PPh}_3)[\text{P}(\text{OCH}_2)_3\text{CEt}](\text{Cl})][\text{Cl}]$, as evidenced by a pair of doublets ($^2J_{\text{PP}} = 60$ Hz) in the ^{31}P NMR spectrum at 131.7 ppm (phosphite) and 45.0 ppm (phosphine). Some minor impurities were also present, including free $\text{P}(\text{OCH}_2)_3\text{CEt}$. The synthesis of complex **2** instead required the reverse process—installing $\text{P}(\text{OCH}_2)_3\text{CEt}$ on the metal center first, followed by coordination of the tris(pyrazolyl)alkane ligand. Refluxing $(p\text{-cymene})\text{Ru}[\text{P}(\text{OCH}_2)_3\text{CEt}](\text{Cl})_2$ and $\text{HC}(\text{pz}^5)_3$ in THF for 7 days resulted in the successful formation of $[\text{HC}(\text{pz}^5)_3]\text{Ru}[\text{P}(\text{OCH}_2)_3\text{CEt}](\text{Cl})_2$ (**2**) in 99% isolated yield (Scheme 3). The ^1H NMR spectrum of **2** reveals $\text{HC}(\text{pz}^5)_3$ methyl resonances in a 1:2 pattern, similarly indicative of a C_s symmetric complex (Figure 2), at 2.60 ppm (3H) and 2.56 ppm (6H) in $\text{DCM-}d_2$. Phosphite resonances are

visible at 4.34 (d, $^3J_{\text{PH}} = 5$ Hz), 1.25 (q, $^3J_{\text{HH}} = 8$ Hz), and 0.83 ppm (t, $^3J_{\text{HH}} = 8$ Hz). Also, a singlet at 127.3 ppm is visible in the ^{31}P NMR spectrum for coordinated $\text{P}(\text{OCH}_2)_3\text{CEt}$. A single crystal suitable for an X-ray diffraction study was grown by layering a $\text{DCM-}d_2$ solution of **2** with hexanes (Figure 3). As expected, the bond angles between *cis* chlorides are close to 90° , showing pseudo-octahedral geometry. The methyl groups in the 5-positions of the pyrazolyl rings are oriented towards the methine proton of the $\text{HC}(\text{pz}^5)_3$ ligand. The bond $\text{Ru}(1)\text{--N}(5)$ (2.137(3) Å), trans to the phosphorus of $\text{P}(\text{OCH}_2)_3\text{CEt}$, is noticeably longer than the corresponding bonds ($\text{Ru}(1)\text{--N}(1)$, 2.046(3) Å; $\text{Ru}(1)\text{--N}(3)$, 2.054(3) Å) trans to the chloride ligands, likely due to $\text{P}(\text{OCH}_2)_3\text{CEt}$ having a larger trans effect than chloride.



Scheme 3. Synthesis of $[\text{HC}(\text{pz}^5)_3]\text{Ru}[\text{P}(\text{OCH}_2)_3\text{CEt}](\text{Cl})_2$ (**2**).

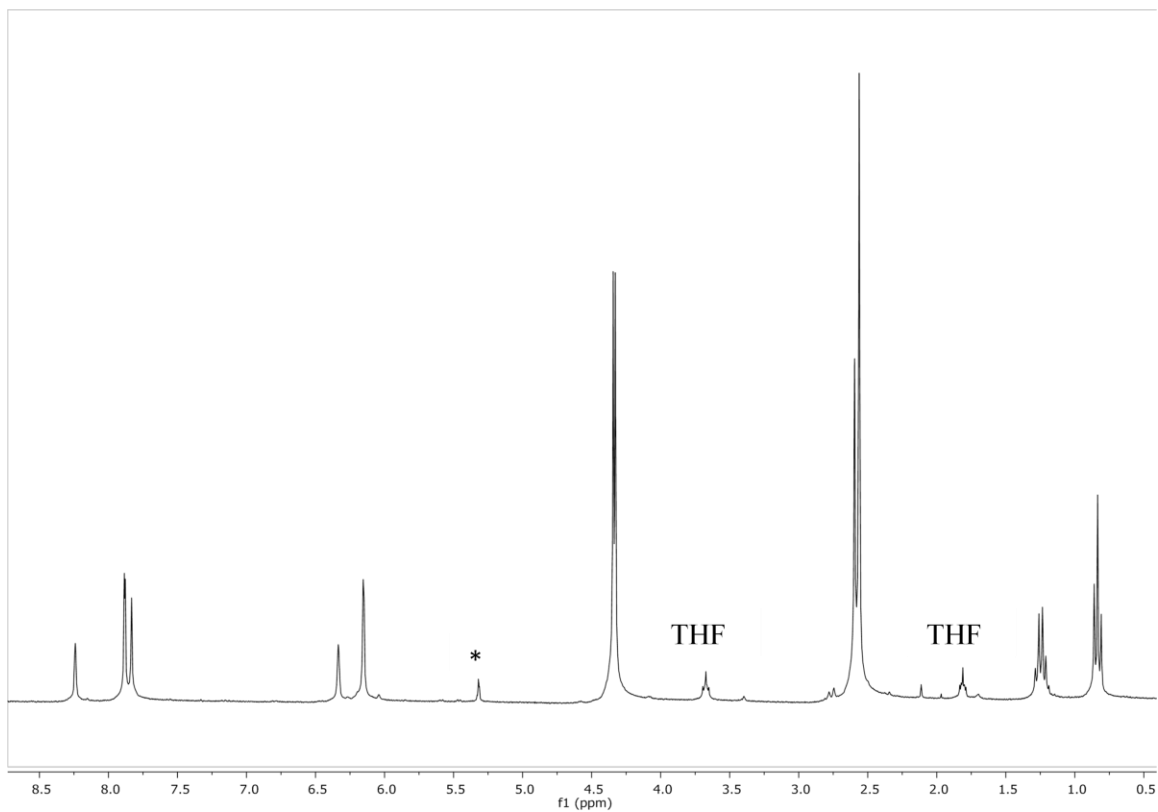


Figure 2. ¹H NMR spectrum (300 MHz, CD₂Cl₂) of [HC(pz⁵)₃]Ru[P(OCH₂)₃CEt](Cl)₂ (**2**). Solvent resonance denoted by *.

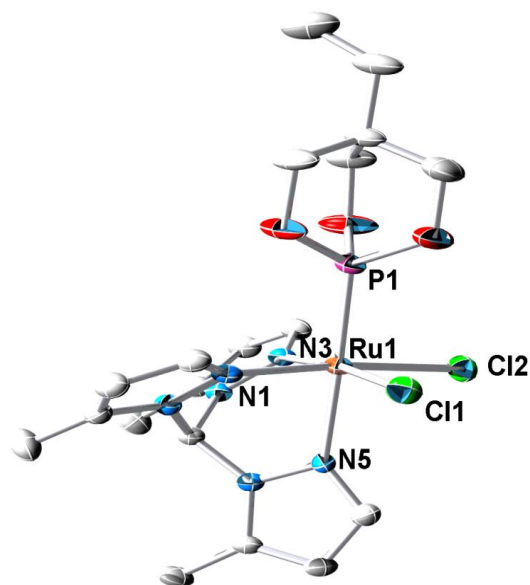
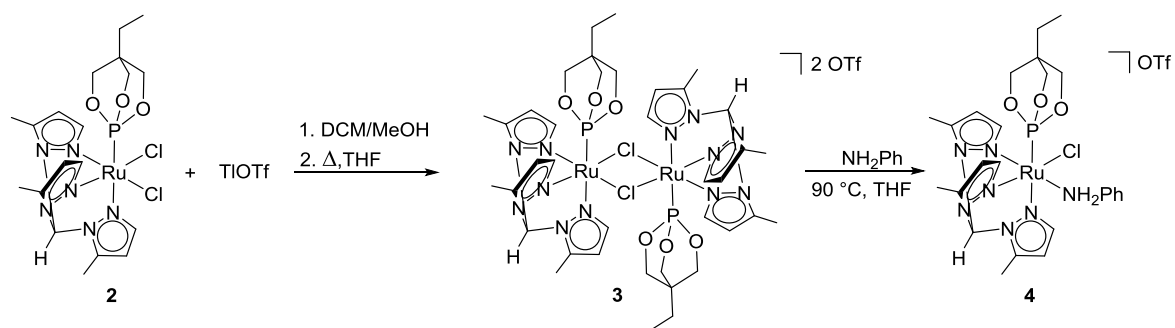


Figure 3. ORTEP of $[\text{HC}(\text{pz}^5)_3]\text{Ru}[\text{P}(\text{OCH}_2)_3\text{CEt}](\text{Cl})_2$ (**2**) (50% probability with H atoms omitted). Selected bond lengths (\AA): Ru(1)-N(1), 2.046(3); Ru(1)-N(3), 2.054(3); Ru(1)-N(5), 2.137(3); Ru(1)-P(1), 2.186(1); Ru(1)-Cl(2), 2.405(1); Ru(1)-Cl(1), 2.410(1). Selected bond angles (deg): N(1)-Ru(1)-N(3), 88.1(1); N(3)-Ru(1)-Cl(2), 90.1(1); N(1)-Ru(1)-Cl(1), 89.4(1); P(1)-Ru(1)-Cl(1), 91.8(4); Cl(2)-Ru(1)-Cl(1), 91.7(4).

Multiple synthetic strategies toward a Ru(II)-amido complex were employed using complex **2**. A methanol solution of TlOTf was added to a DCM solution of complex **2** (discussed in Chapter 2) to form $\{[\text{HC}(\text{pz}^5)_3]\text{Ru}[\text{P}(\text{OCH}_2)_3\text{CEt}](\mu\text{-Cl})_2\}[\text{OTf}]_2$ (**3**) in 90% isolated yield (Scheme 3). Heating complex **3** and NH_2Ph at 90°C in THF afforded $\{[\text{HC}(\text{pz}^5)_3]\text{Ru}[\text{P}(\text{OCH}_2)_3\text{CEt}](\text{NH}_2\text{Ph})(\text{Cl})\}[\text{OTf}]$ (**4**) in 59% isolated yield (Scheme 4). The ^1H NMR spectrum of **4** in $\text{DCM-}d_2$ reveals phenyl resonances of coordinated aniline at 7.08 ppm and 6.71 ppm, and doublets are observed at 5.34 (overlaps with CD_2Cl_2 resonance) and 4.54 ppm ($^2J_{\text{HH}} = 11.5$ Hz) for the diastereotopic NH_2 hydrogen atoms (Figure 5). Three resonances for the methyl groups of $\text{HC}(\text{pz}^5)_3$ are observed in a 1:1:1 ratio characteristic of an asymmetric complex. Resonances for phosphite are visible at 4.44 (d, $^3J_{\text{PH}} = 4.6$ Hz), 1.33 (q), and 0.89 ppm (t) in the ^1H NMR spectrum and at 129.8 ppm in the ^{31}P NMR spectrum.



Scheme 4. Synthesis of $\{[\text{HC}(\text{pz}^5)_3\text{Ru}[\text{P}(\text{OCH}_2)_3\text{CET}](\mu\text{-Cl})]\}_2[\text{OTf}]_2$ (**3**) and $[\text{HC}(\text{pz}^5)_3\text{Ru}[\text{P}(\text{OCH}_2)_3\text{CET}](\text{NH}_2\text{Ph})(\text{Cl})][\text{OTf}]$ (**4**).

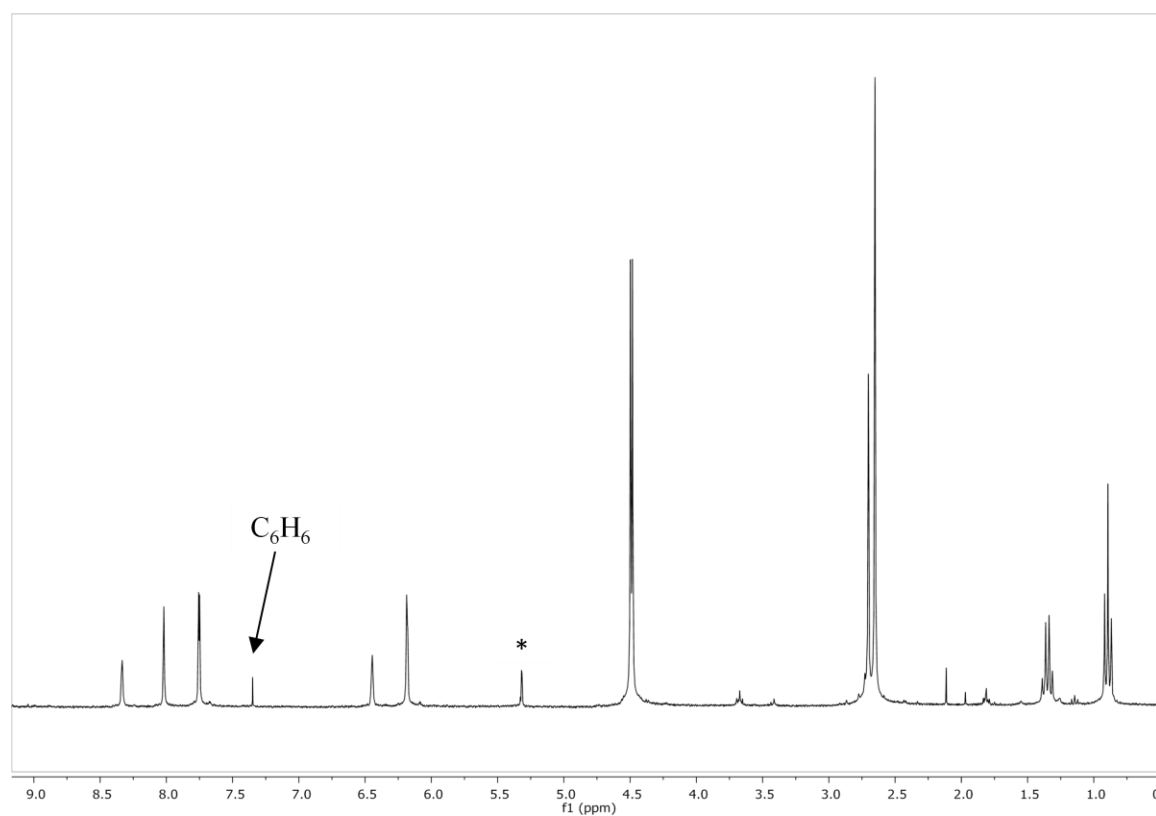


Figure 4. ¹H NMR spectrum (300 MHz, CD₂Cl₂) of $\{[\text{HC}(\text{pz}^5)_3\text{Ru}[\text{P}(\text{OCH}_2)_3\text{CET}](\mu\text{-Cl})]\}_2[\text{OTf}]_2$ (**3**). Solvent resonance denoted by *.

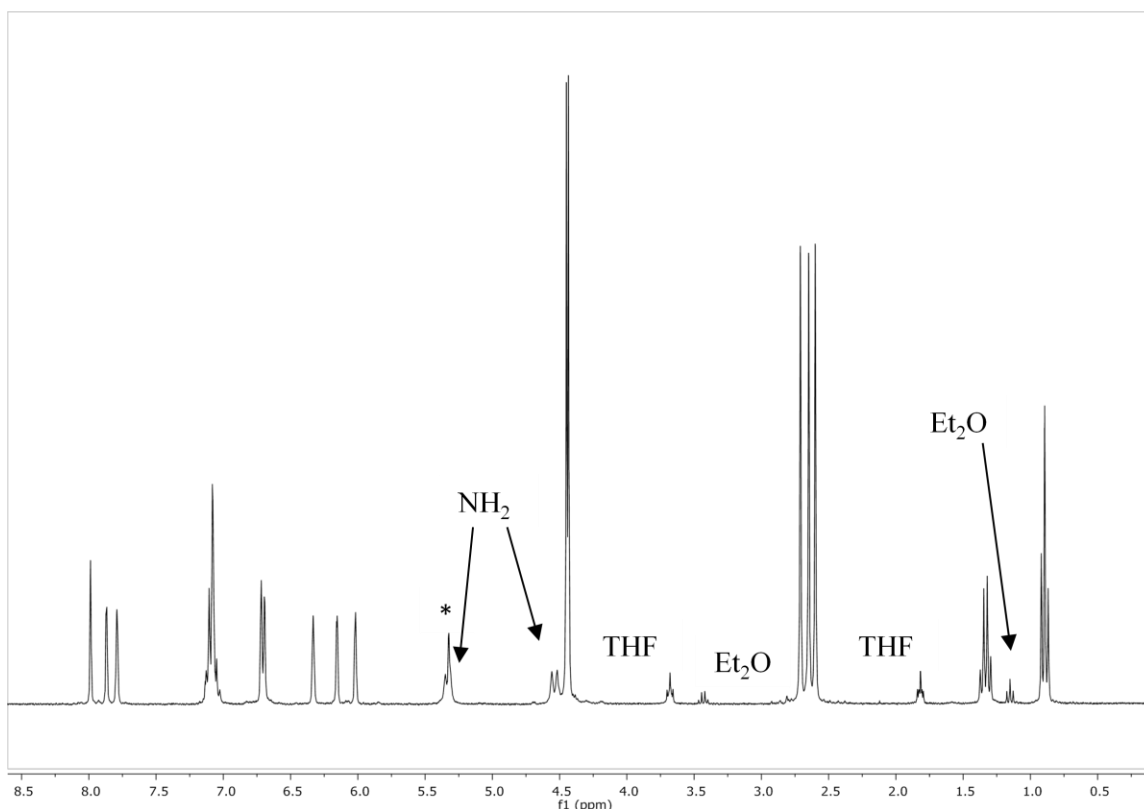


Figure 5. ^1H NMR spectrum (300 MHz, CD_2Cl_2) of $\{[\text{HC}(\text{pz}^5)_3]\text{Ru}[\text{P}(\text{OCH}_2)_3\text{CEt}](\text{NH}_2\text{Ph})(\text{Cl})\}[\text{OTf}]$ (**4**). Solvent resonance denoted by *.

3.3 Reactivity of $\{[\text{HC}(\text{pz}^5)_3]\text{Ru}[\text{P}(\text{OCH}_2)_3\text{CEt}](\text{NH}_2\text{Ph})(\text{Cl})\}[\text{OTf}]$ (**4**)

The synthesis of a Ru–anilido complex suitable for 1,2-addition was attempted by using $\{[\text{HC}(\text{pz}^5)_3]\text{Ru}[\text{P}(\text{OCH}_2)_3\text{CEt}](\text{NH}_2\text{Ph})(\text{Cl})\}[\text{OTf}]$ (**4**), either by first deprotonating the aniline ligand followed by exchanging the chloride for a more labile ligand, or by first exchanging the chloride for a labile ligand followed by deprotonation of coordinated aniline. The reaction of complex **4** with NaH in THF resulted in what appeared to be both deprotonation of the aniline ligand and the undesired deprotonation of the methine carbon of $\text{HC}(\text{pz}^5)_3$, giving the putative complex $\{[:\text{C}(\text{pz}^5)_3]\text{Ru}[\text{P}(\text{OCH}_2)_3\text{CEt}](\text{Cl})(\text{NHPH})\}[\text{Na}]$ (**5**) *in situ* in ~98% ^1H NMR yield (Scheme 5, Figure 6). Integrating the downfield resonances in the ^1H NMR spectrum reveals six pyrazolyl protons. Also, the methine resonance (typically the most downfield resonance of the $\text{HC}(\text{pz}^5)_3$ ligand) is missing, indicating the possibility that the methine C–H of $\text{HC}(\text{pz}^5)_3$ had been

deprotonated. The tris(pyrazolyl)alkane methyl groups are observed in a 1:1:1 pattern. While **5** was not the desired product of the reaction of **4** with NaH, the reactivity of **5** was explored to see if a complex capable of bond activation could be synthesized from this precursor. Attempts to abstract chloride from **5** using AgOTf resulted in the formation of an aniline complex instead of the desired Ru–anilido/triflate complex, in ~23% yield by ^1H NMR. This aniline complex was different from **4** as evident from chemical shifts in the ^1H NMR spectrum (Figure 7), likely indicating that either chloride abstraction was successful or a $\{[\text{HC}(\text{pz}^5)_3]\text{Ru}[\text{P}(\text{OCH}_2)_3\text{CEt}](\text{NH}_2\text{Ph})(\text{Cl})\}-\text{AgOTf}$ adduct was formed. The undesired protonation of the anilido ligand rendered this synthetic route unproductive.

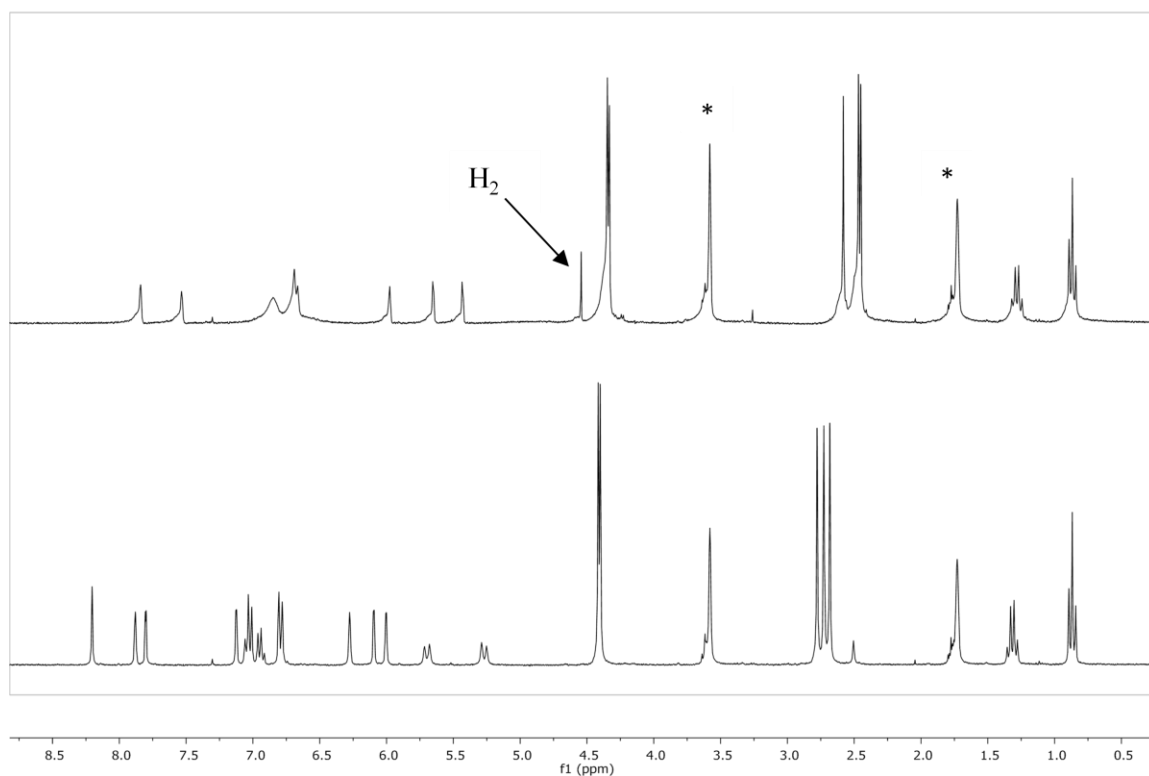


Figure 6. ^1H NMR spectra (THF- d_8 , 300 MHz) of $\{[\text{HC}(\text{pz}^5)_3]\text{Ru}[\text{P}(\text{OCH}_2)_3\text{CEt}](\text{NH}_2\text{Ph})(\text{Cl})\}[\text{OTf}]$ (**4**) (bottom) and $\{[:\text{C}(\text{pz}^5)_3]\text{Ru}[\text{P}(\text{OCH}_2)_3\text{CEt}](\text{Cl})(\text{NHPh})\}[\text{Na}]$ (**5**) (top). Solvent resonances denoted by *.

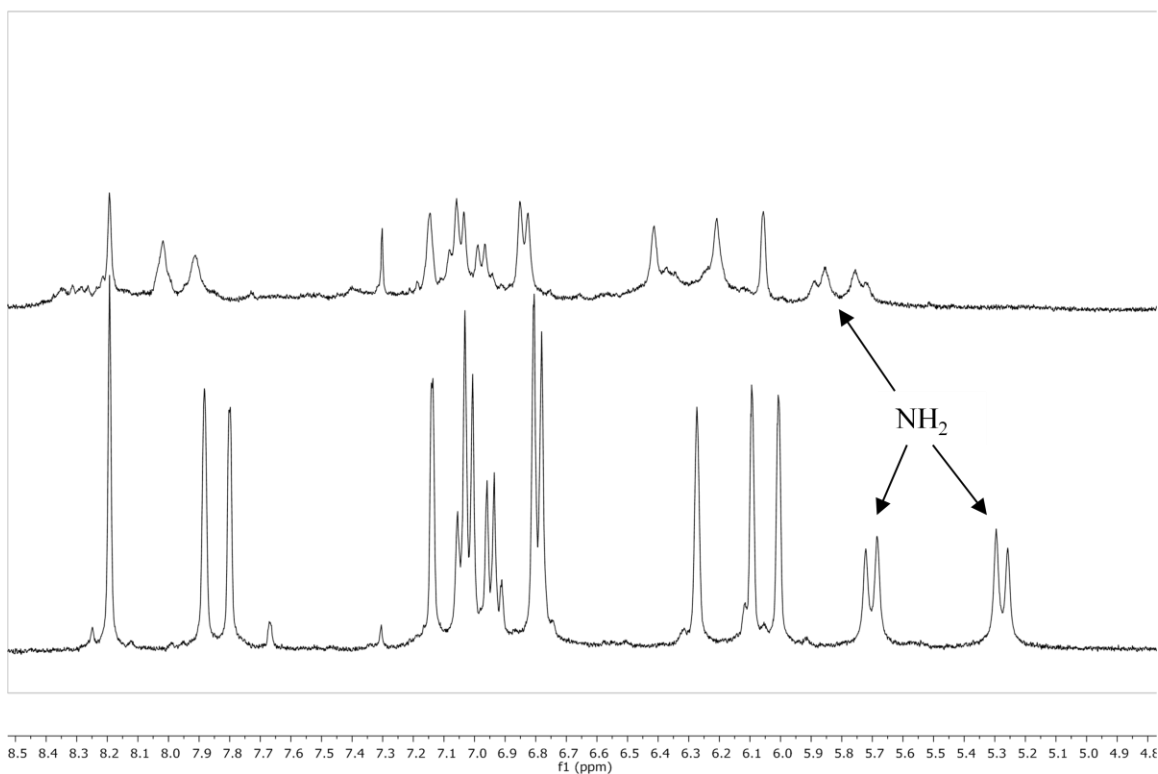
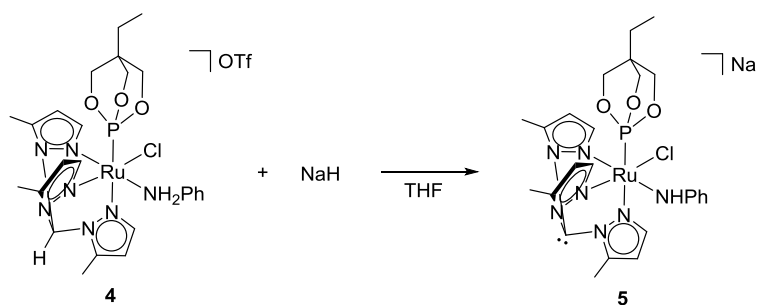


Figure 7. Downfield region of the ^1H NMR spectra (300 MHz, $\text{THF-}d_8$) of **4** (bottom) and aniline complex formed from adding AgOTf to **5** (top).

Adding TlOTf or NaOTf after the *in situ* generation of $\{[:\text{C}(\text{pz}^5)_3]\text{Ru}[\text{P}(\text{OCH}_2)_3\text{CEt}](\text{Cl})(\text{NHPh})\}[\text{Na}]$ resulted in the formation of multiple products. It also appeared that decomposition was taking place, as the intensities of the complex resonances decreased after addition of TlOTf and NaOTf, respectively. Adding NaBAr'_4 to complex **5** (generated *in situ*) in THF resulted in incomplete conversion to the putative THF complex, $[:\text{C}(\text{pz}^5)_3]\text{Ru}[\text{P}(\text{OCH}_2)_3\text{CEt}](\text{THF})(\text{NHPh})$ (50% yield by ^1H NMR).



Scheme 5. Reaction of $\{[\text{HC}(\text{pz}^5)_3]\text{Ru}[\text{P}(\text{OCH}_2)_3\text{CEt}](\text{NH}_2\text{Ph})(\text{Cl})\}[\text{OTf}]$ (**4**) with NaH.

Reactions with **4** and **5** were attempted in the presence of acetonitrile. Since NCMe is generally a better ligand than THF or triflate, Ru–NCMe complexes could potentially be more stable than Ru–THF or Ru–OTf. NaH was added to a CD_3CN solution of complex **4**, to deprotonate the aniline ligand, followed by the addition of NaBAR'_4 to abstract a Cl ligand. However, this reaction resulted in the formation of multiple intractable species. Furthermore, the addition of NaBAR'_4 and NCMe to **5** in $\text{THF-}d_8$ resulted in incomplete conversion to a putative solvento complex in ~20% yield (by ^1H NMR). The only NCMe resonance observed in the ^1H NMR spectrum corresponded to free NCMe, indicating that the desired coordination of acetonitrile had not occurred. Thus, attempts to use acetonitrile as a ligand to isolate $\{[\text{HC}(\text{pz}^5)_3]\text{Ru}[\text{P}(\text{OCH}_2)_3\text{CEt}](\text{NHPh})(\text{NCMe})\}[\text{OTf}]$ or $\{[:\text{C}(\text{pz}^5)_3]\text{Ru}[\text{P}(\text{OCH}_2)_3\text{CEt}](\text{NHPh})(\text{NCMe})\}[\text{Na}]$ were not successful.

Next, methods of abstracting a chloride from **4** followed by deprotonation of the aniline ligand were explored. Adding AgOTf in $\text{THF-}d_8$ to complex **4** produced $\{[\text{HC}(\text{pz}^5)_3]\text{Ru}[\text{P}(\text{OCH}_2)_3\text{CEt}](\text{NH}_2\text{Ph})(\text{OTf})\}[\text{OTf}]$ (**6**) in ~80% yield by ^1H NMR spectroscopy (Scheme 6). Significant changes in chemical shifts for the aniline NH_2 group and the phosphite were observed upon conversion of **4** to **6** (Figure 8). The alternate route of adding TMSOTf (trimethylsilyl trifluoromethanesulfonate) to **4** in $\text{DCM-}d_2$ also appeared to work in ~80% yield, as evidenced by observing a resonance possibly for TMSCl in the ^1H NMR spectrum at 0.44 ppm (Scheme 6). However, the reaction of NaH with **6** did not result in deprotonation to form the

desired product $[\text{HC}(\text{pz}^5)_3]\text{Ru}[\text{P}(\text{OCH}_2)_3\text{CEt}](\text{NHPh})(\text{OTf})$. Rather, complex **6** appeared to revert to complex **4**.

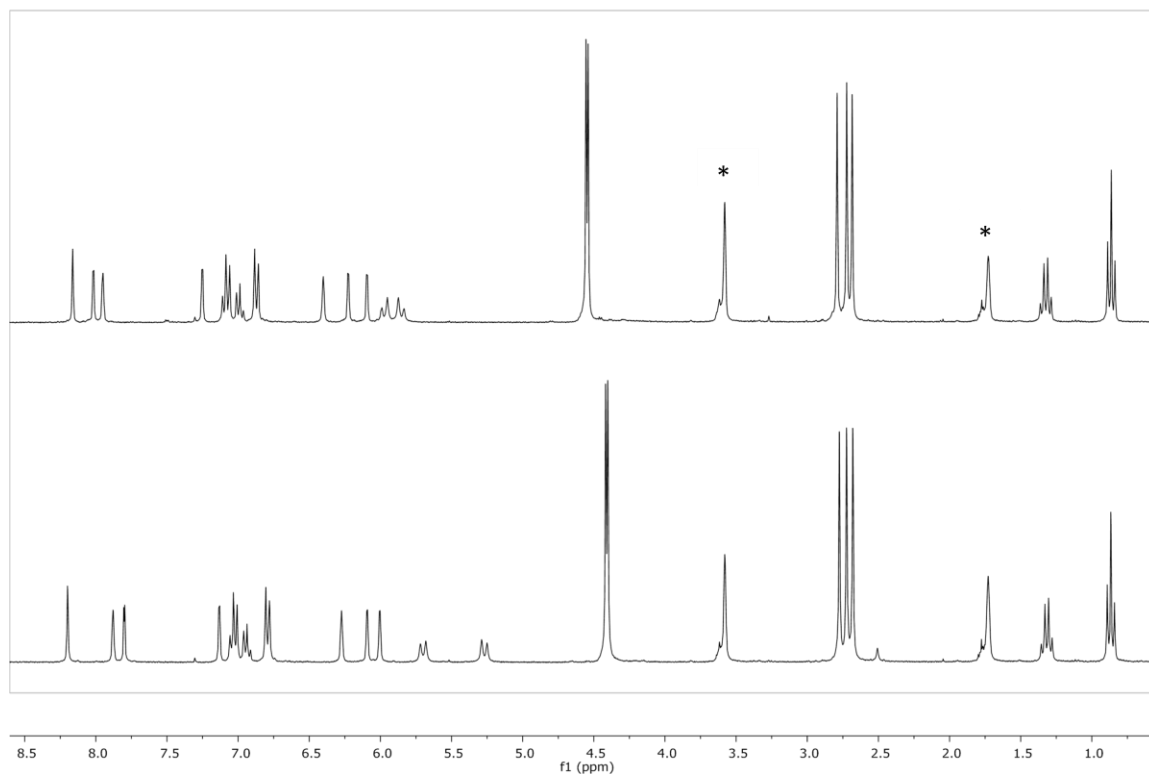
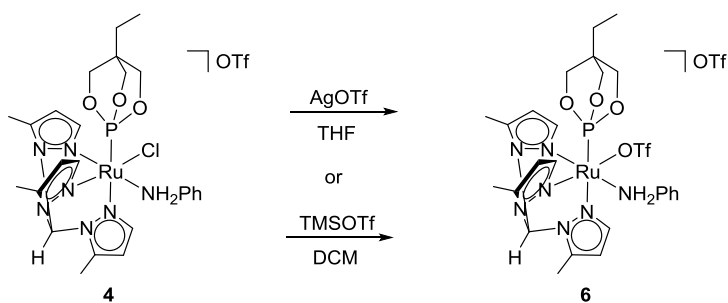


Figure 8. ^1H NMR spectra (300 MHz, $\text{THF-}d_8$) of $[\text{HC}(\text{pz}^5)_3]\text{Ru}[\text{P}(\text{OCH}_2)_3\text{CEt}](\text{NH}_2\text{Ph})(\text{Cl})\{\text{OTf}\}$ (**4**) (bottom) and $[\text{HC}(\text{pz}^5)_3]\text{Ru}[\text{P}(\text{OCH}_2)_3\text{CEt}](\text{NH}_2\text{Ph})(\text{OTf})\{\text{OTf}\}$ (**6**) (top). Solvent resonances denoted by *.



Scheme 6. Synthesis of $[\text{HC}(\text{pz}^5)_3]\text{Ru}[\text{P}(\text{OCH}_2)_3\text{CEt}](\text{NH}_2\text{Ph})(\text{OTf})\{\text{OTf}\}$ (**6**).

Exchanging triflate with acetonitrile on **6** was attempted in an effort to synthesize a precursor to a Ru–anilido complex that would be less susceptible to protonation. Adding NCMe to a $\text{THF-}d_8$ solution of **6** (formed *in situ*) and heating at 70 °C formed the complex

{[HC(pz⁵)₃Ru[P(OCH₂)₃CEt](NH₂Ph)(NCMe)]OTf}₂ (**7**) in quantitative yield by ¹H NMR spectroscopy (Scheme 7). A resonance for coordinated acetonitrile was observed at 2.47 ppm in the ¹H NMR spectrum (Figure 9). The ³¹P NMR spectrum of **7** exhibits a single resonance at 130.8 ppm. Adding NaH to **7** (isolated) formed the putative {[HC(pz⁵)₃Ru[P(OCH₂)₃CEt](NHPh)(NCMe)]OTf} (**8**) in ~62% yield by ¹H NMR spectroscopy (Scheme 7). However, there is a possibility that **8** could actually be the amidinate complex {[HC(pz⁵)₃Ru[P(OCH₂)₃CEt][N(H)C(Me)N(Ph)]]OTf} (Figure 10), as NHPh has been demonstrated to perform intramolecular nucleophilic addition to coordinated acetonitrile in the reaction between (PCP)Ru(CO)(NHPh)(PMe₃) and NCMe.⁴ The broad ¹H NMR spectrum of **8** indicated the possibility of some paramagnetic impurity (Figure 10). A single resonance at 131.7 ppm was visible in the ³¹P NMR spectrum of **8**. Furthermore, complex **8** was found to be very air sensitive, turning from yellow to blue upon reaction with air.

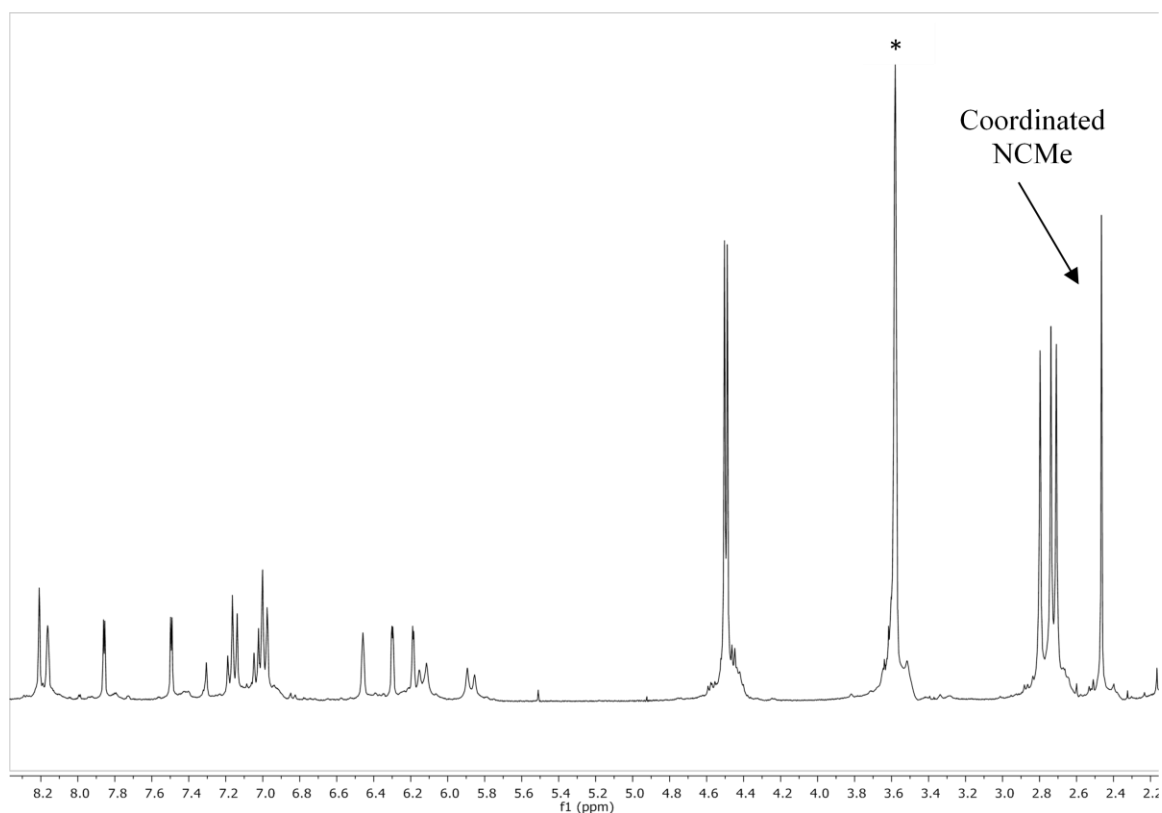


Figure 9. ¹H NMR spectrum (300 MHz, THF-*d*₈) of {[HC(pz⁵)₃Ru[P(OCH₂)₃CEt](NH₂Ph)(NCMe)]OTf}₂ (**7**). Solvent resonance denoted by *.

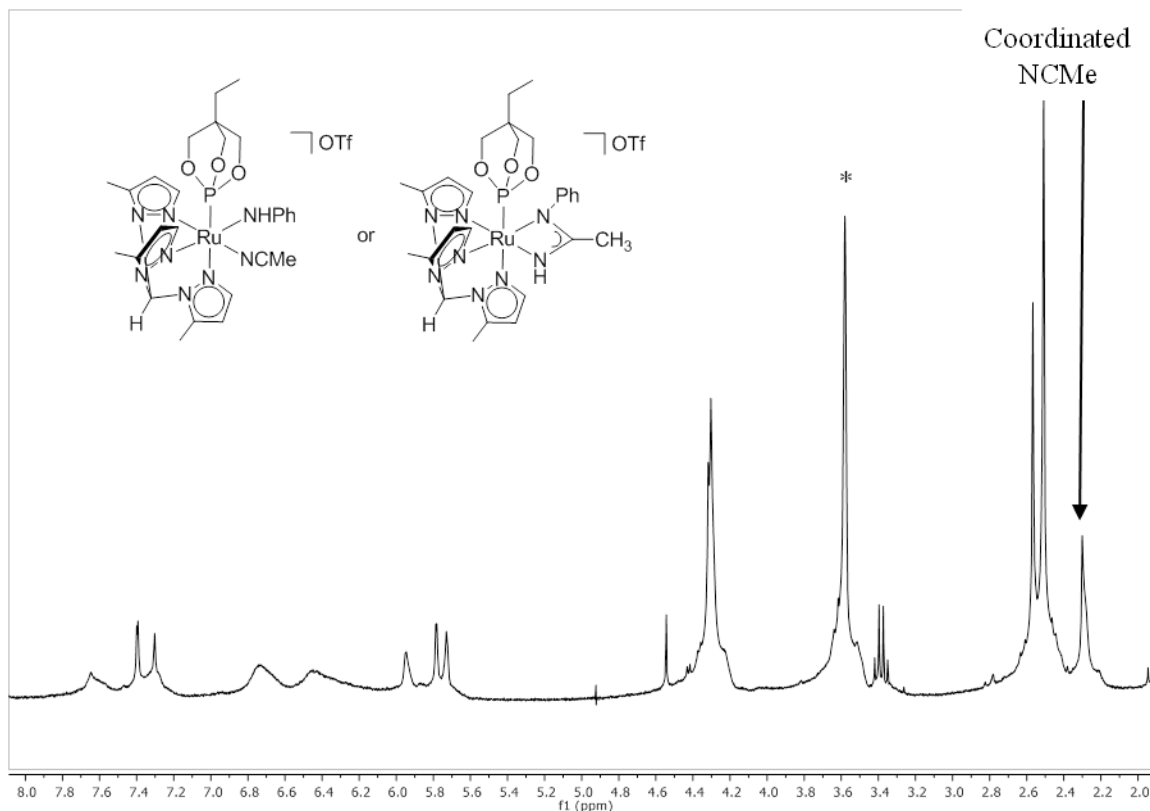
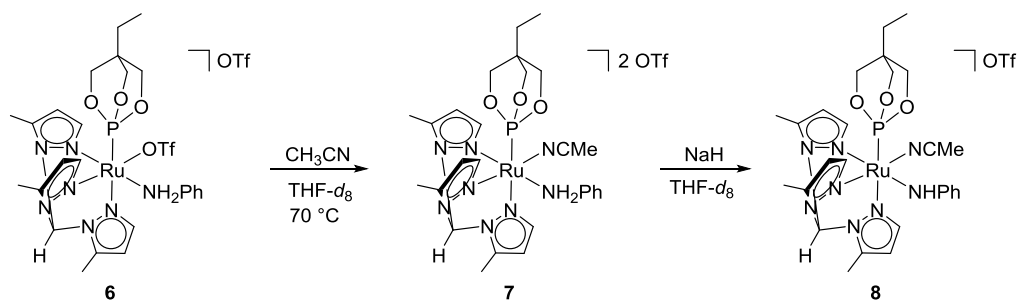


Figure 10. ^1H NMR spectrum (300 MHz, $\text{THF-}d_8$) of $\{[\text{HC}(\text{pz}^5)_3]\text{Ru}[\text{P}(\text{OCH}_2)_3\text{CEt}](\text{NHPh})(\text{NCMe})\}[\text{OTf}]$ or $\{[\text{HC}(\text{pz}^5)_3]\text{Ru}[\text{P}(\text{OCH}_2)_3\text{CEt}][\text{N}(\text{H})\text{C}(\text{Me})\text{N}(\text{Ph})]\}[\text{OTf}]$ (**8**). Solvent resonance denoted by *.

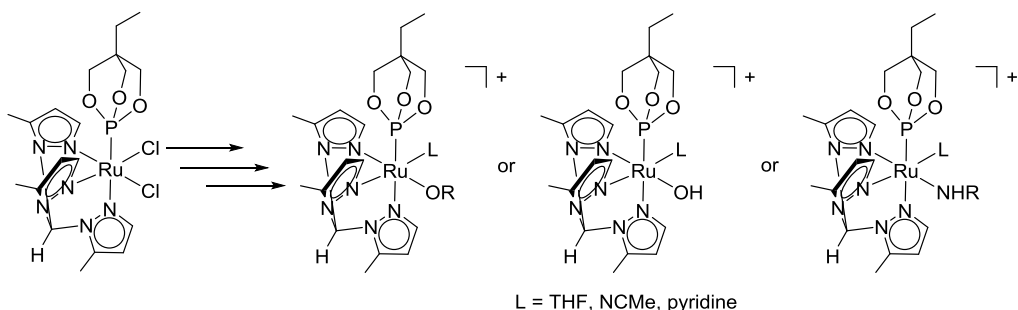
Pyridine was added to **6** and heated at 70 °C in an attempt to exchange triflate with pyridine to synthesize a precursor for a more stable Ru–anilido complex. This reaction did not form the desired Ru–pyridine/aniline complex $\{[\text{HC}(\text{pz}^5)_3]\text{Ru}[\text{P}(\text{OCH}_2)_3\text{CEt}](\text{NH}_2\text{Ph})(\text{py})\}[\text{OTf}]_2$, as no coordinated pyridine resonances were observed by ^1H NMR spectroscopy. Rather, multiple intractable products were formed.



Scheme 7. Reaction of $\{[\text{HC}(\text{pz}^5)_3]\text{Ru}[\text{P}(\text{OCH}_2)_3\text{CEt}](\text{NH}_2\text{Ph})(\text{OTf})\}[\text{OTf}]$ (**6**) with NCMe and subsequent deprotonation.

3.4 Reactivity of $[\text{HC}(\text{pz}^5)_3]\text{Ru}[\text{P}(\text{OCH}_2)_3\text{CEt}](\text{Cl})_2$ (**2**)

The reactivity of $[\text{HC}(\text{pz}^5)_3]\text{Ru}[\text{P}(\text{OCH}_2)_3\text{CEt}](\text{Cl})_2$ (**2**) was explored further by using halide abstractors, acids and bases to exchange chloride for other ligands (Scheme 8). The synthesis of not only Ru–amido complexes but also Ru–alkoxo or –hydroxo complexes was desired with the intent to compare the reactivity of N vs. O donor ligands towards 1,2-CH or HH-addition.

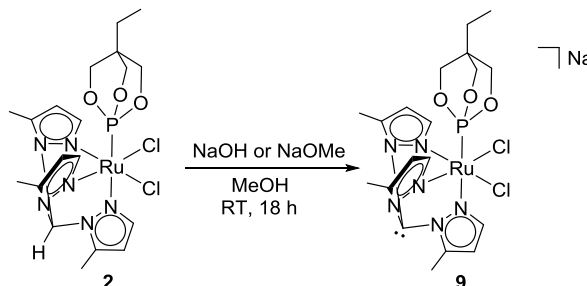


Scheme 8. Target Ru–OR, Ru–OH, and Ru–NHR complexes synthesized by chloride exchange from $[\text{HC}(\text{pz}^5)_3]\text{Ru}[\text{P}(\text{OCH}_2)_3\text{CEt}](\text{Cl})_2$ (**2**).

3.4.1 Attempted Synthesis of a Ru–OMe or Ru–OH Species

The reaction of a methanolic solution of **2** with excess NaOH or NaOMe does not result in chloride abstraction with formation of a desired Ru–OR ($\text{R} = \text{H}$ or Me) species (Scheme 9). Instead, this reaction results in the deprotonated complex $\{[:\text{C}(\text{pz}^5)_3]\text{Ru}[\text{P}(\text{OCH}_2)_3\text{CEt}](\text{Cl})_2\}[\text{Na}]$ (**9**) in 80% isolated yield (^{31}P NMR = 125.2 ppm). The ^1H NMR spectrum of **9** shows that it is C_s symmetric based on the characteristic two resonances for the poly(pyrazolyl)alkane methyl

groups in a 1:2 ratio and a 1:2 pattern for pyrazolyl C–H resonances. Furthermore, the most downfield resonance due to the HC(pz⁵)₃ methine proton is missing, indicative of deprotonation at the methine carbon.



Scheme 9. Reaction of [HC(pz⁵)₃Ru[P(OCH₂)₃CEt](Cl)₂ (**2**) with NaOH or NaOMe.

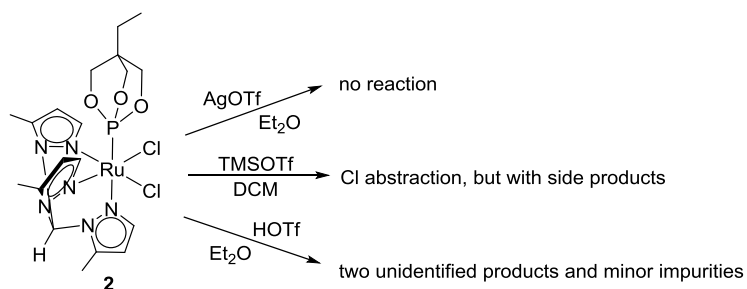
3.4.2 Attempts to Synthesize Ru–OTf or Ru–Solvento Species

As mentioned above, a logical starting point towards synthesizing a Ru–NHR or Ru–OR complexes from **2** was to abstract the chlorides to allow coordination of desired heteroatom ligands. If the desired ligand cannot be exchanged directly with chloride (for example, in the reaction of NaOMe with Ru–Cl to produce Ru–OMe and NaCl), the removal of chloride by salt metathesis to install a triflate or a labile solvent molecule (THF, acetonitrile, etc.) can provide an alternate synthetic route due to the ease of displacement of triflate and solvent ligands. For example, the reaction of Ru–Cl with AgOTf to produce Ru–OTf and AgCl could occur, followed by the displacement of OTf with NH₂Ph to make [Ru–NH₂Ph][OTf].

Various triflate sources and halide abstractors were reacted with complex **2** to exchange one or two chlorides for triflate or solvent (Scheme 10). The use of triflic acid (HOTf) to exchange chloride and triflate has been reported.^{5,6} The reaction of complex **2** with excess HOTf in Et₂O to make a bis(triflate) species resulted in an asymmetric major product in an estimated 70% yield with multiple minor impurities. The ³¹P NMR spectrum showed a resonance at 128.5 ppm for the major product. ¹⁹F NMR showed a single resonance at -79.0 ppm. The identity of

the major product could possibly be $[\text{HC}(\text{pz}^5)_3]\text{Ru}[\text{P}(\text{OCH}_2)_3\text{CEt}](\text{Cl})(\text{OTf})$, although this has not been confirmed due to focusing efforts on other synthetic routes.

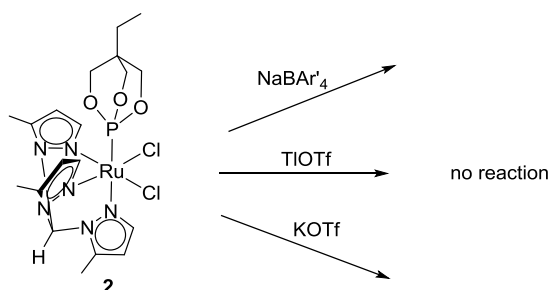
TMSOTf was used to abstract a chloride from complex **2** in 42% yield by ^1H NMR in $\text{DCM}-d_2$ at room temperature, as evidenced by production of an asymmetric complex and the formation of TMSCl observed at 0.43 ppm in the ^1H NMR spectrum. Several unidentified minor side products were also formed. While this reaction provided a route to a $\text{Ru}-\text{OTf}$ species, the synthesis of a $\text{Ru}-\text{OTf}$ complex in better yield and under milder reaction conditions was discovered (discussed in the last paragraph of this section). Thus, synthesis involving TMSOTf was not pursued further.



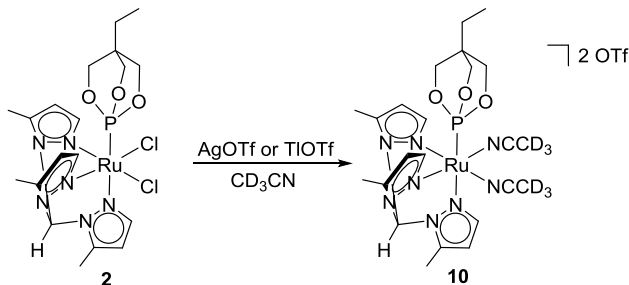
Scheme 10. Reactivity of $[\text{HC}(\text{pz}^5)_3]\text{Ru}[\text{P}(\text{OCH}_2)_3\text{CEt}](\text{Cl})_2$ (**2**) with triflate sources.

No reaction occurred upon addition of NaBAR'_4 to a solution of complex **2** in CD_3CN as evidenced by ^1H and ^{31}P NMR spectroscopy. Excess NaBAR'_4 was added to a solution of $[\text{HC}(\text{pz}^5)_3]\text{Ru}[\text{P}(\text{OCH}_2)_3\text{CEt}](\text{Cl})_2$ (**2**) in THF to synthesize $\{[\text{HC}(\text{pz}^5)_3]\text{Ru}[\text{P}(\text{OCH}_2)_3\text{CEt}](\text{Cl})(\text{THF})\}[\text{BAR}'_4]$ or $\{[\text{HC}(\text{pz}^5)_3]\text{Ru}[\text{P}(\text{OCH}_2)_3\text{CEt}](\text{THF})_2\}[\text{BAR}'_4]_2$. While the presence of NaBAR'_4 made the previously insoluble complex **2** dissolve in THF, it is clear from ^1H NMR spectral data that chloride abstraction had not occurred (the complex observed after addition of NaBAR'_4 is C_s symmetric and exhibits the same ^{31}P NMR shift, 127.3 ppm, as that for **2**) (Scheme 11). Adding NaBAR'_4 and aniline to a THF solution of complex **2** and heating at 70°C did not result in any reaction, supporting the hypothesis that NaBAR'_4 only serves to solubilize **2** in THF.

Alternatively, when AgOTf or TlOTf are added to **2** in CD₃CN, a white precipitate (presumably AgCl or TlCl, respectively) forms, and ¹H and ³¹P NMR spectral data indicate that {[HC(pz⁵)₃]Ru[P(OCH₂)₃CEt](CD₃CN)}[OTf]₂ (**10**) is formed in 86% yield by ¹H NMR spectroscopy for the reaction with AgOTf—the product formed after addition of AgOTf or TlOTf is C_s symmetric, and a single resonance at 129.2 ppm is observed in the ³¹P NMR spectrum (while **2** has a resonance at 127.3 ppm) (Scheme 12).



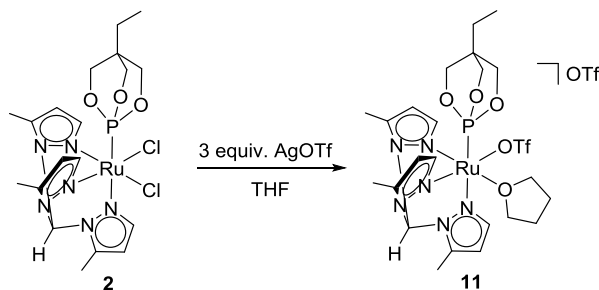
Scheme 11. Reactivity of [HC(pz⁵)₃]Ru[P(OCH₂)₃CEt](Cl)₂ (**2**) with NaBAR'₄, TlOTf and KOTf in THF.



Scheme 12. Reaction of [HC(pz⁵)₃]Ru[P(OCH₂)₃CEt](Cl)₂ (**2**) with triflate salts in CD₃CN.

No reaction occurred upon the addition of TlOTf to a suspension of **2** in THF even with refluxing, and no TlCl was observed to precipitate (Scheme 11). Similarly, no reaction occurred between **2** and KOTf (Scheme 11). Adding AgOTf to a suspension of complex **2** in Et₂O produced no reaction. However, adding 3 equiv of AgOTf to a suspension of **2** in THF solubilized complex **2** in THF. After 5-10 minutes a white precipitate began to form. This reaction resulted in formation of the asymmetric complex

{[HC(pz⁵)₃Ru[P(OCH₂)₃CEt](THF)(OTf)]}[OTf] (**11**) in quantitative yield (Scheme 13) (³¹P NMR = 129.8 ppm). The ¹H NMR spectrum of **11** in THF-*d*₈ reveals a methine C–H and six pyrazolyl resonances as well as phosphite resonances at 4.50 ppm (d, ³J_{PH} = 4 Hz), 1.35 ppm (t, ³J_{HH} = 8 Hz), and 0.88 ppm (q, ³J_{HH} = 8 Hz), and three methyl resonances (Figure 11). The removal of Ag by 2-3 vacuum filtrations through Celite is imperative, as Ag impurities were shown to have adverse effects on subsequent reactions (see Section 3.8). A crystal suitable for an X-ray diffraction study was grown by layering a THF solution of **11** with hexanes (Figure 12). The structure deviates somewhat from strictly octahedral geometry as indicated by the bond angles N(3)-Ru-N(5) (84.8(3) Å), N(5)-Ru-O(4) (97.8(3) Å), N(3)-Ru-O(7) (92.0(3) Å) and O(4)-Ru-O(7) (84.7(3) Å). The trans effect is observable in terms of bond lengths, as Ru–N(1) (2.118(6) Å), trans to P(OCH₂)₃CEt (the ligand with the stronger trans effect), is longer than Ru–N(3), (2.026(6) Å) and Ru–N(5) (2.032(7) Å), trans to triflate and tetrahydrofuran, respectively.



Scheme 13. Synthesis of {[HC(pz⁵)₃Ru[P(OCH₂)₃CEt](THF)(OTf)]}[OTf] (**11**).

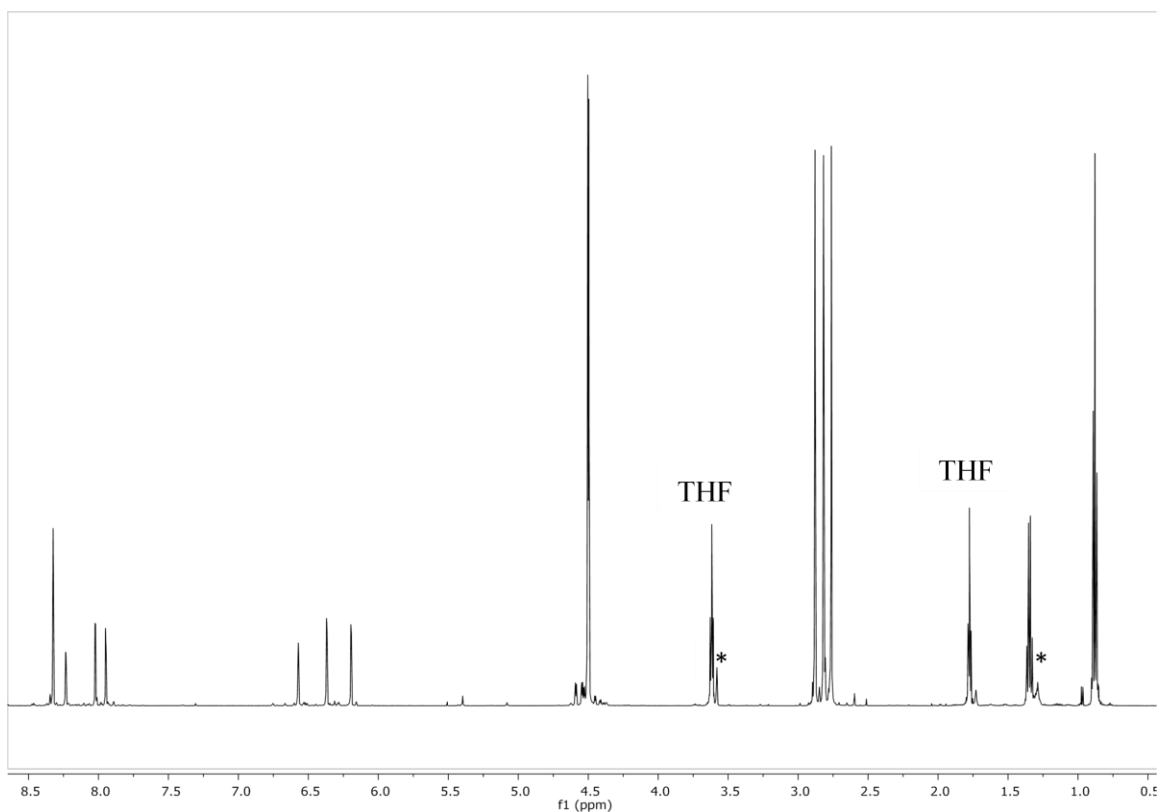


Figure 11. ^1H NMR spectrum (600 MHz, $\text{THF-}d_8$) of $\{[\text{HC}(\text{pz}^5)_3]\text{Ru}[\text{P}(\text{OCH}_2)_3\text{CEt}](\text{THF})(\text{OTf})\}[\text{OTf}]$ (**11**). Solvent resonances denoted by *.

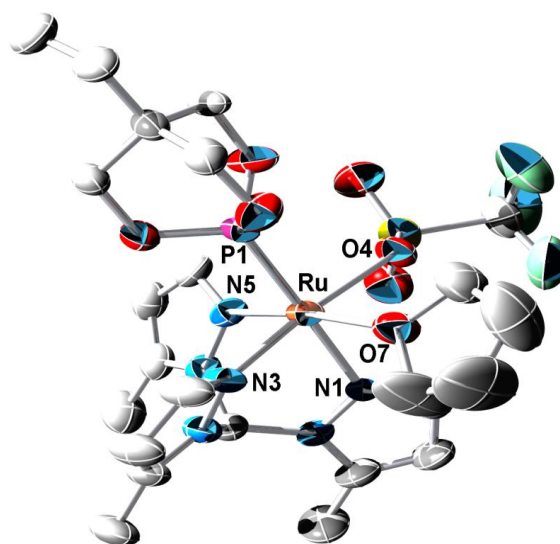
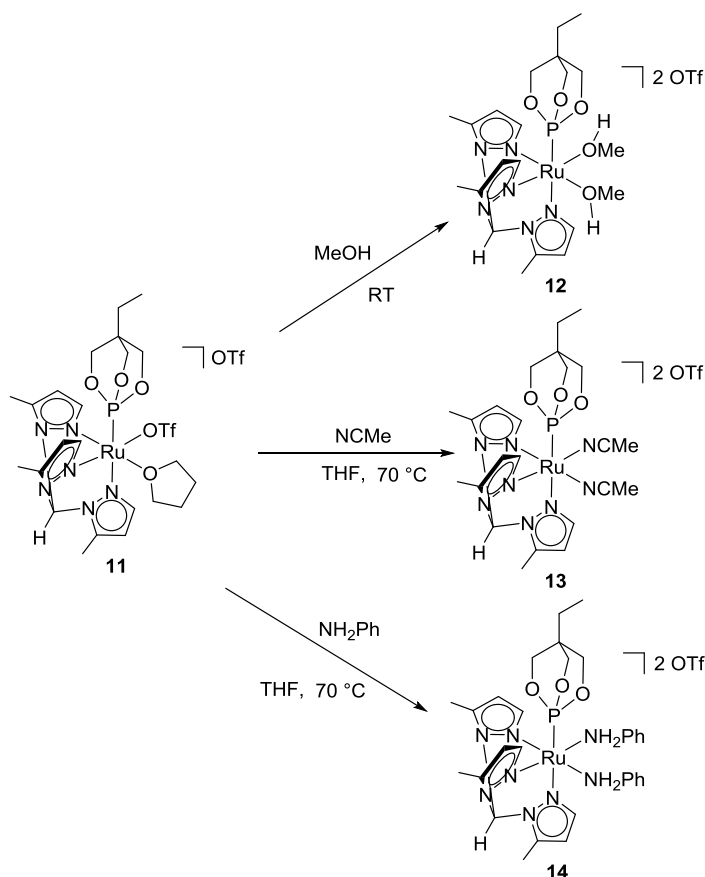


Figure 12. ORTEP of $\{[\text{HC}(\text{pz}^5)_3]\text{Ru}[\text{P}(\text{OCH}_2)_3\text{CEt}](\text{THF})(\text{OTf})\}[\text{OTf}]$ (**11**) (50% probability with H atoms and uncoordinated OTf omitted). Selected bond lengths (\AA): Ru-N(1), 2.118(6); Ru-N(3), 2.026(6); Ru-N(5), 2.032(7); Ru-O(4), 2.153(6); Ru-O(7), 2.138(6); Ru-P(1), 2.205(2). Selected bond angles (deg): N(3)-Ru-N(5), 84.8(3); N(5)-Ru-O(4), 97.8(3); N(3)-Ru-O(7), 92.0(3); O(4)-Ru-O(7), 84.7(3); N(3)-Ru-P(1), 92.4(2); O(4)-Ru-P(1), 92.9(2); O(7)-Ru-P(1), 95.6(2).

3.5 Ligand Substitution Reactions with $\{[\text{HC}(\text{pz}^5)_3]\text{Ru}[\text{P}(\text{OCH}_2)_3\text{CEt}](\text{THF})(\text{OTf})\}[\text{OTf}]$ (**11**)

Since $\{[\text{HC}(\text{pz}^5)_3]\text{Ru}[\text{P}(\text{OCH}_2)_3\text{CEt}](\text{THF})(\text{OTf})\}[\text{OTf}]$ (**11**) possesses two ligands that are likely labile (THF and OTf), attempts were made to coordinate methoxide or anilido. A methanol solution of **11** was stirred overnight to afford the C_s symmetric bis(methanol) complex $\{[\text{HC}(\text{pz}^5)_3]\text{Ru}[\text{P}(\text{OCH}_2)_3\text{CEt}](\text{MeOH})_2\}[\text{OTf}]_2$ (**12**) in ~70-80% yield (Scheme 14) as evidenced by a quartet (5.93 ppm, 1H, $^3J_{\text{HH}} = 4$ Hz) and a doublet (3.35 ppm, 3H, $^3J_{\text{HH}} = 4$ Hz) for coordinated methanol in the ^1H NMR spectrum and a resonance at 130.4 ppm in the ^{31}P NMR spectrum. To confirm that methanol *had* coordinated to the metal center, complex **12** was isolated and reconstituted in THF. Heating the solution resulted in release of free methanol and reversion to **11**. Adding NCMe to a THF- d_8 solution of **11** and heating at 70 °C resulted in the formation of $\{[\text{HC}(\text{pz}^5)_3]\text{Ru}[\text{P}(\text{OCH}_2)_3\text{CEt}](\text{NCMe})_2\}[\text{OTf}]_2$ (**13**) in quantitative yield by ^1H NMR spectroscopy (Scheme 14). A resonance for coordinated NCMe was observed at 2.54 ppm in the ^1H NMR spectrum, and a resonance at 128.8 ppm was visible in the ^{31}P NMR spectrum, in agreement with that of the bis(acetonitrile) complex formed by adding MOTf (M = Ag or Tl) to an CD_3CN solution of **2** (see Section 3.4.2). Adding NH_2Ph to complex **11** in THF- d_8 and heating at 70 °C resulted in the formation of an asymmetric complex $\{[\text{HC}(\text{pz}^5)_3]\text{Ru}[\text{P}(\text{OCH}_2)_3\text{CEt}](\text{NH}_2\text{Ph})(\text{L})\}[\text{OTf}]_n$ (L could be OTf or THF, and n could be 1 or 2, respectively) with two minor products after 20 min in a roughly 4:2:1 ratio. Prolonged heating resulted in formation of $\{[\text{HC}(\text{pz}^5)_3]\text{Ru}[\text{P}(\text{OCH}_2)_3\text{CEt}](\text{NH}_2\text{Ph})_2\}[\text{OTf}]_2$ (**14**) (Scheme 14). LiNHPH was also investigated as a reagent to directly install an anilido ligand, thus circumventing the need to coordinate and deprotonate aniline. The addition of LiNHPH to complex **11** in THF- d_8 at -78 °C appeared to initially deprotonate the methine carbon of $\text{HC}(\text{pz}^5)_3$; however, complex **11** converted to a C_s symmetric species overnight in 38% yield by ^1H NMR spectroscopy, presumably $\{[:\text{C}(\text{pz}^5)_3]\text{Ru}[\text{P}(\text{OCH}_2)_3\text{CEt}](\text{NHPH})_2\}[\text{Li}]$ (**15**). The reaction of **11**

with NaOMe in methanol resulted in decomposition of **11** to intractable products. Most likely, NaOMe deprotonates the methine carbon of HC(pz⁵)₃, which could lead to decomposition.

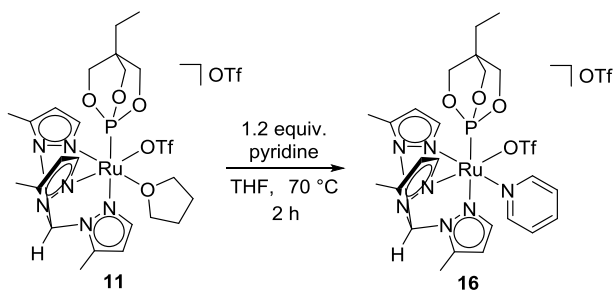


Scheme 14. Reactivity of $\{[\text{HC}(\text{pz}^5)_3]\text{Ru}[\text{P}(\text{OCH}_2)_3\text{CEt}](\text{THF})(\text{OTf})\}[\text{OTf}]$ (**11**) to form dicationic complexes **12-14**.

From these results, it appeared that complex **11** had a strong propensity toward dissociating both THF and OTf to form undesired bis-ligated species $\{[\text{HC}(\text{pz}^5)_3]\text{Ru}[\text{P}(\text{OCH}_2)_3\text{CEt}](\text{L})_2\}[\text{OTf}]_2$ ($\text{L} = \text{NH}_2\text{Ph}$, MeOH, or NCMethylamine) rather than the desired $\{[\text{HC}(\text{pz}^5)_3]\text{Ru}[\text{P}(\text{OCH}_2)_3\text{CEt}](\text{L})(\text{OTf})\}[\text{OTf}]$. Nevertheless, the addition of pyridine to a THF solution of **11** and heating at 70 °C for 2 hours produced $\{[\text{HC}(\text{pz}^5)_3]\text{Ru}[\text{P}(\text{OCH}_2)_3\text{CEt}](\text{py})(\text{OTf})\}[\text{OTf}]$ (**16**) (py = pyridine) in 94% isolated yield (³¹P NMR = 130.0 ppm) (Scheme 15). The ¹H NMR spectrum of **16** shows pyridine resonances at 8.36, 7.81 and 7.31 ppm, and HC(pz⁵)₃ methyl resonances at 2.86 and 2.79 ppm (Figure 13).

While only two methyl resonances were observed, it appears that two of the three methyl resonances coincidentally overlap as six pyrazolyl resonances and a methine resonance are observed supporting the assumption that **16** is asymmetric. A crystal structure was obtained from a crystal grown by layering a DCM solution of **16** with hexanes. While the data for the structure is not of a high enough quality to publish, the structure obtained indicates that the coordinated THF (instead of triflate) of complex **11** was exchanged for pyridine (Figure 14).

Heating the reaction of **11** with pyridine at temperatures higher than 70 °C (e.g., 90 °C) or for longer than 2 hours at 70 °C resulted in conversion to the bis(pyridine) complex $\{[\text{HC}(\text{pz}^5)_3]\text{Ru}[\text{P}(\text{OCH}_2)_3\text{CEt}](\text{py})_2\}[\text{OTf}]_2$ (**17**). It was hypothesized that adding heteroatom ligands to **16** could dissociate triflate to produce asymmetric complexes in which pyridine would serve as a labile ligand. Thus, research efforts were focused on using complex **16** as a precursor to a Ru–X species (X = amido, alkoxo, or hydroxo).



Scheme 15. Synthesis of $\{[\text{HC}(\text{pz}^5)_3]\text{Ru}[\text{P}(\text{OCH}_2)_3\text{CEt}](\text{py})(\text{OTf})\}[\text{OTf}]$ (**16**).

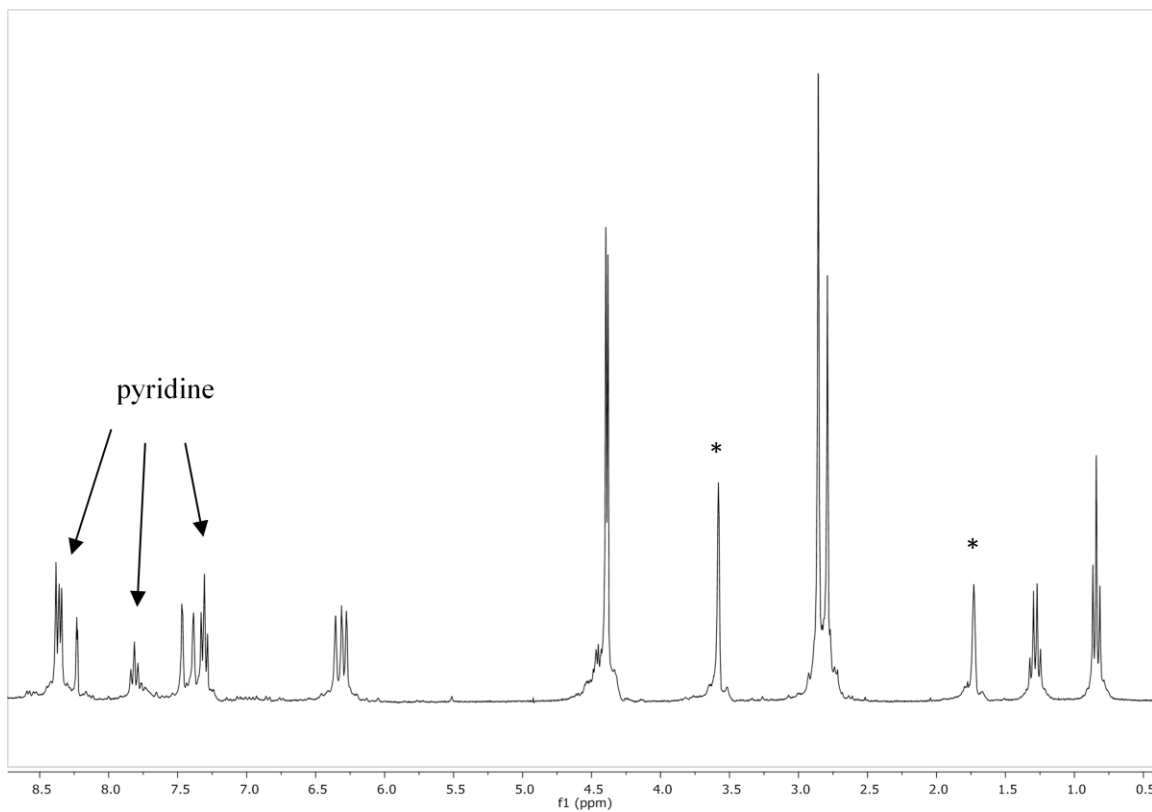


Figure 13. ^1H NMR spectrum (300 MHz, $\text{THF-}d_8$) of $\{[\text{HC}(\text{pz}^5)_3]\text{Ru}[\text{P}(\text{OCH}_2)_3\text{CEt}](\text{py})(\text{OTf})\}[\text{OTf}]$ (**16**). Solvent resonances denoted by *.

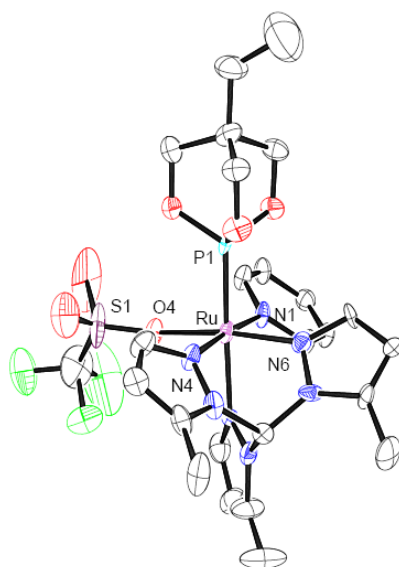
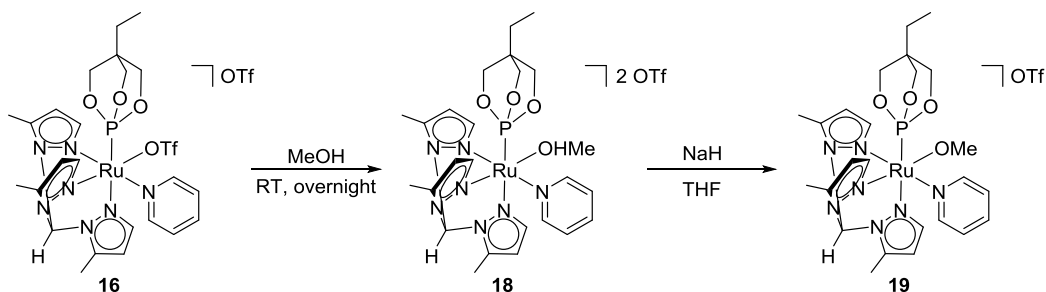


Figure 14. Preliminary crystal structure of $\{[\text{HC}(\text{pz}^5)_3]\text{Ru}[\text{P}(\text{OCH}_2)_3\text{CEt}](\text{py})(\text{OTf})\}[\text{OTf}]$ (**16**).

3.6 Reactivity of $\{[\text{HC}(\text{pz}^5)_3]\text{Ru}[\text{P}(\text{OCH}_2)_3\text{CEt}](\text{py})(\text{OTf})\}[\text{OTf}]$ (**16**)

Stirring a solution of $\{[\text{HC}(\text{pz}^5)_3]\text{Ru}[\text{P}(\text{OCH}_2)_3\text{CEt}](\text{py})(\text{OTf})\}[\text{OTf}]$ (**16**) in H_2O at room temperature for 24 h resulted in recovery of the starting material. Thus, attempting to make Ru–aqua and subsequent Ru–hydroxo complexes via this synthetic route was not successful. Stirring **16** in methanol at room temperature overnight led to the formation of $\{[\text{HC}(\text{pz}^5)_3]\text{Ru}[\text{P}(\text{OCH}_2)_3\text{CEt}](\text{py})(\text{MeOH})\}[\text{OTf}]_2$ (**18**) in ~60% yield as evidenced by coordinated pyridine resonances at 8.32, 7.83, and 7.35 ppm and a quartet at 6.16 ppm ($^3J_{\text{HH}} = 4$ Hz, $-\text{OH}$) and doublet at 3.19 ppm ($^3J_{\text{HH}} = 4$ Hz, $-\text{CH}_3$) for coordinated methanol in the ^1H NMR spectrum ($\text{THF-}d_8$) (Scheme 16, Figure 15). Deprotonation of **18** in $\text{THF-}d_8$ with NaH produced the corresponding methoxide complex $\{[\text{HC}(\text{pz}^5)_3]\text{Ru}[\text{P}(\text{OCH}_2)_3\text{CEt}](\text{py})(\text{OMe})\}[\text{OTf}]$ (**19**) in quantitative yield. The ^1H NMR spectrum of **19** shows the disappearance of the OH resonance and formation of a singlet at 3.09 ppm due to the coordinated methoxide (Scheme 16, Figure 15).



Scheme 16. Synthesis of $\{[\text{HC}(\text{pz}^5)_3]\text{Ru}[\text{P}(\text{OCH}_2)_3\text{CEt}](\text{py})(\text{MeOH})\}[\text{OTf}]_2$ (**18**) and $\{[\text{HC}(\text{pz}^5)_3]\text{Ru}[\text{P}(\text{OCH}_2)_3\text{CEt}](\text{py})(\text{OMe})\}[\text{OTf}]$ (**19**).

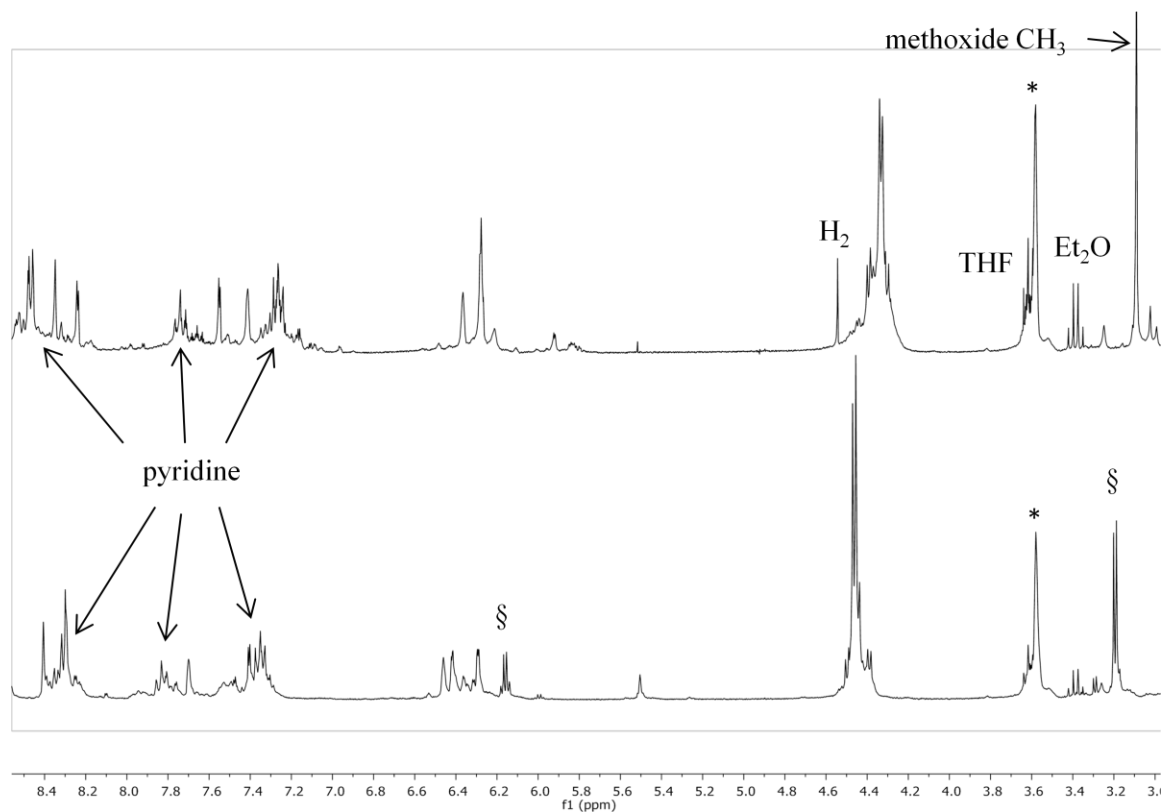
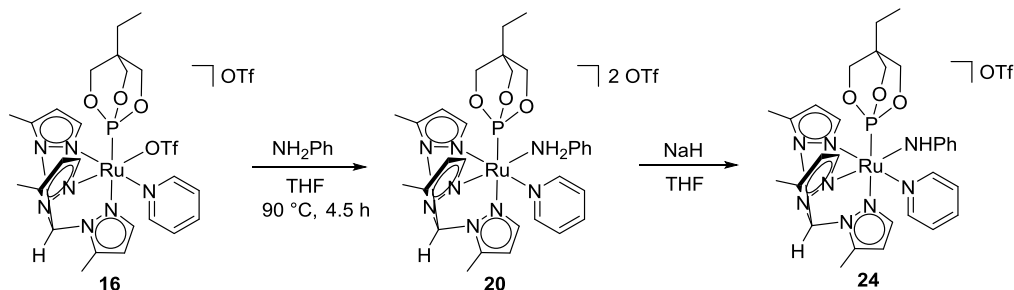


Figure 15. ^1H NMR (300 MHz, $\text{THF-}d_8$) spectra of $\{[\text{HC}(\text{pz}^5)_3]\text{Ru}[\text{P}(\text{OCH}_2)_3\text{CEt}](\text{py})(\text{MeOH})\}[\text{OTf}]_2$ (**18**) (bottom) and $\{[\text{HC}(\text{pz}^5)_3]\text{Ru}[\text{P}(\text{OCH}_2)_3\text{CEt}](\text{py})(\text{OMe})\}[\text{OTf}]$ (**19**) (top). Solvent resonances denoted by *. Coordinated methanol resonances denoted by §.

Combining complex **16** with LiNHPH at -78 $^\circ\text{C}$ to make $\{[\text{HC}(\text{pz}^5)_3]\text{Ru}[\text{P}(\text{OCH}_2)_3\text{CEt}](\text{py})(\text{NHPH})\}[\text{OTf}]$ did not produce a visible reaction. Adding NH_2Ph to a THF solution of **16** and heating at 90 $^\circ\text{C}$ for ~ 4.5 h afforded $\{[\text{HC}(\text{pz}^5)_3]\text{Ru}[\text{P}(\text{OCH}_2)_3\text{CEt}](\text{py})(\text{NH}_2\text{Ph})\}[\text{OTf}]_2$ (**20**) in $\sim 70\%$ yield, as evidenced by the ^1H and ^{31}P NMR spectra (^{31}P NMR = 133.1 ppm) (Scheme 17). The ^1H NMR spectrum of **20** reveals pyridine resonances at 8.54, 7.80, and 7.38 ppm; phenyl resonances are observed at 6.93 and 6.75 ppm, and doublets due to the diastereotopic NH_2 group are observed at 6.33 and 6.05 ppm ($^2J_{\text{HH}} = 12$ Hz) (Figure 16). $\text{HC}(\text{pz}^5)_3$ methyl resonances are observed in 1:1:1 intensity. The ^1H NMR resonance of the diastereotopic methylene groups of $\text{P}(\text{OCH}_2)_3\text{CEt}$ displays a distinctive non-first order splitting pattern at 4.51 ppm (Figure 16 inset), instead of a doublet as usually observed. A

minor symmetric product was also formed and confirmed to be $[[\text{HC}(\text{pz}^5)_3]\text{Ru}[\text{P}(\text{OCH}_2)_3\text{CEt}](\text{py})_2][\text{OTf}]_2$ (**17**) through independent synthesis (the reaction of **14** with pyridine in THF at 90 °C yielded complex **17**).



Scheme 17. Synthesis of $\{[\text{HC}(\text{pz}^5)_3]\text{Ru}[\text{P}(\text{OCH}_2)_3\text{CEt}](\text{py})(\text{NH}_2\text{Ph})\}[\text{OTf}]_2$ (**20**) and $\{[\text{HC}(\text{pz}^5)_3]\text{Ru}[\text{P}(\text{OCH}_2)_3\text{CEt}](\text{py})(\text{NHPh})\}[\text{OTf}]$ (**24**).

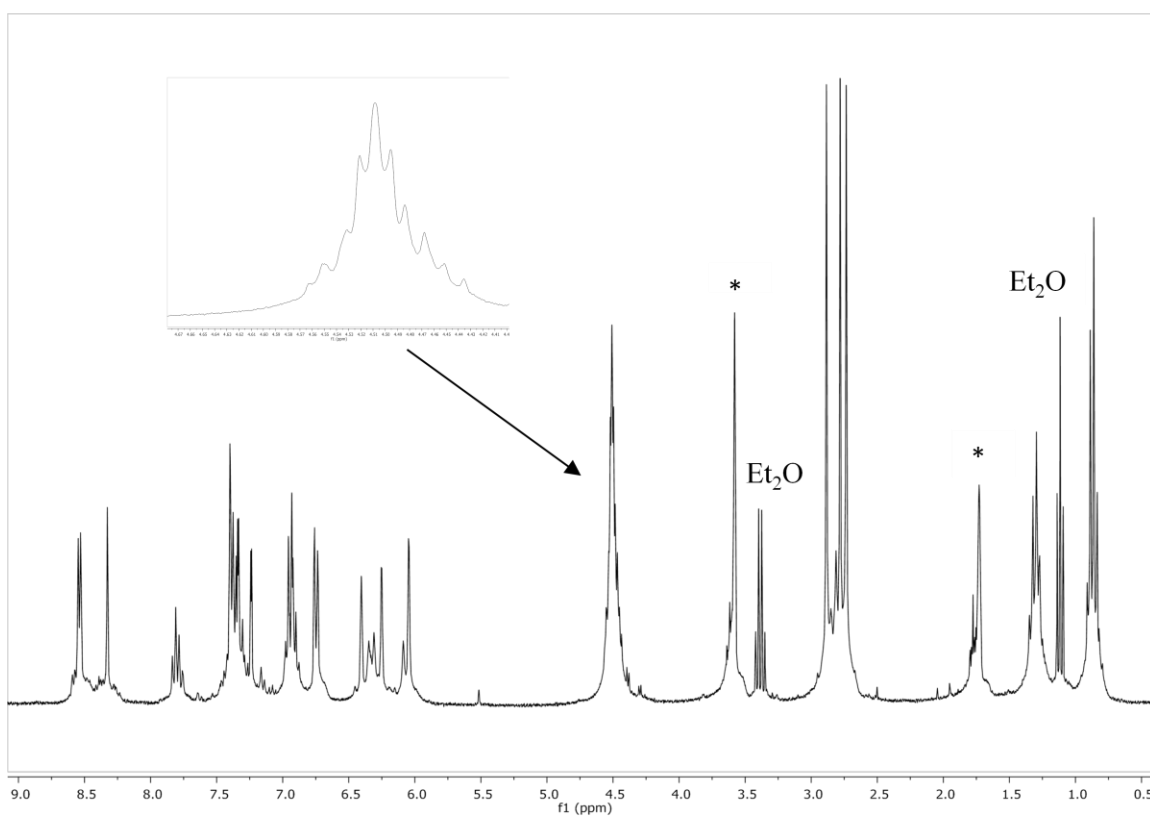
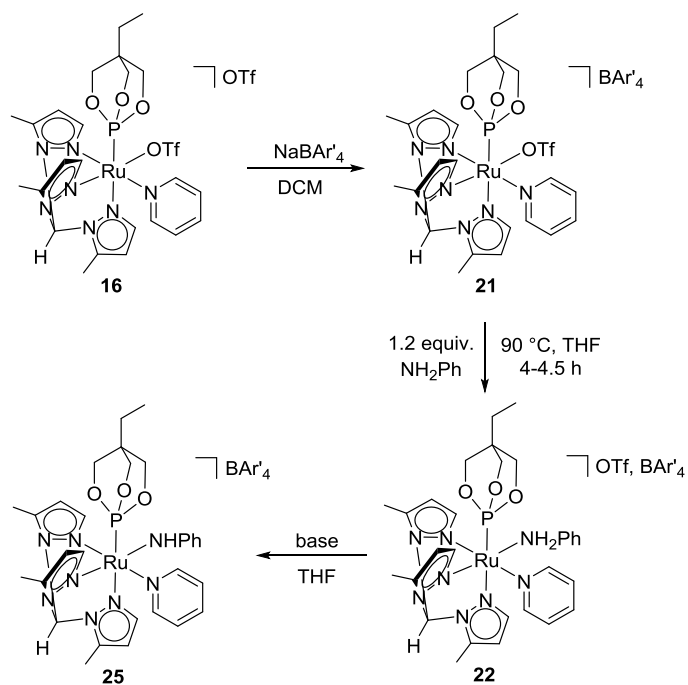


Figure 16. ^1H NMR spectrum (300 MHz, $\text{THF-}d_8$) of $\{[\text{HC}(\text{pz}^5)_3]\text{Ru}[\text{P}(\text{OCH}_2)_3\text{CEt}](\text{py})(\text{NH}_2\text{Ph})\}[\text{OTf}]_2$ (**20**). Solvent resonances denoted by *.

The reaction of complex **16** with NH_2Ph to make complex **20** was observed to decompose to intractable products approximately 50% of the times the reaction was attempted. Experimenting with temperature and reaction time did not improve reaction success rate. It was finally discovered that reaction failure was the result of insufficient removal of Ag impurities from the precursor complexes **11** and **16**. Rigorously removing Ag compounds from $\{[\text{HC}(\text{pz}^5)_3]\text{Ru}[\text{P}(\text{OCH}_2)_3\text{CEt}](\text{THF})(\text{OTf})\}[\text{OTf}]$ (**11**) unfortunately decreased the solubility of $\{[\text{HC}(\text{pz}^5)_3]\text{Ru}[\text{P}(\text{OCH}_2)_3\text{CEt}](\text{py})(\text{OTf})\}[\text{OTf}]$ (**16**) in THF. This issue with solubility also prevented successful synthesis of **20**. A counterion exchange of OTf with BAR'_4 with the complex **16** to produce $\{[\text{HC}(\text{pz}^5)_3]\text{Ru}[\text{P}(\text{OCH}_2)_3\text{CEt}](\text{py})(\text{OTf})\}[\text{BAR}'_4]$ (**21**) improved solubility in THF (Scheme 18). The scaled-up synthesis of $\{[\text{HC}(\text{pz}^5)_3]\text{Ru}[\text{P}(\text{OCH}_2)_3\text{CEt}](\text{py})(\text{NH}_2\text{Ph})\}[\text{OTf}][\text{BAR}'_4]$ (**22**) from **21** was successful and effectively optimized.

The removal of $\{[\text{HC}(\text{pz}^5)_3]\text{Ru}[\text{P}(\text{OCH}_2)_3\text{CEt}](\text{py})_2\}[\text{OTf}][\text{BAR}'_4]$ (**23**), the minor side product formed during the synthesis of $\{[\text{HC}(\text{pz}^5)_3]\text{Ru}[\text{P}(\text{OCH}_2)_3\text{CEt}](\text{py})(\text{NH}_2\text{Ph})\}[\text{OTf}][\text{BAR}'_4]$ (**22**), presented another challenge. Multiple methods of purifying **22** were explored. Complex **23** was finally removed via chromatography on silica gel (see Experimental Section). The ^1H NMR spectrum of $\{[\text{HC}(\text{pz}^5)_3]\text{Ru}[\text{P}(\text{OCH}_2)_3\text{CEt}](\text{py})(\text{NH}_2\text{Ph})\}[\text{OTf}][\text{BAR}'_4]$ (**22**) in $\text{DCM-}d_2$ is shown in Figure 17; coordinated pyridine resonances are visible at 8.02, 7.80, and 7.30 ppm, aniline phenyl resonances are observed at 7.06 (m) and 6.49 ppm (d, $^3J_{\text{HH}} = 8$ Hz), and NH_2 doublets are observed at 5.23 and 5.02 ppm ($^2J_{\text{HH}} = 12$ Hz). $\text{HC}(\text{pz}^5)_3$ methyl resonances are observed in 1:1:1 intensity. The ^1H NMR resonance of the diastereotopic methylene groups of $\text{P}(\text{OCH}_2)_3\text{CEt}$ once again displays a distinctive non-first order splitting pattern at 4.40 ppm (Figure 17 inset). A crystal suitable for an X-ray diffraction study was grown by slow evaporation from a THF solution of **22** (Figure 18). The bond $\text{Ru-N}(7)$ (2.138 Å) trans to $\text{P}(\text{OCH}_2)_3\text{CEt}$ is longer than the corresponding bonds $\text{Ru-N}(3)$ (2.068 Å) and $\text{Ru-N}(5)$ (2.094 Å) trans to aniline and pyridine, respectively. This observation is due to the phosphite ligand having a larger trans effect.



Scheme 18. Synthesis of $\{[\text{HC}(\text{pz}^5)_3\text{Ru}[\text{P}(\text{OCH}_2)_3\text{CEt}](\text{py})(\text{OTf})]\}[\text{BAR}'_4]$ (**21**), $\{[\text{HC}(\text{pz}^5)_3\text{Ru}[\text{P}(\text{OCH}_2)_3\text{CEt}](\text{py})(\text{NH}_2\text{Ph})]\}[\text{OTf}][\text{BAR}'_4]$ (**22**), and $\{[\text{HC}(\text{pz}^5)_3\text{Ru}[\text{P}(\text{OCH}_2)_3\text{CEt}](\text{py})(\text{NHPH})]\}[\text{BAR}'_4]$ (**25**).

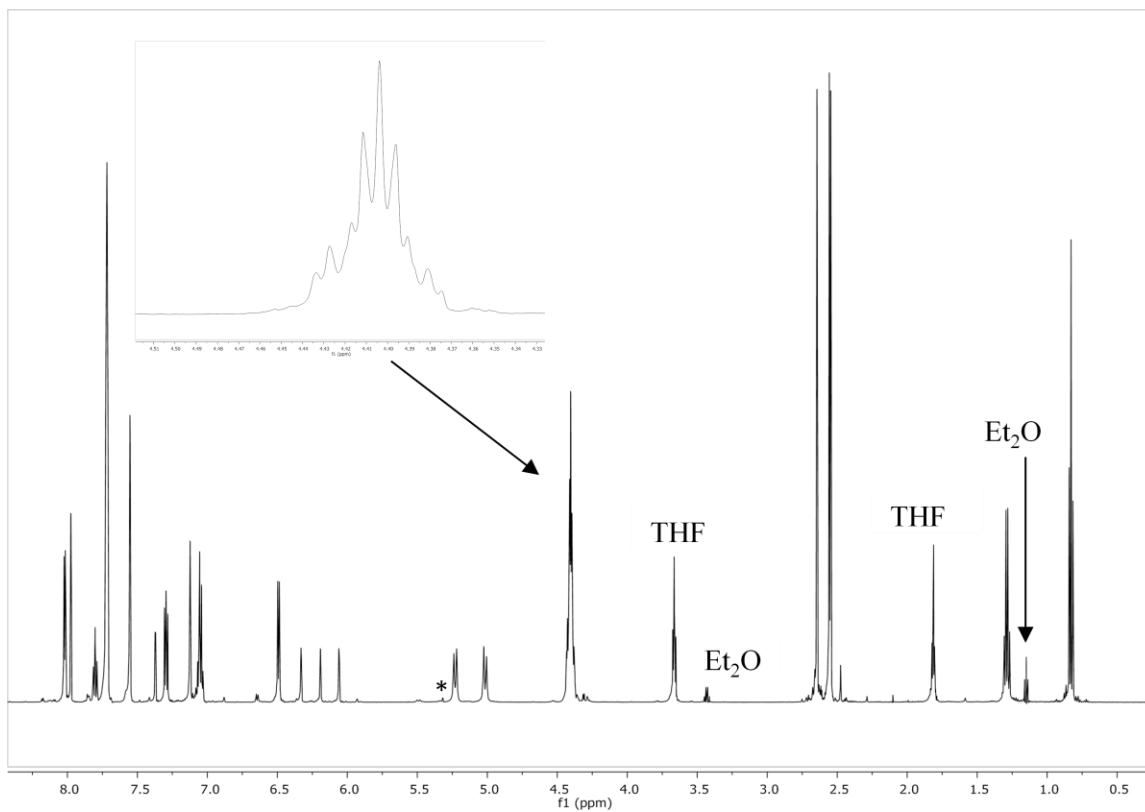


Figure 17. ^1H NMR spectrum (600 MHz, CD_2Cl_2) of $\{[\text{HC}(\text{pz}^5)_3]\text{Ru}[\text{P}(\text{OCH}_2)_3\text{CEt}](\text{py})(\text{NH}_2\text{Ph})\}[\text{OTf}][\text{BAR}'_4]$ (**22**). Inset: Non-first order splitting pattern of $\text{P}(\text{OCH}_2)_3\text{CEt}$ diastereotopic methylene groups. Solvent resonance denoted by *.

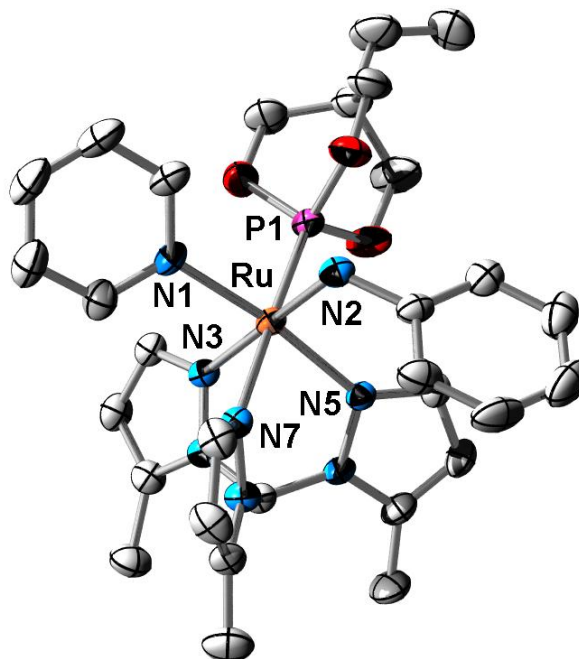


Figure 18. ORTEP of $\{[\text{HC}(\text{pz}^5)_3]\text{Ru}[\text{P}(\text{OCH}_2)_3\text{CEt}](\text{py})(\text{NH}_2\text{Ph})\}[\text{OTf}][\text{BAr}'_4]$ (**22**) (50% probability ellipsoids with H atoms and counterions omitted). Selected bond lengths (Å): Ru-N(1), 2.092; Ru-N(2), 2.155; Ru-N(3), 2.068; Ru-N(5), 2.094; Ru-N(7), 2.138; Ru-P(1), 2.195. Selected bond angles (deg): N(1)-Ru-N(2), 86.77; N(1)-Ru-N(3), 90.83; N(3)-Ru-N(5), 84.46; N(5)-Ru-N(2), 97.39; N(1)-Ru-N(7), 89.20; N(2)-Ru-N(7), 89.04; N(5)-Ru-N(7), 84.95.

Adding NaH to **20** resulted in a deprotonated species, the putative $\{[\text{HC}(\text{pz}^5)_3]\text{Ru}[\text{P}(\text{OCH}_2)_3\text{CEt}](\text{py})(\text{NHPh})\}[\text{OTf}]$ (**24**), in quantitative yield (Scheme 15). Irreproducible results were observed upon pressurizing $\{[\text{HC}(\text{pz}^5)_3]\text{Ru}[\text{P}(\text{OCH}_2)_3\text{CEt}](\text{py})(\text{NHPh})\}^+$ with H_2 and heating (see section whatever)—that is, different Ru hydride complexes would be observed in differing ratios during H_2 activation. At times, the putative anilido complex would decompose upon heating. Improvement of the work-up procedures of precursor complexes **11**, **16** and **22** promoted consistent reactivity with H_2 in terms of product identities and amounts. However, the method of deprotonating $\{[\text{HC}(\text{pz}^5)_3]\text{Ru}[\text{P}(\text{OCH}_2)_3\text{CEt}](\text{py})(\text{NH}_2\text{Ph})\}[\text{OTf}]_2$ (**20**) or $\{[\text{HC}(\text{pz}^5)_3]\text{Ru}[\text{P}(\text{OCH}_2)_3\text{CEt}](\text{py})(\text{NH}_2\text{Ph})\}[\text{OTf}][\text{BAr}'_4]$ (**22**) was found to play a key role in whether the resulting species would successfully activate H_2 . The base initially used to

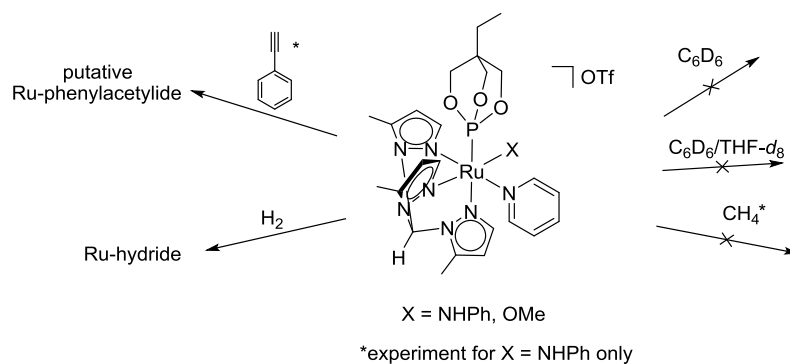
synthesize $\{[\text{HC}(\text{pz}^5)_3]\text{Ru}[\text{P}(\text{OCH}_2)_3\text{CEt}](\text{py})(\text{NHPh})\}[\text{OTf}]$ (**24**) or $\{[\text{HC}(\text{pz}^5)_3]\text{Ru}[\text{P}(\text{OCH}_2)_3\text{CEt}](\text{py})(\text{NHPh})\}[\text{BAr}'_4]$ (**25**) was NaH. NaH is insoluble in THF and can be easily removed via vacuum filtration. However, the heterogeneous reaction between NaH and **24** or **25** is difficult to control. During the reaction between NaH and **24** or **25**, effervescence (presumably due to formation of H_2) is observed along with a reaction solution color change from purple to red. Immediate isolation after the reaction mixture turned red often resulted in incomplete reaction (starting material observed in solution along with product). Extended reaction times would result in the relatively clean formation of an undesired asymmetric complex that was not stable. This undesired product, complex **26**, has not been conclusively identified. Coordinated phenyl resonances are observed at 5.59 ppm (d, $^3J_{\text{HH}} = 8$ Hz) and 5.54 ppm (t, $^3J_{\text{HH}} = 7$ Hz), coordinated pyridine resonances are observed at 8.43, 7.06, and 6.24 ppm, but no methine proton is observed in the ^1H NMR spectrum of **26**. Thus, other bases for the synthesis of **25** were explored.

Adding MeLi to $\{[\text{HC}(\text{pz}^5)_3]\text{Ru}[\text{P}(\text{OCH}_2)_3\text{CEt}](\text{py})(\text{NH}_2\text{Ph})\}[\text{OTf}][\text{BAr}'_4]$ (**22**) in THF at -78 °C resulted in multiple intractable products. Adding ~1 equivalent of KO^tBu to **22** in THF resulted in **26**. Adding 1.1 eq of NaHMDS to **22** in THF at room temperature resulted in formation of the desired major and minor putative anilido complexes, at first thought to be rotamers. However, high temperature VT NMR spectroscopy (from room temperature to 105 °C) did not show the coalescence of these two species that was expected if the complexes had been rotamers. The identities of these two complexes will be discussed in depth in Chapter 4.

Adding too much NaHMDS (> 1.2 eq) to **22** was discovered to result in formation of **26**. These observations indicated that the synthesis of **25** is very sensitive to the amount of base added, consistent with the results of reactions between **20** and **22**. Going forward, NaHMDS was used in the synthesis of **25**.

3.7 Initial Experiments Exploring the Reactivity of $\{[\text{HC}(\text{pz}^5)_3]\text{Ru}[\text{P}(\text{OCH}_2)_3\text{CEt}](\text{py})(\text{X})\}^+$ ($\text{X} = \text{NHPH}, \text{OMe}$)

Preliminary experiments were conducted to probe the reactivity of $\{[\text{HC}(\text{pz}^5)_3]\text{Ru}[\text{P}(\text{OCH}_2)_3\text{CEt}](\text{py})(\text{X})\}^+$ ($\text{X} = \text{NHPH}, \text{OMe}$) towards C–H and H₂ bond activation (Scheme 19). $\{[\text{HC}(\text{pz}^5)_3]\text{Ru}[\text{P}(\text{OCH}_2)_3\text{CEt}](\text{py})(\text{NHPH})\}^+$ exhibited no desired C–H activation of C₆D₆, either in neat C₆D₆ at 70–120 °C or in a mixture of THF-*d*₈ and C₆D₆ at 110 °C or 120 °C. Instead, decomposition to multiple products was observed under these conditions. Pressurizing $\{[\text{HC}(\text{pz}^5)_3]\text{Ru}[\text{P}(\text{OCH}_2)_3\text{CEt}](\text{py})(\text{NHPH})\}^+$ with 25 psi of CH₄ in THF-*d*₈ and heating at 110 °C also led to multiple intractable products, none of which appeared to be the result of C–H activation of methane as no resonances due to a Ru–Me group were observed by ¹H NMR spectroscopy. However, the reaction of $\{[\text{HC}(\text{pz}^5)_3]\text{Ru}[\text{P}(\text{OCH}_2)_3\text{CEt}](\text{py})(\text{NHPH})\}^+$ with phenylacetylene in THF-*d*₈ at room temperature produced the putative $\{[\text{HC}(\text{pz}^5)_3]\text{Ru}[\text{P}(\text{OCH}_2)_3\text{CEt}](\text{NH}_2\text{Ph})(\text{phenylacetylidide})\}^+$ (**27**) in an ~1:1 ratio with an unidentified species. Evidence for formation of **27** includes observation of an AB pattern for an NH₂ group (²J_{HH} = 10 Hz) at 4.92 ppm. The reaction did not go to completion at room temperature, and heating the reaction mixture at 70 °C resulted in decomposition. It was found that pressurizing a solution of $\{[\text{HC}(\text{pz}^5)_3]\text{Ru}[\text{P}(\text{OCH}_2)_3\text{CEt}](\text{py})(\text{NHPH})\}^+$ in THF-*d*₈ with 25 psi of H₂ and heating at 110 °C resulted in the formation of hydride species with resonances at -14.2, -15.6, and -17.3 ppm (all doublets, ²J_{PH} = 40 Hz) and free aniline, suggestive of H₂ activation.



Scheme 19. Initial 1,2-CH and HH-addition experiments with $\{[\text{HC}(\text{pz}^5)_3]\text{Ru}[\text{P}(\text{OCH}_2)_3\text{CEt}](\text{py})(\text{X})\}^+$ (X = NHPH, OMe).

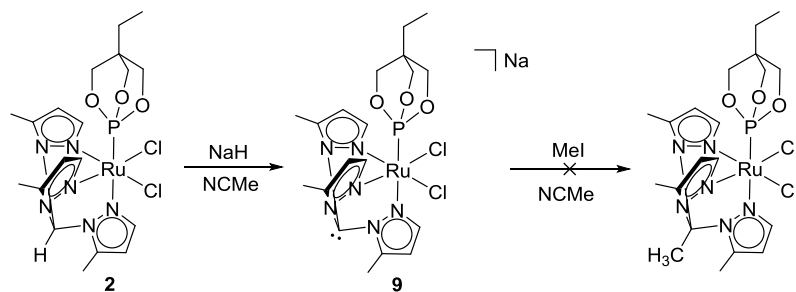
Furthermore, pressurizing a solution of $\{[\text{HC}(\text{pz}^5)_3]\text{Ru}[\text{P}(\text{OCH}_2)_3\text{CEt}](\text{py})(\text{OMe})\}^+$ with H_2 in $\text{THF-}d_8$ and heating at $80\text{ }^\circ\text{C}$ was found to produce a hydride complex and free methanol. The final hydride product of both the Ru–NHPH and Ru–OMe H_2 activation reactions are identical.

3.8 Attempted Methylation of the $\text{HC}(\text{pz}^5)_3$ Backbone

Attempts to install a methyl group on the methine carbon of $\text{HC}(\text{pz}^5)_3$ were conducted with the desire to eliminate potential issues arising from the deprotonation of the acidic methine of $\text{HC}(\text{pz}^5)_3$ (Scheme 20). The steric hindrance of the methyl groups in the 5-positions of the pyrazolyl rings could make alkylating the methine position difficult, and to our knowledge, a procedure for the synthesis of $\text{MeC}(\text{pz}^5)_3$ has not been published at the time the following experiments were conducted.

$[\text{HC}(\text{pz}^5)_3]\text{Ru}[\text{P}(\text{OCH}_2)_3\text{CEt}](\text{Cl})_2$ (**2**) was deprotonated with NaH in acetonitrile and in THF to form $\{[:\text{C}(\text{pz}^5)_3]\text{Ru}[\text{P}(\text{OCH}_2)_3\text{CEt}](\text{Cl})_2\}[\text{Na}]$ (**8**) as evidenced by the $\text{HC}(\text{pz}^5)_3$ methine C–H resonance missing in the ^1H NMR spectra. The solution was decanted off the NaH and MeI was added to the deprotonated complex **8**. Conversion to a new C_s symmetric complex was observed by ^1H NMR spectroscopy. The new complex exhibits four pyrazolyl resonances integrating to 6 protons in a 2:1:2:1 pattern. A resonance due to the C–H group of $\text{HC}(\text{pz}^5)_3$ was not observed. It was difficult to determine if any of the resonances in the upfield region

corresponded to a new methyl group due to impurities formed by the reaction with MeI. Therefore, the product was isolated and reconstituted in DCM- d_2 . The ^1H NMR spectrum of putative $[\text{MeC}(\text{pz}^5)_3]\text{Ru}[\text{P}(\text{OCH}_2)_3\text{CEt}](\text{Cl})_2$ appeared to show a methyl resonance at 3.41 ppm. However, when the sample was dried and reconstituted in DCM- d_2 a second time, this resonance decreased in intensity. A third isolation and reconstitution in NCMe- d_3 decreased the peak even more, indicating that this resonance was actually an impurity being removed. The addition of MeI to $\{[:\text{C}(\text{pz}^5)_3]\text{Ru}[\text{P}(\text{OCH}_2)_3\text{CEt}](\text{Cl})_2\}[\text{Na}]$ was repeated, and the putative methyl resonance was not present in the ^1H NMR spectrum, confirming that the methide carbon of $:\text{C}(\text{pz}^5)_3$ had not been successfully methylated. The identity of the product of the reaction between $\{[:\text{C}(\text{pz}^5)_3]\text{Ru}[\text{P}(\text{OCH}_2)_3\text{CEt}](\text{Cl})_2\}[\text{Na}]$ and MeI was not confirmed, but a halide exchange to produce $\{[:\text{C}(\text{pz}^5)_3]\text{Ru}[\text{P}(\text{OCH}_2)_3\text{CEt}](\text{I})_2\}[\text{Na}]$ was hypothesized. Attempts at methylating $\text{HC}(\text{pz}^5)_3$ were no longer pursued.



Scheme 20. Attempted methylation of the $\text{HC}(\text{pz}^5)_3$ backbone.

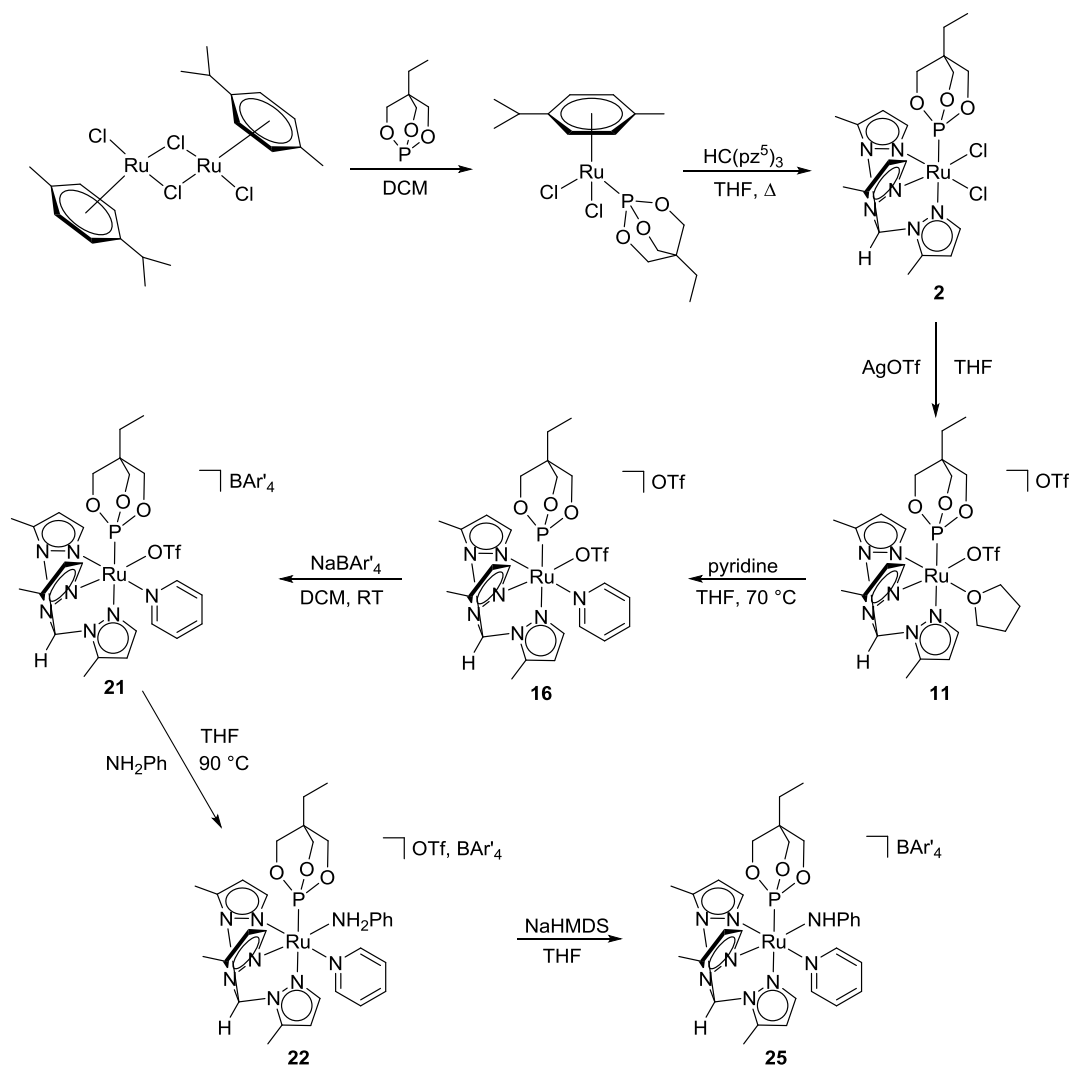
3.9 Conclusions

$[\text{HC}(\text{pz}^5)_3]\text{Ru}[\text{P}(\text{OCH}_2)_3\text{CEt}](\text{Cl})_2$ was synthesized by refluxing $\text{HC}(\text{pz}^5)_3$ with (p-cymene) $\text{Ru}[\text{P}(\text{OCH}_2)_3\text{CEt}](\text{Cl})_2$. Using multiple ligand exchange reactions, the $\text{Ru}-\text{X}$ ($\text{X} = \text{OMe}$ or NHPH) complexes $\{[\text{HC}(\text{pz}^5)_3]\text{Ru}[\text{P}(\text{OCH}_2)_3\text{CEt}](\text{py})(\text{OMe})\}^+$ and $\{[\text{HC}(\text{pz}^5)_3]\text{Ru}[\text{P}(\text{OCH}_2)_3\text{CEt}](\text{py})(\text{NHPH})\}^+$ were synthesized using $[\text{HC}(\text{pz}^5)_3]\text{Ru}[\text{P}(\text{OCH}_2)_3\text{CEt}](\text{Cl})_2$ as a precursor. $\{[\text{HC}(\text{pz}^5)_3]\text{Ru}[\text{P}(\text{OCH}_2)_3\text{CEt}](\text{py})(\text{OMe})\}^+$

and $\{[\text{HC}(\text{pz}^5)_3]\text{Ru}[\text{P}(\text{OCH}_2)_3\text{CEt}](\text{py})(\text{NHPh})\}^+$ were found to be capable of H_2 activation to produce a Ru–hydride complex and free methanol and aniline, respectively.

Attempting to methylate the backbone of $\text{HC}(\text{pz}^5)_3$ while the ligand was coordinated to Ru was unsuccessful. This is probably due to steric influences of the methyl groups on the pyrazolyl rings. Evidently, coordination to the metal center does not “spread” the methyl groups far apart enough to allow sufficient space for a methylating reagent to react with the methide carbon of the poly(pyrazolyl)alkane. This strategy might work, however, if $\text{HC}(\text{pz}^5)_3$ were coordinated to a smaller metal atom such as Fe—the bite angles of the ligand would decrease with a smaller metal, thus pulling the methyl groups farther from the backbone carbon.⁷ The synthesis of the ligand $\text{MeC}(\text{pz}^5)_3$ and its coordination to Fe(II) ($[(\text{MeC}(\text{pz}^5)_3)\text{Fe}][\text{BF}_4]_2$) has since been reported.⁷

The overall synthetic procedure to produce $\{[\text{HC}(\text{pz}^5)_3]\text{Ru}[\text{P}(\text{OCH}_2)_3\text{CEt}](\text{py})(\text{NHPh})\}[\text{BAr}'_4]$, the focus of chapter 4, is as follows (Scheme 21):



Scheme 21. Overall synthetic procedure for $\{[\text{HC}(\text{pz}^5)_3]\text{Ru}[\text{P}(\text{OCH}_2)_3\text{CEt}](\text{py})(\text{NHPh})\}[\text{BAR}'_4]$ (**25**).

3.10 Experimental Section

General Considerations. Unless otherwise noted, all synthetic procedures were performed under anaerobic conditions in a nitrogen-filled glovebox or by using standard Schlenk techniques. Glovebox purity was maintained by periodic nitrogen purges and was monitored by an oxygen analyzer ($\text{O}_2 < 15$ ppm for all reactions). Tetrahydrofuran and *n*-pentane were dried by distillation from sodium/benzophenone and P_2O_5 , respectively. Diethyl ether and acetonitrile was distilled over CaH_2 . Benzene, methylene chloride, and hexanes were purified by passage through

a column of activated alumina. Benzene-*d*₆, acetone-*d*₆, CD₃CN, CD₂Cl₂, and CDCl₃ were used as received and stored under a N₂ atmosphere over 4Å molecular sieves. THF-*d*₈ was distilled over sodium/benzophenone and stored over 4Å molecular sieves. ¹H NMR spectra were recorded on a Varian 300 MHz, Varian 500 MHz or a Bruker 600 MHz or 800 MHz spectrometer, and ¹³C{¹H} NMR spectra were recorded on a Bruker 600 MHz (operating frequency = 150 MHz) or a Bruker 800 MHz (operating frequency = 201 MHz). All ¹H and ¹³C spectra are referenced against residual proton signals (¹H NMR) or ¹³C resonances (¹³C NMR) of the deuterated solvents. ³¹P{¹H} NMR spectra were obtained on a Varian 300 MHz (operating frequency = 121 MHz), Varian 500 MHz (operating frequency = 201 MHz) or Varian 600 MHz (operating frequency = 243 MHz) spectrometer and referenced against an external standard of H₃PO₄ (δ = 0). ¹⁹F{¹H} NMR spectra were obtained on a Varian 300 MHz (operating frequency = 282 MHz) or a Varian 600 MHz (operating frequency = 565 MHz) and referenced against an internal standard of hexafluorobenzene (δ = -164.9). High-resolution mass spectra were acquired in electrospray ionization (ESI) mode from samples dissolved in a 3:1 acetonitrile/water solution containing sodium trifluoroacetate (NaTFA). Mass spectra are reported for M⁺ for monocationic complexes, M²⁺ for dicationic complexes, or [M + Na⁺] for neutral complexes, using [Na(NaTFA)_{*x*}]⁺ clusters as an internal standard. In all cases, observed isotopic envelopes were consistent with the molecular composition reported. Spectra were collected by Dr. William Myers (University of Richmond) on a Bruker BioTOF-Q, a PerkinElmer Axion2 TOF, a Shimadzu IT-TOF, a Bruker MaXis Impact, an Agilent 6230 TOF, or a Waters Xevo G2Qtof. X-ray diffraction studies were performed by Dr. Michal Sabat (Department of Materials Science and Engineering, University of Virginia). Tris(5-methyl-pyrazolyl)methane was synthesized according to a previously reported procedure.⁸ All other reagents were used as received from the manufacturers.

[HC(pz⁵)₃]Ru(PPh₃)(Cl)₂ (1). Tris(5-methyl-pyrazolyl)methane (0.054 g, 0.208 mmol) was added to a solution of Ru(PPh₃)₃(Cl)₂ (0.223 g, 0.233 mmol) in ~30 mL of toluene. The

reaction mixture was refluxed for 18 h, after which it was cooled. Hexanes were added to further precipitate the yellow solid that had formed; solid was collected on a fine porosity frit and washed with toluene, followed by washing with pentane to yield **1** in 99% yield (0.119 g). ^1H NMR (300 MHz, CDCl_3) δ = 8.43 (1H, $\text{HC}(\text{pz}^5)_3$), 6.42 (2H, d, $^3J_{\text{HH}} = 2$ Hz, pz 3-position), 6.20 (1H, pz 4-position), 5.69 (2H, pz 4-position), 7.79 (m, phenyl), 7.26 (m, phenyl), 2.56 (6H, $\text{HC}(\text{pz}^5)_3$ 5-methyl), 2.50 (3H, $\text{HC}(\text{pz}^5)_3$ 5-methyl). ^{31}P NMR (121 MHz, CDCl_3) δ = 52. ^{13}C NMR (201 MHz, CD_2Cl_2) δ = 149.3 (pz 3 or 5-position), 145.7 (pz 3 or 5-position), 141.4 (pz 3 or 5-position), 139.9 (pz 3 or 5-position), 136.0 (pz 3 or 5-position), 135.8 (pz 3 or 5-position), 135.4 (d, $^2J_{\text{PC}} = 9$ Hz, phenyl ipso), 129.2 (phenyl meta and para), 127.9 (d, $^2J_{\text{PC}} = 9$ Hz, phenyl ortho), 108.7 (pz 4-position), 108.5 (pz 4-position), 69.3 ($\text{HC}(\text{pz}^5)_3$), 11.6 ($\text{HC}(\text{pz}^5)_3$ methyls, one resonance missing due to coincidental overlap), 11.1 ($\text{HC}(\text{pz}^5)_3$ methyl).

[HC(pz⁵)₃Ru[P(OCH₂)₃CEt](Cl)₂ (2). Tris(5-methyl-pyrazolyl)methane (0.425 g, 1.639 mmol) and (p-cymene)Ru[P(OCH₂)₃CEt](Cl)₂ (0.768 g, 1.640 mmol) were combined in ~170 mL of THF and refluxed for 7 days. The yellow product was collected via vacuum filtration while still hot. Product was washed with THF and hexanes to yield **2** in 99% yield (0.966 g). ^1H NMR (300 MHz, CD_2Cl_2) δ = 8.24 (1H, $\text{HC}(\text{pz}^5)_3$), 7.88 (2H, d, $^3J_{\text{HH}} = 2$ Hz, pz 3-position), 7.83 (1H, pz 3-position), 6.34 (1H, pz 4-position), 6.15 (2H, pz 4-position), 4.34 (6H, d, $^3J_{\text{PH}} = 5$ Hz, $\text{P}(\text{OCH}_2)_3\text{CEt}$), 2.60 (3H, $\text{HC}(\text{pz}^5)_3$ 5-methyl), 2.56 (6H, $\text{HC}(\text{pz}^5)_3$ 5-methyl), 1.25 (2H, q, $^3J_{\text{HH}} = 8$ Hz, $-\text{CH}_2\text{CH}_3$), 0.83 (3H, t, $^3J_{\text{HH}} = 8$ Hz, $-\text{CH}_2\text{CH}_3$). ^{31}P NMR (121 MHz, CD_2Cl_2) δ = 127.3. ^{13}C NMR (150 MHz, CD_2Cl_2) δ = 149.6 (pz 3 or 5-position), 145.1 (pz 3 or 5-position), 141.6 (pz 3 or 5-position), 140.3 (pz 3 or 5-position) (2 resonances missing likely due to coincidental overlap), 108.6 (pz 4-position), 108.6 (pz 4-position), 108.4 (pz 4-position), 74.6 (d, $^2J_{\text{PC}} = 7$ Hz, $-\text{OCH}_2$), 69.1 ($\text{HC}(\text{pz}^5)_3$), 35.7 (d, $^3J_{\text{PC}} = 31$ Hz, $-\text{OCH}_2\text{C}-$), 24.0 ($-\text{CH}_2\text{CH}_3$), 11.6 ($\text{HC}(\text{pz}^5)_3$ methyls, one resonance missing due to coincidental overlap), 11.2 ($\text{HC}(\text{pz}^5)_3$ methyl), 7.4 ($-\text{CH}_2\text{CH}_3$). HR-MS: [M^+] obsd (%), calcd (%), ppm: 587.0300 (29), 587.0315 (30), -2.5; 588.0298 (35), 588.0302 (38), -0.7; 589.0307 (60), 589.0305 (63), 0.4; 590.0290 (100), 590.0296

(100), -1.1; 591.0283 (49), 591.0298 (48), -2.5; 592.0288 (92), 592.0289 (96), -0.1; 593.0330 (24), 593.0305 (25), 4.2; 594.0281 (38), 594.0276 (37), 0.9.

[M+Na⁺]: obsd (%), calcd (%), ppm: 610.0209 (31), 610.0213 (30), -0.6; 611.0171 (36), 611.0200 (38), -4.7; 612.0183 (63), 612.0202 (63), -3.1; 613.0171 (100), 613.0194 (100), -3.8; 614.0171 (47), 614.0195 (48), -3.9; 615.0170 (97), 615.0186 (96), -2.7; 616.0190 (24), 616.0203 (25), -2.1; 617.0147 (34), 617.0173 (37), -4.3.

{[HC(pz⁵)₃Ru[P(OCH₂)₃CEt](μ-Cl)]₂[OTf]₂ (3). [HC(pz⁵)₃Ru[P(OCH₂)₃CEt](Cl)₂ (2) (0.104 g, 0.175 mmol) was dissolved in ~30 mL of DCM. TlOTf (0.068 g, 0.192 mmol) was dissolved in a minimal amount of methanol and added to the solution of **2** in DCM. The reaction mixture was allowed to stir for 4 h at room temperature, after which the reaction mixture was filtered to remove a dark gray precipitate. The orange filtrate was reduced to dryness, then reconstituted in THF and refluxed for 30 min. The cream-beige product was collected via vacuum filtration. Product was washed with THF and pentane to give **3** in 90% yield (0.112 g). ¹H NMR (300 MHz, CD₂Cl₂) δ = 8.33 (1H, HC(pz⁵)₃), 8.02 (1H, pz 3-position), 7.75 (2H, d, ³J_{HH} = 2 Hz, pz 3-position), 6.45 (1H, pz 4-position), 6.19 (2H, dd, ³J_{HH} = 2 Hz, pz 4-position), 4.49 (6H, d, ³J_{PH} = 5 Hz, P(OCH₂)₃CEt), 2.70 (3H, HC(pz⁵)₃ 5-methyl), 2.65 (6H, HC(pz⁵)₃ 5-methyl), 1.35 (2H, q, ³J_{HH} = 8 Hz, -CH₂CH₃), 0.89 (3H, t, ³J_{HH} = 8 Hz, -CH₂CH₃). ³¹P NMR (121 MHz, CD₂Cl₂) δ = 128.3. ¹⁹F NMR (282 MHz, CD₂Cl₂) δ = -79.4. ¹³C NMR (201 MHz, CD₂Cl₂) δ = 149.8 (pz 3 or 5-position), 145.4 (pz 3 or 5-position), 143.3 (pz 3 or 5-position), 141.9 (pz 3 or 5-position) (2 resonances missing likely due to coincidental overlap), 109.2 (pz 4-position), 108.9 (pz 4-position), 75.4 (d, ²J_{PC} = 7 Hz, -(OCH₂)₃), 69.5 (HC(pz⁵)₃), 36.3 (d, ³J_{PC} = 31 Hz, -(OCH₂)₃C-), 24.0 (-CH₂CH₃), 11.8 (HC(pz⁵)₃ methyls, one resonance missing due to coincidental overlap), 11.3 (HC(pz⁵)₃ methyl), 7.5 (-CH₂CH₃).

{[HC(pz⁵)₃Ru[P(OCH₂)₃CEt](NH₂Ph)(Cl)] [OTf] (4). A suspension of {[HC(pz⁵)₃Ru[P(OCH₂)₃CEt](μ-Cl)]₂[OTf]₂ (**3**) (0.047 g, 0.033 mmol) was made in ~10 mL of

THF in a pressure tube equipped with a stir bar. Aniline (22 μL , 0.24 mmol) was added to the reaction mixture. The tube was sealed and set in a 90 $^{\circ}\text{C}$ oil bath for ~ 3 days, during which time the solution turned mauve and a white precipitate formed. In the glovebox, the reaction mixture was filtered to remove the white precipitate; Et_2O was then added to the filtrate to precipitate the product. The pale lilac product was collected via vacuum filtration and washed with Et_2O and pentane to give **4** in 59% yield (0.031 g). ^1H NMR (300 MHz, CD_2Cl_2) δ = 7.99 (1H, $\text{HC}(\text{pz}^5)_3$), 7.87 (1H, d, $^3J_{\text{HH}} = 2$ Hz, pz 3-position), 7.79 (1H, pz 3-position), 6.33 (1H, pz 4-position), 6.16 (1H, pz 4-position), 6.02 (1H, pz 4-position) (1 pyrazolyl resonance missing due to coincidental overlap with phenyl resonances), 7.08 (m, phenyl), 6.71 (m, phenyl), 5.34 (1H, d, NH_2 , overlaps with CD_2Cl_2 resonance), 4.54 (1H, d, $^2J_{\text{HH}} = 11.5$ Hz, NH_2), 4.44 (6H, d, $^3J_{\text{PH}} = 5$ Hz, $\text{P}(\text{OCH}_2)_3\text{CEt}$), 2.71 (3H, $\text{HC}(\text{pz}^5)_3$ 5-methyl), 2.65 (3H, $\text{HC}(\text{pz}^5)_3$ 5-methyl), 2.60 (3H, $\text{HC}(\text{pz}^5)_3$ 5-methyl), 1.33 (2H, q, $^3J_{\text{HH}} = 8$ Hz, $-\text{CH}_2\text{CH}_3$), 0.89 (3H, t, $^3J_{\text{HH}} = 8$ Hz, $-\text{CH}_2\text{CH}_3$). ^{31}P NMR (121 MHz, CD_2Cl_2) δ = 129.8. ^{19}F NMR (282 MHz, CD_2Cl_2) δ = -79.1, -79.8. ^{13}C NMR (201 MHz, $\text{THF}-d_8$) δ = 150.0 (pz 3 or 5-position), 149.9 (pz 3 or 5-position), 146.2 (pz 3 or 5-position), 145.2 (pz 3 or 5-position), 144.7 (pz 3 or 5-position), 144.2 (pz 3 or 5-position), 143.9 (phenyl ipso), 129.6 (phenyl ortho), 125.0 (phenyl para), 122.2 (phenyl meta), 108.6 (pz 4-position), 108.4 (pz 4-position), 108.3 (pz 4-position), 75.2 (d, $^2J_{\text{PC}} = 6$ Hz, $-(\text{OCH}_2)_3$), 70.3 ($\text{HC}(\text{pz}^5)_3$), 36.5 (d, $^3J_{\text{PC}} = 31$ Hz, $-(\text{OCH}_2)_3\text{C}-$), 24.2 ($-\text{CH}_2\text{CH}_3$), 11.9 ($\text{HC}(\text{pz}^5)_3$ methyl), 11.6 ($\text{HC}(\text{pz}^5)_3$ methyl), 11.5 ($\text{HC}(\text{pz}^5)_3$ methyl), 7.6 ($-\text{CH}_2\text{CH}_3$).



$\{[\text{HC}(\text{pz}^5)_3]\text{Ru}[\text{P}(\text{OCH}_2)_3\text{CEt}](\text{NH}_2\text{Ph})(\text{Cl})\}[\text{OTf}]$ (**4**) (0.0067 g, 0.0084 mmol) was dissolved in ~ 300 μL of $\text{THF}-d_8$. NaH (~ 2 mg, 0.083 mmol) was added to the solution. Effervescence likely due to H_2 was observed, but solution remained yellow. Complex **5** was formed in 80% yield by ^1H NMR spectroscopy. ^1H NMR (600 MHz, $\text{THF}-d_8$) δ = 7.84 (1H, pz 3-position), 7.51 (1H, pz 3-position), 5.97 (1H, pz 4-position), 5.65 (1H, pz 4-position), 5.44 (1H, pz 4-position), (1 pz 3-position resonance obscured due to coincidental overlap with phenyl resonance at 6.70), 6.88

(broad, phenyl), 6.70 (phenyl), 4.99 (1H, very broad, NH), 4.34 (6H, d, $^3J_{\text{PH}} = 3$ Hz, $\text{P}(\text{OCH}_2)_3\text{CEt}$), 2.58 (3H, $\text{HC}(\text{pz}^5)_3$ 5-methyl), 2.47 (3H, $\text{HC}(\text{pz}^5)_3$ 5-methyl), 2.46 (3H, $\text{HC}(\text{pz}^5)_3$ 5-methyl), 1.27 (2H, q, $^3J_{\text{HH}} = 8$ Hz, $-\text{CH}_2\text{CH}_3$), 0.86 (3H, t, $^3J_{\text{HH}} = 8$ Hz, $-\text{CH}_2\text{CH}_3$). ^{31}P NMR (243 MHz, $\text{THF-}d_8$) $\delta = 132.8$. ^{19}F NMR (565 MHz, $\text{THF-}d_8$) $\delta = -79.4$. ^{13}C NMR (201 MHz, $\text{THF-}d_8$) $\delta = 145.3$ (pz 3 or 5-position), 145.0 (pz 3 or 5-position), 144.6 (pz 3 or 5-position), 144.4 (pz 3 or 5-position), 141.2 (pz 3 or 5-position), 141.0 (pz 3 or 5-position), 129.0 (phenyl), 104.2 (pz 4-position), 103.7 (pz 4-position), 103.5 (pz 4-position), 74.6 (d, $^2J_{\text{PC}} = 6$ Hz, $-\text{OCH}_2)_3$), 72.7 ($\text{HC}(\text{pz}^5)_3$), 36.0 (d, $^3J_{\text{PC}} = 30$ Hz, $-\text{OCH}_2)_3\text{C-}$), 24.5 ($-\text{CH}_2\text{CH}_3$), 12.8 ($\text{HC}(\text{pz}^5)_3$ methyl), 12.6 ($\text{HC}(\text{pz}^5)_3$ methyl), 12.3 ($\text{HC}(\text{pz}^5)_3$ methyl), 7.6 ($-\text{CH}_2\text{CH}_3$).

{[HC(pz⁵)₃]Ru[P(OCH₂)₃CEt](THF)(OTf)][OTf] (11). AgOTf (0.290 g, 1.129 mmol) was dissolved in a minimal amount of THF and added dropwise to a suspension of **2** (0.216 g, 0.364 mmol) in THF. Complex **2** began to dissolve in THF upon addition of AgOTf. After ~5-10 minutes, AgCl began to precipitate. Reaction vessel was covered with Al foil. Solution was allowed to stir at room temperature for ~18 h, after which the reaction mixture was filtered through Celite to remove AgCl. The yellow filtrate was reduced to dryness and reconstituted in DCM to allow AgCl and AgOTf to precipitate out ~18 h. The DCM solution was filtered through Celite to remove Ag⁺ salts. Volatiles were removed in vacuo, after which solid was reconstituted in ~15 mL of THF, transferred to a pressure tube, sealed, and heated at 90 °C overnight. THF solution was filtered through Celite. Hexanes were added to precipitate out the pale yellow product to yield **11** in 98% yield (0.318 g). ^1H NMR (600 MHz, $\text{THF-}d_8$) $\delta = 8.32$ (1H, $\text{HC}(\text{pz}^5)_3$), 8.23 (1H, bs, pz 3-position), 8.02 (1H, d, $^3J_{\text{HH}} = 2$ Hz, pz 3-position), 7.95 (1H, d, $^3J_{\text{HH}} = 2$ Hz, pz 3-position), 6.57 (1H, pz 4-position), 6.37 (1H, dd, $^3J_{\text{HH}} = 2$ Hz, pz 4-position), 6.20 (1H, dd, $^3J_{\text{HH}} = 2$ Hz, pz 4-position), 4.50 (6H, d, $^3J_{\text{PH}} = 4$ Hz, $\text{P}(\text{OCH}_2)_3\text{CEt}$), 2.88 (3H, $\text{HC}(\text{pz}^5)_3$ 5-methyl), 2.82 (3H, $\text{HC}(\text{pz}^5)_3$ 5-methyl), 2.76 (3H, $\text{HC}(\text{pz}^5)_3$ 5-methyl), 1.35 (2H, q, $^3J_{\text{HH}} = 8$ Hz, $-\text{CH}_2\text{CH}_3$), 0.88 (3H, t, $^3J_{\text{HH}} = 8$ Hz, $-\text{CH}_2\text{CH}_3$), coordinated THF resonances not visible due to exchange with $\text{THF-}d_8$. ^{31}P NMR (121 MHz, $\text{THF-}d_8$) $\delta = 129.82$. ^{19}F NMR (282 MHz, $\text{THF-}d_8$)

$\delta = -79.1, -79.3, -79.8$. ^{13}C NMR (150 MHz, THF- d_8) $\delta = 153.1$ (pz 3 or 5-position), 152.7 (pz 3 or 5-position), 146.3 (pz 3 or 5-position), 146.3 (pz 3 or 5-position), 146.1 (pz 3 or 5-position), 144.9 (pz 3 or 5-position), 109.9 (pz 4-position), 109.5 (d, $J = 4$ Hz, pz 4-position), 108.9 (pz 4-position), 122.3 (q, $^1J_{\text{FC}} = 321$ Hz, CF_3SO_3^-), 119.7 (q, $^1J_{\text{FC}} = 320$ Hz, CF_3SO_3^-), 75.6 (d, $^2J_{\text{PC}} = 6$ Hz, $-(\text{OCH}_2)_3$), 70.5 ($\text{HC}(\text{pz}^5)_3$), 36.9 (d, $^3J_{\text{PC}} = 32$ Hz, $-(\text{OCH}_2)_3\text{C}-$), 24.1 ($-\text{CH}_2\text{CH}_3$), 11.9 ($\text{HC}(\text{pz}^5)_3$ methyl), 11.7 ($\text{HC}(\text{pz}^5)_3$ methyl), 11.4 ($\text{HC}(\text{pz}^5)_3$ methyl), 7.5 ($-\text{CH}_2\text{CH}_3$).

{[HC(pz⁵)₃Ru[P(OCH₂)₃CEt](py)(OTf)]}[OTf] (16).

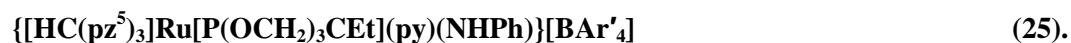
{[HC(pz⁵)₃Ru[P(OCH₂)₃CEt](THF)(OTf)]}[OTf] (**11**) (0.318 g, 0.358 mmol) was dissolved in 11.0 mL of THF in a pressure tube equipped with a stir bar. Pyridine (35 μL , 0.434 mmol) was added to the solution. The pressure tube was sealed and set in a 70 °C oil bath for 2 hours, after which reaction mixture was filtered to remove any precipitate that had formed. Hexanes were added to precipitate the beige product; volatiles were removed under vacuum in a vial to yield **16** in 94% (0.317 g). Note: complex **16** can be made without isolation of **11** after heating over night at 90 °C. After the removal of Ag^+ salts, **11** can be reconstituted in ((x mmol **11**/0.1660) x 5) mL of THF, heated overnight at 90 °C and cooled. Pyridine can then be directly added to this solution, and the reaction mixture can be heated at 70 °C for 2 hours, followed by workup. ^1H NMR (300 MHz, THF- d_8) $\delta = 8.34$ (1H, $\text{HC}(\text{pz}^5)_3$), 8.23 (1H, d, $^3J_{\text{HH}} = 2$ Hz, pz 3-position), 7.47 (1H, d, $^3J_{\text{HH}} = 2$ Hz, pz 3-position), 7.39 (1H, pz 3-position), 6.35 (1H, pz 4-position), 6.31 (1H, pz 4-position), 6.28 (1H, pz 4-position), 8.37 (d, $^3J_{\text{HH}} = 7$ Hz, pyridine), 7.81 (t, $^3J_{\text{HH}} = 7$ Hz, pyridine), 7.31 (t, $^3J_{\text{HH}} = 7$ Hz, pyridine), 4.39 (6H, d, $^3J_{\text{PH}} = 5$ Hz, $\text{P}(\text{OCH}_2)_3\text{CEt}$), 2.86 (6H, $\text{HC}(\text{pz}^5)_3$ methyl), 2.79 (3H, $\text{HC}(\text{pz}^5)_3$ methyl), 1.28 (2H, q, $^3J_{\text{HH}} = 8$ Hz, $-\text{CH}_2\text{CH}_3$), 0.84 (3H, t, $^3J_{\text{HH}} = 8$ Hz, $-\text{CH}_2\text{CH}_3$). ^{31}P NMR (121 MHz, THF- d_8) $\delta = 130.0$. ^{19}F NMR (282 MHz, THF- d_8) $\delta = -79.0, -79.7$. ^{13}C NMR (150 MHz, CD_2Cl_2) $\delta = 155.8$ (pyridine), 151.5 (pz 3 or 5-position), 151.1 (pz 3 or 5-position), 145.6 (d, $J = 3$ Hz, pz 3 or 5-position), 145.5 (pz 3 or 5-position), 143.5 (d, $J = 2$ Hz, pz 3 or 5-position), 143.4 (pz 3 or 5-position), 138.0 (pyridine), 125.3 (pyridine), 121.1 (q, outer resonances not resolved, $^1J_{\text{FC}} = 320$ Hz, OTf), 118.94 (q, outer

resonances not resolved, $^1J_{\text{FC}} = 319$ Hz, OTf), 110.0 (pz 4-position), 109.4 (d, $J = 4$ Hz, pz 4-position), 108.8 (pz 4-position), 75.4 (d, $^2J_{\text{PC}} = 7$ Hz, $-(\text{OCH}_2)_3$), 69.6 ($\text{HC}(\text{pz}^5)_3$), 36.4 (d, $^3J_{\text{PC}} = 32$ Hz, $-(\text{OCH}_2)_3\text{C}-$), 23.8 ($-\text{CH}_2\text{CH}_3$), 12.1 ($\text{HC}(\text{pz}^5)_3$ methyl), 11.8 ($\text{HC}(\text{pz}^5)_3$ methyl), 11.5 ($\text{HC}(\text{pz}^5)_3$ methyl), 7.5 ($-\text{CH}_2\text{CH}_3$). HR-MS: $[\text{M}^+]$ obsd (%), calcd (%), ppm: 745.0884 (31), 745.0880 (35), 0.6; 746.0911 (41), 746.0872 (44), 5.2; 747.0845 (58), 747.0878 (58), -4.4; 748.0866 (100), 748.0869 (100), -0.3; 749.0905 (28), 749.0889 (31), 2.1; 750.0862 (65), 750.0874 (58), -1.6.

{[HC(pz⁵)₃Ru[P(OCH₂)₃CEt](py)(OTf)]BAR'₄} (21). Complex **16** (0.635 g, 0.675 mmol) was dissolved in ~30 mL of DCM. NaBAR'₄ (0.659 g, 0.744 mmol) was added to the solution and allowed to stir at room temperature for ~40 min, after which the reaction solution was filtered through Celite to remove NaOTf. Filtrate was reduced to dryness under vacuum to give **21** in 91% yield (0.985 g). ¹H NMR (600 MHz, THF-*d*₈) $\delta = 8.27$ (1H, $\text{HC}(\text{pz}^5)_3$), 8.21 (1H, pz 3-position), 7.55 (1H, pz 3-position), 6.47 (1H, pz 4-position), 6.35 (2H, pz 4-position), (1 pyrazolyl resonance missing likely due to coincidental overlap with BAR'₄) 8.24 (d, $^3J_{\text{HH}} = 6$ Hz, pyridine), 7.88 (t, $^3J_{\text{HH}} = 8$ Hz, pyridine), 7.33 (t, $^3J_{\text{HH}} = 7$ Hz, pyridine), 7.79 (BAR'₄), 7.58 (BAR'₄), 4.39 (6H, d, $^3J_{\text{PH}} = 4$ Hz, P(OCH₂)₃CEt), 2.81 (3H, $\text{HC}(\text{pz}^5)_3$ methyl), 2.77 (3H, $\text{HC}(\text{pz}^5)_3$ methyl), 2.75 (3H, $\text{HC}(\text{pz}^5)_3$ methyl), 1.28 (2H, q, $^3J_{\text{HH}} = 8$ Hz, $-\text{CH}_2\text{CH}_3$), 0.84 (3H, t, $^3J_{\text{HH}} = 8$ Hz, $-\text{CH}_2\text{CH}_3$). ³¹P NMR (243 MHz, CD₂Cl₂) $\delta = 129.2$. ¹⁹F NMR (565 MHz, CD₂Cl₂) $\delta = -63.4, -63.9, -79.2, -79.5$.

{[HC(pz⁵)₃Ru[P(OCH₂)₃CEt](py)(NH₂Ph)]OTf]BAR'₄} (22). Complex **21** (0.859 g, 0.519 mmol) was dissolved in 4.0 mL of THF in a pressure tube equipped with a stir bar. Aniline (57 μL , 0.625 mmol) was added to the solution. The tube was sealed and set in a 90 °C oil bath for ~4 h, after which solution was cooled and filtered to remove a gray precipitate. Volatiles were removed in vacuo from the dark purple filtrate. Pure complex **22** was isolated after the following chromatography conditions: about ¾ inch of a silica gel/hexanes mixture was prepared

in a 15 mL fine porosity frit, onto which complex **22** was dry-loaded. A yellow impurity, found to include free aniline by ^1H NMR spectroscopy, was first eluted with Et_2O . Then, the product (a violet band) was eluted with THF. This eluent was then reduced to dryness under vacuum, and the solid was dry-loaded again onto a fresh $\frac{3}{4}$ in mixture of silica/hexanes in a 15 mL fine porosity frit. Product **22** was then eluted once more with THF; volatiles were removed in vacuo to give the dark purple **22** in 43% yield (0.378 g). ^1H NMR (600 MHz, CD_2Cl_2) δ = 7.98 (1H, $\text{HC}(\text{pz}^5)_3$), 7.37 (1H, d, $^3J_{\text{HH}} = 2$ Hz, pz 3-position), 7.12 (2H, d, $^3J_{\text{HH}} = 2$ Hz, pz 3-position), 6.33 (1H, pz 4-position), 6.19 (1H, pz 4-position), 6.06 (1H, pz 4-position), 7.72 (BAr'_4), 7.55 (BAr'_4), 8.02 (d, $^3J_{\text{HH}} = 5$ Hz, pyridine), 7.80 (pyridine), 7.30 (pyridine), 7.06 (m, phenyl), 6.49 (d, $^3J_{\text{HH}} = 8$ Hz, phenyl), 5.23 (1H, d, $^2J_{\text{HH}} = 12$ Hz, NH_2), 5.02 (1H, d, $^2J_{\text{HH}} = 12$ Hz, NH_2), 4.40 (6H, m, $\text{P}(\text{OCH}_2)_3\text{CEt}$), 2.64 (3H, $\text{HC}(\text{pz}^5)_3$ 5-methyl), 2.56 (3H, $\text{HC}(\text{pz}^5)_3$ 5-methyl), 2.55 (3H, $\text{HC}(\text{pz}^5)_3$ 5-methyl), 1.29 (2H, q, $^3J_{\text{HH}} = 8$ Hz, $-\text{CH}_2\text{CH}_3$), 0.83 (3H, t, $^3J_{\text{HH}} = 8$ Hz, $-\text{CH}_2\text{CH}_3$). ^{31}P NMR (243 MHz, THF) δ = 133.1. ^{13}C NMR (150 MHz, CD_2Cl_2) δ = 162.3 (4 line pattern, $^1J_{\text{BC}} = 50$ Hz, BAr'_4), 155.6 (pyridine), 149.8 (pz 3 or 5-position), 149.6 (pz 3 or 5-position), 146.4 (pz 3 or 5-position), 143.6 (pz 3 or 5-position), 143.0 (pz 3 or 5-position), 142.9 (pz 3 or 5-position), 138.8 (pyridine), 135.4 (BAr'_4), 130.2 (phenyl ipso), 129.8 (phenyl ortho), 129.5 (q, $^1J_{\text{CF}} = 32$ Hz, BAr'_4), 126.4 (pyridine), 126.0 (phenyl), 124.2 (phenyl), 118.1 (BAr'_4), 110.5 (pz 4-position), 110.3 (pz 4-position), 109.4 (pz 4-position), 76.0 (d, $^2J_{\text{PC}} = 7$ Hz, $-(\text{OCH}_2)_3$), 68.9 ($\text{HC}(\text{pz}^5)_3$), 36.7 (d, $^3J_{\text{PC}} = 32$ Hz, $-(\text{OCH}_2)_3\text{C}-$), 23.7 ($-\text{CH}_2\text{CH}_3$), 11.5 ($\text{HC}(\text{pz}^5)_3$ methyl), 11.48 ($\text{HC}(\text{pz}^5)_3$ methyl), 11.4 ($\text{HC}(\text{pz}^5)_3$ methyl), 7.4 ($-\text{CH}_2\text{CH}_3$). HR-MS: [M^{2+}] obsd (%), calcd (%), ppm: 344.5963 (32), 344.5966 (35), -1.0; 345.0971 (43), 345.0963 (45), 2.2; 345.5971 (57), 345.5967 (58), 1.3; 346.0959 (100), 346.0962 (100), -0.8; 346.5989 (33), 346.5974 (33), 4.3; 347.0971 (56), 347.0966 (54), 1.5.



$\{[\text{HC}(\text{pz}^5)_3]\text{Ru}[\text{P}(\text{OCH}_2)_3\text{CEt}](\text{py})(\text{NH}_2\text{Ph})\}[\text{OTf}][\text{BAr}'_4]$ (**22**) (0.0053 g, 0.0034 mmol) was

dissolved in ~0.5 mL of THF- d_8 . NaHMDS (~0.0037 mmol) was added to the solution to give **1** in 92% yield. ^1H NMR (600 MHz, THF- d_8) δ = 7.83 (HC(pz 5) $_3$, obscured by BAr' $_4$, as indicated by ^1H - ^{13}C HMQC NMR spectroscopy), 7.12 (1H, pz 3-position), 7.06 (1H, pz 3-position), 7.03 (1H, pz 3-position), 6.06 (1H, pz 4-position), 5.87 (1H, pz 4-position), 5.75 (1H, pz 4-position), 8.10 (pyridine), 7.75 (pyridine), 7.17 (pyridine), 7.79 (BAr' $_4$), 7.58 (BAr' $_4$), 6.68 (broad, phenyl), 4.41 (NH, typically obscured by P(OCH $_2$) $_3$ CEt), 4.37 (6H, P(OCH $_2$) $_3$ CEt), 2.66 (3H, HC(pz 5) $_3$ 5-methyl), 2.58 (3H, HC(pz 5) $_3$ 5-methyl), 2.55 (3H, HC(pz 5) $_3$ 5-methyl), 1.28 (2H, q, $^3J_{\text{HH}}$ = 8 Hz, -CH $_2$ CH $_3$), 0.84 (3H, t, $^3J_{\text{HH}}$ = 8 Hz, -CH $_2$ CH $_3$). ^{31}P NMR (201 MHz, THF- d_8) δ = 132.0 (broad). ^{13}C NMR (201 MHz, THF- d_8) δ = 163.0 (4 line pattern, $^1J_{\text{BC}}$ = 50 Hz, BAr' $_4$), 157.3 (pyridine), 156.2 (pz 3 or 5-position), 151.1 (pz 3 or 5-position), 148.4 (pz 3 or 5-position), 145.2 (pz 3 or 5-position), 144.2 (pz 3 or 5-position), 140.4 (pyridine), 135.8 (BAr' $_4$), 130.2 (q, $^1J_{\text{CF}}$ = 32 Hz, BAr' $_4$), 129.2 (phenyl ipso), 129.1 (bs, phenyl), 124.8 (phenyl), 126.4 (pyridine), 118.3 (BAr' $_4$), 105.3 (pz 4-position), 105.2 (pz 4-position), 104.4 (pz 4-position), 75.0 (-OCH $_2$) $_3$, 70.1 (HC(pz 5) $_3$), 36.3 (d, $^3J_{\text{PC}}$ = 30 Hz, -(OCH $_2$) $_3$ C-), 24.2 (-CH $_2$ CH $_3$), 12.8 (HC(pz 5) $_3$ methyl), 12.8 (HC(pz 5) $_3$ methyl), 12.7 (HC(pz 5) $_3$ methyl), 7.4 (-CH $_2$ CH $_3$).

References

- (1) Joslin, E. E.; Quillian, B.; Gunnoe, T. B.; Cundari, T. R.; Sabat, M.; Myers, W. H. *Inorg. Chem.* **2014**, *53*, 6270.
- (2) Burgess, S. A.; Joslin, E. E.; Gunnoe, T. B.; Cundari, T. R.; Sabat, M.; Myers, W. H. *Chem. Sci.* **2014**, *5*, 4355.
- (3) McKeown, B. A.; Lee, J. P.; Mei, J.; Cundari, T. R.; Gunnoe, T. B. *Eur. J. Inorg. Chem.* **2016**, *2016*, 2296.
- (4) Zhang, J.; Gunnoe, T. B.; Boyle, P. D. *Organometallics* **2004**, *23*, 3094.
- (5) Bolinger, C. M.; Story, N.; Sullivan, B. P.; Meyer, T. J. *Inorg. Chem.* **1988**, *27*, 4582.
- (6) Burgess, S. A.; Devarajan, D.; Bolano, T.; Ess, D. H.; Gunnoe, T. B.; Sabat, M.; Myers, W. H. *Inorg. Chem.* **2014**, *53*, 5328.
- (7) Goodman, M. A.; DeMarco, M. J.; Tarasek, S. E.; Nazarenko, A. Y.; Brennessel, W.; Goodman, M. S. *Inorganica Chimica Acta* **2014**, *423*, Part A, 358.
- (8) Goodman, M. A.; Nazarenko, A. Y.; Casavant, B. J.; Li, Z.; Brennessel, W. W.; DeMarco, M. J.; Long, G.; Goodman, M. S. *Inorg. Chem.* **2012**, *51*, 1084.

4 Dihydrogen Activation by {[HC(pz⁵)₃]Ru[P(OCH₂)₃CEt](py)(NHAr)}[BAr'₄] Complexes

4.1 Introduction

Dihydrogen activation provides a useful model for C–H bond activation, as an H–H bond is similar to C–H bonds in both polarity and bond dissociation energy (e.g., BDEs of H₃C–H and H–H are both 104 kcal/mol).¹⁻³ Although bond polarity and BDEs are similar, dihydrogen permits the study of bond activation in some cases where C–H activation is not always observed. This is because H₂ is a better ligand than hydrocarbons such as propane or methane, and the more facile coordination allows H₂ activation by a larger number of complexes.³ As discussed in Chapter 3, {[HC(pz⁵)₃]Ru[P(OCH₂)₃CEt](py)(NHPh)}[BAr'₄] (**1**) activates H₂ in THF to form several Ru–hydride species and release free aniline at temperatures ranging from 80 to 110 °C. With a complex capable of H₂ activation in hand, we set out to extend studies of the H₂ activation reaction. For example, we sought to probe the effect of amido basicity on H₂ activation by using a series of {[HC(pz⁵)₃]Ru[P(OCH₂)₃CEt](py)(NHAr)}[BAr'₄] complexes in which Ar = 4-(trifluoromethyl)phenyl, 4-fluorophenyl, 4-chlorophenyl, phenyl, 4-methylphenyl, and 4-isopropylphenyl (Figure 1). The substituents in the 4-position of the phenyl rings include a range of electron-donating and electron-withdrawing groups, thus presumably altering basicity of the respective anilido ligands compared with that of complex **1**. Computational studies performed by Ess and co-workers indicated that less basic lone pairs could promote lower overall activation barriers to bond activation (see Chapter 1), and observations from the work described herein would give experimental insight into whether bond activation is favored by more or less basic anilido ligands.⁴

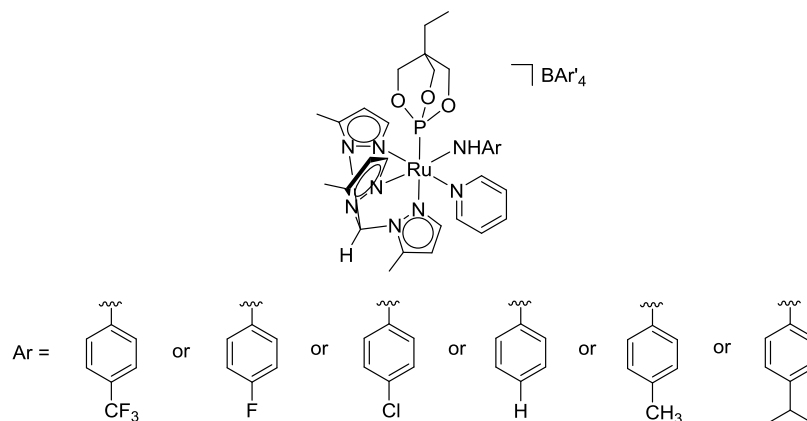


Figure 1. $\{[\text{HC}(\text{pz}^5)_3]\text{Ru}[\text{P}(\text{OCH}_2)_3\text{CET}](\text{py})(\text{NHAr})\}[\text{BAR}'_4]$ targets for this study.

4.2 Nature of $\{[\text{HC}(\text{pz}^5)_3]\text{Ru}[\text{P}(\text{OCH}_2)_3\text{CET}](\text{py})(\text{NHPh})\}[\text{BAR}'_4]$ (**1**)

As discussed in Chapter 3, both a major and minor asymmetric species, believed to be $\{[\text{HC}(\text{pz}^5)_3]\text{Ru}[\text{P}(\text{OCH}_2)_3\text{CET}](\text{py})(\text{NHPh})\}[\text{BAR}'_4]$ (**1**) (major) and $\{[:\text{C}(\text{pz}^5)_3]\text{Ru}[\text{P}(\text{OCH}_2)_3\text{CET}](\text{py})(\text{NH}_2\text{Ph})\}[\text{BAR}'_4]$ (**1'**) (minor) in equilibrium (Scheme 1), were typically observed in a 6:1 to a 4:1 ratio in solution upon synthesis of the Ru–anilido complex. Analysis by ^1H NMR and two dimensional ^1H - ^1H COSY spectroscopy revealed $\text{P}(\text{OCH}_2)_3\text{CET}$, phenyl, pyridine, and pyrazolyl resonances for both complexes. Analysis of $\{[\text{HC}(\text{pz}^5)_3]\text{Ru}[\text{P}(\text{OCH}_2)_3\text{CET}](\text{py})(^{15}\text{NHPh})\}[\text{BAR}'_4]$ by ^1H NMR and two dimensional ^1H - ^{15}N NMR correlation spectroscopy revealed an anilido N–H proton belonging to the major species. A doublet integrating for the same value as a pyrazolyl resonance (1 H) of the major complex was observed at 4.37 ppm with $^1J_{\text{H}^{15}\text{N}} = 82$ Hz by ^1H NMR spectroscopy (Figure 2). Furthermore, a cross peak for the ^{15}NH resonance of the anilido ligand was observed by ^1H - ^{15}N NMR correlation spectroscopy (Figure 3).

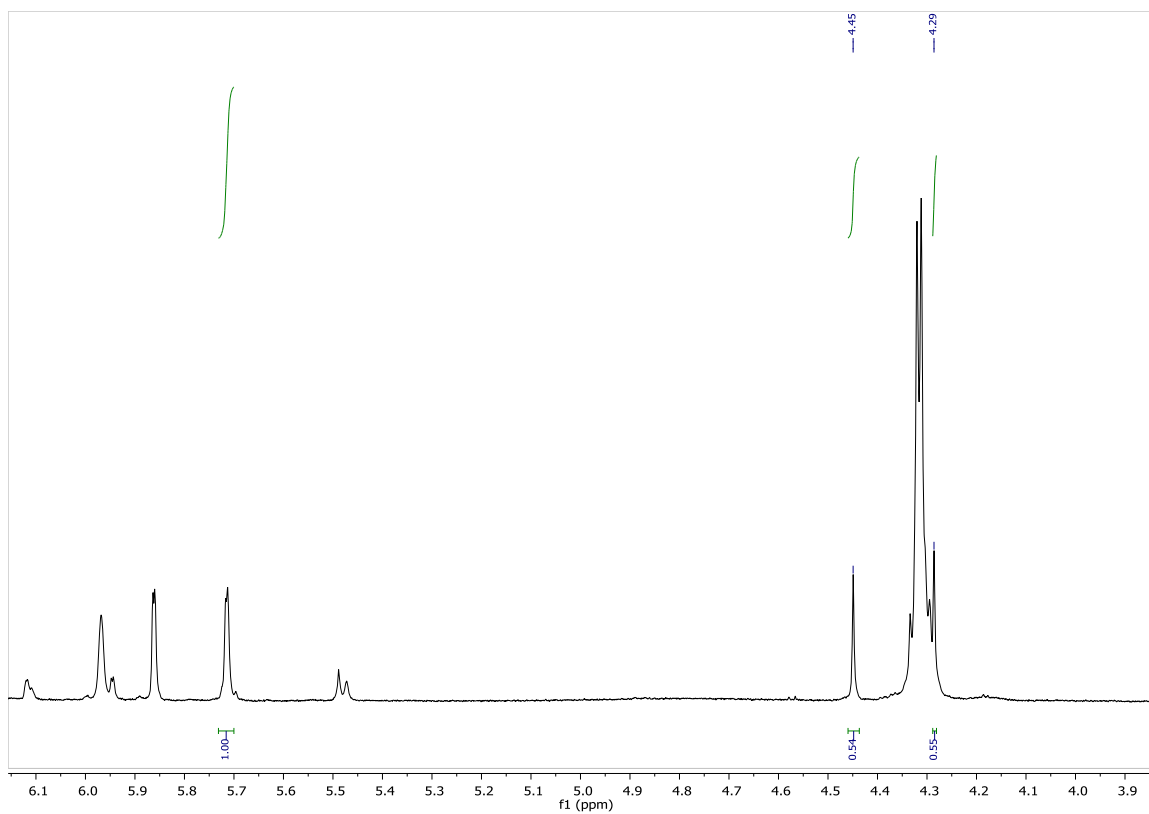


Figure 2. Portion of ^1H NMR (500 MHz, $\text{THF-}d_8$) spectrum of $\{[\text{HC}(\text{pz}^5)_3]\text{Ru}[\text{P}(\text{OCH}_2)_3\text{CEt}](\text{py})(^{15}\text{NPh})\}[\text{BAR}'_4]$ showing ^{15}NH doublet partially obscured by $\text{P}(\text{OCH}_2)_3\text{CEt}$ resonance.

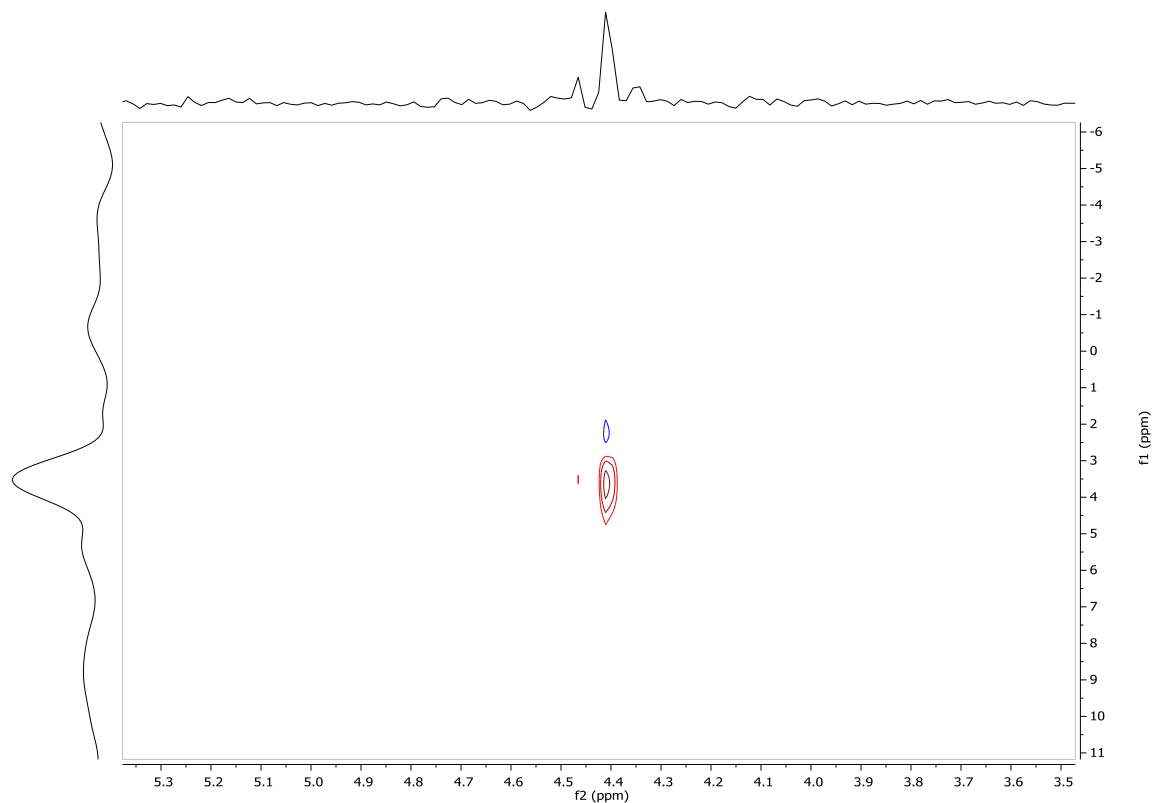
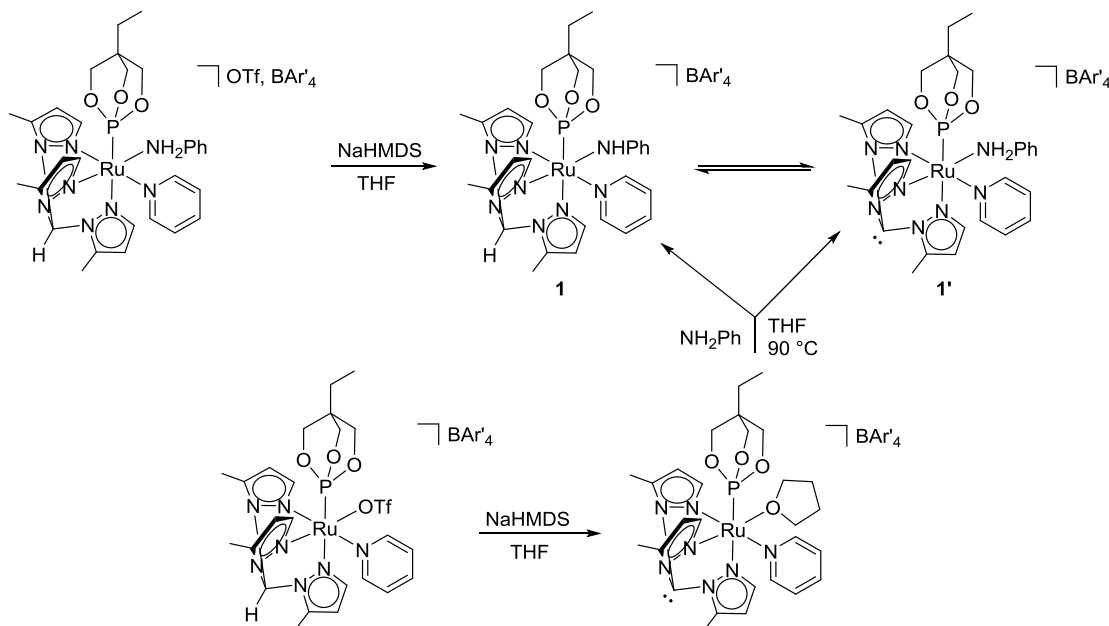


Figure 3. ^1H - ^{15}N correlation NMR spectrum of $\{[\text{HC}(\text{pz}^5)_3]\text{Ru}[\text{P}(\text{OCH}_2)_3\text{CEt}](\text{py})(^{15}\text{NHPH})\}[\text{BAr}'_4]$.

While the two species were originally hypothesized to be rotamers of $\{[\text{HC}(\text{pz}^5)_3]\text{Ru}[\text{P}(\text{OCH}_2)_3\text{CEt}](\text{py})(\text{NHPH})\}[\text{BAr}'_4]$ (**1**), data obtained from variable temperature ^1H NMR did not support this assumption because the resonances from the two species did not coalesce with an increase in temperature. Attempts to remove the minor species via filtration were not successful. The identities of **1** and **1'** were supported by the deprotonation of the methine carbon of $\{[\text{HC}(\text{pz}^5)_3]\text{Ru}[\text{P}(\text{OCH}_2)_3\text{CEt}](\text{py})(\text{OTf})\}[\text{BAr}'_4]$ with NaHMDS in THF- d_8 , followed by the addition of aniline to the solution. After heating this reaction mixture at 90 °C for 30 minutes, the same major and minor species that form from adding NaHMDS to $\{[\text{HC}(\text{pz}^5)_3]\text{Ru}[\text{P}(\text{OCH}_2)_3\text{CEt}](\text{py})(\text{NH}_2\text{Ph})\}[\text{OTf}][\text{BAr}'_4]$ were observed by ^1H NMR spectroscopy (in a 4:1 ratio) along with a symmetric bis(pyridine) product (Scheme 1). For simplicity, the major species $\{[\text{HC}(\text{pz}^5)_3]\text{Ru}[\text{P}(\text{OCH}_2)_3\text{CEt}](\text{py})(\text{NHPH})\}[\text{BAr}'_4]$ (**1**) will be

discussed in the following sections. However, the equilibrium between **1** and **1'** likely plays an important role in explaining the nature of a side reaction observed during H₂ activation experiments, which will be addressed further in Section 4.3.

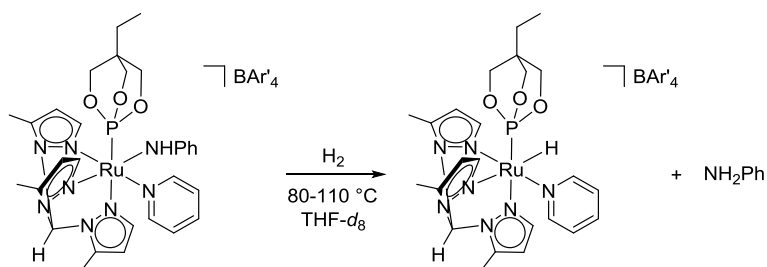


Scheme 1. Alternate synthetic pathways to $\{[\text{HC}(\text{pz}^5)_3]\text{Ru}[\text{P}(\text{OCH}_2)_3\text{CEt}](\text{py})(\text{NHPh})\}[\text{BAR}'_4]$ (**1**) and $\{[:\text{C}(\text{pz}^5)_3]\text{Ru}[\text{P}(\text{OCH}_2)_3\text{CEt}](\text{py})(\text{NH}_2\text{Ph})\}[\text{BAR}'_4]$ (**1'**).

4.3 H₂ Activation by $\{[\text{HC}(\text{pz}^5)_3]\text{Ru}[\text{P}(\text{OCH}_2)_3\text{CEt}](\text{py})(\text{NHPh})\}[\text{BAR}'_4]$ (**1**)

Upon pressurizing a THF-*d*₈ solution of $\{[\text{HC}(\text{pz}^5)_3]\text{Ru}[\text{P}(\text{OCH}_2)_3\text{CEt}](\text{py})(\text{NHPh})\}[\text{BAR}'_4]$ (**1**) with H₂ and heating (80-110 °C) (Scheme 2), the formation of three distinct Ru–hydride species was observed (Figure 4 and Figure 5). Monitoring this reaction over time by ¹H NMR spectroscopy showed that $\{[\text{HC}(\text{pz}^5)_3]\text{Ru}[\text{P}(\text{OCH}_2)_3\text{CEt}](\text{py})(\text{NH}_2\text{Ph})(\text{H})\}^+$ (**2**) with a hydride resonance at -14.9 ppm (doublet, ²J_{PH} = 39 Hz) appears first and then is likely converted to $[\text{HC}(\text{pz}^5)_3\text{Ru}[\text{P}(\text{OCH}_2)_3\text{CEt}](\text{py})(\text{H})]^+$ (**3**) with a hydride resonance at -14.3 ppm (doublet, ²J_{PH} = 40 Hz), the final Ru complex of the reaction (see Section 4.4.1 and 4.4.2). The integrations of the hydride resonances for these complexes support a single hydride ligand for each complex, as opposed to possible η²-H₂ complexes. A third minor species with a hydride resonance at -16.7 ppm (doublet, ²J_{PH} = 41 Hz),

thought to be $\{[\text{HC}(\text{pz}^5)_3]\text{Ru}[\text{P}(\text{OCH}_2)_3\text{CEt}](\text{THF})(\text{H})\}^+$ (**4**) (see section 4.4.3), also grew in and was consumed over the course of the reaction, presumably decomposing as integrations of the hydride resonances did not support conversion of -16.7 to the -14.3 ppm complex (the integration of -14.3 corresponded to the conversion of -14.9 rather than -14.9 + -16.7 ppm). During the reaction, doublets due to the NH_2 group of coordinated aniline grow in as the anilido ligand is protonated, and then free aniline is produced.



Scheme 2. H_2 activation by $\{[\text{HC}(\text{pz}^5)_3]\text{Ru}[\text{P}(\text{OCH}_2)_3\text{CEt}](\text{py})(\text{NHPH})\}[\text{BAR}'_4]$ (**1**).

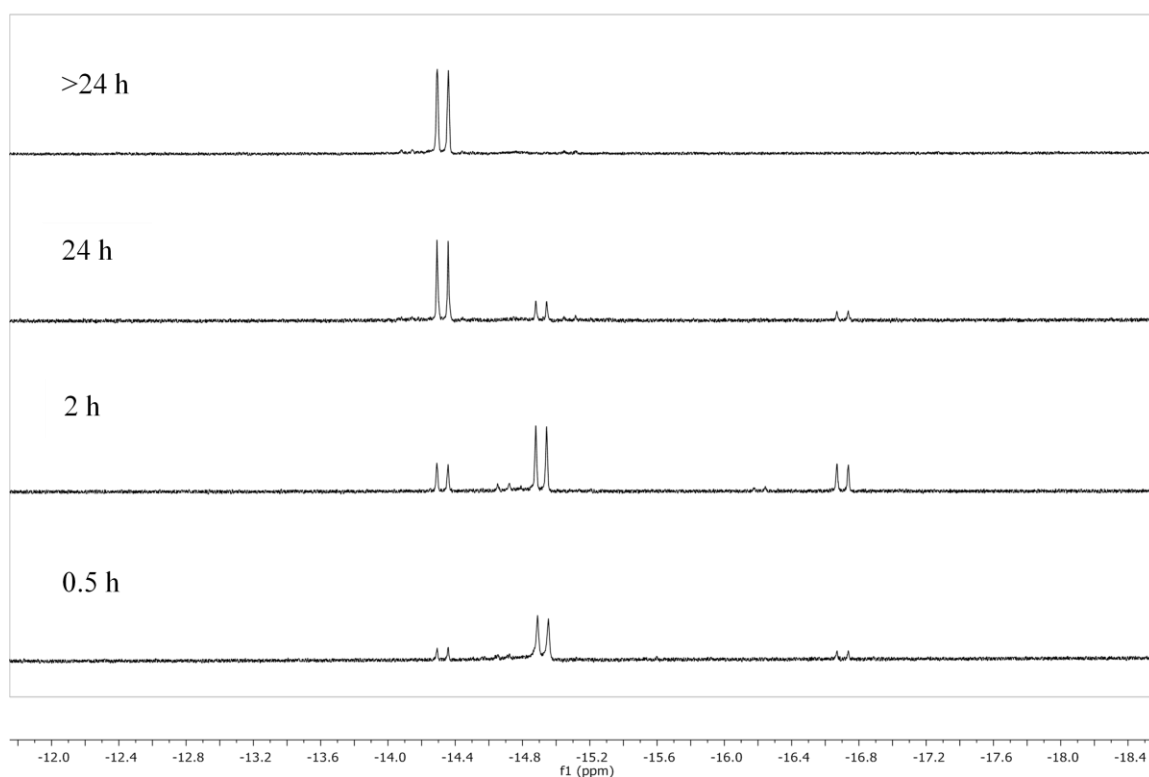


Figure 4. Hydride region of the ^1H NMR spectra (600 MHz, $\text{THF-}d_8$) during the reaction of $\{[\text{HC}(\text{pz}^5)_3]\text{Ru}[\text{P}(\text{OCH}_2)_3\text{CEt}](\text{py})(\text{NHPH})\}[\text{BAR}'_4]$ (**1**) with 25 psi H_2 at 90 °C.

Furthermore, a C_s symmetric Ru complex without a hydride ligand (**5**) forms concomitantly with the products of the H_2 activation reaction and was present at the end of the reaction. However, complex **5** is thought to be the product of a competing reaction rather than a product of H_2 activation. A THF- d_8 solution of complex **1** was pressurized with 25 psi N_2 and heated at 110 °C for ~ 4 h, leading to conversion to **5** and free aniline. A 1H NMR spectrum of the isolated complex **5** showed two pyridine resonances at 8.40 (doublet) and 7.27 (triplet), four pyrazolyl resonances integrating for six protons, and $HC(pz^5)_3$ methyl resonances at 2.69 and 2.63 ppm (Figure 6). The ^{31}P NMR spectrum showed a single resonance at 131.4 ppm.

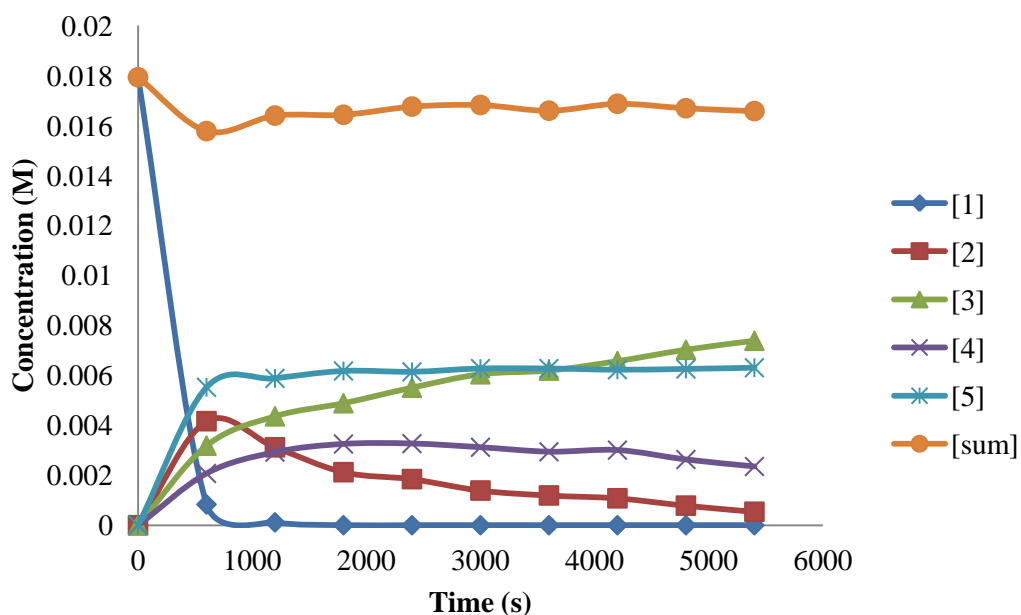


Figure 5. Example of concentration of complexes **1-5** over the course of H_2 activation by **1** at 110 °C and 55 psig H_2 .

Integration of the pyridine resonances revealed a 2:1 ratio of pyridine to Ru complex, indicating that **5** is actually a bis(pyridine) species. No methine proton was observed by 1H NMR spectroscopy, indicating that the methine carbon of $HC(pz^5)_3$ had been deprotonated. Thus, complex **5** was hypothesized to be $\{[:C(pz^5)_3]Ru[P(OCH_2)_3CEt](py)_2\}[BAr'_4]$.

To confirm the identity of **5**, the bis(pyridine) complex was independently synthesized. Heating a THF- d_8 solution of **1** under 50 psig N_2 to 110 °C for ~4.5 h afforded formation of **5** in 47% yield by 1H NMR spectroscopy (theoretical maximum yield = 50%). Addition of excess pyridine to an identical sample resulted in quantitative conversion to **5** in ~1.25 h. These results suggest that two equivalents of Ru complex react to form $\{[:C(pz^5)_3]Ru[P(OCH_2)_3CEt](py)_2\}[BAr'_4]$ and a decomposition product (unidentified).

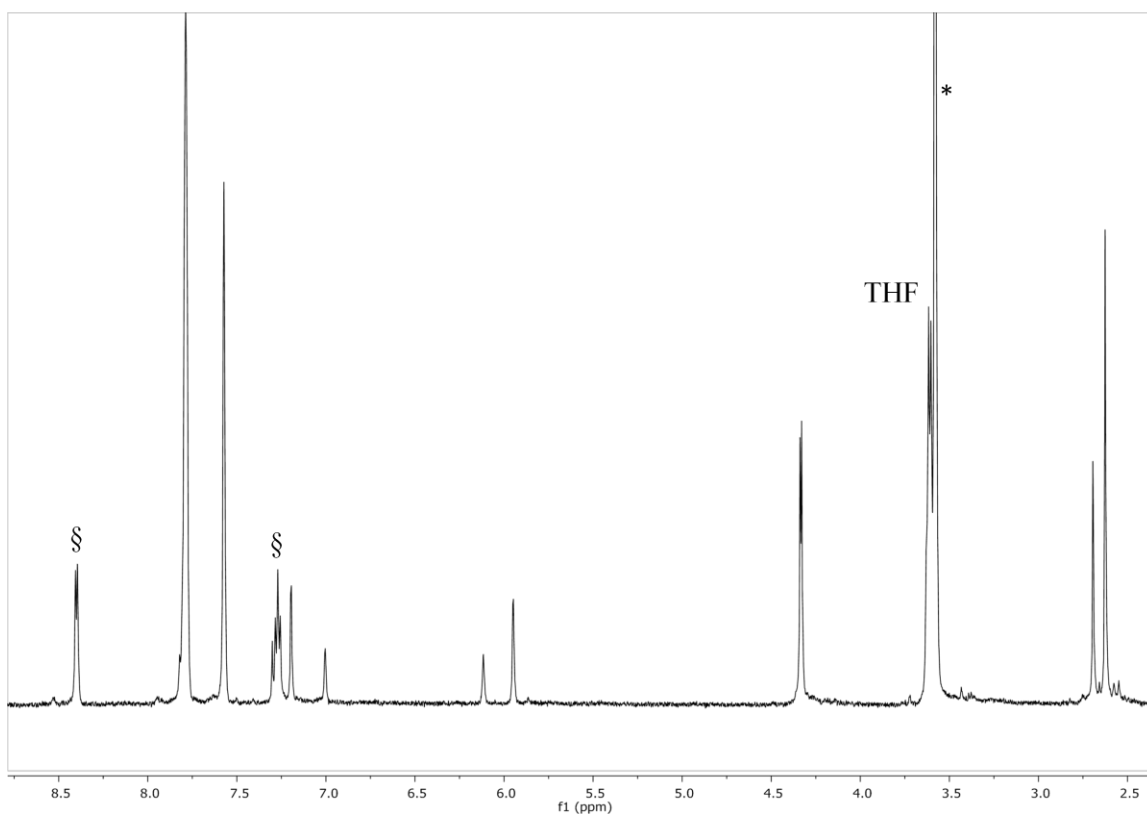


Figure 6. 1H NMR spectrum (500 MHz, THF- d_8) of complex **5**. Solvent resonance denoted by *. Coordinated pyridine resonances denoted by §.

Adding HCl to **5** in THF- d_8 turned the solution from brown to purple and converted **5** to $\{[HC(pz^5)_3]Ru[P(OCH_2)_3CEt](py)_2\}[BAr'_4][Cl]$ by protonating the poly(pyrazolyl)alkane ligand—ligand resonances in the downfield region integrated for seven protons after reaction with HCl (Figure 7). Addition of DCl to **5** in THF- d_8 produced the same result but with one resonance still missing due to deuterium incorporation. Comparison of the HCl and DCl products revealed

that the ligand position being protonated was the most downfield resonance, the methide/methine carbon. Furthermore, dissolving **5** in DCM- d_2 had the same effect as adding HCl. The solution turned from brown to purple, and the reaction was slow enough to observe both **5** and the protonated species in solution. Adding HCl to $\{[:C(pz^5)_3]Ru[P(OCH_2)_3CEt](py-d_5)_2\}[BAR'_4]$ (**5-py- d_5**) further confirmed that the methide carbon of $:C(pz^5)_3$ is protonated and no proton incorporation into the pyridine ligands is observed (no H–D coupling was observed in the pyridine resonances). A COSY NMR spectrum revealed the third pyridine resonance of complex **5** to coincidentally overlap with a BAR'_4 resonance. The COSY NMR spectrum of $\{[HC(pz^5)_3]Ru[P(OCH_2)_3CEt](py)_2\}[BAR'_4][Cl]$ revealed that two pyrazolyl resonances (integrating to 3 H) coincidentally overlap with a BAR'_4 resonance. A crystal suitable for an X-ray diffraction study was grown by layering a THF solution of $\{[HC(pz^5)_3]Ru[P(OCH_2)_3CEt](py)_2\}^+$ with hexanes (Figure 8). This confirmed the presence of two pyridines, and the methide carbon had been protonated, likely due to complex **5** picking up a proton over time from some source in its environment and converting to $\{[HC(pz^5)_3]Ru[P(OCH_2)_3CEt](py)_2\}[BAR'_4]_2$. The bond length of Ru1–N3 (2.1561(2) Å), trans to P(OCH₂)₃CEt (the ligand with a greater trans effect) is noticeably longer than for Ru1–N5, (2.0828(2) Å) and Ru1–N3 (2.1561(2) Å), which are trans to pyridine.

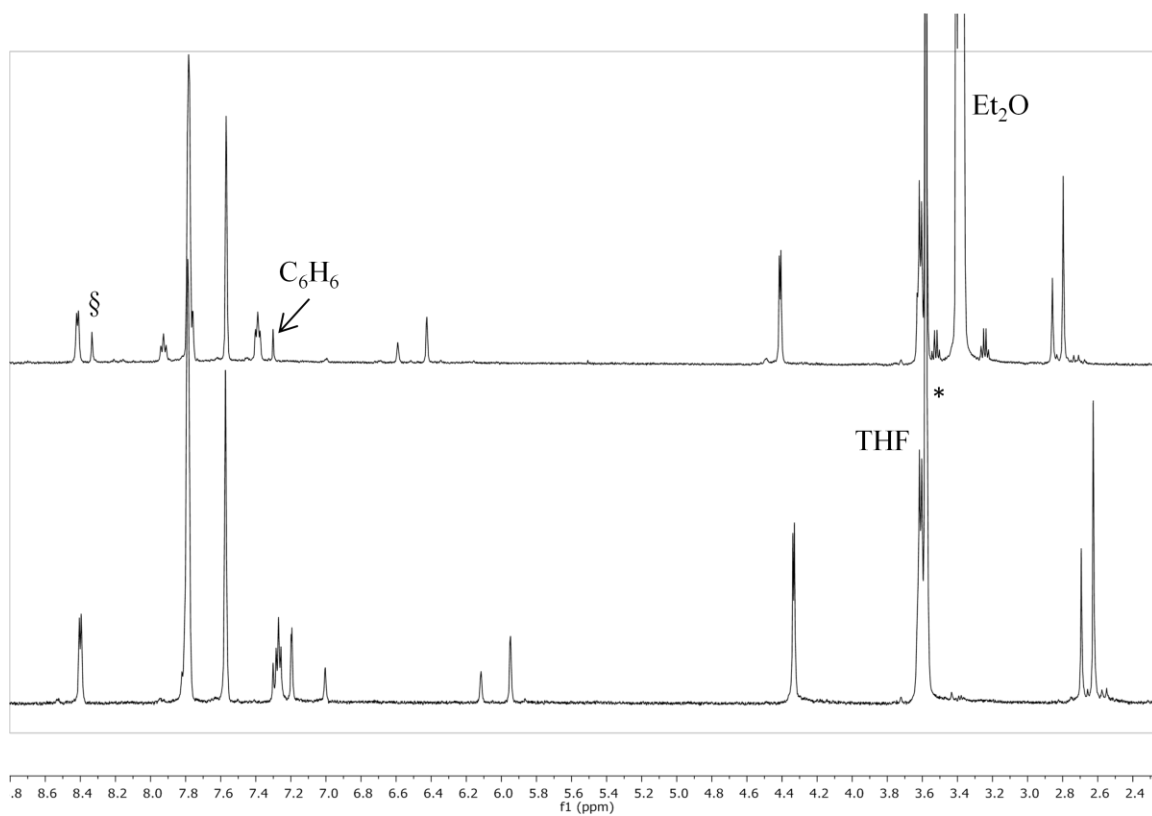


Figure 7. ^1H NMR spectra (500 MHz, $\text{THF-}d_8$) of complex **5** before addition of HCl (bottom) and after addition of HCl (top). Solvent resonance denoted by *. Methine proton denoted by §.

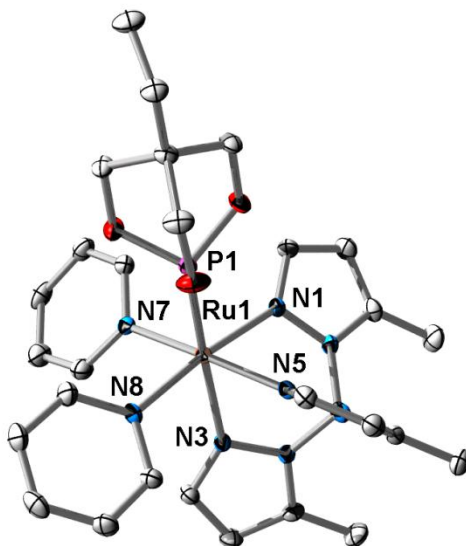
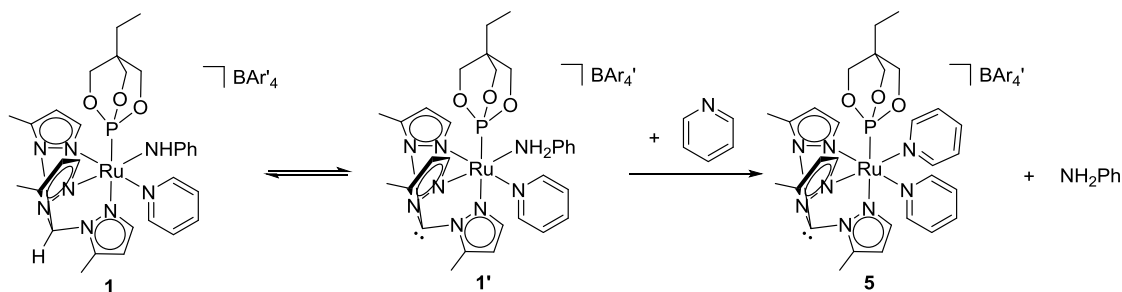


Figure 8. ORTEP of $\{[\text{HC}(\text{pz}^5)_3\text{Ru}[\text{P}(\text{OCH}_2)_3\text{CET}](\text{py})_2][\text{BAr}'_4]\}$ (50% probability with H atoms and BAr'_4 omitted). Selected bond lengths (\AA): Ru1-N5, 2.0828(19); Ru1-N1, 2.1043(18); Ru1-N3, 2.1561(18); Ru1-N8, 2.0963(19); Ru1-N7, 2.1160(19); Ru1-P1, 2.2049(6). Selected bond angles (deg): N5-Ru1-N8, 92.52(7); N5-Ru1-N1, 84.10(7); N8-Ru1-N7, 90.39(7); N1-Ru1-N7, 92.50(7); N5-Ru1-N3, 83.77(7); N8-Ru1-N3, 87.74(7); N1-Ru1-N3, 86.80(7); N7-Ru1-N3 90.92(7).

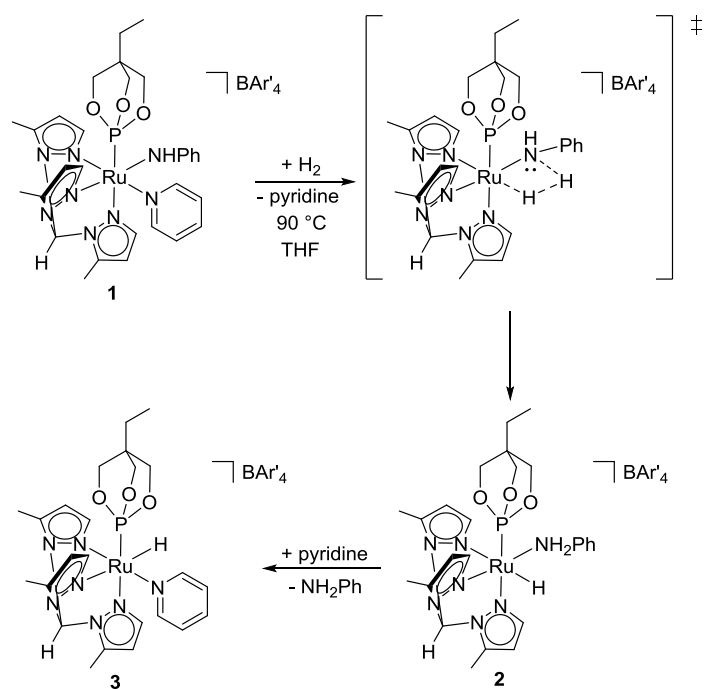
One can envision the side reaction involving a bimolecular pathway in which complex **1** reverts to $\{[:\text{C}(\text{pz}^5)_3]\text{Ru}[\text{P}(\text{OCH}_2)_3\text{CET}](\text{py})(\text{NH}_2\text{Ph})\}[\text{BAr}'_4]$ (**1'**) via proton transfer, releases aniline and abstracts a pyridine from either another equivalent of $\{[:\text{C}(\text{pz}^5)_3]\text{Ru}[\text{P}(\text{OCH}_2)_3\text{CET}](\text{py})(\text{NH}_2\text{Ph})\}[\text{BAr}'_4]$ or complex **1**, leading to formation of complex **5**— $\{[:\text{C}(\text{pz}^5)_3]\text{Ru}[\text{P}(\text{OCH}_2)_3\text{CET}](\text{py})_2\}[\text{BAr}'_4]$ (Scheme 3). Thus, the equilibrium between **1** and **1'** provides a considerable source of error during kinetic and mechanistic studies, and the k_{obs} values discussed in Section 4.6 are likely representative of the upper limit of those values.



Scheme 3. Formation of $\{[:C(pz^5)_3]Ru[P(OCH_2)_3CET](py)_2\}[BAR'_4]$ (**5**).

4.4 Analysis of Hydride Species Formed During H_2 Activation by $\{[HC(pz^5)_3]Ru[P(OCH_2)_3CET](py)(NHPh)\}[BAR'_4]$ (**1**)

Examining the 1H NMR spectrum of the products of the H_2 activation reaction by complex **1** indicated that $HC(pz^5)_3$, pyridine and $P(OCH_2)_3CET$ were coordinated to the final hydride product (-14.3 ppm) (Figure 9). These observations indicate that this species is $\{[HC(pz^5)_3]Ru[P(OCH_2)_3CET](py)(H)\}[BAR'_4]$ (**3**) (Scheme 4). Thus, the hydride resonance that first grows in at -14.9 ppm likely corresponds to $\{[HC(pz^5)_3]Ru[P(OCH_2)_3CET](NH_2Ph)(H)\}[BAR'_4]$ (**2**), which was supported by the observation that NH_2 doublets appear simultaneously at 5.13 and 5.03 ppm ($^2J_{HH} = 11$ Hz) with formation of the -14.9 ppm species. $\{[HC(pz^5)_3]Ru[P(OCH_2)_3CET](THF)(H)\}^+$ (**4**), the species with a hydride resonance at -16.7 ppm was hypothesized to most likely be an intermediate or side product of H_2 activation, appearing to ultimately decompose by the end of the reaction. To confirm these hypotheses, attempts were made to synthesize each of the hydride species independently.



Scheme 4. H₂ activation by $\{[\text{HC}(\text{pz}^5)_3]\text{Ru}[\text{P}(\text{OCH}_2)_3\text{CEt}](\text{py})(\text{NHPH})\}[\text{BAr}'_4]$ (**1**) with intermediate $\{[\text{HC}(\text{pz}^5)_3]\text{Ru}[\text{P}(\text{OCH}_2)_3\text{CEt}](\text{NH}_2\text{Ph})(\text{H})\}[\text{BAr}'_4]$ (**2**).

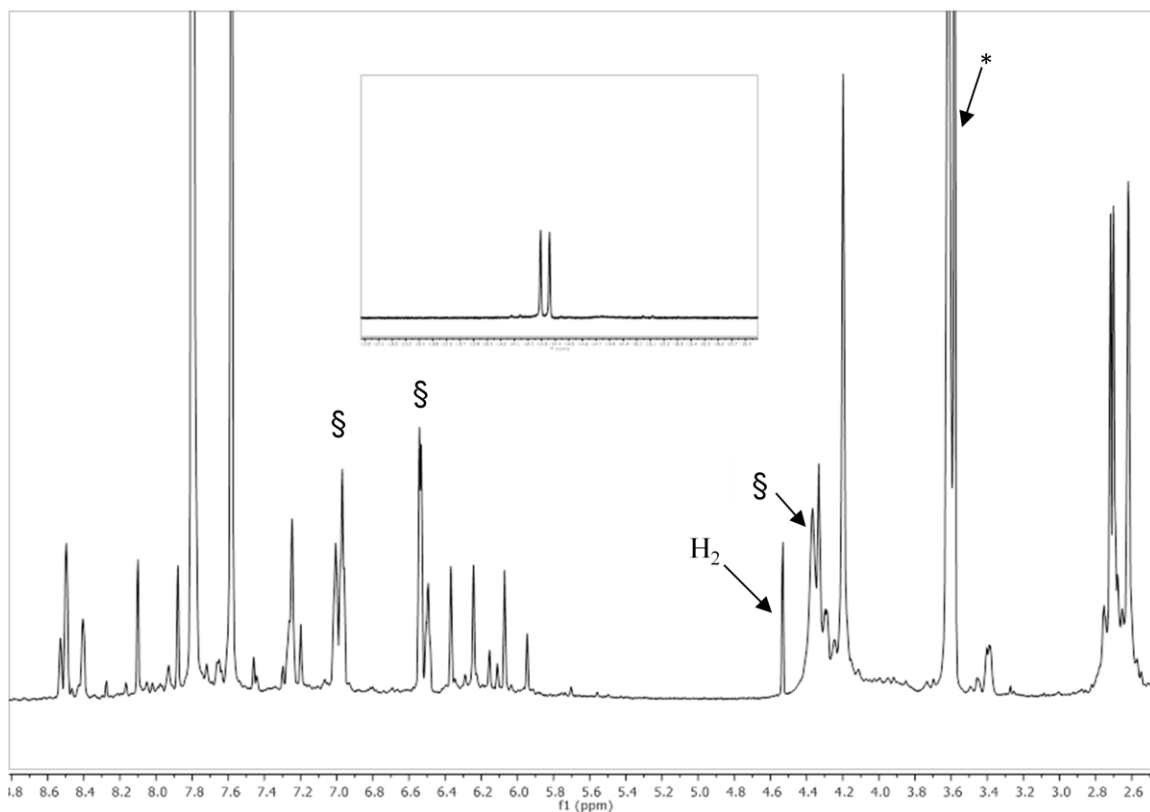
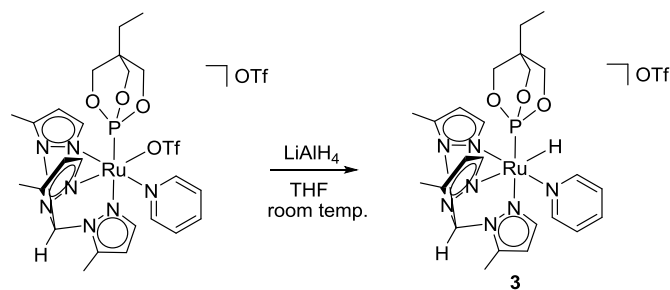


Figure 9. ¹H NMR spectrum (500 MHz, THF-*d*₈) at the end of the reaction between $\{[\text{HC}(\text{pz}^5)_3]\text{Ru}[\text{P}(\text{OCH}_2)_3\text{CEt}](\text{py})(\text{NHPh})\}[\text{BAr}'_4]$ (**1**) and H₂. Inset: The hydride region, showing the final hydride resonance at -14.3 ppm. Solvent resonance denoted by *. Free aniline denoted by §.

4.4.1 Synthesis of $\{[\text{HC}(\text{pz}^5)_3]\text{Ru}[\text{P}(\text{OCH}_2)_3\text{CEt}](\text{py})(\text{H})\}^+$ (**3**)

At room temperature, lithium aluminum hydride (LiAlH₄) was added to a THF solution of $\{[\text{HC}(\text{pz}^5)_3]\text{Ru}[\text{P}(\text{OCH}_2)_3\text{CEt}](\text{py})(\text{OTf})\}[\text{OTf}]$ resulting in the conversion of the Ru–pyridine/triflate complex to $\{[\text{HC}(\text{pz}^5)_3]\text{Ru}[\text{P}(\text{OCH}_2)_3\text{CEt}](\text{py})(\text{H})\}^+$ (**3**) in ~80% yield, as indicated by six pyrazolyl resonances and a methine resonance, coordinated pyridine resonances at 8.50, 7.59, and 7.01 ppm, and a hydride resonance at -14.3 ppm (d, ²J_{PH} = 40 Hz) in the ¹H NMR spectrum (Scheme 5, Figure 10). A resonance at 136.5 ppm is observed in the ³¹P NMR spectrum of **3**.



Scheme 5. Synthesis of $\{[\text{HC}(\text{pz}^5)_3]\text{Ru}[\text{P}(\text{OCH}_2)_3\text{CEt}](\text{py})(\text{H})\}[\text{OTf}]$ (**3**).

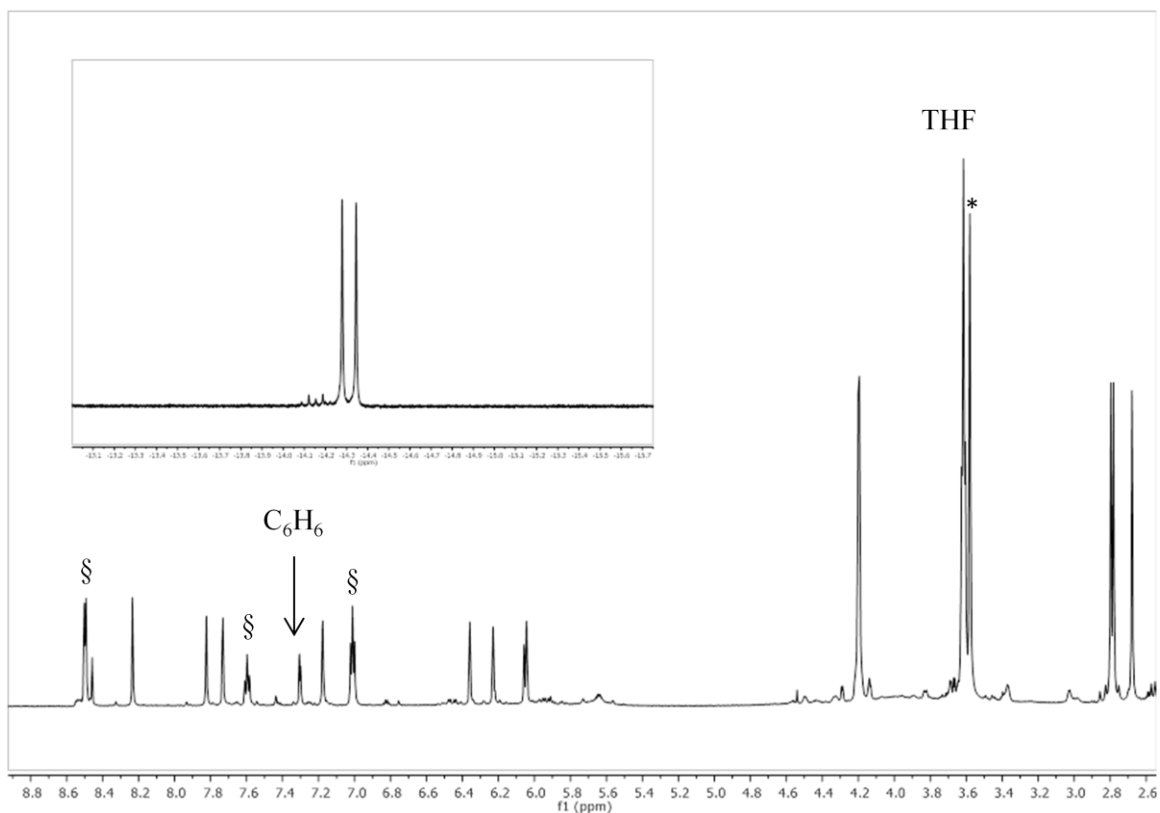


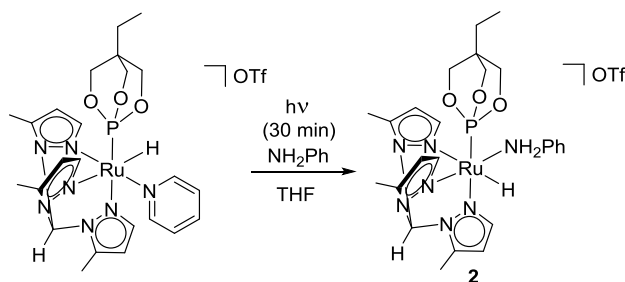
Figure 10. ^1H NMR spectrum (500 MHz, $\text{THF-}d_8$) of $\{[\text{HC}(\text{pz}^5)_3]\text{Ru}[\text{P}(\text{OCH}_2)_3\text{CEt}](\text{py})(\text{H})\}[\text{OTf}]$ (**2**). Solvent resonance denoted by *. Pyridine resonances denoted by §.

4.4.2 Synthesis of $\{[\text{HC}(\text{pz}^5)_3]\text{Ru}[\text{P}(\text{OCH}_2)_3\text{CEt}](\text{NH}_2\text{Ph})(\text{H})\}[\text{OTf}]$ (**2**)

The independent synthesis of complex **2** proved to be much more challenging than that for complex **3**. Multiple synthetic routes to afford **2** were explored. The addition of LiAlH_4 to a THF solution of $\{[\text{HC}(\text{pz}^5)_3]\text{Ru}[\text{P}(\text{OCH}_2)_3\text{CEt}](\text{NH}_2\text{Ph})(\text{Cl})\}[\text{OTf}]$ at room temperature gave multiple intractable species with trace hydride resonances appearing at -11.5, -15.7 and -16.7 ppm

in the ^1H NMR spectrum. Reactions involving either sodium borohydride (NaBH_4) or lithium triethylborohydride (LiEt_3BH) with $\{[\text{HC}(\text{pz}^5)_3]\text{Ru}[\text{P}(\text{OCH}_2)_3\text{CEt}](\text{NH}_2\text{Ph})(\text{Cl})\}[\text{OTf}]$ afforded the liberation of $\text{HC}(\text{pz}^5)_3$ (in the case of NaBH_4) and formation of multiple intractable products. Attempts at Cl/OTf exchange followed by hydride transfer using AgOTf and LiAlH_4 , respectively, were similarly unsuccessful.

As synthesizing a Ru–aniline/hydride complex directly from $\{[\text{HC}(\text{pz}^5)_3]\text{Ru}[\text{P}(\text{OCH}_2)_3\text{CEt}](\text{NH}_2\text{Ph})(\text{Cl})\}[\text{OTf}]$ did not prove successful, photolysis of $\{[\text{HC}(\text{pz}^5)_3]\text{Ru}[\text{P}(\text{OCH}_2)_3\text{CEt}](\text{py})(\text{H})\}[\text{OTf}]$ in the presence of excess aniline was carried out to exchange the coordinated pyridine with aniline. After several attempts, it was determined that photolysis of a THF solution of **3** and NH_2Ph for 30 min produced the desired product, $\{[\text{HC}(\text{pz}^5)_3]\text{Ru}[\text{P}(\text{OCH}_2)_3\text{CEt}](\text{NH}_2\text{Ph})(\text{H})\}[\text{OTf}]$ (**2**), in ~36% yield by ^1H NMR spectroscopy (Scheme 6). The ^1H NMR spectrum of the product is consistent with that of the -14.9 ppm hydride species observed in H_2 activation reactions. A hydride resonance is observed at -14.9 ppm (d, $^2J_{\text{PH}} = 39$ Hz), coordinated aniline NH_2 doublets are observed at 5.12 and 4.99 ppm ($^2J_{\text{HH}} = 11$ Hz) and phenyl resonances are observed at 7.02 (m), 6.90 (m), and 6.74 ppm (d, $^3J_{\text{HH}} = 7$ Hz) (Figure 11). Pyridine is not observed in the ^1H NMR spectrum of **2**.



Scheme 6. Synthesis of $\{[\text{HC}(\text{pz}^5)_3]\text{Ru}[\text{P}(\text{OCH}_2)_3\text{CEt}](\text{NH}_2\text{Ph})(\text{H})\}[\text{OTf}]$ (**2**).

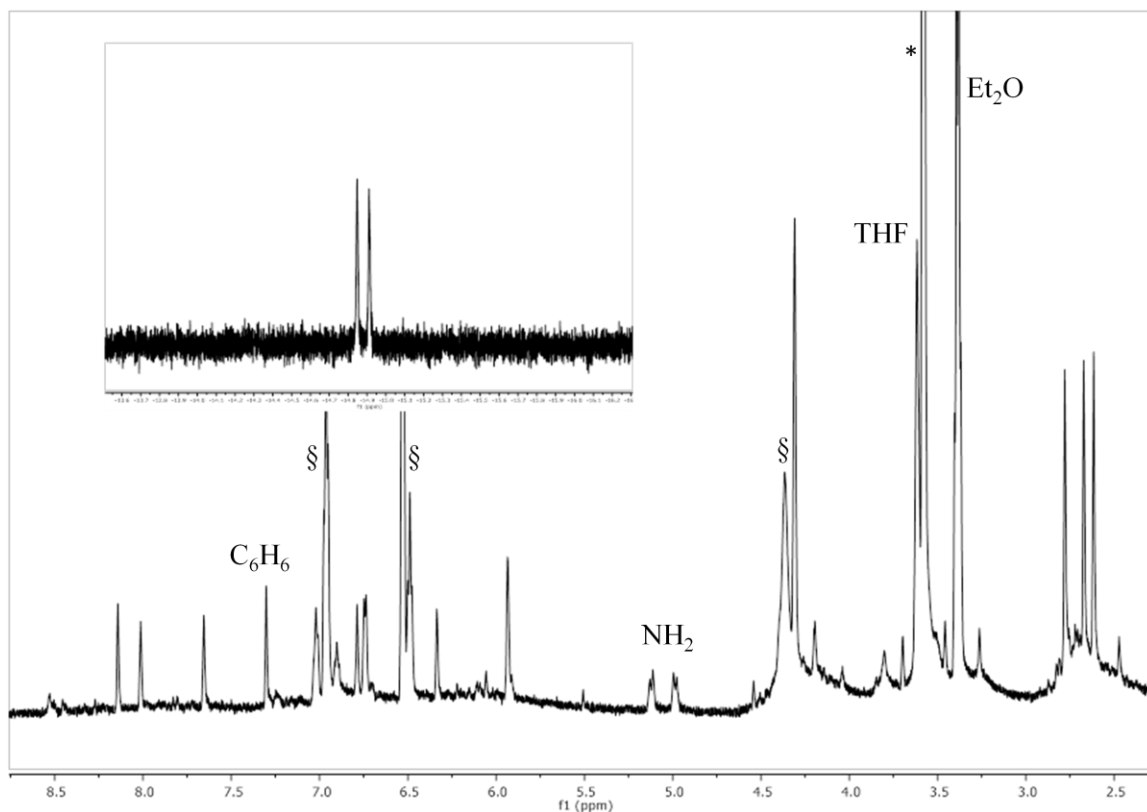


Figure 11. ^1H NMR spectrum (500 MHz, $\text{THF-}d_8$) of $\{[\text{HC}(\text{pz}^5)_3]\text{Ru}[\text{P}(\text{OCH}_2)_3\text{CEt}](\text{NH}_2\text{Ph})(\text{H})\}[\text{OTf}]$ (**3**). Solvent resonance denoted by *. Free aniline denoted by §.

4.4.3 Attempted synthesis of $\{[\text{HC}(\text{pz}^5)_3]\text{Ru}[\text{P}(\text{OCH}_2)_3\text{CEt}](\text{THF})(\text{H})\}^+$ (**4**)

With the confirmation of the identities of the hydride complexes with resonances at -14.3 and -14.9 ppm, multiple attempts were made to independently synthesize the -16.7 ppm species thought to be $\{[\text{HC}(\text{pz}^5)_3]\text{Ru}[\text{P}(\text{OCH}_2)_3\text{CEt}](\text{THF})(\text{H})\}^+$ (**4**). LiAlH_4 was added to a THF solution of $[\text{HC}(\text{pz}^5)_3]\text{Ru}[\text{P}(\text{OCH}_2)_3\text{CEt}](\text{Cl})_2$ in THF at room temperature for 3 h, resulting in the formation of a complex with deprotonated $\text{HC}(\text{pz}^5)_3$ and trace complexes with hydride resonances at -10.2, -15.3, and -16.6 ppm. Addition of LiEt_3BH to $[\text{HC}(\text{pz}^5)_3]\text{Ru}[\text{P}(\text{OCH}_2)_3\text{CEt}](\text{Cl})_2$ at 60 °C in THF resulted in complexes with hydride resonances at -9.2, -15.3, -16.6 and -16.7 ppm. Reactions of $\{[\text{HC}(\text{pz}^5)_3]\text{Ru}[\text{P}(\text{OCH}_2)_3\text{CEt}](\text{THF})(\text{OTf})\}[\text{OTf}]$ with either LiAlH_4 , NaBH_4 or LiEt_3BH either resulted in decomposition with trace hydrides or minimal reaction in the case of LiEt_3BH (except for a minor hydride resonance at -9.6 ppm). A THF solution of

{[HC(pz⁵)₃Ru[P(OCH₂)₃CEt](THF)(OTf)]}[OTf] was pressurized with H₂ (25 or 30 psi) and heated at either 70 or 110 °C, but no reaction occurred to produce either an η²-H₂ complex or a hydride species after days of heating; the starting material was stable in solution under these conditions. Finally, heating a THF-*d*₈ solution of LiAlH₄ and the dimer {[HC(pz⁵)₃Ru[P(OCH₂)₃CEt](μ-Cl)]₂[OTf]₂ at 60 °C for 30 minutes resulted in the formation of an asymmetric species with coordinated HC(pz⁵)₃, P(OCH₂)₃CEt, and a hydride resonance at -16.7 ppm, as observed by ¹H NMR spectroscopy (Figure 13 inset). The ¹H NMR spectrum showed an impure mixture, but the ³¹P NMR spectrum showed one product with a resonance at 125.7 ppm (Figure 13). However, this resonance was not observed in the ³¹P NMR spectrum of the H₂ activation reaction mixture, and this complex could not be confirmed to be the same as the -16.7 ppm hydride complex formed by H₂ activation by {[HC(pz⁵)₃Ru[P(OCH₂)₃CEt](py)(NHPh)]}[BAR'₄] (**1**).

In reactions that produced a complex with a -16.7 ppm hydride resonance ([HC(pz⁵)₃Ru[P(OCH₂)₃CEt](Cl)₂ with LiEt₃BH and {[HC(pz⁵)₃Ru[P(OCH₂)₃CEt](μ-Cl)]₂[OTf]₂ with LiAlH₄), pyridine was not present as pyridine was neither bound to Ru or added to the reaction solution. Coordinated NH₂Ph was present in only *one* of the reactions that produced a -16.7 ppm hydride complex ({[HC(pz⁵)₃Ru[P(OCH₂)₃CEt](NH₂Ph)(Cl)]}[OTf] with LiAlH₄, see Section 4.4.2). These observations indicate that neither pyridine nor aniline is coordinated to Ru in complex **4**. While chlorides are coordinated to the Ru complexes that are reacted with hydride reagents to produce a resonance at -16.7 ppm, chloride is not present during the H₂ activation reaction. Thus, chloride is also not bound to **4**, leaving THF as a possible substrate available to coordinate to Ru. There was no evidence by ¹H and ³¹P NMR spectroscopy that a second P(OCH₂)₃CEt was coordinated to complex **4**, as the hydride resonance would have been split into a doublet of doublets by two phosphite ligands in an asymmetric complex (two doublets would also have been visible by ³¹P NMR spectroscopy, each exhibiting a ²J_{PP} coupling constant). For a C_s symmetric complex, the hydride resonance would be split into a triplet by the

equivalent phosphite resonances. Therefore, **4** is proposed to be $\{[\text{HC}(\text{pz}^5)_3]\text{Ru}[\text{P}(\text{OCH}_2)_3\text{CEt}](\text{THF})(\text{H})\}^+$ (Figure 12). This hypothesis is reasonable, as both pyridine and aniline have been observed to dissociate over the course of the reaction by ^1H NMR and the temporary coordination of THF (the solvent for the reaction) is known to be common for complexes with an open coordination site. Furthermore, the addition of only 0.3 equiv. of free pyridine to the reaction solution effectively prohibited the formation of **4** during H_2 activation by **1**, giving further evidence that **4** is a THF adduct.

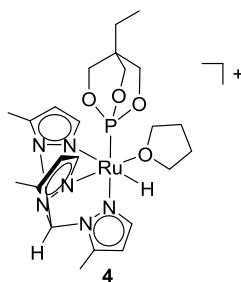


Figure 12. Proposed identity of complex **4**.

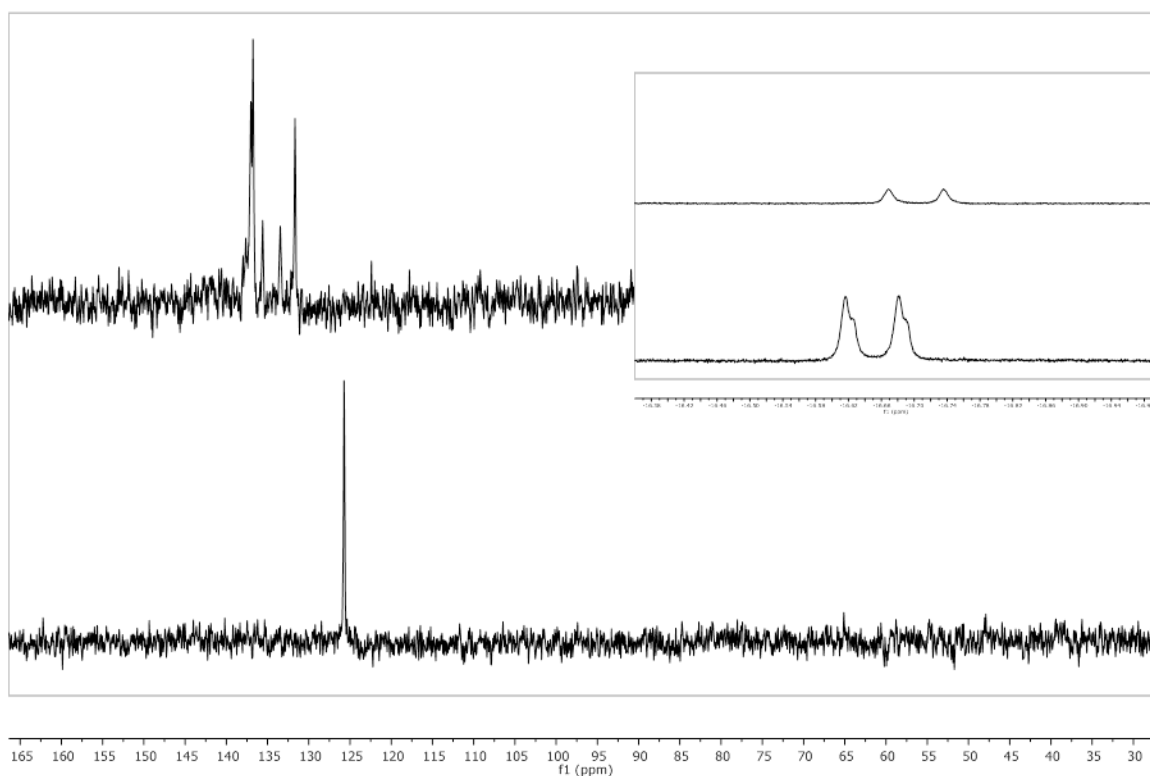
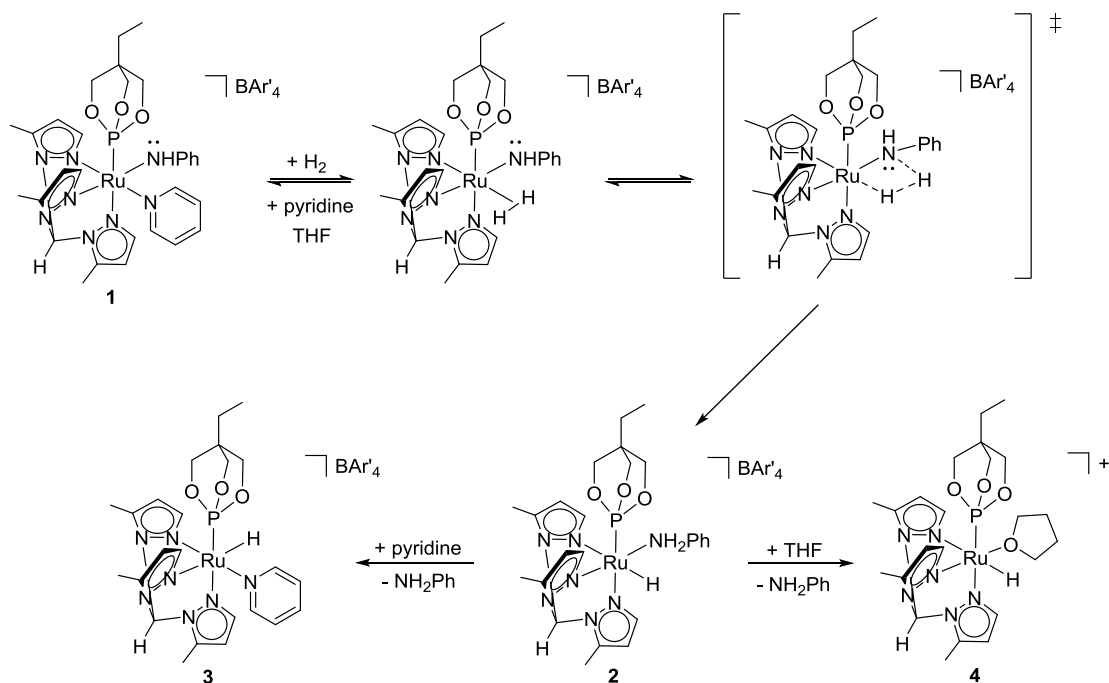


Figure 13. ^{31}P NMR spectra (500 MHz, $\text{THF-}d_8$) of the H_2 activation reaction by $\{[\text{HC}(\text{pz}^5)_3]\text{Ru}[\text{P}(\text{OCH}_2)_3\text{CEt}](\text{py})(\text{NHPh})\}[\text{BAR}'_4]$ (**1**) in progress (top) and the product of the reaction of $\{[\text{HC}(\text{pz}^5)_3]\text{Ru}[\text{P}(\text{OCH}_2)_3\text{CEt}](\mu\text{-Cl})\}_2[\text{OTf}]_2$ with LiAlH_4 (bottom). Inset: respective hydride resonances.

4.5 Proposed Mechanism for H_2 Activation and Formation of Hydride Complexes

The identification of the hydride complexes formed during H_2 activation led to the proposal of the following reaction mechanism for H_2 activation by $\{[\text{HC}(\text{pz}^5)_3]\text{Ru}[\text{P}(\text{OCH}_2)_3\text{CEt}](\text{py})(\text{NHPh})\}[\text{BAR}'_4]$ (**1**) (Scheme 7). First, pyridine dissociates from **1** to open a coordination site at the metal center. Dihydrogen then binds to the metal center and is activated by the anilido ligand to form complex **2**. No $\eta^2\text{-H}_2$ complexes are observed by ^1H NMR spectroscopy and are transient if formed. Net exchange of aniline with pyridine or THF forms complex **3** or **4**, respectively.



Scheme 7. Proposed mechanism of H₂ activation by $\{[\text{HC}(\text{pz}^5)_3]\text{Ru}[\text{P}(\text{OCH}_2)_3\text{CEt}](\text{py})(\text{NHPh})\}[\text{BAR}'_4]$ (**1**) with formation of $\{[\text{HC}(\text{pz}^5)_3]\text{Ru}[\text{P}(\text{OCH}_2)_3\text{CEt}](\text{THF})(\text{H})\}^+$ (**4**) in THF.

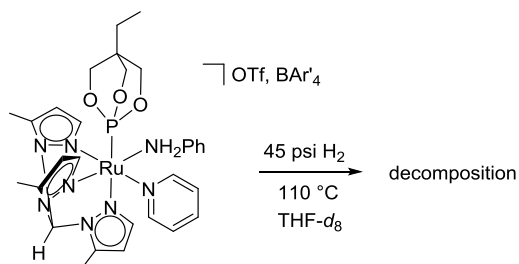
4.6 Kinetic and Mechanistic Studies of H₂ Activation by

$\{[\text{HC}(\text{pz}^5)_3]\text{Ru}[\text{P}(\text{OCH}_2)_3\text{CEt}](\text{py})(\text{NHPh})\}[\text{BAR}'_4]$ (**1**)

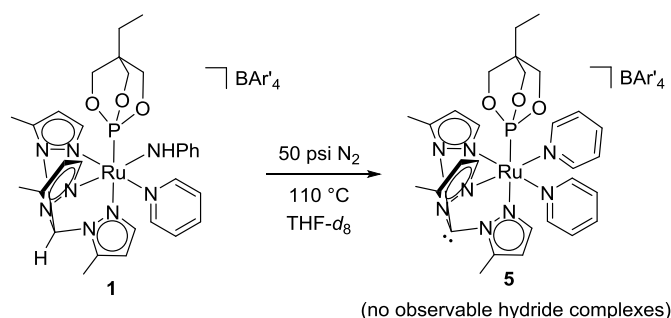
4.6.1 Control Experiments

Pressurizing a THF-*d*₈ solution of $\{[\text{HC}(\text{pz}^5)_3]\text{Ru}[\text{P}(\text{OCH}_2)_3\text{CEt}](\text{py})(\text{NH}_2\text{Ph})\}[\text{OTf}][\text{BAR}'_4]$ with 45 psi H₂ and subsequent heating to 110 °C resulted in decomposition without production of any observable Ru hydride species, indicating that the hydride species do not likely form from H₂ activation by the aniline complex (Scheme 8). Adding $\{[\text{HC}(\text{pz}^5)_3]\text{Ru}[\text{P}(\text{OCH}_2)_3\text{CEt}](\text{py})(\text{NH}_2\text{Ph})\}[\text{OTf}][\text{BAR}'_4]$ to a THF-*d*₈ solution of $\{[\text{HC}(\text{pz}^5)_3]\text{Ru}[\text{P}(\text{OCH}_2)_3\text{CEt}](\text{py})(\text{NHPh})\}[\text{BAR}'_4]$ (**1**), pressurizing with 45 psi H₂, and heating at 110 °C did not appear to have any effect on H₂ activation by **1**, and $\{[\text{HC}(\text{pz}^5)_3]\text{Ru}[\text{P}(\text{OCH}_2)_3\text{CEt}](\text{py})(\text{NH}_2\text{Ph})\}[\text{OTf}][\text{BAR}'_4]$ decomposed over the course of the reaction. Heating a THF solution of complex **1** under nitrogen pressure afforded conversion to

the C_s symmetric complex $\{[C(pz^5)_3]Ru[P(OCH_2)_3CEt](py)_2\}[BAR'_4]$ (~50% yield) formed by the competing side reaction unrelated to the pathway for H_2 activation (Scheme 9, see Section 4.2). Thus, $\{[HC(pz^5)_3]Ru[P(OCH_2)_3CEt](py)(NHPh)\}[BAR'_4]$ produces no observable Ru hydride complexes in the absence of H_2 .



Scheme 8. Reaction of $\{[HC(pz^5)_3]Ru[P(OCH_2)_3CEt](py)(NH_2Ph)\}[OTf][BAR'_4]$ with H_2 .



Scheme 9. Reaction of $\{[HC(pz^5)_3]Ru[P(OCH_2)_3CEt](py)(NHPh)\}[BAR'_4]$ (**1**) under N_2 .

4.6.2 General Reaction Setup for Kinetic Studies involving $\{[HC(pz^5)_3]Ru[P(OCH_2)_3CEt](py)(NHPh)\}[BAR'_4]$ (**1**)

Kinetic studies were performed in triplicate. A stock solution containing Ru–NHAr complex (Ar = aryl group) [0.0528 M], hexamethyldisilane (HMDS, internal standard) [0.0049 M], and THF- d_8 (1 mL) was prepared in a volumetric flask. An aliquot (280 μ L) of stock solution was added to each of three high pressure NMR tubes. The tubes were sealed and degassed through three consecutive freeze-pump-thaw cycles (for experiments involving H_2) and subsequently pressurized with the desired gas (H_2 or N_2). Each tube was then heated to 90 $^\circ$ C in

the probe of an NMR spectrometer, and arrayed data collection was used to collect ^1H NMR spectra every 3.7 minutes.

4.6.3 H_2 Pressure Dependence Studies

We hoped to carefully elucidate kinetic experiments to shed light on the details of H_2 activation by $\{[\text{HC}(\text{pz}^5)_3]\text{Ru}[\text{P}(\text{OCH}_2)_3\text{CEt}](\text{py})(\text{NHAr})\}[\text{BAr}'_4]$ ($\text{Ar} = 4\text{-isopropylphenyl}$, 4-methylphenyl , phenyl , 4-chlorophenyl , 4-fluorophenyl) complexes. However, as outlined below, challenges associated with multi-phase reactions (gas/liquid) and possibly the equilibrium between $\{[\text{HC}(\text{pz}^5)_3]\text{Ru}[\text{P}(\text{OCH}_2)_3\text{CEt}](\text{py})(\text{NHPh})\}[\text{BAr}'_4]$ (**1**) (major) and $\{[:\text{C}(\text{pz}^5)_3]\text{Ru}[\text{P}(\text{OCH}_2)_3\text{CEt}](\text{py})(\text{NH}_2\text{Ph})\}[\text{BAr}'_4]$ (**1'**) complicated the ability to get reproducible results. Attempts were made to study the effect of H_2 pressure on the rate of H_2 activation by **1**. Using the ideal gas law and an estimate of the volume of the NMR tube minus the volume of the sample, it was determined that H_2 should be in excess relative to **1** when pressurizing with 35 psi (~ 0.12 mmol H_2 , 8 fold excess relative to **1**), 45 psi (~ 0.15 mmol H_2 , 10 fold excess relative to **1**), 55 psi (~ 0.18 mmol H_2 , 12 fold excess relative to **1**), and 65 psi (~ 0.22 mmol H_2 , 15 fold excess relative to **1**) of H_2 . Thus, our hope was to achieve pseudo first order conditions since H_2 would be present in excess (this would require fast diffusion relative to reaction rate). Assuming pseudo first order conditions in H_2 (under the assumption that H_2 diffusion is faster than the rate of the reaction), the reaction rates at 90°C were obtained by plotting $\ln[\mathbf{1}]$, which was determined from integrations of ^1H NMR spectra relative to an internal standard, vs. time and fitting the data to a linear function (Figure 14). The linear fits are reasonable, if not perfect. At H_2 pressures of 35, 45, 55 and 65 psig, the k_{obs} (s^{-1}) values were found to be values of $1.28(3) \times 10^{-3}$, $5.6(8) \times 10^{-4}$, $9.4(6) \times 10^{-4}$, $9.5(4) \times 10^{-4}$, respectively (Table 1). However, the concentration of H_2 in solution vs concentration of **1** was determined by ^1H NMR spectroscopy and showed that concentration of H_2 in solution was not in excess relative to **1**. Furthermore, we were not able to achieve a consistent starting $[\text{H}_2]$ as indicated by deviations in initial $[\text{H}_2]$ among the three samples for each pressure (reactions were performed in triplicate) (Table 1). Yet, pseudo first order conditions

might be achieved if H₂ diffusion into solution was faster than the rate of H₂ consumption by the reaction with **1**, as mentioned above. A plot of [H₂] vs time over the course of the reaction showed that [H₂] remained relatively constant, indicating that the rate of H₂ diffusion into solution is faster than the rate of the reaction (Figure 15). Plots of k_{obs} vs H₂ pressure (psig) and k_{obs} vs initial [H₂] for each of the three NMR samples showed no trend (Figure 16 and 17).

In principle, the reaction rate can be obtained by monitoring the disappearance of starting complex (**1**) over time. However, analysis of the H₂ pressure studies by this method is further complicated by the equilibrium between $\{[\text{HC}(\text{pz}^5)_3]\text{Ru}[\text{P}(\text{OCH}_2)_3\text{CEt}](\text{py})(\text{NHPh})\}[\text{BAr}'_4]$ (**1**) and $\{[:\text{C}(\text{pz}^5)_3]\text{Ru}[\text{P}(\text{OCH}_2)_3\text{CEt}](\text{py})(\text{NH}_2\text{Ph})\}[\text{BAr}'_4]$ (**1'**). Conversion of complex **1'** to **1** could skew the rate at which **1** is converted to $\{[\text{HC}(\text{pz}^5)_3]\text{Ru}[\text{P}(\text{OCH}_2)_3\text{CEt}](\text{H})(\text{NH}_2\text{Ph})\}[\text{BAr}'_4]$ (**2**). Another significant source of error arises from the competing side reaction wherein complexes **1** and **1'** produce $\{[:\text{C}(\text{pz}^5)_3]\text{Ru}[\text{P}(\text{OCH}_2)_3\text{CEt}](\text{py})_2\}[\text{BAr}'_4]$ (**5**) and an unidentified decomposition product. The rate of reaction can also be obtained by monitoring the appearance of product over time, circumventing some sources of error. As three hydride complexes (**2**, **3**, and **4**) were formed over the course of the reaction, the sum of the concentrations of these hydride species was used in the following analysis. Plotting $\ln[\text{sum of } \mathbf{2}, \mathbf{3}, \text{ and } \mathbf{4}]$ gave k_{obs} (s⁻¹) values of 4.8(1) x 10⁻⁴, 3.3(7) x 10⁻⁴, 8.7(10) x 10⁻⁴, and 1.7(7) x 10⁻⁴ for pressures of 35, 45, 55, and 65 psig H₂, respectively (Table 1, Figure 18). These k_{obs} values obtained from product formation analysis are lower than those obtained from monitoring the disappearance of starting material (complex **1**) as expected, as the disappearance of **1** includes consumption of **1** by the side reaction to form complex **5**. Nevertheless, no trend can be seen from these values, either, likely resulting from different amounts of possible impurities in the starting material and irreproducibility in the extent of the side reaction to form **5**. Therefore, reaching definitive conclusions is not possible.

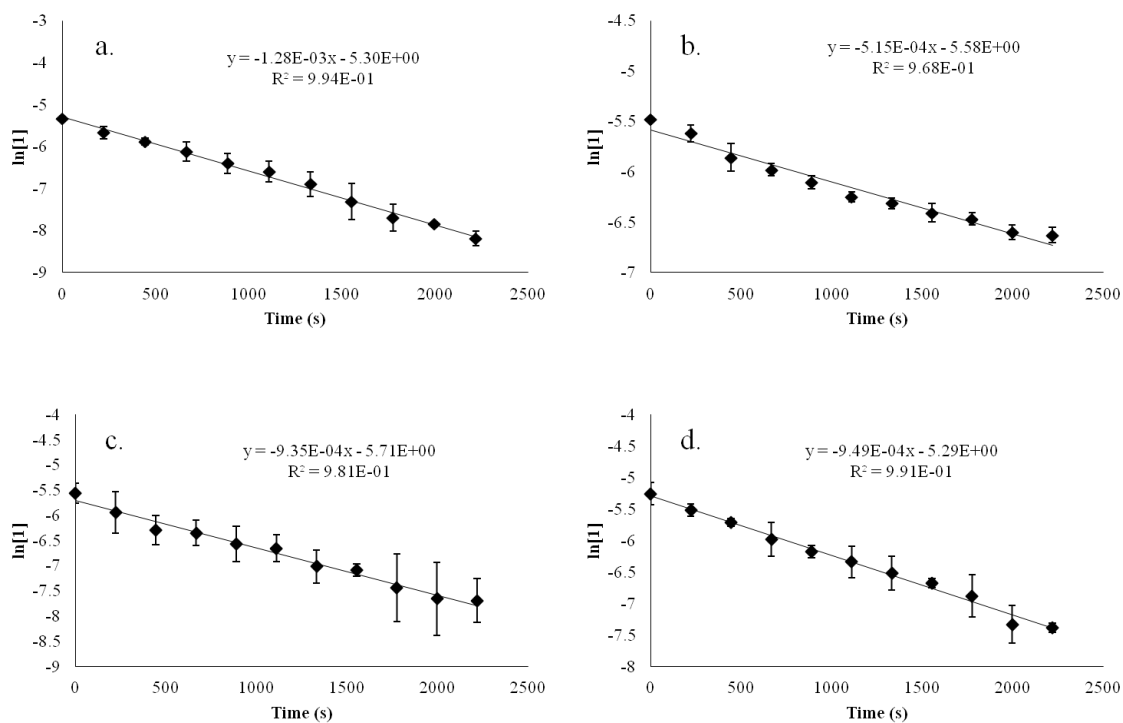


Figure 14. Plot of $\ln[1]$ vs time (s) for the reactions of **1** (0.0528 M) with H_2 at 35 (a.), 45 (b.), 55 (c.), 65 (d.) psig at 90 °C.

Table 1. H_2 pressure dependence on experimental rates of H_2 activation.

H_2 pressure (psig)	Initial $[H_2]$ in triplicate			$k_{obs} (s^{-1})$	$k_{obs} (s^{-1})$
				(disappearance of 1)	(appearance of total hydride complexes)
35	0.0035	0.0027	0.0018	$1.28(3) \times 10^{-3}$	$4.8(1) \times 10^{-4}$
45	0.0041	0.0035	0.0023	$5.2(3) \times 10^{-4}$	$3.3(7) \times 10^{-4}$
55	0.0050	0.0060	0.0038	$9.4(6) \times 10^{-4}$	$8.7(10) \times 10^{-4}$
65	0.0069	0.0067	0.0053	$9.5(4) \times 10^{-4}$	$1.7(7) \times 10^{-4}$

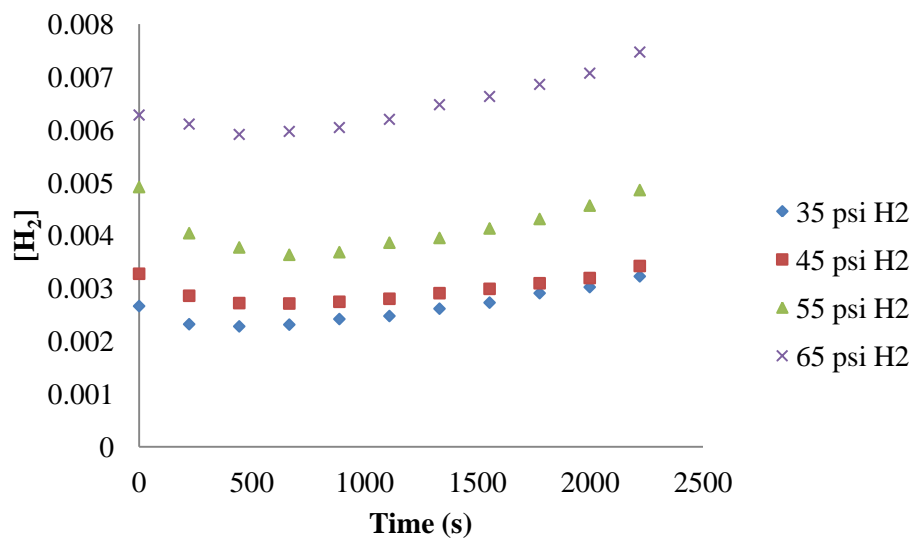
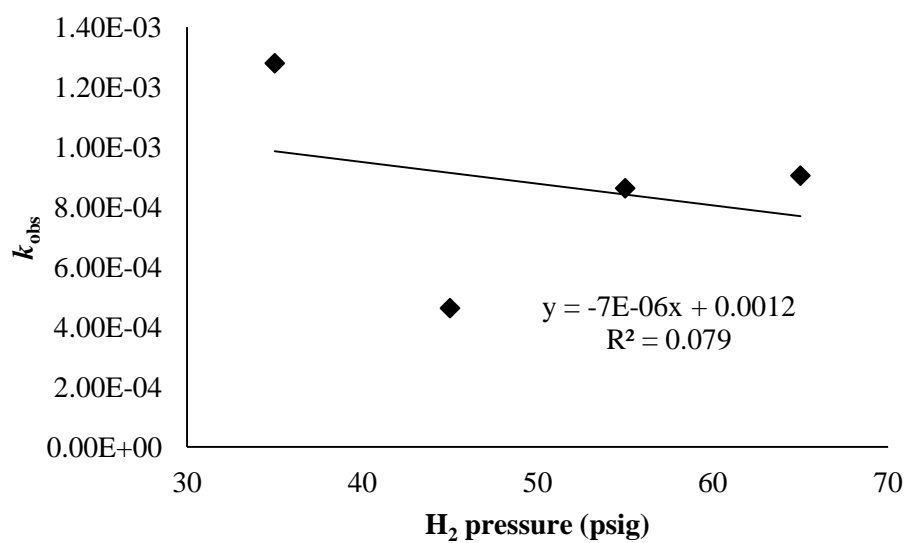


Figure 15. Concentration of H₂ in solution over reaction time.



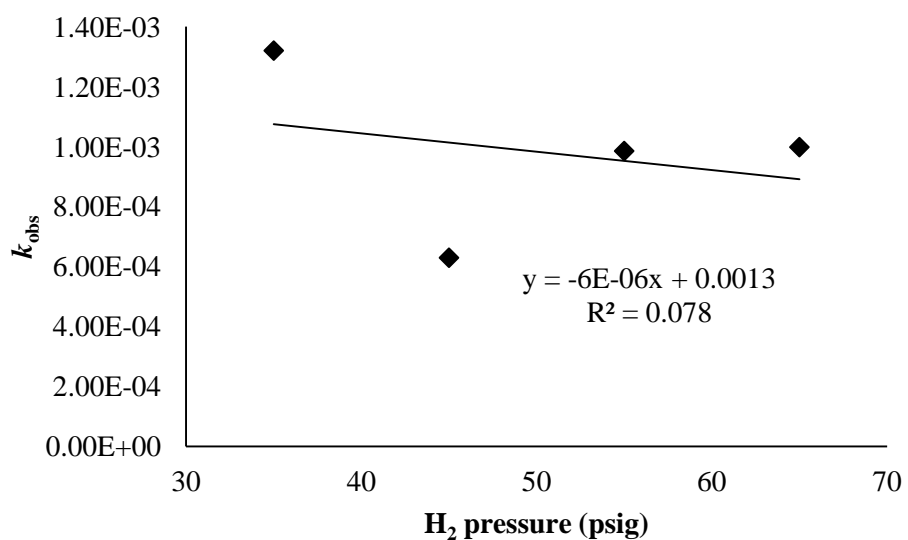
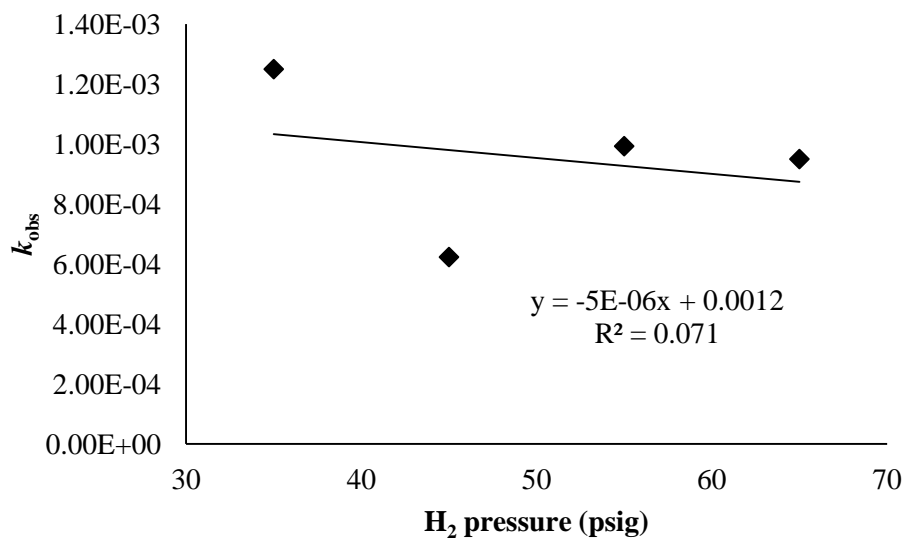
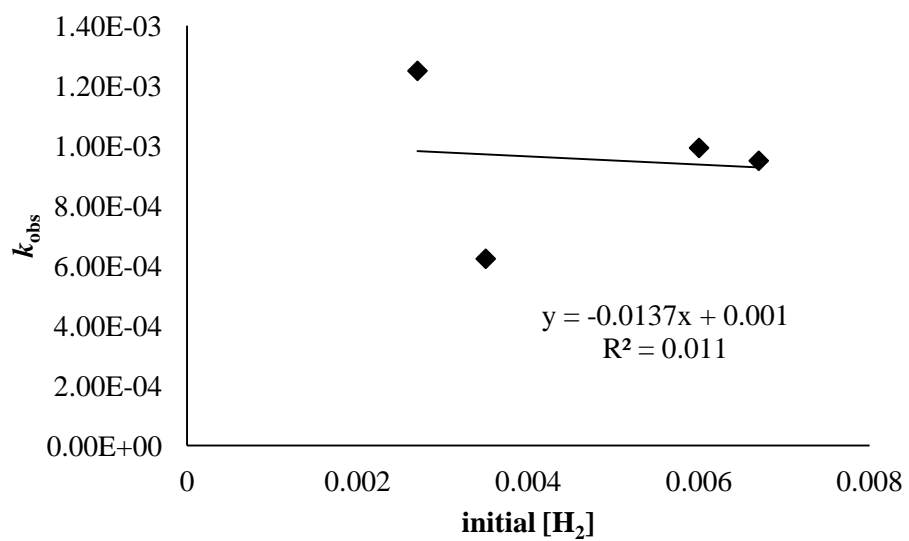
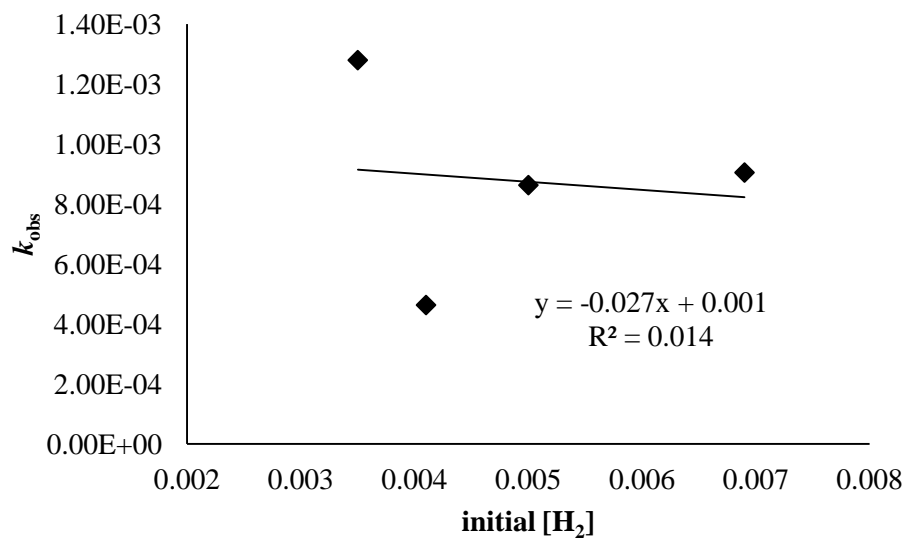


Figure 16. Three plots of k_{obs} vs H_2 pressure (35, 45, 55, 65 psig) obtained by performing H_2 activation experiments in triplicate. .



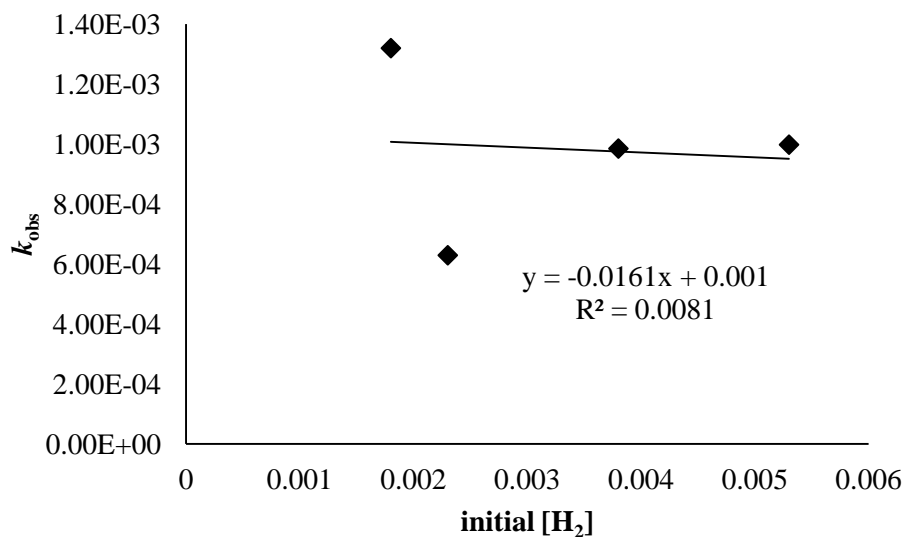


Figure 17. Three plots of k_{obs} vs initial $[\text{H}_2]$ for 35, 45, 55 and 65 psig H_2 obtained by performing H_2 activation experiments in triplicate.

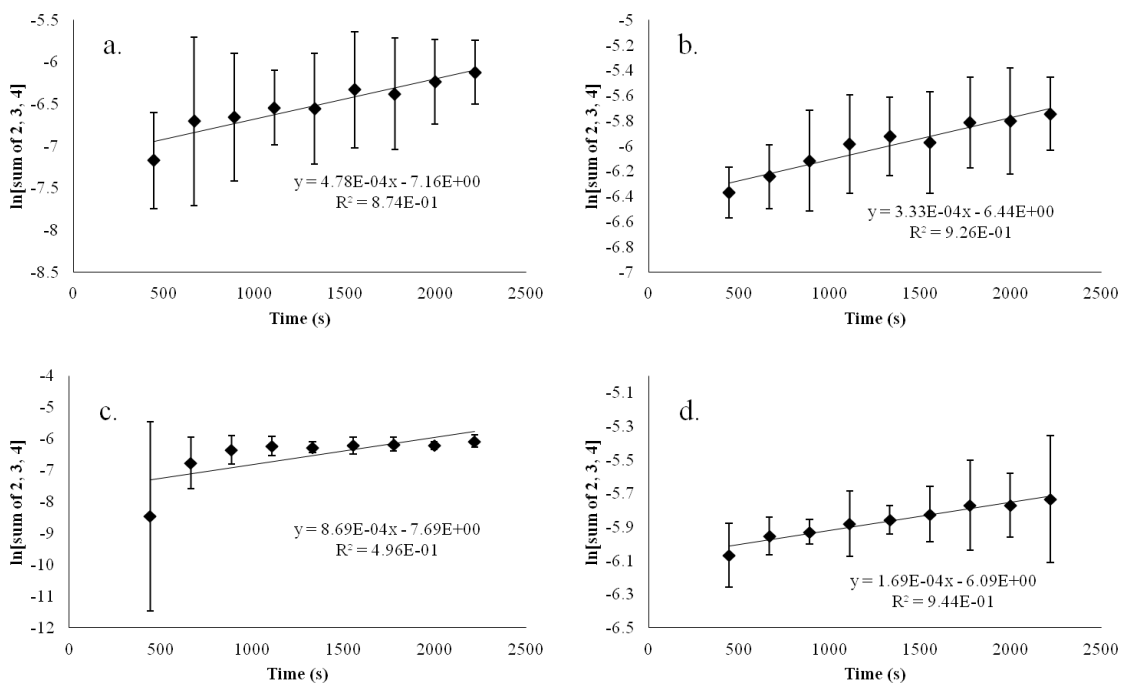


Figure 18. Plot of $\ln[\text{sum of 2, 3, and 4}]$ vs time (s) for the reactions of 1 (0.0528 M) with H_2 at 35 (a.), 45 (b.), 55 (c.), 65 (d.) psig at 90°C .

4.6.4 D₂ Activation by Complex 1

D₂ activation (55 psig) by **1** was studied at 90 °C. The measurement of a KIE was attempted. However, as stated above, the reactions do not proceed under pseudo first order conditions of H₂ or D₂ in solution and no real conclusions can be made from a KIE study.

The hydride resonances at -14.3, -14.9, and -16.7 ppm were observed by ²H NMR spectroscopy, further demonstrating that the hydride resonances originate from H₂ (D₂) activation rather than from some intramolecular reaction. Interestingly, it was observed by ²H NMR spectroscopy that a significant amount of H/D scrambling occurs within the Ru complex framework during reactions with D₂. Deuterium incorporation was observed in the 4-position of the pyrazolyl rings and the methine position of the ligand; furthermore, in the ¹H NMR spectrum, a 1:1:1 triplet for HD gas and proton resonances in the hydride positions were observed in reactions involving D₂. These observations are not unexpected, as H/D exchange has been observed between OH and NPh ligands of TpRu(PMe₃)₂(X) (X = OH or NPh) and the pyrazolyl rings of Tp, especially in the pyrazolyl 4-positions.⁵

4.6.5 Pyridine Dependence Studies

Next, the dependence of the rate of H₂ activation by complex **1** on free pyridine was probed. Assuming pseudo first order conditions in H₂, plots of ln[**1**] vs. time for H₂ activation reactions (90 °C, 55 psig H₂) with 0, 0.3, 0.5, and 1.0 equiv. of free pyridine relative to complex **1** gave *k*_{obs} (s⁻¹) values of 9.4(6) × 10⁻⁴, 3.8(4) × 10⁻⁴, 2.5(4) × 10⁻⁴, and 2.4(2) × 10⁻⁴, respectively (Figure 19, Table 2). Performing these experiments with higher equivalents of pyridine would not yield useful data, as excess free pyridine promotes the side reaction that forms {[C(pz⁵)₃Ru[P(OCH₂)₃CEt](py)₂][BAr'₄]} (**5**). However, these concentrations of added pyridine did not appear to have a large effect on the amount of complex **5** formed during the reaction. Yields (determined by ¹H NMR spectroscopy) of **5** formed at the end of monitoring kinetic reactions are included in Table 2. From the data, it can be concluded that adding free pyridine suppresses the rate of H₂ activation, and it is possible that saturation kinetics are observed since

there is little difference in rate for the addition of 0.3, 0.5, and 1.0 equivalents of pyridine. But, quantitative interpretation of the data is difficult due to the challenges in achieving reliable rate constants under the experimental conditions. As with the H₂ pressure studies, it was found that [H₂] in solution was not under pseudo first order conditions as observed by ¹H NMR spectroscopy. Also, the competitive formation of **5** complicates analysis. At best, probably the only definitive statement is that added pyridine slows the H₂ activation reaction.

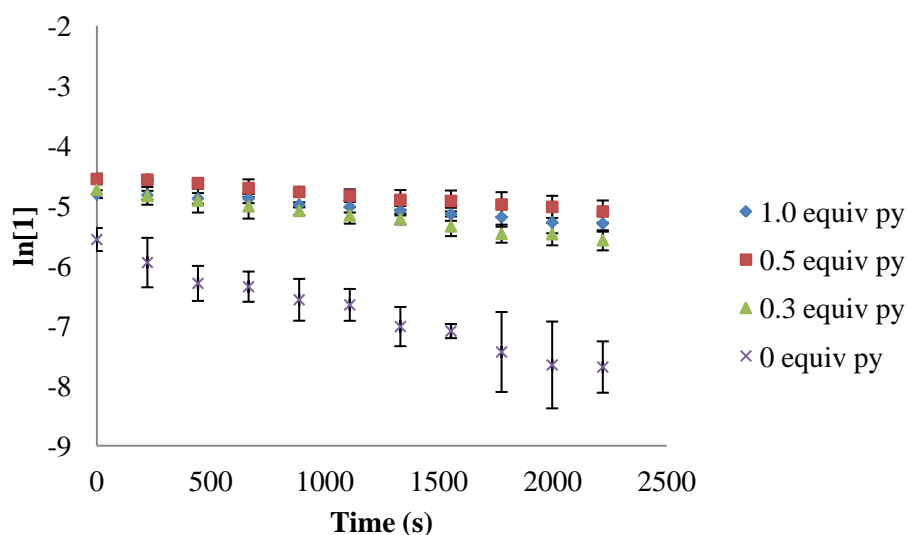


Figure 19. Plot of ln[1] vs time (s) for the reactions of **1** (0.0528 M) with added pyridine (0, 0.3, 0.5, 1.0 eq) and 55 psig H₂ at 90 °C.

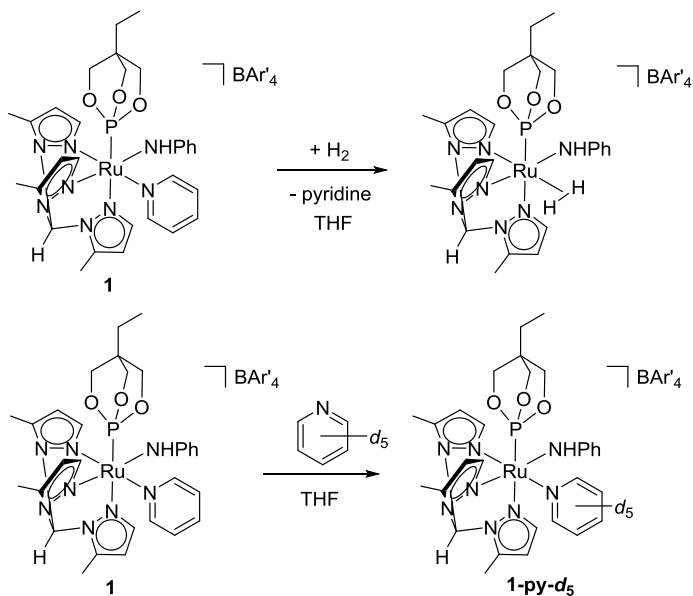
Table 2. Concentration of pyridine dependence on experimental rates for H₂ activation.

Equiv. of added pyridine	k_{obs} (s ⁻¹)	% yield of complex 5
0.0	9.4(6) x 10 ⁻⁴	20%
0.3	3.8(4) x 10 ⁻⁴	11%
0.5	2.5(4) x 10 ⁻⁴	11%
1.0	2.4(2) x 10 ⁻⁴	21%

4.6.6 Degenerative Pyridine Exchange Studies

A coordination site on {[HC(pz⁵)₃]Ru[P(OCH₂)₃CEt](py)(NHPh)}[BAr'₄] (**1**) is likely necessary to allow coordination and activation of H₂ (Scheme 10). The ligand most likely

dissociates to generate a vacant coordination site is pyridine (Scheme 10). In order to assess the lability of the pyridine ligand of **1**, degenerative pyridine exchange studies were performed (Figure 20).



Scheme 10. Dissociation of pyridine from **1** to allow coordination of H_2 (top) and dissociation of pyridine from **1** to allow exchange with pyridine- d_5 (bottom).

Heating (90 °C) THF- d_8 solutions of complex **1** with 5 or 10 equiv. of pyridine- d_5 under nitrogen pressure (50 psig) gave k_{obs} values of $1.2(1) \times 10^{-3}$ and $1.1(2) \times 10^{-3}$ respectively. These k_{obs} show that pyridine exchange is faster than the observed values are comparable to the observed of H_2 activation, ($k_{\text{obs}} = 9.4(6) \times 10^{-4}$), indicating that pyridine dissociation is viable in H_2 activation by **1**. However, the presence of pyridine- d_5 promoted competition between degenerative exchange and the side reaction synthesizing $\{[\text{:C}(\text{pz}^5)_3]\text{Ru}[\text{P}(\text{OCH}_2)_3\text{CEt}](\text{py})_2\}[\text{BAR}'_4]$ (**5**). Yields (determined by ^1H NMR spectroscopy) of **5** formed at the end of monitoring kinetic reactions are included in Table 3, and show a marked increase in the amount of **5** formed with increasing equivalents of added pyridine.

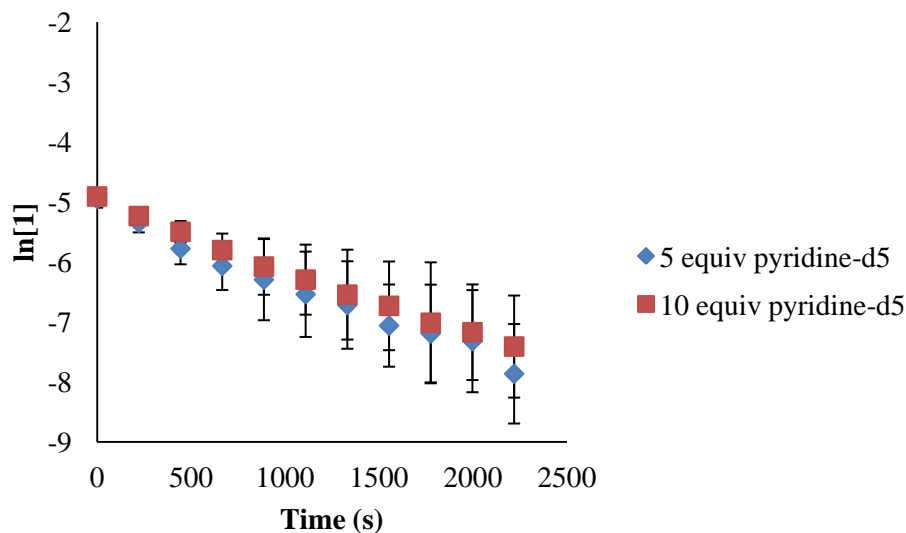


Figure 20. Plot of the $\ln[1]$ vs time (s) for the degenerative exchange of pyridine- d_5 with **1** at 50 psi N_2 , 90 °C.

Table 3. % Yield of complex **5** as a function of added pyridine.

Equiv. of added pyridine	% yield of complex 5
0*	20%*
5	31%
10	43%

*This value is for complex **5** formed during the H_2 activation reaction with **1** at 55 psig H_2 .

4.7 H_2 activation by $\{[HC(pz^5)_3]Ru[P(OCH_2)_3CET](py)(NHAr)][BAr'_4]\}$ (Ar = 4-isopropylphenyl, 4-methylphenyl, 4-chlorophenyl, 4-fluorophenyl)

Following the synthetic procedure for $\{[HC(pz^5)_3]Ru[P(OCH_2)_3CET](py)(NH_2Ph)]OTf[BAr'_4]\}$ discussed in Chapter 3, a series of Ru-substituted aniline complexes were made: $\{[HC(pz^5)_3]Ru[P(OCH_2)_3CET](py)(4\text{-isopropylaniline})\}OTf[BAr'_4]$ (**6**), $\{[HC(pz^5)_3]Ru[P(OCH_2)_3CET](py)(4\text{-methylaniline})\}OTf[BAr'_4]$ (**7**), $\{[HC(pz^5)_3]Ru[P(OCH_2)_3CET](py)(4\text{-chloroaniline})\}OTf[BAr'_4]$ (**8**), $\{[HC(pz^5)_3]Ru[P(OCH_2)_3CET](py)(4\text{-fluoroaniline})\}OTf[BAr'_4]$ (**9**) and $\{[HC(pz^5)_3]Ru[P(OCH_2)_3CET](py)(4\text{-$

(trifluoromethyl)aniline)}[OTf][BAR'₄] (**10**). Furthermore, the corresponding anilido complexes were synthesized by deprotonation using NaHMDS: {[HC(pz⁵)₃]Ru[P(OCH₂)₃CEt](py)(4-isopropylanilido)}[BAR'₄] (**11**), {[HC(pz⁵)₃]Ru[P(OCH₂)₃CEt](py)(4-methylanilido)}[BAR'₄] (**12**), {[HC(pz⁵)₃]Ru[P(OCH₂)₃CEt](py)(4-chloroanilido)}[BAR'₄] (**13**), and {[HC(pz⁵)₃]Ru[P(OCH₂)₃CEt](py)(4-fluoroanilido)}[BAR'₄] (**14**) (Scheme 11). The attempted synthesis of {[HC(pz⁵)₃]Ru[P(OCH₂)₃CEt](py)(4-(trifluoromethyl)anilido)}[BAR'₄] (**15**) resulted in decomposition, indicating that the CF₃ group is somehow incompatible with the deprotonation conditions. Interestingly, syntheses of complexes **11-14** were observed to form major and minor products ($\{[HC(pz^5)_3]Ru[P(OCH_2)_3CEt](py)(NHAr)\}[BAR'_4]$ and $\{[:C(pz^5)_3]Ru[P(OCH_2)_3CEt](py)(NH_2Ar)\}[BAR'_4]$, respectively). K_{eq} was determined by integrating resonances for the major and minor complexes against an internal standard and using the following equation:

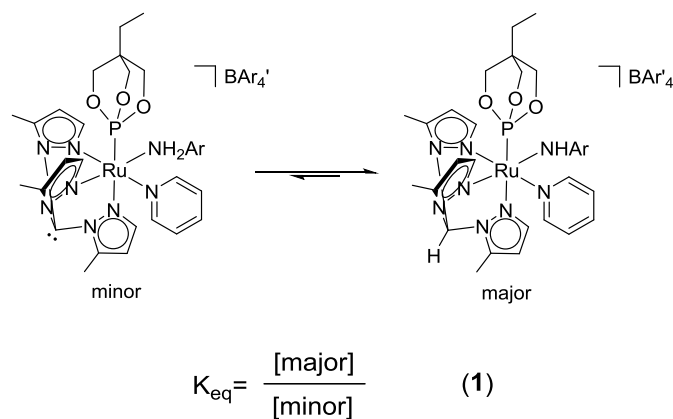
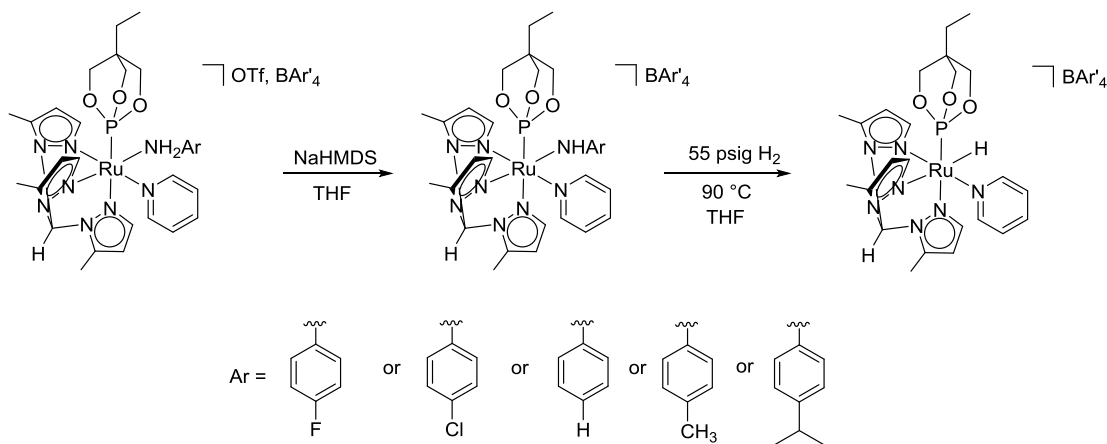


Table 4. Experimental K_{eq} values of the equilibrium between and $\{[HC(pz^5)_3]Ru[P(OCH_2)_3CEt](py)(NHAr)\}[BAR'_4]$ and $\{[:C(pz^5)_3]Ru[P(OCH_2)_3CEt](py)(NH_2Ar)\}$.

Substituent	σ_p^+ value ⁶	K_{eq}
Cl	0.11	1.9
F	-0.07	3.9
H	0.00	11
isopropyl	-0.28	21
CH ₃	-0.31	27

K_{eq} for the different $\{[\text{HC}(\text{pz}^5)_3]\text{Ru}[\text{P}(\text{OCH}_2)_3\text{CEt}](\text{py})(\text{NHAr})\}[\text{BAr}'_4]$ and $\{[:\text{C}(\text{pz}^5)_3]\text{Ru}[\text{P}(\text{OCH}_2)_3\text{CEt}](\text{py})(\text{NHAr})\}$ complexes are listed in Table 4 along with each substituent's σ_{p}^+ value. The data do not appear to show any trend between σ_{p}^+ and K_{eq} . It is currently not understood why these experimental K_{eq} values are found for the respective complexes.

H_2 activation by complexes **11-14** were studied in triplicate at 90 °C and 55 psi H_2 . The following rates were observed for each complex: **11**, $k_{\text{obs}} = 1.6(1) \times 10^{-4}$; **12**, $k_{\text{obs}} = 2.8(3) \times 10^{-4}$; **13**, $k_{\text{obs}} = 7.4(7) \times 10^{-4}$; **14**, $k_{\text{obs}} = 7.8(4) \times 10^{-4}$, assuming pseudo first order conditions in H_2 . A Hammett plot of $\log(k_{\text{substituent}}/k_{\text{H}})$ vs the σ_{p}^+ parameters of H, F, Cl, CH_3 and isopropyl has a reaction constant (ρ) of 1.6. This positive value for ρ is consistent with the trend that more electron-withdrawing groups (i.e., a less basic lone pair) generally promoted faster reaction rates than electron-donating groups (Table 5, Figure 21).



Scheme 11. H_2 activation by $\{[\text{HC}(\text{pz}^5)_3]\text{Ru}[\text{P}(\text{OCH}_2)_3\text{CEt}](\text{py})(\text{NHAr})\}[\text{BAr}'_4]$.

Table 5. Experimental k_{obs} (s^{-1}) values for H_2 activation by $\{[\text{HC}(\text{pz}^5)_3]\text{Ru}[\text{P}(\text{OCH}_2)_3\text{CEt}](\text{py})(\text{NHAr})\}[\text{BAR}'_4]$ complexes at 90°C and 55 psig H_2 .

Substituent	σ_{p}^+ value ⁶	k_{obs} (s^{-1})
F	-0.07	$7.8(4) \times 10^{-4}$
Cl	0.11	$7.4(7) \times 10^{-4}$
H	0.00	$9.4(6) \times 10^{-4}$
CH_3	-0.31	$2.8(3) \times 10^{-4}$
isopropyl	-0.28	$1.6(1) \times 10^{-4}$

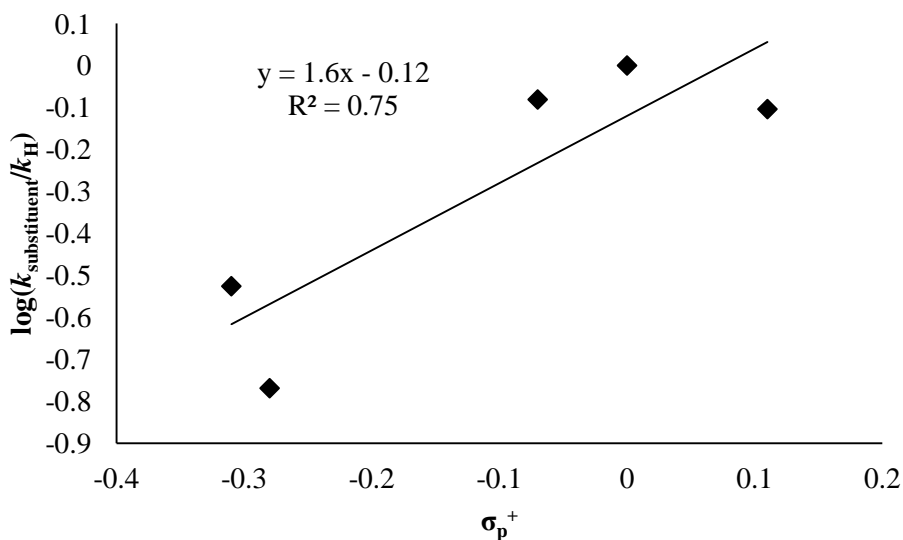


Figure 21. Hammett plot of $\log(k_{\text{substituent}}/k_{\text{H}})$ vs σ_{p}^+ .

Computational studies by Ess and coworkers indicate that an octahedral TpRu-X ($\text{X} = \text{OH}, \text{OMe}, \text{NH}_2$) complex rearranges to a trigonal bipyramidal geometry upon dissociation of a ligand to allow coordination of a substrate for 1,2-CH-addition (Figure 22, see Chapter 1). This geometry puts the heteroatom lone pair electrons in a position to be donated into the metal center's d orbitals, stabilizing the five-coordinate intermediate. Thus, although increased basicity of the ligand receiving the activated proton can facilitate the CH bond breaking step, the overall energy barrier for 1,2-CH-addition can be increased if more basic lone pair electrons stabilize the

trigonal bipyramidal intermediate. The experimental observations in the H₂ activation reactions would seem to indicate that, for the {[HC(pz⁵)₃]Ru[P(OCH₂)₃CEt](py)(NH₂Ar)}[BAr'₄] series, the lone pair stabilizes a coordinatively unsaturated trigonal bipyramidal intermediate more than it lowers the energy barrier for H₂ activation, thus increasing the overall activation barrier and giving lower *k*_{obs} values for anilido ligands with more basic lone pairs. Nevertheless, the proposed equilibrium of complex **1** with {[:C(pz⁵)₃]Ru[P(OCH₂)₃CEt](py)(NH₂Ph)}[BAr'₄] (**1'**) and the observed H/D scrambling in reactions involving D₂ indicate that reactivity could be more complicated than simple 1,2-addition of H₂ across the Ru–N bond, making it impossible to draw definitive conclusions concerning basicity.

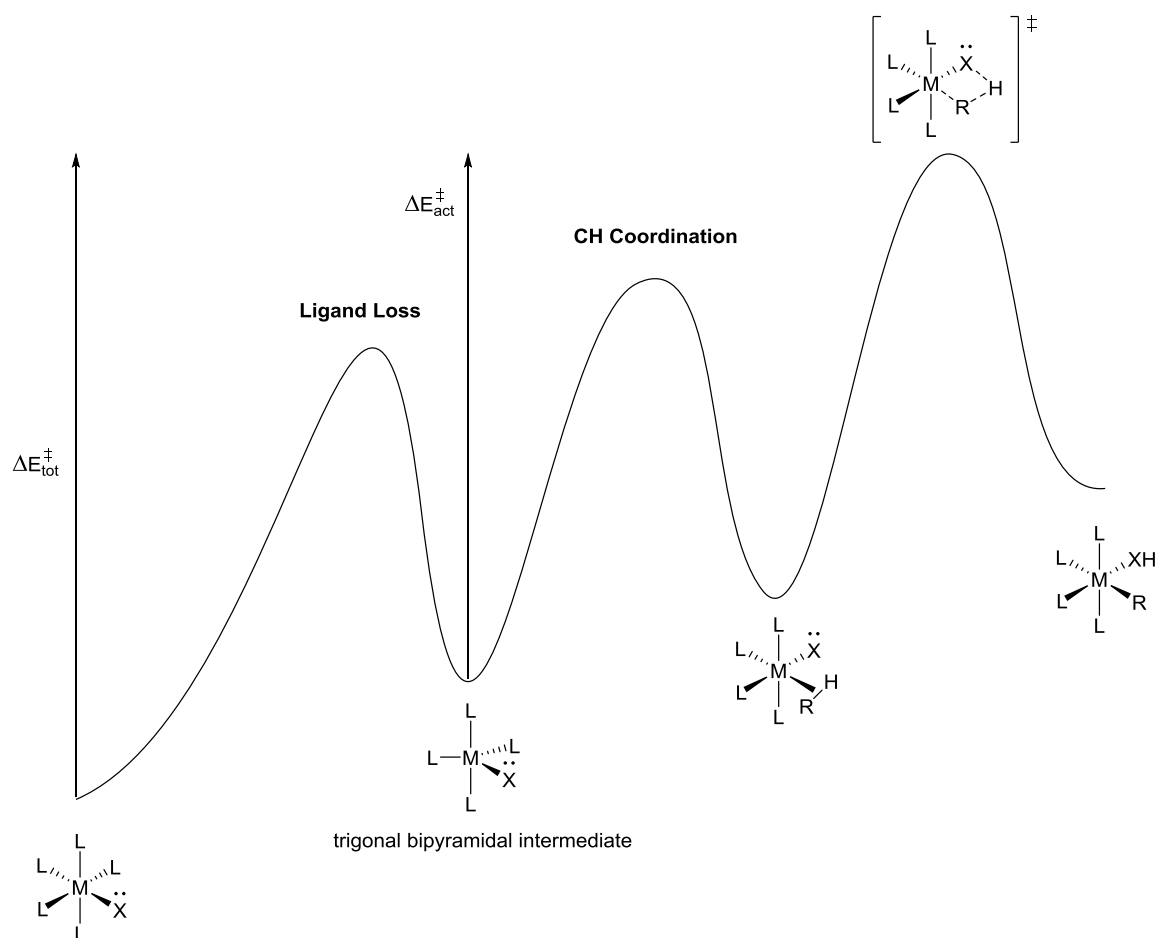


Figure 22. 1,2-Addition reaction coordinate

4.8 Conclusions

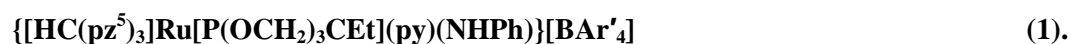
{[HC(pz⁵)₃]Ru[P(OCH₂)₃CEt](py)(NHPh)}[BAR'₄] (**1**) is capable of H₂ activation in THF to form {[HC(pz⁵)₃]Ru[P(OCH₂)₃CEt](NH₂Ph)(H)}[BAR'₄] (**2**) at 80-110 °C. Over the course of the reaction, complex **2** converts to {[HC(pz⁵)₃]Ru[P(OCH₂)₃CEt](py)(H)}[BAR'₄] (**3**) and free aniline. This H₂ activation reaction is slowed as pyridine concentration increases, consistent with the hypothesis that pyridine dissociates to allow coordination of H₂. The equilibrium between {[HC(pz⁵)₃]Ru[P(OCH₂)₃CEt](py)(NHPh)}[BAR'₄] (**1**) and {[:C(pz⁵)₃]Ru[P(OCH₂)₃CEt](py)(NH₂Ph)}[BAR'₄] (**1'**) promotes a bimolecular reaction to produce {[:C(pz⁵)₃]Ru[P(OCH₂)₃CEt](py)₂}[BAR'₄] (**5**) and aniline, and serves as a significant source of error by competing with H₂ activation by **1**. Generally, the production of **5** increases with increasing concentration of pyridine. Conclusions cannot be drawn from kinetic analysis as pseudo first order conditions in H₂ concentration in solution could not be obtained.

Larger *k*_{obs} values were observed for H₂ activation reactions involving complexes with less basic anilido ligands (such as 4-fluoroanilido), which was consistent with the observed trend and ρ value of 1.6 in the Hammett plot. Nevertheless, it is difficult to conclude exactly how basicity effects 1,2-HH-addition due to the reaction conditions and the extensive amount of exchange that occurs among the hydride, NH, and pyrazolyl positions as evidenced by ²H NMR spectroscopy for reactions with D₂.

4.9 Experimental Section

General Considerations. Unless otherwise noted, all synthetic procedures were performed under anaerobic conditions in a nitrogen-filled glovebox or by using standard Schlenk techniques. Glovebox purity was maintained by periodic nitrogen purges and was monitored by an oxygen analyzer (O₂ < 15 ppm for all reactions). Tetrahydrofuran and *n*-pentane were dried by distillation from sodium/benzophenone and P₂O₅, respectively. Diethyl ether and acetonitrile was distilled over CaH₂. Benzene, methylene chloride, and hexanes were purified by passage through a column of activated alumina. Benzene-*d*₆, acetone-*d*₆, CD₃CN, CD₂Cl₂, and CDCl₃ were used as

received and stored under a N₂ atmosphere over 4Å molecular sieves. THF-*d*₈ was distilled over sodium/benzophenone and stored over 4Å molecular sieves. ¹H NMR spectra were recorded on a Varian 300 MHz, Varian 500 MHz or a Bruker 600 MHz or 800 MHz spectrometer, and ¹³C{¹H} NMR spectra were recorded on a Bruker 600 MHz (operating frequency = 150 MHz) or a Bruker 800 MHz (operating frequency = 201 MHz). All ¹H and ¹³C spectra are referenced against residual proton signals (¹H NMR) or ¹³C resonances (¹³C NMR) of the deuterated solvents. ³¹P{¹H} NMR spectra were obtained on a Varian 300 MHz (operating frequency = 121 MHz), Varian 500 MHz (operating frequency = 201 MHz) or Varian 600 MHz (operating frequency = 243 MHz) spectrometer and referenced against an external standard of H₃PO₄ (δ = 0). ¹⁹F{¹H} NMR spectra were obtained on a Varian 300 MHz (operating frequency = 282 MHz) or a Varian 600 MHz (operating frequency = 565 MHz) and referenced against an internal standard of hexafluorobenzene (δ = -164.9). X-ray diffraction studies were performed by Dr. Jeffrey Petersen (West Virginia University). Tris(5-methyl-pyrazolyl)methane was synthesized according to a previously reported procedure.⁷ All other reagents were used as received from the manufacturers.



{[HC(pz⁵)₃Ru[P(OCH₂)₃CEt](py)(NH₂Ph)]}[OTf][BAr'₄] (0.0053 g, 0.0034 mmol) was dissolved in ~0.5 mL of THF-*d*₈. NaHMDS (~0.0037 mmol) was added to the solution to give **1** in 92% yield. Scaled-up reactions: {[HC(pz⁵)₃Ru[P(OCH₂)₃CEt](py)(NH₂Ph)]}[OTf][BAr'₄] (0.0202 g, 0.012 mmol) was dissolved in ~1 mL of THF. NaHMDS (~0.013 mmol) was added to the solution. Volatiles were removed in vacuo. Solid was gently rinsed with C₆H₆. Benzene was pipetted off, and solid was reconstituted in THF. Volatiles were removed in vacuo and product was dried overnight to yield **1** in ~83% isolated yield (0.0151 g). ¹H NMR (600 MHz, THF-*d*₈) δ = 7.83 (HC(pz⁵)₃, obscured by BA r'₄, as indicated by ¹H-¹³C HMQC NMR spectroscopy), 7.12 (1H, pz 3-position), 7.06 (1H, pz 3-position), 7.03 (1H, pz 3-position), 6.06 (1H, pz 4-position), 5.87 (1H, pz 4-position), 5.75 (1H, pz 4-position), 8.10 (pyridine), 7.75 (pyridine), 7.17

(pyridine), 7.79 (BAR'₄), 7.58 (BAR'₄), 6.68 (broad, phenyl), 4.41 (NH, typically obscured by P(OCH₂)₃CEt), 4.37 (6H, P(OCH₂)₃CEt), 2.66 (3H, HC(pz⁵)₃ 5-methyl), 2.58 (3H, HC(pz⁵)₃ 5-methyl), 2.55 (3H, HC(pz⁵)₃ 5-methyl), 1.28 (2H, q, ³J_{HH} = 8 Hz, -CH₂CH₃), 0.84 (3H, t, ³J_{HH} = 8 Hz, -CH₂CH₃). ³¹P NMR (201 MHz, THF-*d*₈) δ = 132.0 (broad). ¹³C NMR (201 MHz, THF-*d*₈) δ = 163.0 (4 line pattern, ¹J_{BC} = 50 Hz, BAR'₄), 157.3 (pyridine), 156.2 (pz 3 or 5-position), 151.1 (pz 3 or 5-position), 148.4 (pz 3 or 5-position), 145.2 (pz 3 or 5-position), 144.2 (pz 3 or 5-position), 140.4 (pyridine), 135.8 (BAR'₄), 130.2 (q, ¹J_{CF} = 32 Hz, BAR'₄), 129.2 (phenyl ipso), 129.1 (bs, phenyl), 124.8 (phenyl), 126.4 (pyridine), 118.3 (BAR'₄), 105.3 (pz 4-position), 105.2 (pz 4-position), 104.4 (pz 4-position), 75.0 (-OCH₂)₃, 70.1 (HC(pz⁵)₃), 36.3 (d, ³J_{PC} = 30 Hz, -OCH₂)₃C-, 24.2 (-CH₂CH₃), 12.8 (HC(pz⁵)₃ methyl), 12.8 (HC(pz⁵)₃ methyl), 12.7 (HC(pz⁵)₃ methyl), 7.4 (-CH₂CH₃).

{[:C(pz⁵)₃]Ru[P(OCH₂)₃CEt](py)(NH₂Ph)]BAR'₄} (1'). Complex

{[HC(pz⁵)₃]Ru[P(OCH₂)₃CEt](py)(NH₂Ph)]OTf]BAR'₄] (0.0053 g, 0.0034 mmol) was dissolved in ~1-2 mL of THF. NaHMDS (~0.0037 mmol) was added to the solution to give **1'** in ~8 % yield. ¹H NMR (600 MHz, THF-*d*₈) δ = 7.75 (1H), 7.66 (1H), 7.50 (1H), 6.33 (2H), 6.12 (1H), 8.48 (pyridine), 7.75 (pyridine), 7.24 (pyridine), 6.27 (phenyl), 5.70 (phenyl), 5.48 (d, ³J_{HH} = 8 Hz, phenyl), 4.30 (6H, P(OCH₂)₃CEt). NH₂ resonances have not been resolved.

{[HC(pz⁵)₃]Ru[P(OCH₂)₃CEt](py)(H)]OTf} (3). LiAlH₄ was added to {[HC(pz⁵)₃]Ru[P(OCH₂)₃CEt](py)(OTf)]OTf] (0.0324 g, 0.361 mmol) in 0.8 mL THF. Solution was filtered to remove a black precipitate. Hexanes were added to the yellow filtrate to precipitate **2**, a yellow solid, in ~80% yield. ¹H NMR (600 MHz, THF-*d*₈) δ = 8.23 (HC(pz⁵)₃), 7.82 (1H, pz 3-position), 7.73 (1H, pz 3-position), 7.18 (1H, pz 3-position), 6.36 (1H, pz 4-position), 6.23 (1H, pz 4-position), 6.04 (1H, pz 4-position), 8.50 (d, ³J_{HH} = 5 Hz, pyridine), 7.59 (t, ³J_{HH} = 8 Hz, pyridine), 7.01 (t, ³J_{HH} = 7 Hz, pyridine), 4.20 (6H, d, ³J_{PH} = 4 Hz, P(OCH₂)₃CEt), 2.80 (3H, HC(pz⁵)₃ 5-methyl), 2.78 (3H, HC(pz⁵)₃ 5-methyl), 2.68 (3H, HC(pz⁵)₃ 5-methyl), 1.20 (2H, q, ³J_{HH} = 8 Hz, -CH₂CH₃), 0.80 (3H, t, ³J_{HH} = 8 Hz, -CH₂CH₃), -14.3 (1H, d, ²J_{PH} = 40 Hz,

hydride). ^{31}P NMR (243 MHz, THF- d_8) $\delta = 136.5$. ^{19}F (565 MHz, THF- d_8) $\delta = -79.7$. ^{13}C NMR (150 MHz, THF- d_8) $\delta = 159.0$ (pyridine), 146.4 (pz 3 or 5-position), 145.4 (pz 3 or 5-position), 143.2 (pz 3 or 5-position), 143.1 (pz 3 or 5-position), 143.0 (pz 3 or 5-position), 141.1 (pz 3 or 5-position), 139.9 (pyridine), 124.5 (pyridine), 108.8 (pz 4-position), 108.7 (pz 4-position), 108.0 (pz 4-position), 121.8 (q, $^1J_{\text{FC}} = 320$ Hz, CF_3SO_3), 74.5 (d, $^2J_{\text{PC}} = 7$ Hz, $-(\text{OCH}_2)_3$), 70.2 ($\text{HC}(\text{pz}^5)_3$), 35.7 (d, $^3J_{\text{PC}} = 31$ Hz, $-(\text{OCH}_2)_3\text{C}-$), 24.4 ($-\text{CH}_2\text{CH}_3$), 11.6 ($\text{HC}(\text{pz}^5)_3$ methyl), 11.4 ($\text{HC}(\text{pz}^5)_3$ methyl), 10.9 ($\text{HC}(\text{pz}^5)_3$ methyl), 7.5 ($-\text{CH}_2\text{CH}_3$).

$\{[\text{HC}(\text{pz}^5)_3]\text{Ru}[\text{P}(\text{OCH}_2)_3\text{CEt}](\text{NH}_2\text{Ph})(\text{H})\}[\text{OTf}]$ (2). NH_2Ph (~ 60 μL) was added to an NMR sample of $\{[\text{HC}(\text{pz}^5)_3]\text{Ru}[\text{P}(\text{OCH}_2)_3\text{CEt}](\text{py})(\text{H})\}[\text{OTf}]$ (3) in THF- d_8 . The solution was photolyzed for 30 minutes (after a 15 min lamp warm-up time). Volatiles were removed from product in vacuo. Product was washed with Et_2O to yield **3**. ^1H NMR (600 MHz, THF- d_8) $\delta = 8.14$ ($\text{HC}(\text{pz}^5)_3$), 8.01 (1H, pz 3-position), 7.66 (1H, pz 3-position), 6.79 (1H, pz 3-position), 6.34 (1H, pz 4-position), and 5.94 ppm (2H, pz 4-position), 7.02 (m, phenyl), 6.90 (m, phenyl), and 6.74 (d, $^3J_{\text{HH}} = 7$ Hz, phenyl), 5.12 (d, $^2J_{\text{HH}} = 11$ Hz, NH_2), 4.99 (d, $^2J_{\text{HH}} = 11$ Hz, NH_2), 4.31 (6H, unresolved d, $\text{P}(\text{OCH}_2)_3\text{CEt}$), 2.78 (3H, $\text{HC}(\text{pz}^5)_3$ 5-methyl), 2.67 (3H, $\text{HC}(\text{pz}^5)_3$ 5-methyl), 2.62 (3H, $\text{HC}(\text{pz}^5)_3$ 5-methyl), 1.28 (2H, q, $^3J_{\text{HH}} = 8$ Hz, $-\text{CH}_2\text{CH}_3$), 0.86 (3H, t, $^3J_{\text{HH}} = 8$ Hz, $-\text{CH}_2\text{CH}_3$), -14.9 ppm (d, $^2J_{\text{PH}} = 39$ Hz). ^{31}P NMR (243 MHz, THF- d_8) $\delta = 136.1$. ^{19}F NMR (565 MHz, THF- d_8) $\delta = -79.4$.

$\{[:\text{C}(\text{pz}^5)_3]\text{Ru}[\text{P}(\text{OCH}_2)_3\text{CEt}](\text{py})_2\}[\text{BAR}'_4]$ (5). Pyridine (6 μL , 0.07 mmol) was added to a THF solution of $\{[\text{HC}(\text{pz}^5)_3]\text{Ru}[\text{P}(\text{OCH}_2)_3\text{CEt}](\text{py})(\text{NHPh})\}[\text{BAR}'_4]$ (1) (~ 30 mg, 0.02 mmol) in a high pressure NMR tube. Tube was pressurized with 40 psi N_2 and heated at 110 or 90 C to give 5 in quantitative yield. ^1H NMR (600 MHz, THF- d_8) $\delta = 7.19$ (2H, pz 3-position), 7.00 (1H, pz 3-position), 6.12 (1H, pz 4-position), 5.95 (2H, pz 4-position), 7.79 (BAR'_4), 7.57 (BAR'_4), 8.40 (d, $^3J_{\text{HH}} = 6$ Hz, pyridine), 7.27 (t, $^3J_{\text{HH}} = 7$ Hz, pyridine), 1 pyridine resonance missing due to coincidental overlap with BAR'_4 at 7.79, 4.33 (d, $^3J_{\text{PH}} = 5$ Hz, $\text{P}(\text{OCH}_2)_3\text{CEt}$), 2.69 (3 H, $\text{HC}(\text{pz}^5)_3$ 5-methyl), 2.63 (6 H, $\text{HC}(\text{pz}^5)_3$ 5-methyl), 1.26 (2H, q, $^3J_{\text{HH}} = 8$ Hz, $-\text{CH}_2\text{CH}_3$), 0.81 (3H, t, $^3J_{\text{HH}}$

= 8 Hz, $-\text{CH}_2\text{CH}_3$). ^{31}P NMR (201 MHz, THF- d_8) δ = 131.5. ^{13}C NMR (201 MHz, THF- d_8) δ = 163.3 (4 line pattern, $^1J_{\text{BC}} = 50$ Hz, BAr'_4), 157.3 (pyridine), 147.4 (pz 3 or 5-position), 146.9 (pz 3 or 5-position), 144.9 (pz 3 or 5-position), 143.0 (pz 3 or 5-position), 140.7 (pz 3 or 5-position), (1 pz 3 or 5-position resonance missing due to coincidental overlap), 138.1 (pyridine), 135.8 (BAr'_4), 130.1 (q, $^1J_{\text{CF}} = 32$ Hz, BAr'_4), 125.7 (q, $^1J_{\text{FC}} = 274$ Hz, CF_3SO_3), 125.6 (pyridine), 118.4 (BAr'_4), 106.5 (1H, pz 4-position), 105.7 (1H, pz 4-position), 75.5 (d, $^2J_{\text{PC}} = 6$ Hz, $-(\text{OCH}_2)_3$), 72.6 ($:\text{C}(\text{pz}^5)_3$), 36.4 (d, $^3J_{\text{PC}} = 35$ Hz, $-(\text{OCH}_2)_3\text{C}-$), 24.1 ($-\text{CH}_2\text{CH}_3$), 12.8 ($\text{HC}(\text{pz}^5)_3$ methyl), 12.4 ($\text{HC}(\text{pz}^5)_3$ methyl), 7.4 ($-\text{CH}_2\text{CH}_3$).

Substituted aniline complexes. The syntheses for $\{[\text{HC}(\text{pz}^5)_3]\text{Ru}[\text{P}(\text{OCH}_2)_3\text{CEt}](\text{py})(\text{NH}_2\text{Ar})\}[\text{OTf}][\text{BAr}'_4]$ (Ar = 4-isopropylphenyl, 4-methylphenyl, 4-chlorophenyl, 4-fluorophenyl, 4-(trifluoromethyl)phenyl) is the same as the synthetic procedure for $\{[\text{HC}(\text{pz}^5)_3]\text{Ru}[\text{P}(\text{OCH}_2)_3\text{CEt}](\text{py})(\text{NH}_2\text{Ph})\}[\text{OTf}][\text{BAr}'_4]$ (see Experimental Section of Chapter 3). Spectral data are provided below for complexes **6-10**.

$\{[\text{HC}(\text{pz}^5)_3]\text{Ru}[\text{P}(\text{OCH}_2)_3\text{CEt}](\text{py})(4\text{-isopropylaniline})\}[\text{OTf}][\text{BAr}'_4]$ (6). ^1H NMR (800 MHz, THF- d_8) δ = 8.23 (2H, $\text{HC}(\text{pz}^5)_3$ and pz 3-position), 7.46 (1H, pz 3-position), 7.40 (1H, pz 3-position), 6.48 (1H, pz 4-position), 6.33 (1H, pz 4-position), 6.15 (1H, pz 4-position), 8.34 (d, $^3J_{\text{HH}} = 6$ Hz, pyridine), 7.90 (t, $^3J_{\text{HH}} = 8$ Hz, pyridine), 7.38 (t, $^3J_{\text{HH}} = 7$ Hz, pyridine), 6.88 (d, $^3J_{\text{HH}} = 8$ Hz, phenyl), 7.81 (BAr'_4), 7.60 (BAr'_4), 6.88 (d, $^3J_{\text{HH}} = 8$ Hz, phenyl), 6.61 (d, $^3J_{\text{HH}} = 8$ Hz, phenyl), 6.13 (d, $^2J_{\text{HH}} = 12$ Hz, NH_2), 5.97 (d, $^2J_{\text{HH}} = 12$ Hz, NH_2), 4.49 (m, $\text{P}(\text{OCH}_2)_3\text{CEt}$), 2.84 (3H, $\text{HC}(\text{pz}^5)_3$ 5-methyl), 2.74 (3H, $\text{HC}(\text{pz}^5)_3$ 5-methyl), 2.72 (3H, $\text{HC}(\text{pz}^5)_3$ 5-methyl), 1.32 (2H, q, $^3J_{\text{HH}} = 8$ Hz, $-\text{CH}_2\text{CH}_3$), 1.17 (d, $^3J_{\text{HH}} = 7$ Hz, $-\text{CH}(\text{CH}_3)_2$), 1.12 (dd, $^3J_{\text{HH}} = 7$ Hz, $-\text{CH}(\text{CH}_3)_2$) 0.85 (3H, t, $^3J_{\text{HH}} = 8$ Hz, $-\text{CH}_2\text{CH}_3$). ^{31}P NMR (201 MHz, THF- d_8) δ = 133.3. ^{13}C NMR (201 MHz, THF- d_8) δ = 163.0 (4 line pattern, $^1J_{\text{BC}} = 50$ Hz, BAr'_4), 157.3 (pyridine), 149.8 (pz 3 or 5-position), 149.6 (pz 3 or 5-position), 147.0 (pz 3 or 5-position), 146.2 (pz 3 or 5-position), 145.7 (pz 3 or 5-position), 145.2 (pz 3 or 5-position), 145.0 (phenyl), 142.9 (pyridine), 138.9 (phenyl), 135.8 (BAr'_4), 130.2 (q, $^1J_{\text{CF}} = 32$ Hz, BAr'_4), 128.0 (phenyl), 126.5

(pyridine), 125.7 (q, $^1J_{CF} = 272$ Hz, CF_3), 122.1 (phenyl), 118.4 (BAr'_4), 110.1 (pz 4-position), 110.1 (pz 4-position), 109.0 (pz 4-position), 76.1 ($-(OCH_2)_3$), 69.9 ($HC(pz^5)_3$), 37.0 (d, $^3J_{PC} = 31$ Hz, $-(OCH_2)_3C-$), 34.6 ($-C(CH_3)_2$), 24.5 ($-C(CH_3)_2$), 24.4 ($-C(CH_3)_2$), 24.0 ($-CH_2CH_3$), 11.2 ($HC(pz^5)_3$ methyl), 11.1 ($HC(pz^5)_3$ methyl), 11.0 ($HC(pz^5)_3$ methyl), 7.4 ($-CH_2CH_3$).

{[HC(pz⁵)₃]Ru[P(OCH₂)₃CEt](py)(4-methylaniline)}[OTf][BAr'₄] (7). 1H NMR (800 MHz, THF-*d*₈) $\delta = 8.21$ (1H, $HC(pz^5)_3$), 7.45 (1H, pz 3-position), 7.40 (1H, pz 3-position), 7.36 (1H, pz 3-position), 6.50 (1H, pz 4-position), 6.34 (1H, pz 4-position), 6.17 (1H, pz 4-position), 8.32 (pyridine), 7.92 (pyridine), 7.38 (pyridine), 7.79 (BAr'_4), 7.58 (BAr'_4), 6.80 (d, $^3J_{HH} = 8$ Hz, phenyl), 6.57 (d, $^3J_{HH} = 7$ Hz, phenyl), 6.13 (d, $^2J_{HH} = 12$ Hz, NH_2), 5.97 (d, $^2J_{HH} = 13$ Hz, NH_2), 4.49 (m, $P(OCH_2)_3CEt$), 2.83 (3H, $HC(pz^5)_3$ 5-methyl), 2.74 (3H, $HC(pz^5)_3$ 5-methyl), 2.71 (3H, $HC(pz^5)_3$ 5-methyl), 2.14 ($-CH_3$), 1.32 (2H, q, $^3J_{HH} = 8$ Hz, $-CH_2CH_3$), 0.85 (3H, t, $^3J_{HH} = 8$ Hz, $-CH_2CH_3$). ^{31}P NMR (201 MHz, THF-*d*₈) $\delta = 134.2$. ^{13}C NMR (201 MHz, THF-*d*₈) $\delta = 163.0$ (4 line pattern, $^1J_{BC} = 50$ Hz, BAr'_4), 157.3 (pyridine), 149.9 (pz 3 or 5-position), 149.7 (pz 3 or 5-position), 146.3 (pz 3 or 5-position), 145.6 (pz 3 or 5-position), 145.2 (pz 3 or 5-position), 144.9 (pz 3 or 5-position), 142.4 (pyridine), 139.0 (phenyl), 135.8 (BAr'_4), 130.53 (q, $^1J_{CF} = 32$ Hz, BAr'_4), 130.1 (phenyl), 126.5 (pyridine), 125.7 (q, $^1J_{CF} = 273$ Hz, CF_3), 122.2 (phenyl), 118.4 (BAr'_4), 110.2 (pz 4-position), 110.1 (pz 4-position), 109.0 (pz 4-position), 76.2 (d, $^2J_{CP} = 6$ Hz, $-(OCH_2)_3$), 69.9 ($HC(pz^5)_3$), 37.0 (d, $^3J_{CP} = 31$ Hz, $-(OCH_2)_3C-$), 24.0 ($-CH_2CH_3$), 20.8 ($-CH_3$), 11.1 ($HC(pz^5)_3$ methyl), 11.1 ($HC(pz^5)_3$ methyl), 10.9 ($HC(pz^5)_3$ methyl), 7.4 ($-CH_2CH_3$).

{[HC(pz⁵)₃]Ru[P(OCH₂)₃CEt](py)(4-chloroaniline)}[OTf][BAr'₄] (8). 1H NMR (800 MHz, THF-*d*₈) $\delta = 8.24$ ($HC(pz^5)_3$), 7.67 (1H, pz 3-position), 7.46 (1H, pz 3-position), 7.35 (1H, pz 3-position), 6.56 (1H, pz 4-position), 6.34 (1H, pz 4-position), 6.20 (1H, pz 4-position), 8.32 (d, $^3J_{HH} = 6$ Hz, pyridine), 7.91 (t, $^3J_{HH} = 7$ Hz, pyridine), 7.39 (t, $^3J_{HH} = 7$ Hz, pyridine), 7.82 (BAr'_4), 7.60 (BAr'_4), 7.05 (d, $^3J_{HH} = 8$ Hz, phenyl), 6.76 (d, $^3J_{HH} = 8$ Hz, phenyl), 6.26 (d, $^2J_{HH} = 12$ Hz, NH_2), 6.11 (d, $^2J_{HH} = 12$ Hz, NH_2), 4.50 (m, $P(OCH_2)_3CEt$), 2.86 (3H, $HC(pz^5)_3$ 5-methyl), 2.75 (3H, $HC(pz^5)_3$ 5-methyl), 2.73 (3H, $HC(pz^5)_3$ 5-methyl), 1.32 (2H, q, $^3J_{HH} = 8$ Hz, $-$

CH_2CH_3), 0.85 (3H, t, $^3J_{\text{HH}} = 8$ Hz, $-\text{CH}_2\text{CH}_3$). ^{31}P NMR (201 MHz, $\text{THF-}d_8$) $\delta = 134.8$. ^{13}C NMR (201 MHz, $\text{THF-}d_8$) $\delta = 163.0$ (4 line pattern, $^1J_{\text{BC}} = 50$ Hz, BAr'_4), 157.3 (pyridine), 150.0 (pz 3 or 5-position), 149.7 (pz 3 or 5-position), 146.4 (pz 3 or 5-position), 145.8 (pz 3 or 5-position), 145.4 (pz 3 or 5-position), 145.2 (pz 3 or 5-position), 144.1 (pyridine), 139.0 (phenyl), 135.8 (BAr'_4), 131.2 (phenyl), 130.2 (q, $^1J_{\text{CF}} = 32$ Hz, BAr'_4), 130.1 (phenyl), 129.6, 126.5 (phenyl), 125.7 (q, $^1J_{\text{CF}} = 273$ Hz, CF_3), 124.1 (pyridine), 118.4 (BAr'_4), 110.4 (pz 4-position), 110.1 (pz 4-position), 109.2 (pz 4-position), 76.2 (d, $^2J_{\text{CP}} = 6$ Hz, $-(\text{OCH}_2)_3$), 70.0 ($\text{HC}(\text{pz}^5)_3$), 37.0 (d, $^3J_{\text{CP}} = 32$ Hz, $-(\text{OCH}_2)_3\text{C-}$), 24.0 ($-\text{CH}_2\text{CH}_3$), 11.2 ($\text{HC}(\text{pz}^5)_3$ methyl), 11.2 ($\text{HC}(\text{pz}^5)_3$ methyl), 11.1 ($\text{HC}(\text{pz}^5)_3$ methyl), 7.4 ($-\text{CH}_2\text{CH}_3$).

{[HC(pz⁵)₃]Ru[P(OCH₂)₃CEt](py)(4-fluoroaniline)}[OTf][BAr'₄] (9). ^1H NMR (500 MHz, $\text{THF-}d_8$) $\delta = 8.22$ ($\text{HC}(\text{pz}^5)_3$), 7.60 (1H, pz 3-position), 7.46 (1H, pz 3-position), 7.33 (1H, pz 3-position), 6.57 (1H, pz 4-position), 6.35 (1H, pz 4-position), 6.20 (1H, pz 4-position), 8.30 (d, $^3J_{\text{HH}} = 5$ Hz, pyridine), 7.92 (t, $^3J_{\text{HH}} = 8$ Hz, pyridine), 7.39 (t, $^3J_{\text{HH}} = 8$ Hz, pyridine), 6.79-6.72 (m, phenyl), 6.26 (d, $^2J_{\text{HH}} = 12$ Hz, NH_2), 6.05 (d, $^2J_{\text{HH}} = 12$ Hz, NH_2), 4.49 (m, $\text{P}(\text{OCH}_2)_3\text{CEt}$), 2.85 (3H, $\text{HC}(\text{pz}^5)_3$ 5-methyl), 2.74 (3H, $\text{HC}(\text{pz}^5)_3$ 5-methyl), 2.72 (3H, $\text{HC}(\text{pz}^5)_3$ 5-methyl), 1.32 (2H, q, $^3J_{\text{HH}} = 8$ Hz, $-\text{CH}_2\text{CH}_3$), 0.85 (3H, t, $^3J_{\text{HH}} = 8$ Hz, $-\text{CH}_2\text{CH}_3$). ^{31}P NMR (201 MHz, $\text{THF-}d_8$) $\delta = 133.70$. ^{19}F NMR (565 MHz, $\text{THF-}d_8$) $\delta = -63.5, -79.3, -118.7$. ^{13}C NMR (201 MHz, $\text{THF-}d_8$) $\delta = 163.0$ (4 line pattern, $^1J_{\text{BC}} = 50$ Hz, BAr'_4), 161.1 (d, $^1J_{\text{CF}} = 244$ Hz, phenyl $-\text{CF}$), 157.3 (pyridine), 150.0 (pz 3 or 5-position), 149.7 (pz 3 or 5-position), 146.4 (pz 3 or 5-position), 145.6 (pz 3 or 5-position), 145.3 (pz 3 or 5-position), 145.1 (pz 3 or 5-position), 141.2 (pyridine), 139.0 (phenyl), 135.8 (BAr'_4), 130.2 (q, $^1J_{\text{CF}} = 32$ Hz, BAr'_4), 126.6 (phenyl), 125.7 (q, $^1J_{\text{CF}} = 273$ Hz, CF_3), 124.0 (phenyl), 118.4 (BAr'_4), 110.4 (pz 4-position), 110.2 (pz 4-position), 109.2 (pz 4-position), 76.2 (d, $^2J_{\text{CP}} = 6$ Hz, $-(\text{OCH}_2)_3$), 69.9 ($\text{HC}(\text{pz}^5)_3$), 37.0 (d, $^3J_{\text{CP}} = 32$ Hz, $-(\text{OCH}_2)_3\text{C-}$), 24.0 ($-\text{CH}_2\text{CH}_3$), 11.1 ($\text{HC}(\text{pz}^5)_3$ methyl), 11.1 ($\text{HC}(\text{pz}^5)_3$ methyl), 10.9 ($\text{HC}(\text{pz}^5)_3$ methyl), 7.4 ($-\text{CH}_2\text{CH}_3$).

{[HC(pz⁵)₃]Ru[P(OCH₂)₃CEt](py)(4-(trifluoromethyl)anilino)}[OTf][BAr'₄] (10). ¹H NMR (800 MHz, THF-*d*₈) δ = 8.23 (HC(pz⁵)₃), 7.69 (1H, pz 3-position), 7.47 (1H, pz 3-position), 7.28 (1H, pz 3-position), 6.57 (1H, pz 4-position), 6.35 (1H, pz 4-position), 6.15 (1H, pz 4-position), 8.33 (d, ³J_{HH} = 6 Hz, pyridine), 7.93 (t, ³J_{HH} = 8 Hz, pyridine), 7.39 (t, ³J_{HH} = 7 Hz, pyridine), 7.37 (d, ³J_{HH} = 8 Hz, phenyl), 6.94 (d, ³J_{HH} = 8 Hz, phenyl), 6.48 (d, ²J_{HH} = 12 Hz, NH₂), 6.30 (d, ²J_{HH} = 12 Hz, NH₂), 4.51 (m, P(OCH₂)₃CEt), 2.86 (3H, HC(pz⁵)₃ 5-methyl), 2.74 (3H, HC(pz⁵)₃ 5-methyl), 2.71 (3H, HC(pz⁵)₃ 5-methyl), 1.32 (2H, q, ³J_{HH} = 8 Hz, -CH₂CH₃), 0.85 (3H, t, ³J_{HH} = 8 Hz, -CH₂CH₃). ³¹P NMR (201 MHz, THF-*d*₈) δ = 132.1. ¹⁹F NMR (565 MHz, THF-*d*₈) δ = -63.6, -79.3, -197.4. ¹³C NMR (201 MHz, THF-*d*₈) δ = 163.0 (4 line pattern, ¹J_{BC} = 50 Hz, BAr'₄), 157.3 (pyridine), 149.9 (pz 3 or 5-position), 149.8 (pz 3 or 5-position), 149.4 (pz 3 or 5-position), 146.4 (pz 3 or 5-position), 145.8 (pz 3 or 5-position), 145.5 (pz 3 or 5-position), 145.3 (pyridine), 139.1 (phenyl), 135.8 (BAr'₄), 130.2 (q, ¹J_{CF} = 32 Hz, BAr'₄), 128.0 (q, ¹J_{CF} = 33 Hz, -CF₃), 127.4 (phenyl), 126.6 (phenyl), 1 phenyl resonance missing due to coincidental overlap, 125.7 (q, ¹J_{CF} = 272 Hz, (SO₃)CF₃), 123.1 (pyridine), 118.4 (BAr'₄), 110.4 (pz 4-position), 110.2 (pz 4-position), 109.1 (pz 4-position), 76.2 (d, ²J_{CP} = 6 Hz, -(OCH₂)₃), 69.9 (HC(pz⁵)₃), 37.0 (d, ³J_{CP} = 32 Hz, -(OCH₂)₃C-), 24.0 (-CH₂CH₃), 11.2 (HC(pz⁵)₃ methyl), 11.1 (HC(pz⁵)₃ methyl), 1 HC(pz⁵)₃ methyl resonance missing due to coincidental overlap, 7.4 (-CH₂CH₃).

Substituted anilido complexes. The syntheses for {[HC(pz⁵)₃]Ru[P(OCH₂)₃CEt](py)(NHAr)}[OTf][BAr'₄] (Ar = 4-isopropylphenyl, 4-methylphenyl, 4-chlorophenyl, 4-fluorophenyl) is the same as the synthetic procedure for {[HC(pz⁵)₃]Ru[P(OCH₂)₃CEt](py)(NHPh)}[OTf][BAr'₄] (1). Spectral data are provided below for complexes **11-14**.

{[HC(pz⁵)₃]Ru[P(OCH₂)₃CEt](py)(4-isopropylanilido)}[BAr'₄] (11). ¹H NMR (600 MHz, THF-*d*₈) δ = 7.09 (1H, pz 3-position), 7.04 (1H, pz 3-position), 7.01 (1H, pz 3-position), 6.04 (1H, pz 4-position), 5.87 (1H, pz 4-position), 5.74 (1H, pz 4-position), 7.80 (BAr'₄), 7.58

(BAr'₄), 8.13 (d, ³J_{HH} = 6 Hz, pyridine), 7.74 (t, ³J_{HH} = 8 Hz, pyridine), 7.17 (t, ³J_{HH} = 7 Hz, pyridine), 6.88 (d, ³J_{HH} = 8 Hz, phenyl), 6.85 (d, ³J_{HH} = 8 Hz, phenyl), 4.37 (d, ³J_{PH} = 4 Hz, P(OCH₂)₃CEt), 2.66 (3 H, HC(pz⁵)₃ 5-methyl), 2.57 (3 H, HC(pz⁵)₃ 5-methyl), 2.55 (3 H, HC(pz⁵)₃ 5-methyl), 1.28 (2H, q, ³J_{HH} = 8 Hz, -CH₂CH₃), 1.14 (d, ³J_{HH} = 7 Hz, -CH(CH₃)₂), 0.84 (3H, t, ³J_{HH} = 8 Hz, -CH₂CH₃). ³¹P NMR (201 MHz, THF-*d*₈) δ = 133.3. ¹³C NMR (201 MHz, THF-*d*₈) δ = 163.0 (4 line pattern, ¹J_{BC} = 50 Hz, BAr'₄), 159.1 (pyridine), 150.9 (pz 3 or 5-position), 147.4 (pz 3 or 5-position), 143.0 (pz 3 or 5-position), 140.0 (pyridine), 138.2 (pz3 or 5-position), 137.6 (pz 3 or 5-position), 135.7 (BAr'₄), 130.1 (q, ¹J_{CF} = 32 Hz, BAr'₄), 129.6 (phenyl), 129.2 (phenyl), 127.4 (phenyl), 125.8 (q, ¹J_{CF} = 272 Hz, CF₃), 124.5 (pyridine), 120.6 (phenyl), 118.3 (BAr'₄), 104.8 (pz 4-position), 104.0 (pz 4-position), 1 pz 4-position missing due to coincidental overlap, 74.7 (-(OCH₂)₃), 67.9 (-CH(CH₃)₂), 27.7 (-CH(CH₃)₂), 24.4 (-CH₂CH₃), 12.8 (HC(pz⁵)₃ methyl), 12.4 (HC(pz⁵)₃ methyl), 7.5 (-CH₂CH₃).

{[HC(pz⁵)₃]Ru[P(OCH₂)₃CEt](py)(4-methylanilido)}[BAr'₄] (12). ¹H NMR (600 MHz, THF-*d*₈) δ = 7.19 (1H, pz 3-position), 7.09 (1H, pz 3-position), 7.00 (1H, pz 3-position), 6.00 (1H, pz 3-position), 5.86 (1H, pz 3-position), 5.73 (1H, pz 3-position), 8.17 (pyridine), 7.71 (pyridine), 7.14 (pyridine), 7.79 (BAr'₄), 7.57 (BAr'₄), 6.64 (broad, phenyl), 6.33 (broad, phenyl), 4.33 (P(OCH₂)₃CEt), 2.65 (3H, HC(pz⁵)₃ 5-methyl), 2.58 (3H, HC(pz⁵)₃ 5-methyl), 2.55 (3H, HC(pz⁵)₃ 5-methyl), 2.09 (3H, -CH₃), 1.27 (2H, q, ³J_{HH} = 8 Hz, -CH₂CH₃), 0.84 (3H, t, ³J_{HH} = 8 Hz, -CH₂CH₃). ³¹P NMR (201 MHz, THF-*d*₈) δ = 132.3. ¹³C NMR (201 MHz, THF-*d*₈) δ = 163.1 (4 line pattern, ¹J_{BC} = 50 Hz, BAr'₄), 157.4 (pyridine), 145.2 (pz 3 or 5-position), 144.4 (pz 3 or 5-position), 140.5 (pz 3 or 5-position), 137.2 (phenyl), 135.9 (BAr'₄), 130.3 (q, ¹J_{CF} = 32 Hz, BAr'₄), 130.0 (phenyl), 125.8 (q, ¹J_{CF} = 273 Hz, CF₃), 125.0 (pyridine), 118.4 (BAr'₄), 105.5 (pz 4-position), 105.4 (pz 4-position), 104.6 (pz 4-position), 75.2 (-(OCH₂)₃), 36.2 (d, ³J_{PC} = 30 Hz, -(OCH₂)₃C-), 24.4 (-CH₂CH₃), 21.0 (-C(CH₃)₂), 12.9 (HC(pz⁵)₃ methyl), 12.5 (HC(pz⁵)₃ methyl), 7.6 (-CH₂CH₃).

{[HC(pz⁵)₃]Ru[P(OCH₂)₃CEt](py)(4-chloroanilido)}[BAr'₄] (13). ¹H NMR (500 MHz, THF-*d*₈) δ = 8.25 (HC(pz⁵)₃), 7.73 (1H, pz 3-position), 7.70 (1H, pz 3-position), 7.46 (1H, pz 3-position), 6.34 (1H, pz 4-position), 6.18 (1H, pz 4-position), (1 resonance missing due to coincidental overlap), 8.42 (d, ³J_{HH} = 5 Hz, pyridine), 7.24 (t, ³J_{HH} = 7 Hz, pyridine), (1 pyridine resonance missing due to coincidental overlap), 7.79 (BAr'₄), 7.58 (BAr'₄), 6.35 (d, ³J_{HH} = 8 Hz, phenyl), 6.21 (d, ³J_{HH} = 8 Hz, phenyl), 4.31 (d, ³J_{PH} = 4 Hz, P(OCH₂)₃CEt), 2.83 (3H, HC(pz⁵)₃ 5-methyl), 2.76 (6H, coincidental overlap, HC(pz⁵)₃ 5-methyl), 1.24 (2H, q, ³J_{HH} = 8 Hz, -CH₂CH₃), 0.80 (3H, t, ³J_{HH} = 8 Hz, -CH₂CH₃). ³¹P NMR (243 MHz, THF-*d*₈) δ = 130.8. ¹³C NMR (201 MHz, THF-*d*₈) δ = 163.0 (4 line pattern, ¹J_{BC} = 50 Hz, BAr'₄), 157.4 (pyridine), 150.0 (pz 3 or 5-position), 149.4 (pz 3 or 5-position), 146.3 (pz 3 or 5-position), 135.8 (BAr'₄), 130.2 (q, ¹J_{CF} = 32 Hz, BAr'₄), 126.7 (pyridine), 125.7 (q, ¹J_{CF} = 272 Hz, CF₃), 122.9 (phenyl), 121.3 (phenyl), 118.4 (BAr'₄), 110.1 (pz 4-position), 109.9 (pz 4-position), 109.1 (pz 4-position), 76.0 (-OCH₂)₃, 36.8 (d, ³J_{PC} = 32 Hz, -(OCH₂)₃C-), 24.0 (-CH₂CH₃), 11.1 (HC(pz⁵)₃ methyl), 11.1 (HC(pz⁵)₃ methyl), 10.9 (HC(pz⁵)₃ methyl), 7.4 (-CH₂CH₃).

{[HC(pz⁵)₃]Ru[P(OCH₂)₃CEt](py)(4-fluoroanilido)}[BAr'₄] (14). ¹H NMR (500 MHz, THF-*d*₈) δ = 7.20 (1H, pz 3-position), 7.18 (1H, pz 3-position), 7.08 (1H, pz 3-position), 6.04 (1H, pz 4-position), 5.87 (1H, pz 4-position), 5.75 (1H, pz 4-position), (1 missing due to coincidental overlap), 8.19 (pyridine), 7.75 (pyridine), 7.24 (pyridine), 6.61 (broad, phenyl), 6.45 (broad, phenyl), 7.80 (BAr'₄), 7.58 (BAr'₄), 4.35 (P(OCH₂)₃CEt), 2.66 (3H, HC(pz⁵)₃ 5-methyl), 2.58 (3H, HC(pz⁵)₃ 5-methyl), 2.55 (3H, HC(pz⁵)₃ 5-methyl), 1.26 (2H, q, ³J_{HH} = 8 Hz, -CH₂CH₃), 0.82 (3H, t, ³J_{HH} = 8 Hz, -CH₂CH₃). ³¹P NMR (243 MHz, THF-*d*₈) δ = 130.7. ¹⁹F NMR (565 MHz, THF-*d*₈) δ = -63.6, -79.5, -140.3. ¹³C NMR (201 MHz, THF-*d*₈) δ = 163.1 (4 line pattern, ¹J_{BC} = 50 Hz, BAr'₄), 157.4 (pz 3 or 5-position), 157.3 (pyridine), 156.3 (pz 3 or 5-position), 151.1 (pz 3 or 5-position), 148.5 (pz 3 or 5-position), 145.4 (pz 3 or 5-position), 144.3 (pz 3 or 5-position), 140.4 (pyridine), 135.9 (BAr'₄), 130.3 (q, ¹J_{CF} = 32 Hz, BAr'₄), 125.8 (q, ¹J_{CF} = 272 Hz, CF₃), 124.9 (pyridine), 118.5 (BAr'₄), 105.4 (pz 4-position), 105.3 (pz 4-position),

104.5 (pz 4-position), 75.1 $-(\text{OCH}_2)_3$, 70.2 $(\text{HC}(\text{pz}^5)_3)$, 24.4 $(-\text{CH}_2\text{CH}_3)$, 12.9 $(\text{HC}(\text{pz}^5)_3$ methyl), 12.5 $(\text{HC}(\text{pz}^5)_3$ methyl), 7.6 $(-\text{CH}_2\text{CH}_3)$.

References

- (1) Sen, A. *Accounts Chem. Res.* **1998**, *31*, 550.
- (2) Webb, J. R.; Burgess, S. A.; Cundari, T. R.; Gunnoe, T. B. *Dalton Trans.* **2013**, *42*, 16646.
- (3) Kubas, G. J. *Metal Dihydrogen and sigma-Bond Complexes Structure, Theory, and Reactivity*; Kluwer Academic/Plenum Publishers: New York, 2001.
- (4) Ess, D. H.; Gunnoe, T. B.; Cundari, T. R.; Goddard, W. A.; Periana, R. A. *Organometallics* **2010**, *29*, 6801.
- (5) Feng, Y. L., M.; Foley, N. A.; Gunnoe, T. B.; Barakat, K. A.; Cundari, T. R.; Petersen, J. L. *J. Am. Chem. Soc.* **2006**, *128*, 7982.
- (6) Hansch, C.; Leo, A.; Taft, R. W. *Chem. Rev.* **1991**, *91*, 165.
- (7) Goodman, M. A.; Nazarenko, A. Y.; Casavant, B. J.; Li, Z.; Brennessel, W. W.; DeMarco, M. J.; Long, G.; Goodman, M. S. *Inorg. Chem.* **2012**, *51*, 1084.

5 Combined Furan C–H Activation and Furyl Ring-Opening by an Iron(II) Complex

5.1 Introduction

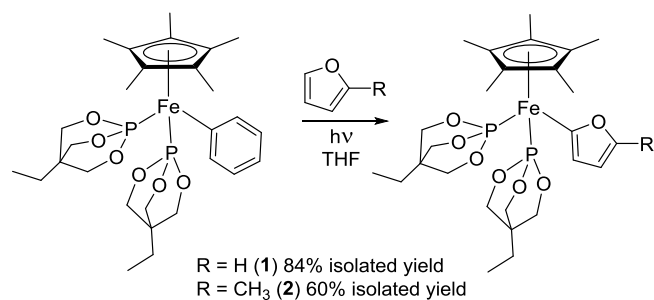
Furan is an important motif in biologically active molecules and fine chemicals,¹⁻⁸ and furan plays a key role in cycloadditions (e.g., Diels–Alder reactions) and transition-metal-mediated reactions to produce aromatic feedstocks and compounds useful in natural product and fine chemical synthesis.⁹⁻¹⁸ Reactions using furan can involve ring opening. For example, furan ring opening and hydrodeoxygenation of bioderived furan compounds to produce linear alkanes has been achieved in high yields and selectivity.^{19,20} Since the furyl moiety is prevalent in lignocellulosic biomass, this type of transformation could prove a viable renewable energy source as petroleum supplies dwindle.^{9,16-20} Transition-metal catalysts, such as pentacarbonyl(η^2 -cis-cyclooctene)chromium(0) and $\text{Rh}_2(\text{OAc})_4$, have been reported to ring-open furan compounds to produce substituted organic products.¹³⁻¹⁵ Our interest in this area focuses on the utilization of earth abundant metals for aromatic C–H activation and functionalization catalysis.²¹⁻²³ Organometallic Fe complexes display a versatile range of chemistry,²²⁻²⁹ and Cp^*Fe complexes are known to perform oxy-insertion³⁰ and C–H activation,³¹ both of which are industrially important transformations. C–H activation of furan by Fe complexes has been reported;³¹⁻³³ when it is coupled with functionalization of the furyl ring and/or furyl ring opening, transition metal-mediated furan C–H activation can lead to a wide range of useful products. The work described herein involves the C–H activation of furan and 2-methylfuran by $\text{Cp}^*\text{Fe}[\text{P}(\text{OCH}_2)_3\text{CEt}]_2\text{Ph}$ ($\text{Cp}^* = \eta^5$ -1,2,3,4,5-pentamethylcyclopentadienyl, $\text{P}(\text{OCH}_2)_3\text{CEt} = 2,6,7$ -trioxa-1-phosphabicyclo[2,2,1]octane) to produce $\text{Cp}^*\text{Fe}[\text{P}(\text{OCH}_2)_3\text{CEt}]_2(2\text{-furyl})$ (**1**) and $\text{Cp}^*\text{Fe}[\text{P}(\text{OCH}_2)_3\text{CEt}]_2[2\text{-}(5\text{-methylfuryl})]$ (**2**), respectively. Iron complexes often exhibit a predisposition toward single-electron chemistry and C–H bond homolysis by radical pathways,³⁴⁻³⁸ the reported C–H activations of furan by $\text{Cp}^*\text{Fe}[\text{P}(\text{OCH}_2)_3\text{CEt}]_2\text{Ph}$ are among the few examples of a likely nonradical pathway.^{31-33,39-43} Also, furyl ring opening occurs upon reaction of complex **1** with 2-butyne under photolytic conditions to form the sandwich complex $\text{Cp}^*\text{Fe}[\eta^5$ -

$\text{C}_5\text{Me}_4(\text{CH}=\text{CHCHO})$] (**3**). Complex **1** is capable of analogous reactions with other internal alkynes. Furthermore, the methylfuryl variant **2** reacts with 2-butyne to form $\text{Cp}^*\text{Fe}[\eta^5\text{-C}_5\text{Me}_4(\text{CH}=\text{CHCOCH}_3)]$ (**4**). To our knowledge, the only previously reported example of a net alkyne insertion that results in heteroaryl ring-opening involving an iron complex consists of the net insertion of 2 equiv of phenylacetylene or diphenylacetylene into an Fe–NHC bond with ring opening of the NHC ligand to form a diimine moiety.⁴⁴

The work presented herein was done together with Dr. Steven Kalman, a former member of the Gunnoe Laboratory. Dr. Kalman developed the C–H activation and furyl ring-opening reactions discussed below and gathered much of the characterization data, including growing crystals and determining the identities of reaction intermediates.

5.2 Furyl C–H activation by $\text{Cp}^*\text{Fe}[\text{P}(\text{OCH}_2)_3\text{CEt}]_2\text{Ph}$

The complex $\text{Cp}^*\text{Fe}(\text{CO})(\text{NCMe})\text{Ph}$ is capable of C–H activation of benzene in addition to the regioselective C–H activation of furan, 2-methylfuran, thiophene, and thiazole.³¹ Thus, we sought to probe the ability of $\text{Cp}^*\text{Fe}[\text{P}(\text{OCH}_2)_3\text{CEt}]_2\text{Ph}$ to activate the C–H bonds of furans. Excess furan was added to a solution of $\text{Cp}^*\text{Fe}[\text{P}(\text{OCH}_2)_3\text{CEt}]_2\text{Ph}$ ³⁰ in THF and photolyzed to produce $\text{Cp}^*\text{Fe}[\text{P}(\text{OCH}_2)_3\text{CEt}]_2(2\text{-furyl})$ (**1**) (84% isolated yield) and free benzene (Scheme 1, Figure 2). A crystal suitable for X-ray diffraction study was grown by cooling a saturated solution of **1** in a 1:1 mixture of diethyl ether and *n*-pentane (Figure 1). The Fe–C13 bond length of **1** is 1.930(5) Å, which is shorter than the Fe–C_{phenyl} bond of $\text{Cp}^*\text{Fe}[\text{P}(\text{OCH}_2)_3\text{CEt}]_2\text{Ph}$ (Fe–C_{phenyl} bond length of 1.9993(2) Å); this difference in bond lengths is indicative of Fe–C_{furyl} being stronger than Fe–C_{phenyl}.³⁰



Scheme 1. Reaction of Cp*Fe[P(OCH₂)₃CEt]₂Ph with furan and 2-methylfuran.

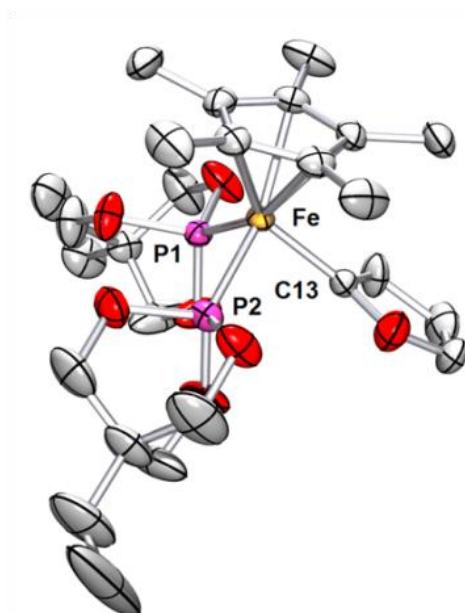


Figure 1. ORTEP of Cp*Fe[P(OCH₂)₃CEt]₂(2-furyl) (**1**) (30% probability ellipsoids; H atoms omitted). Selected bond lengths (Å): Fe–C13 1.930(5), Fe–P1 2.096(1), Fe–P2 2.075(1). Selected bond angles (°): C13–Fe–P1 90.8(2), C13–Fe–P2 91.1(1), P1–Fe–P2 92.27(5).

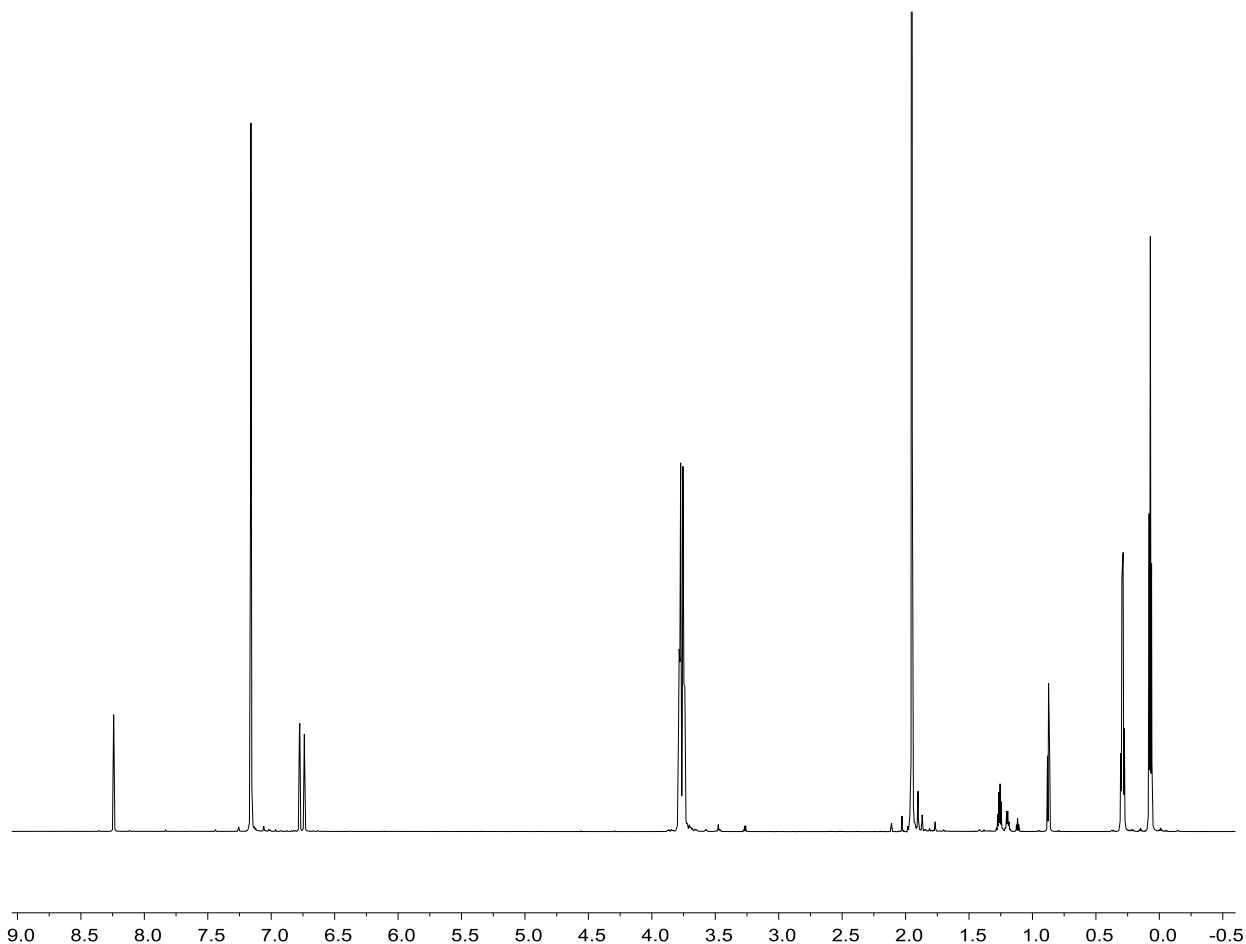


Figure 2. ^1H NMR spectrum for $\text{Cp}^*\text{Fe}[\text{P}(\text{OCH}_2)_3\text{CEt}]_2(2\text{-furyl})$ (**1**) in C_6D_6 .

The corresponding photolytic C–H activation of 2-methylfuran by $\text{Cp}^*\text{Fe}[\text{P}(\text{OCH}_2)_3\text{CEt}]_2\text{Ph}$ produced $\text{Cp}^*\text{Fe}[\text{P}(\text{OCH}_2)_3\text{CEt}]_2[2\text{-(5-methylfuryl)}]$ (**2**) in 60% isolated yield (Scheme 1). The presence of a doublet at 5.80 ppm ($^3J_{\text{HH}} = 3$ Hz) and a multiplet at 5.60 ppm for the coordinated furyl ring as well as a methyl resonance at 2.19 ppm in the ^1H NMR spectrum demonstrates that C–H activation is selective for the α -C–H position of the furan ring (Figure 3). Since the C–H bond dissociation energy of the α -C–H bond (120.4 ± 1 kcal/mol)⁴⁵ is greater than the methyl C–H bond dissociation energy (86.5 ± 2 kcal/mol),⁴⁶ selective C–H activation at the α -C–H position supports C–H activation by a nonradical mechanism.

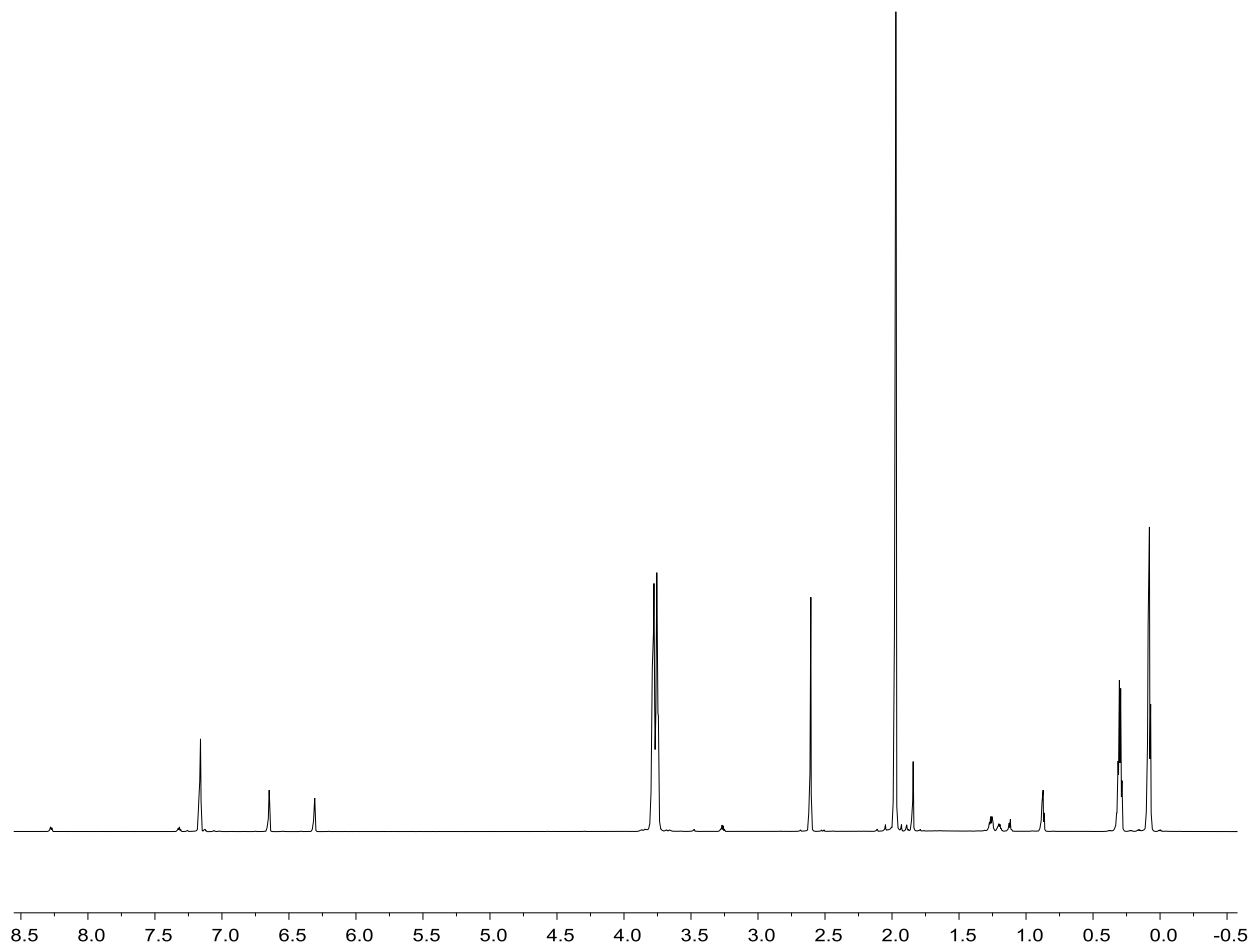
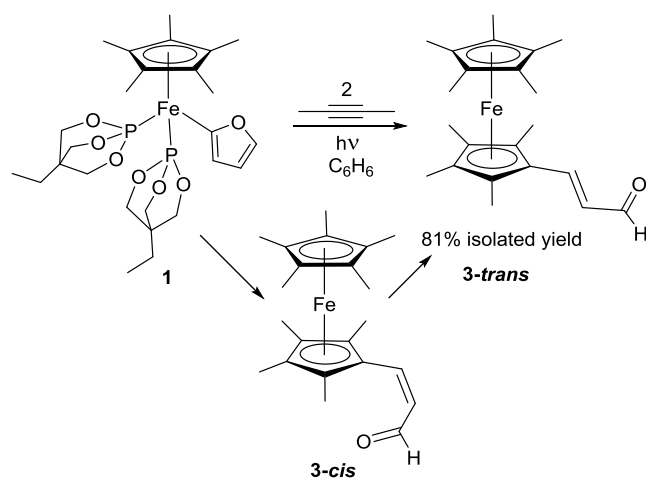


Figure 3. ^1H NMR spectrum of $\text{Cp}^*\text{Fe}[\text{P}(\text{OCH}_2)_3\text{CEt}]_2[2\text{-(5-methylfuryl)}]$ (**2**) in C_6D_6 .

5.3 Photolytic reactions of $\text{Cp}^*\text{Fe}[\text{P}(\text{OCH}_2)_3\text{CEt}]_2(2\text{-furyl})$ (**1**) and $\text{Cp}^*\text{Fe}[\text{P}(\text{OCH}_2)_3\text{CEt}]_2[2\text{-(5-methylfuryl)}]$ (**2**) with 2-butyne.

Under photolytic conditions, the complex $\text{Cp}^*\text{Fe}[\text{P}(\text{OCH}_2)_3\text{CEt}]_2(2\text{-furyl})$ (**1**) reacts with 2-butyne to form the sandwich complex $\text{Cp}^*\text{Fe}[\eta^5\text{-C}_5\text{Me}_4(\text{CH}=\text{CHCHO})]$ (**3-trans**) in 81% isolated yield (Scheme 2, Figure 5). Both $\text{P}(\text{OCH}_2)_3\text{CEt}$ ligands are displaced, allowing 2 equiv of 2-butyne to react with complex **1**. Although the final isolated product is **3-trans**, following the reaction by ^1H NMR spectroscopy provides evidence for the formation of both *cis* and *trans* isomers of the product (**3-cis** and **3-trans**). The intermediate **3-cis** is indicated by the presence of a doublet with $^3J_{\text{HH}} = 11$ Hz at 6.98 ppm, while **3-trans** is indicated by a doublet with $^3J_{\text{HH}} = 16$

Hz at 7.11 ppm. Monitoring the reaction reveals that **3-cis** is likely the kinetic product, which converts to **3-trans** as the reaction proceeds. The identity of **3-trans** was confirmed by an X-ray diffraction study of a single crystal grown by slow evaporation of an *n*-pentane/diethyl ether solution (Figure 4). The crystal structure of **3-trans** confirms that C7–C6 is a double bond (1.324(5) Å) in comparison to the longer adjacent single bonds C6–C1 (1.442(4) Å) and C8–C7 (1.428(5) Å). The trans geometry about the double bond is clearly visible.



Scheme 2. Reaction of Cp*Fe[P(OCH₂)₃CEt]₂(2-furyl) (**1**) with 2-butyne.

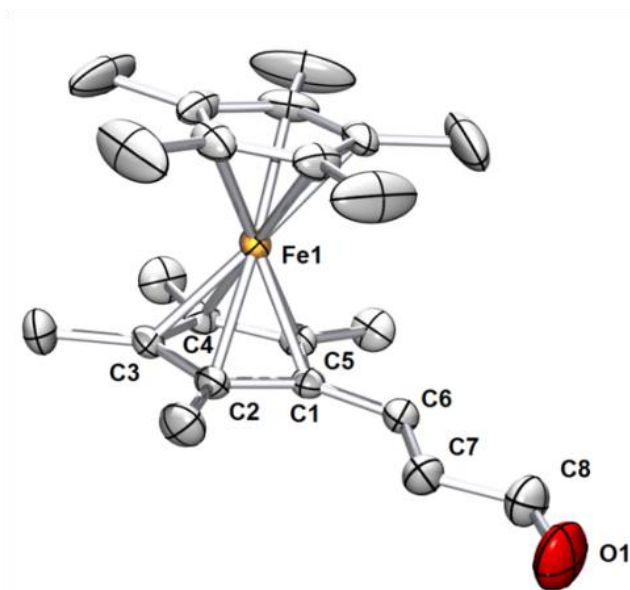


Figure 4. ORTEP of $\text{Cp}^*\text{Fe}[\eta^5\text{-C}_5\text{Me}_4(\text{CH}=\text{CHCHO})]$ (**3-trans**) (50% probability ellipsoids; H atoms omitted). Selected bond lengths (\AA): O1–C8 1.205(5), C8–C7 1.428(5), C7–C6 1.324(5), C6–C1 1.442(4), Fe1–C1 2.051(3), Fe1–C2 2.049(3), Fe1–C3 2.060(3), Fe1–C4 2.059(3), Fe1–C5 2.042(3). Selected bond angles ($^\circ$): C8–C7–C6 121.2(4), C7–C6–C1 130.2(3).

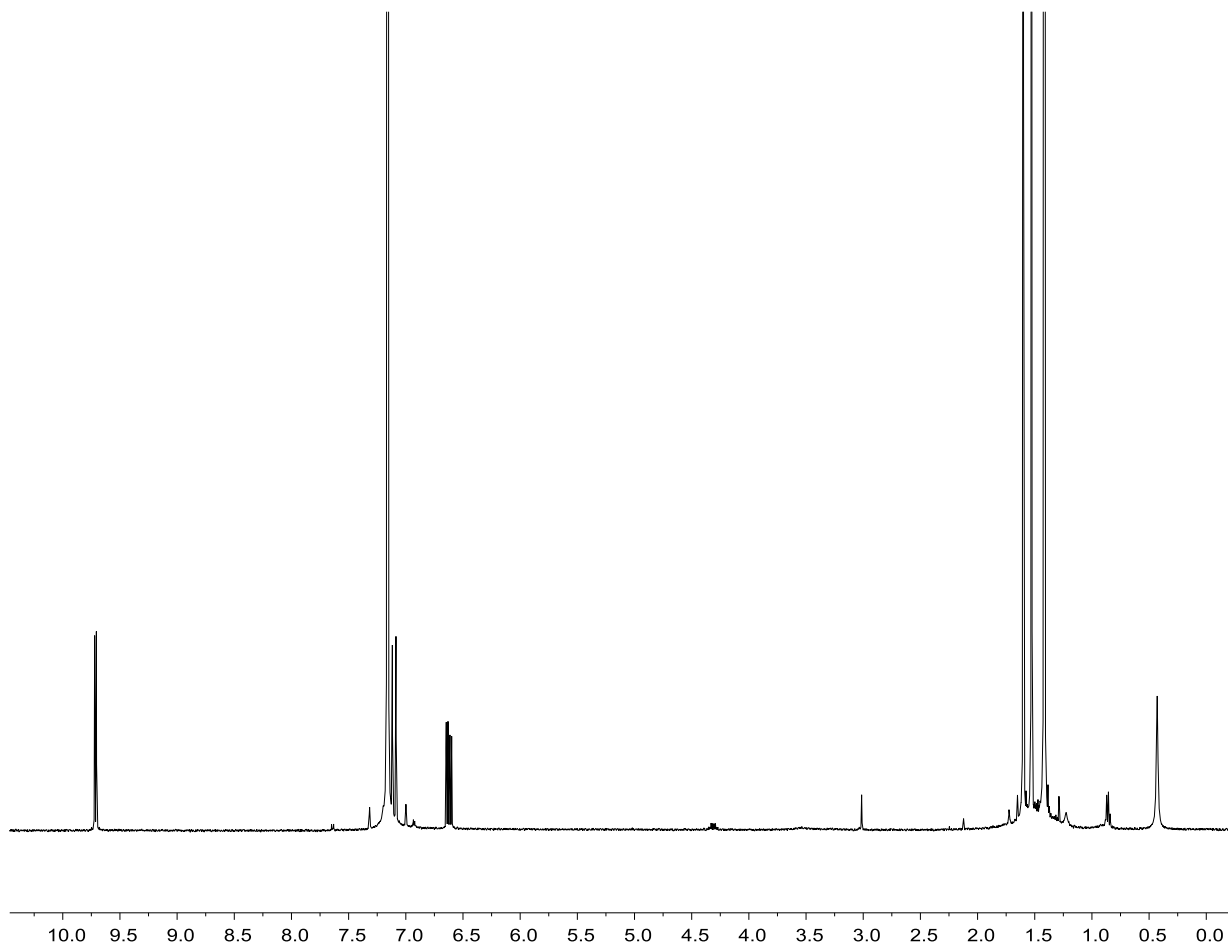
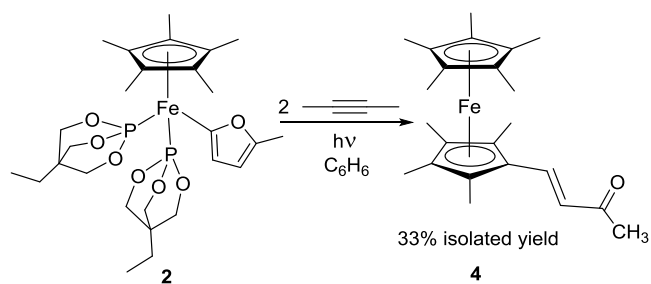


Figure 5. ^1H NMR spectrum of $\text{Cp}^*\text{Fe}[\eta^5\text{-C}_5\text{Me}_4(\text{CH}=\text{CHCOH})](\mathbf{3})$ in C_6D_6 .

The corresponding transformation of $\text{Cp}^*\text{Fe}[\text{P}(\text{OCH}_2)_3\text{CEt}]_2[2\text{-(5-methylfuryl)}]$ (**2**) to produce $\text{Cp}^*\text{Fe}[\eta^5\text{-C}_5\text{Me}_4(\text{CH}=\text{CHCOCH}_3)]$ (**4**) in 33% isolated yield also occurs under photolytic conditions (Scheme 3, Figure 6). ^1H NMR spectroscopy reveals doublets at 7.59 ppm ($^3J_{\text{HH}} = 16$ Hz) and 6.56 ppm ($^3J_{\text{HH}} = 16$ Hz) for the olefin protons; furthermore, a singlet corresponding to the ketone methyl group appears at 2.12 ppm.



Scheme 3. Reaction of $\text{Cp}^*\text{Fe}[\text{P}(\text{OCH}_2)_3\text{CEt}]_2[2\text{-(5-methylfuryl)}]$ (**2**) with 2-butyne.

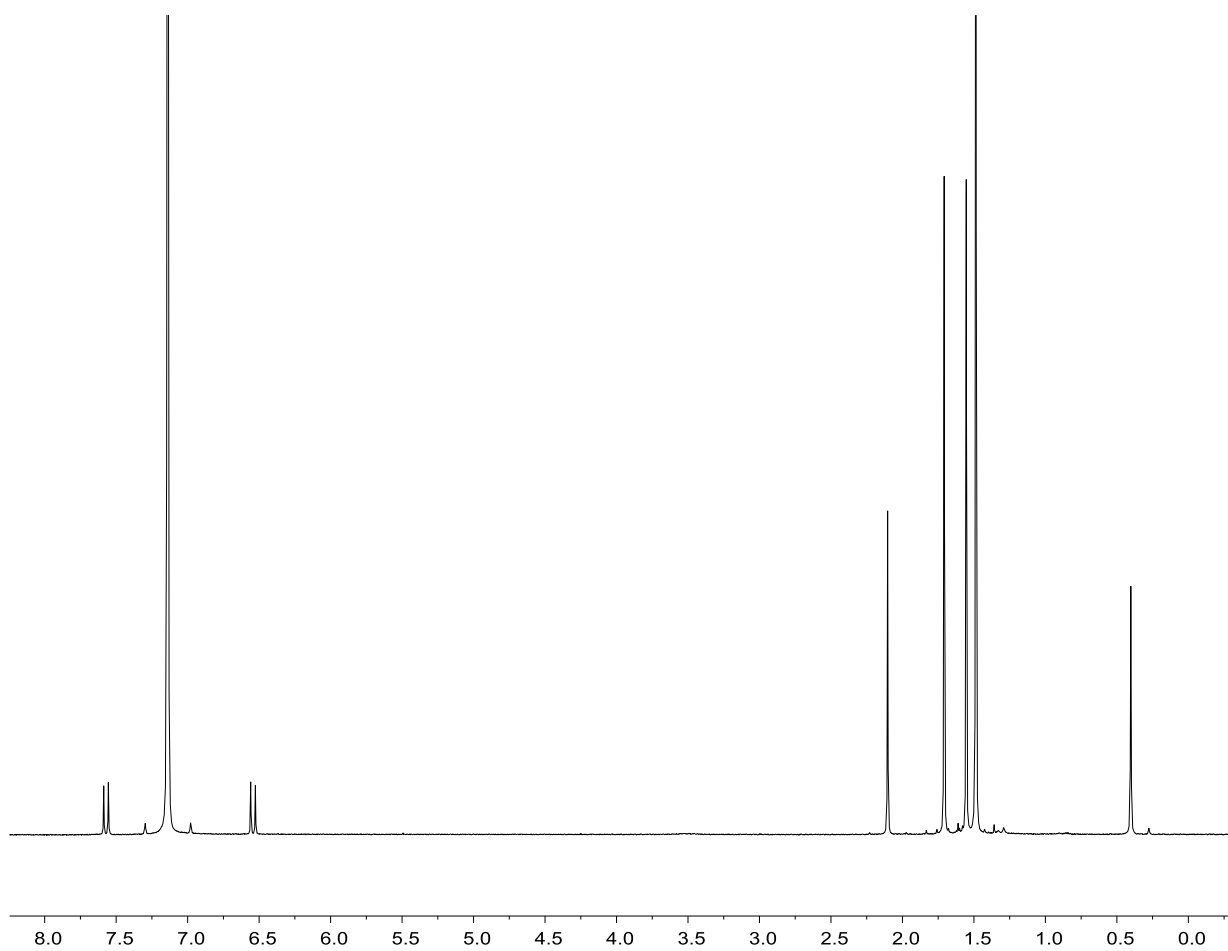


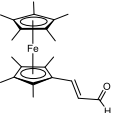
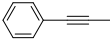
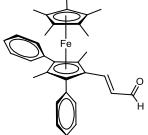
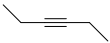
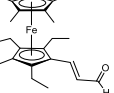
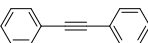
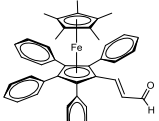
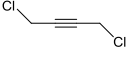
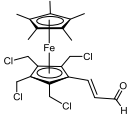
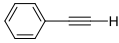
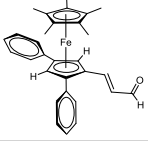
Figure 6. ^1H NMR spectrum of $\text{Cp}^*\text{Fe}[\text{C}_5\text{Me}_4(\text{CH}=\text{CHOMe})]$ (**4**) in C_6D_6 .

5.4 Substrate scope study of reaction of $\text{Cp}^*\text{Fe}[\text{P}(\text{OCH}_2)_3\text{CEt}]_2[2\text{-furyl}]$ (**1**) with alkynes

We probed reactions of **1** with other alkynes (Table 1). 1-Phenyl-1-propyne (entry 2) and 3-hexyne (entry 3) both react to give the ring-opened products. The reaction with 3-hexyne is faster than that with 1-phenyl-1-propyne. Photolysis of diphenylacetylene (Table 1, entry 4) with

1 produced only a small amount of the desired product, while the majority of starting material decomposed to unidentified products. Photolysis with 1,4-dichloro-2-butyne (entry 5) resulted in very broad ^1H NMR spectra, possibly due to formation of paramagnetic species; the desired product was not observed. The reaction of phenylacetylene with **1** (entry 6) produced multiple products, and attempts to drive the reaction to a single product resulted in decomposition to intractable products. The acidic proton of the terminal alkyne of phenylacetylene, which might serve to protonate the furyl ligand (free furan was observed) and ultimately lead to multiple unidentified species, is most likely problematic. The lack of success with phenylacetylene indicates that an internal alkyne is likely necessary for the furyl ring-opening reaction to occur with **1**.

Table 1. Alkyne substrate scope and percent yield of corresponding furyl ring-opening product.

Entry	Substrate ^a	Product	% Yield ^b	Time (h)
1			82	4.5
2			57	16.5
3			59	7.0
4			9	16.5
5			0	---
6			0	---

^aTen equivalents of substrate was added to a 0.069 M solution of **1** in C₆D₆ and photolyzed.

^bYields were determined by ¹H NMR spectroscopy using CH₃NO₂ as an internal standard.

The furyl ring-opening reaction of **1** with 2-butyne does not occur under thermal conditions (70–110 °C). Complex **1** is observed to slowly decompose over time to intractable products with heat in the presence of 2-butyne. Also, this transformation does not appear to involve free radical intermediates, as addition of the radical trap 2,2,6,6-tetramethyl-1-piperindinyloxy (TEMPO) does not inhibit the reaction of **1** with 2-butyne.

5.5 Mechanistic and kinetic studies of the reaction of Cp*Fe[P(OCH₂)₃CEt]₂(2-furyl) (**1**) with 2-butyne

5.5.1 Intermediates and products formed from the reaction of Cp*Fe[P(OCH₂)₃CEt]₂(2-furyl) (**1**) with 2-butyne

In order to explore the alkyne insertion–furyl ring-opening reactions, the reaction of **1** with 2-butyne was monitored. Multiple species involved in the reaction of **1** with 2-butyne can be observed by ¹H NMR spectroscopy before the reaction is complete (Figure 7). Using two-dimensional NMR spectroscopy, we have been able to identify some intermediates during the reaction. Notably, **3-cis** has the following resonances: 9.72 ppm (doublet, aldehyde proton), 6.98 ppm (doublet, ³J_{HH} = 11 Hz, indicative of cis olefin H), and a doublet of doublets at 6.20 ppm (olefin H). Alternately, **3-trans** has the following resonances: 9.71 ppm (doublet, aldehyde proton), 7.11 ppm (doublet, ³J_{HH} = 16 Hz, indicative of trans olefin H), and a doublet of doublets at 6.61 ppm (olefin H). An intermediate species (not **3-cis** or **3-trans**) was found to have furyl resonances at 7.37, 6.38, and 6.19 ppm, methyl resonances occurring at 2.68 and 2.49 ppm, and a Cp* resonance at 1.96 ppm. We propose that this complex (**1a**) is the intermediate formed upon a single insertion of 2-butyne into the Fe–furyl moiety of **1**.

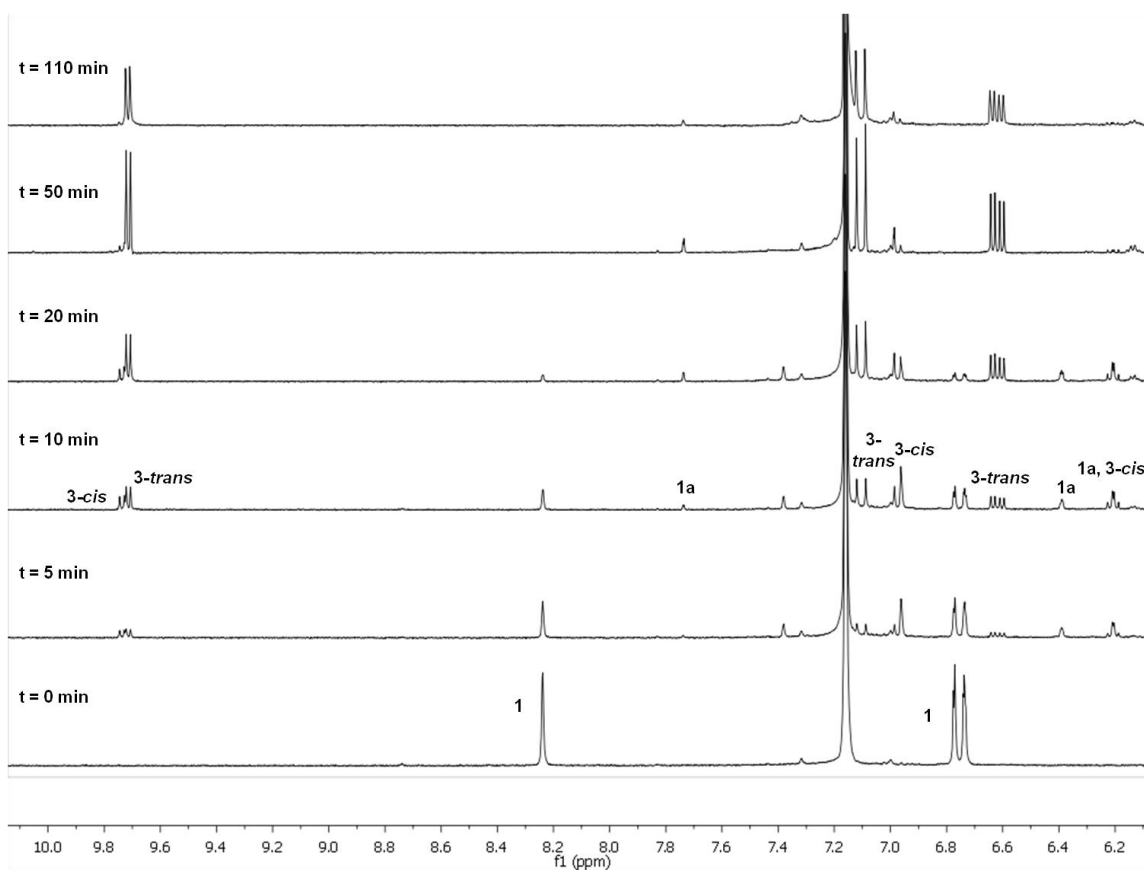
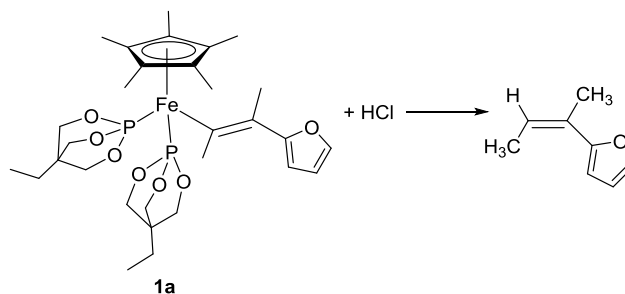


Figure 7. ^1H NMR spectra of the downfield region for the reaction between **1** and 2-butyne in C_6D_6 under photolytic conditions.

The addition of a Brønsted acid (HCl) to the reaction mixture of **1** with 2-butyne after 0.5 h of photolysis was used to indirectly confirm the identity of proposed intermediate **1a** by releasing the organic product dimethylvinylfuran (Scheme 4). The ^1H NMR spectrum after addition of HCl showed furyl resonances at 7.29, 6.38, and 6.32 ppm, a quartet corresponding to the olefin proton at 4.44 ppm ($^3J_{\text{HH}} = 7$ Hz), and methyl resonances at 2.82 and 2.78 ppm. Furthermore, a GC/MS analysis of the reaction solution is consistent with the formation of dimethylvinylfuran.



Scheme 4. Reaction of intermediate **1a** with HCl.

5.5.2 Dependence of free $\text{P}(\text{OCH}_2)_3\text{CEt}$ on the reaction of $\text{Cp}^*\text{Fe}[\text{P}(\text{OCH}_2)_3\text{CEt}]_2(\text{2-furyl})$ (**1**) with 2-butyne

Rigorous kinetic studies were not possible due to inherent variations in photolytic conditions; therefore, each set of experimental conditions for the following mechanistic studies was performed once and photolyzed simultaneously. The dependence of the rate of reaction on free phosphite was probed by ^1H NMR spectroscopy. To identical samples of complex **1** and 2-butyne were added 0, 0.5, 1, and 2 equiv (relative to **1**) of free $\text{P}(\text{OCH}_2)_3\text{CEt}$. The samples were then photolyzed for 30 min intervals, and ^1H NMR analysis after each period of photolysis demonstrated that adding excess phosphite slows the rate of reaction. Monitoring the concentration of **1** over the reaction time shows that the rate of the reaction of **1** with 2-butyne decreases with each **1** equiv of added $\text{P}(\text{OCH}_2)_3\text{CEt}$ (Figure 8). A plot of $\log k_{\text{obs}}$ vs $\log [\text{P}(\text{OCH}_2)_3\text{CEt}]$ confirms the reaction has an inverse first-order dependence on $\text{P}(\text{OCH}_2)_3\text{CEt}$ (Figure 9).

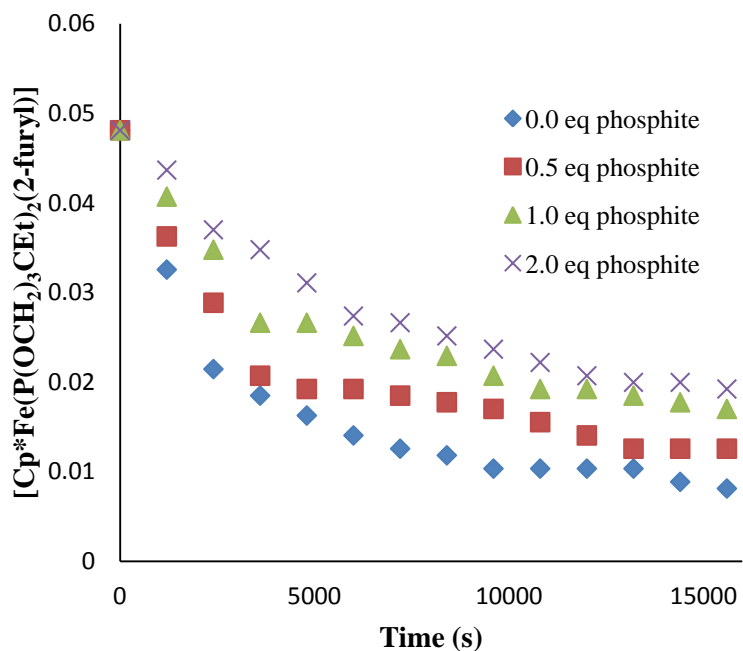


Figure 8. Concentration (M) of **1** vs time for the reaction of **1** with 2-butyne as a function of added $\text{P}(\text{OCH}_2)_3\text{CEt}$.

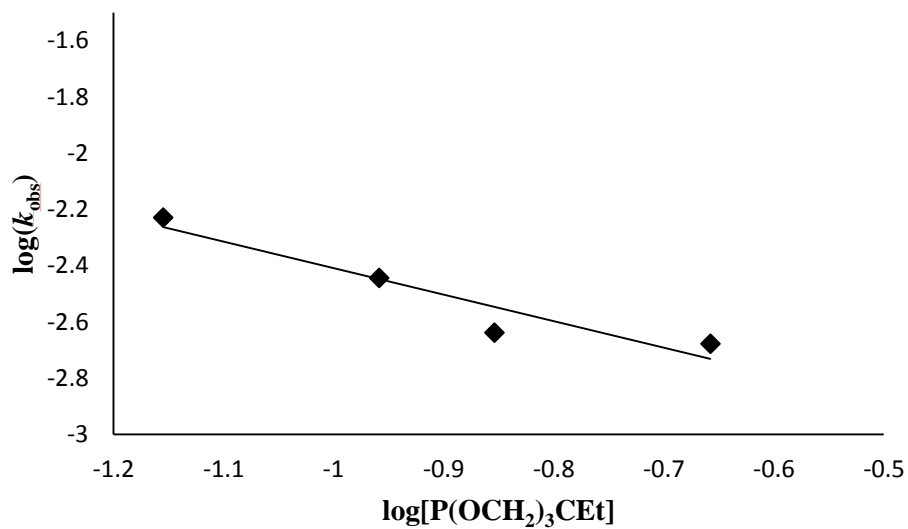


Figure 9. Plot of $\log(k_{\text{obs}})$ vs $\log[\text{P}(\text{OCH}_2)_3\text{CEt}]$ for the reaction of **1** (0.069 M) with 2-butyne (0.141 M) in the presence of varying amounts of added $\text{P}(\text{OCH}_2)_3\text{CEt}$ (slope = -0.94, $R^2 = 0.90$).

5.5.3 Dependence of 2-butyne on the reaction of **1** with 2-butyne

A study of the dependence of the reaction of **1** with 2-butyne on the concentration of 2-butyne was also conducted. Four identical samples of a solution of **1** were prepared; 10, 15, 20, and 25 equiv of 2-butyne (relative to **1**) were added to each NMR tube and photolyzed for 30 min intervals. The ^1H NMR data show that the reaction is zero-order in 2-butyne under pseudo-first-order conditions (Figures 10 and 11). However, one noteworthy observation was that, upon addition of such a large excess of 2-butyne, **1** began to convert to a minor species at room temperature under ambient light. This reaction was especially noticeable at ≥ 25 equiv of 2-butyne. In situ ^1H and ^{31}P NMR spectroscopy is consistent with a ligand exchange reaction between phosphite and 2-butyne, and we propose that this complex is $\text{Cp}^*\text{Fe}[\text{P}(\text{OCH}_2)_3\text{CEt}](\eta^2\text{-2-butyne})(2\text{-furyl})$ (**5**). Three identical samples of a solution of **1** and $\text{P}(\text{OCH}_2)_3\text{CEt}$ (0.5 equiv relative to **1**) were prepared. We then added 10, 20, and 30 equiv of 2-butyne (relative to **1**) to each sample and photolyzed the mixtures for 30 min intervals. Under these conditions, the reaction displays a first-order dependence on 2-butyne (Figure 12).

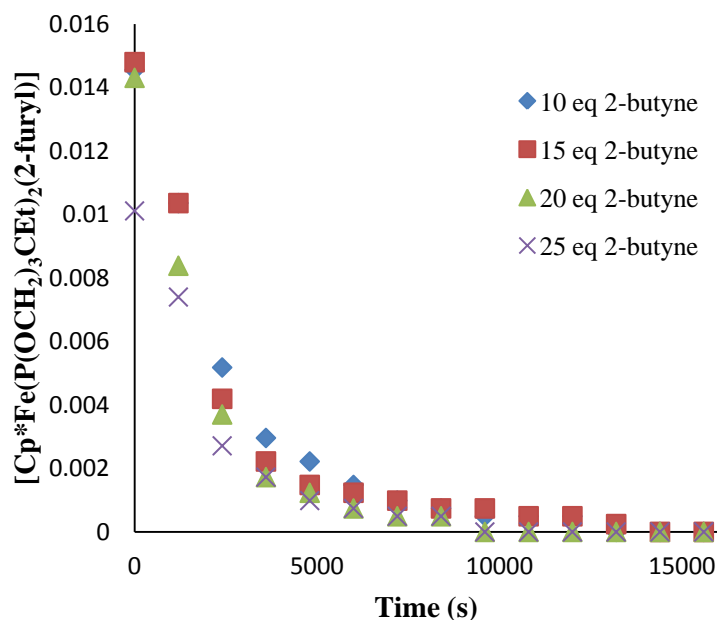


Figure 10. Concentration (M) of **1** vs. time as a function of 2-butyne concentration.

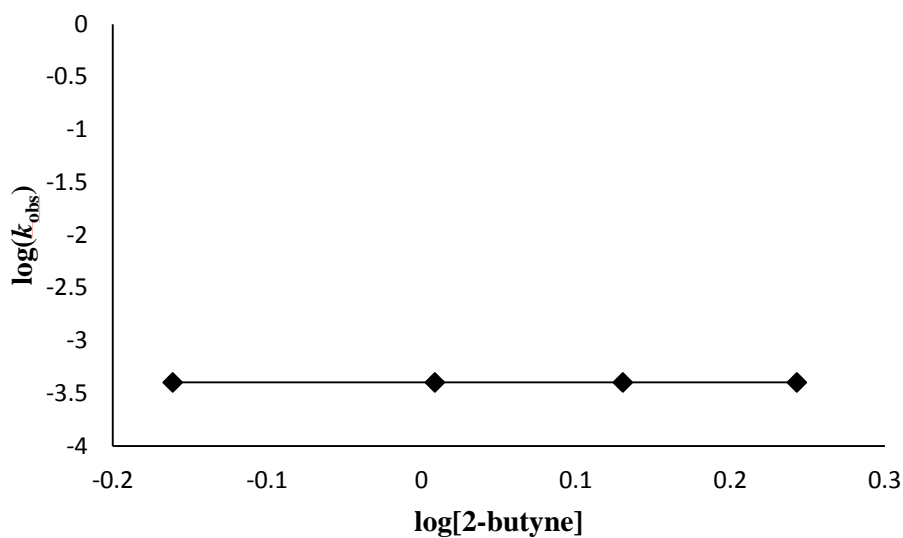


Figure 11. Plot of $\log k_{\text{obs}}$ vs $\log [2\text{-butyne}]$ for the reaction of **1** (0.069 M) with varying amounts of 2-butyne ($R^2 = 0.99$).

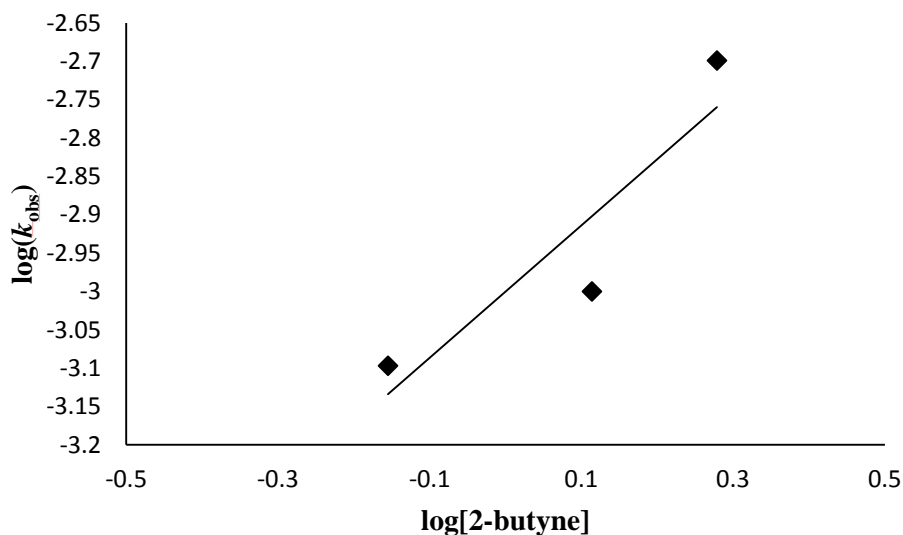
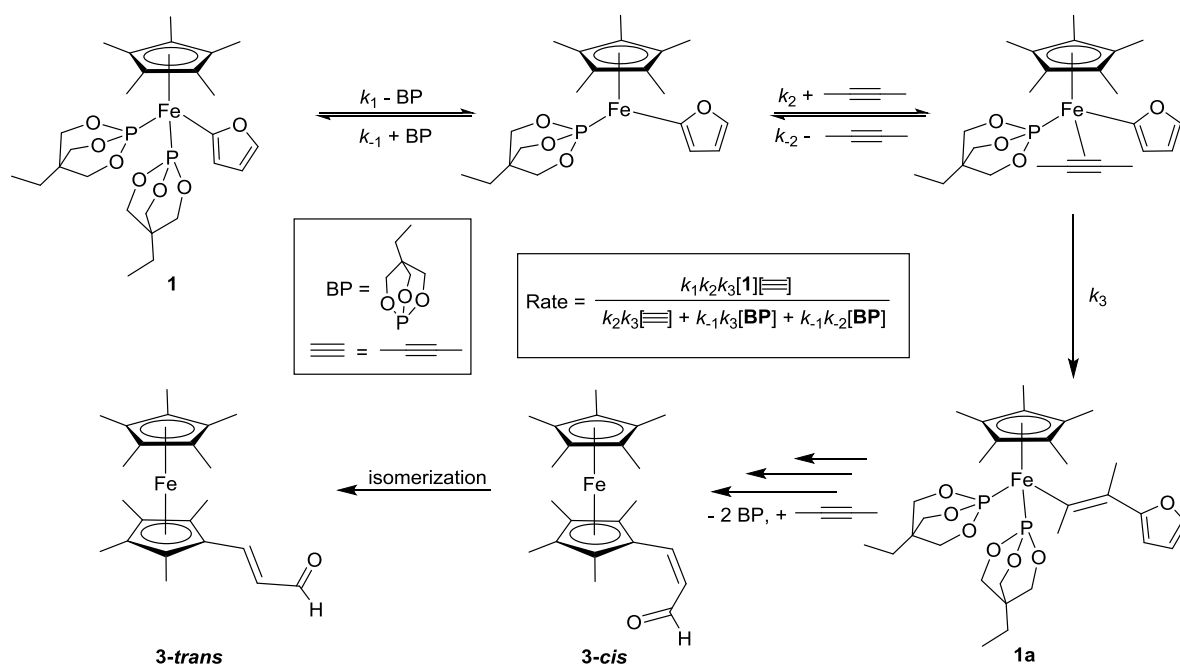


Figure 12. Plot of $\log k_{\text{obs}}$ vs $\log [2\text{-butyne}]$ for the reaction of **1** (0.069 M) with varying amounts of 2-butyne in the presence of 0.5 equiv of $\text{P}(\text{OCH}_2)_3\text{CEt}$ (relative to **1**) (slope = 0.9, $R^2 = 0.8$).

5.6 Proposed rate law for the reaction of **1** with 2-butyne

We propose the following mechanism and rate law on the basis of experimental observations (Scheme 5). Photolysis promotes the dissociation of phosphite followed by

coordination and insertion of 2-butyne into the Fe–furyl bond; subsequent recoordination of phosphite gives intermediate **1a**. The following steps of the reaction involve a net insertion of 1 equiv more of 2-butyne, ring opening of the furyl fragment, and ring closure of the butadienyl fragment to form the cis isomer of $\text{Cp}^*\text{Fe}[\eta^5\text{-C}_5\text{Me}_4(\text{CH}=\text{CHCHO})]$ (**3-cis**). This complex isomerizes to produce the final trans product (**3-trans**). The observed first-order dependence on 2-butyne in the presence of added $\text{P}(\text{OCH}_2)_3\text{CEt}$ and zero-order dependence on 2-butyne without added $\text{P}(\text{OCH}_2)_3\text{CEt}$ are consistent with the proposed rate law and indicate that either the phosphite terms or the 2-butyne term in the denominator can dominate depending on reaction conditions. In one limiting form of the rate law, in the presence of excess 2-butyne the term $k_2k_3[2\text{-butyne}]$ dominates and is much greater than the $k_{-1}k_3[\text{BP}]$ and $k_{-1}k_{-2}[\text{BP}]$ terms. Under these conditions, the rate law is reduced to $\text{rate} = k_1[\mathbf{1}]$, which is consistent with the observed zero-order dependence on 2-butyne under these conditions for reactions performed in the absence of added $\text{P}(\text{OCH}_2)_3\text{CEt}$ and using excess 2-butyne. When excess $\text{P}(\text{OCH}_2)_3\text{CEt}$ is added, the terms containing bicyclic phosphite become larger and, in one limiting form, the $k_2k_3[2\text{-butyne}]$ term will be negligible, which should result in a first-order dependence on the concentration of 2-butyne. Indeed, under conditions with 0.5 equiv of $\text{P}(\text{OCH}_2)_3\text{CEt}$ (relative to complex **1**) added, a first-order dependence on 2-butyne is observed (Figure 12).



Scheme 5. Proposed reaction mechanism of $\text{Cp}^*\text{Fe}[\text{P}(\text{OCH}_2)_3\text{CET}]_2(2\text{-furyl})$ (**1**) with 2-butyne under photolytic conditions.

Cyclization reactions by iron complexes are not without precedent. A reaction was reported by Allison et al. in which the photolysis of $\text{CpFe}(\text{CO})_2(\text{butadienyl})$ complexes promoted insertion of CO into the butadienyl ligand followed by electrocyclic ring closure of the pentadienyl moiety and subsequent rearrangement to give the corresponding hydroxyferrocene complex.⁴⁷ Another notable example of Fe-mediated carbocyclization includes the reaction of $\text{Cp}^*\text{Fe}(\text{CO})(\text{NCMe})\text{Ph}$ with internal alkynes.⁴⁸ This chemistry involves insertion of 1 equiv of alkyne into the Fe–Ph bond, followed by C–H activation, CO insertion, cyclization, and tautomerization to produce $\text{Cp}^*\text{Fe}(\text{hydroxyindenyl})$ type sandwich complexes under mild thermal conditions.⁴⁸

5.7 Conclusions

$\text{Cp}^*\text{Fe}[\text{P}(\text{OCH}_2)_3\text{CET}]_2\text{Ph}$ activates $\alpha\text{-C-H}$ bonds of furan and 2-methylfuran by a nonradical pathway to give $\text{Cp}^*\text{Fe}[\text{P}(\text{OCH}_2)_3\text{CET}]_2(2\text{-furyl})$ (**1**) and $\text{Cp}^*\text{Fe}[\text{P}(\text{OCH}_2)_3\text{CET}]_2[2\text{-}(5\text{-methylfuryl})]$ (**2**). Complexes **1** and **2** react with 2-butyne under photolytic conditions to give

$\text{Cp}^*\text{Fe}[\eta^5\text{-C}_5\text{Me}_4(\text{CH}=\text{CHCHO})]$ (**3-trans**) and $\text{Cp}^*\text{Fe}[\eta^5\text{-C}_5\text{Me}_4(\text{CH}=\text{CHCOCH}_3)]$ (**4**), respectively.

5.8 Experimental Section

General Considerations. Unless otherwise noted, all synthetic procedures were performed under anaerobic conditions in a nitrogen filled glovebox or by using standard Schlenk techniques. Glovebox purity was maintained by periodic nitrogen purges and was monitored by an oxygen analyzer ($\text{O}_2 < 15$ ppm for all reactions). Tetrahydrofuran and n-pentane were dried by distillation from sodium/benzophenone and P_2O_5 , respectively. Diethyl ether was distilled over CaH_2 . Benzene, methylene chloride, and hexanes were purified by passage through a column of activated alumina. Benzene- d_6 , acetone- d_6 , CD_3CN , 1,4-dioxane- d_8 , and THF- d_8 were used as received and stored under a N_2 atmosphere over 4 Å molecular sieves. Tetrabutylammonium hexafluorophosphate ($[\text{Bu}_4\text{N}][\text{PF}_6]$) and ferrocene were purchased from Sigma-Aldrich. Prior to use, $[\text{Bu}_4\text{N}][\text{PF}_6]$ was recrystallized in ethanol and dried under vacuum at 50 °C. ^1H NMR spectra were recorded on a Varian 300, a Varian 500 MHz, or a Bruker 600 or 800 MHz spectrometer, and $^{13}\text{C}\{^1\text{H}\}$ NMR spectra were recorded on a Varian 500 MHz (operating frequency 125 MHz), a Bruker 600 MHz (operating frequency 150 MHz), or a Bruker 800 MHz spectrometer (operating frequency 201 MHz). All ^1H and ^{13}C spectra are referenced against residual proton signals (^1H NMR) or ^{13}C resonances (^{13}C NMR) of the deuterated solvents. $^{31}\text{P}\{^1\text{H}\}$ NMR spectra were obtained on a Varian 300 MHz (operating frequency 121 MHz), a Varian 500 MHz (operating frequency 201 MHz), or a Varian 600 MHz spectrometer (operating frequency 243 MHz) and referenced against an external standard of H_3PO_4 (δ 0). GC/MS was performed using a Shimadzu GCMS-QP2010 Plus system with a 30 m \times 0.25 mm SHRXI-5MS column with 0.25 μm film thickness using electron impact ionization. Electrochemical experiments were performed under a nitrogen atmosphere using a BASi Epsilon potentiostat. Cyclic voltammograms were recorded in NCMe from 800 to -800 mV at 100 mV/s using a 3 mm glassy-carbon working electrode, a platinum-wire auxiliary electrode, and a Ag/AgNO_3 nonaqueous reference electrode

immersed in 5 mL of 0.1 M [Bu₄N][PF₆] solution for analysis. All potentials are referenced to ferrocene as the internal standard. Photolysis experiments were performed using UV–vis radiation generated by a 450 W power supply (Model No. 17830, Ace Glass, Inc.). The complex Cp*Fe[P(OCH₂)₃CET]₂Ph was prepared according to the literature procedure.³⁰ All other reagents were used as purchased from commercial sources. Elemental analyses were performed by Atlantic Microlab, Inc.

Cp*Fe[P(OCH₂)₃CET]₂(2-furyl) (1). Cp*Fe[P(OCH₂)₃CET]₂Ph (0.078 g, 0.13 mmol) was dissolved in THF (~2 mL), and furan (0.24 mL, 3.3 mmol) was added. The resulting solution was placed in a screw-cap NMR tube and photolyzed for ~4 h. Reaction progress was monitored by ³¹P NMR spectroscopy. The reaction solution was dried in vacuo, and the resulting residue was extracted with diethyl ether and filtered through a plug of Celite. After removal of the volatiles from the filtrate in vacuo, the resulting yellow solid was washed with pentane (2 × 1 mL) to give the product (0.064 g, 84% isolated yield). Single crystals suitable for an X-ray diffraction study were grown from a saturated solution of product in n-pentane and diethyl ether at –35 °C. ¹H NMR (600 MHz, CD₃CN): δ 7.59 (br s, 1H, furyl 5), 6.07 (br s, 1H, furyl 3/4), 5.97 (br s, 1H, furyl 3/4), 4.07 (br s, 12H, P(OCH₂)₃CET), 1.47 (s, 15H, Cp*), 1.16 (q, 4H, ³J_{HH} = 7 Hz, P(OCH₂)₃CCH₂CH₃), 0.77 (t, ³J_{HH} = 7 Hz, 6H, P(OCH₂)₃CCH₂CH₃). ³¹P NMR (201 MHz, CD₃CN): δ 168.1 (s). ¹³C NMR (201 MHz, C₆D₆): 179.2 (t, ²J_{CP} = 37 Hz, furyl ipso), 147.2 (furyl), 122.0 (furyl), 111.3 (d, ⁴J_{CP} = 17 Hz, furyl 4), 91.4 (s, C₅Me₅), 73.6 (P(OCH₂)₃CCH₂CH₃), 34.5 (t, ³J_{CP} = 15 Hz, P(OCH₂)₃CCH₂CH₃), 23.4 (P(OCH₂)₃CCH₂CH₃), 10.5 (C₅Me₅), 6.8 (P(OCH₂)₃CCH₂CH₃). Anal. Calcd for C₂₆H₄₀FeO₇P₂: C, 53.62; H, 6.92. Found: C, 53.82; H, 7.04.

Cp*Fe[P(OCH₂)₃CET]₂[2-(5-methylfuryl)] (2). A mixture of Cp*Fe[P(OCH₂)₃CET]₂Ph (0.038 g, 0.064 mmol), 2-methylfuran (0.30 mL, 3.4 mmol), and THF (1 mL) was placed in a J. Young NMR tube. The reaction solution was photolyzed for a total of ~22 h while being monitored by ³¹P NMR spectroscopy. After the reaction was complete, the resulting mixture was

dried in vacuo. The residue was extracted with diethyl ether and filtered through Celite. The filtrate was dried in vacuo, reconstituted in ~2 mL of a 1/1 mixture of *n*-pentane and diethyl ether, and stored at -35 °C. The resulting yellow solid was collected, washed with *n*-pentane, and dried in vacuo to give the product as a yellow-orange solid (0.023 g, 60% yield). ¹H NMR (600 MHz, CD₃CN): δ 5.80 (d, ³J_{HH} = 3 Hz, 1H, furyl 3), 5.60 (m, 1H, furyl 4), 4.06 (s, 12H, P(OCH₂)₃CEt), 2.19 (s, 3H, furyl methyl), 1.50 (s, 15H, Cp*), 1.14 (q, ³J_{HH} = 8 Hz, 4H, P(OCH₂)₃CCH₂CH₃), 0.79 (t, ³J_{HH} = 8 Hz, 6H, P(OCH₂)₃CCH₂CH₃). ³¹P NMR (201 MHz, CD₃CN): δ 168.1 (s). ¹³C NMR (201 MHz, C₆D₆): 175.0 (t, ²J_{CP} = 44 Hz, furyl ipso), 155.1 (furyl), 123.1 (furyl), 107.9 (furyl), 91.4 (C₅Me₅), 73.6 (P(OCH₂)₃CCH₂CH₃), 34.5 (t, ³J_{CP} = 19 Hz, P(OCH₂)₃CCH₂CH₃), 23.4 (P(OCH₂)₃CCH₂CH₃), 15.0 (furyl methyl), 10.6 (C₅Me₅), 6.8 (P(OCH₂)₃CCH₂CH₃). Anal. Calcd for C₂₇H₄₂FeO₇P₂: C, 54.37; H, 7.10. Found: C, 54.08; H, 7.30.

Cp*Fe[η⁵-C₅Me₄(CH=CHCHO)] (3). Cp*Fe[P(OCH₂)₃CEt]₂Ph (0.063 g, 0.11 mmol) was dissolved in furan (~1.5 mL) and placed in a screw-cap NMR tube. The reaction mixture was photolyzed for 5 h until complete conversion to Cp*Fe[P(OCH₂)₃CEt]₂(2-furyl) was observed by ³¹P NMR spectroscopy. At this point, the NMR tube was brought back into the glovebox and 2-butyne (0.17 mL, 2.2 mmol) was added. The resulting mixture was photolyzed for an additional 2 h until the reaction was complete by ³¹P NMR spectroscopy. The purple solution was brought back into the glovebox, and the volatiles were removed in vacuo. The purple residue was chromatographed on a plug of silica gel in a 15 mL frit, with a 10/1 mixture of hexanes and THF as eluent. A purple band was collected, and the volatiles were removed in vacuo. The purple residue was brought outside the glovebox and dissolved in ~4 mL of methanol. To this stirred solution was added H₂O (~15 mL) to precipitate a purple solid, which was collected over a plug of Celite in a frit. The plug was washed with copious amounts of water (~60 mL total). The purple solid was eluted with MeOH and dried in vacuo to yield the desired product as a dihydrate (0.036 g, 81% yield). ¹H NMR (600 MHz, CD₃CN): δ 9.53 (d, ³J_{HH} = 8 Hz, 1H, -CHO), 7.41 (d, ³J_{HH} = 16 Hz, 1H, C₅Me₄CH=CH), 6.33 (dd, ³J_{HH} = 16, 8 Hz, 1H, C₅Me₄CH=CH), 1.88 (s, 6H, 2

of C_5Me_4 adjacent to olefin), 1.79 (s, 6H, 2 of C_5Me_4 not adjacent to olefin), 1.60 (s, 15H, Cp*). ^{13}C NMR (201 MHz, CD_3CN): δ 194.5 (CHO), 157.7 ($C_5Me_4CH=CH$), 126.1 ($C_5Me_4CH=CH$), 86.1 (2 of C_5Me_4 β to olefin), 82.2 (2 of C_5Me_4 γ to olefin), 80.9 (C_5Me_5), 73.7 (C_5Me_4 α to olefin), 10.7 (Me's on C_5Me_4 C β), 9.6 (Me's on C_5Me_4 C γ), 9.4 (C_5Me_5). Anal. Calcd for $C_{22}H_{30}FeO$: C, 72.13; H, 8.25. Found: C, 71.63; H, 8.24. CV (NCMe): $E_{1/2} = -0.26$ V Fe(III/II).

Cp*Fe[η^5 - $C_5Me_4(CH=CHC(Me)O)$] (4). Cp*Fe[P(OCH $_2$) $_3$ CEt] $_2$ Ph (0.064 g, 0.11 mmol) and 2-methylfuran (0.26 mL, 2.9 mmol) were dissolved in THF (~2 mL) and placed in a screw-cap NMR tube. The reaction mixture was photolyzed for 29 h until complete conversion to Cp*Fe[P(OCH $_2$) $_3$ CEt] $_2$ [2-(5-methylfuryl)] was observed by ^{31}P NMR spectroscopy. At this point, the NMR tube was brought back into the glovebox and 2-butyne (0.17 mL, 2.2 mmol) was added. The resulting mixture was photolyzed for an additional 3 h until the reaction was complete by ^{31}P NMR spectroscopy. The purple solution was brought back into the glovebox, and the volatiles were removed in vacuo. The purple residue was chromatographed on a plug of silica gel in a 15 mL frit, eluting with a 20:1 mixture of hexanes and THF. A purple band was collected, and the volatiles were removed in vacuo. The purple residue was brought outside the glovebox and dissolved in ~5 mL of methanol. To this stirred solution was added H $_2$ O (~15 mL) to precipitate a purple solid, which was collected over a plug of Celite on a frit. The plug was washed with copious amounts of water (~75 mL total). The purple solid was eluted with MeOH and dried in vacuo to yield the desired product as a hydrate (0.015 g, 33% yield). 1H NMR (800 MHz, C_6D_6): δ 7.59 (d, $^3J_{HH} = 16$ Hz, 1H, CH=CHC(O)Me), 6.56 (d, $^3J_{HH} = 16$ Hz, 1H, CH=CHC(O)Me), 2.12 (s, 3H, CH=CHC(O)Me), 1.73 (s, 6H, cyclopentadienyl methyls), 1.58 (s, 6H, cyclopentadienyl methyls), 1.51 (s, 15H, C_5Me_5). ^{13}C NMR (201 MHz, C_6D_6): δ 195.7 (CH=CHC(O)Me), 144.8 (CH=CHC(O)Me), 124.0 (CH=CHC(O)Me), 83.8 (cyclopentadienyl), 81.1 (cyclopentadienyl), 80.0 (C_5Me_5), 72.4 (cyclopentadienyl), 27.5 (CH=CHC(O)Me), 10.6 (cyclopentadienyl methyl), 9.5 (C_5Me_5). One ^{13}C resonance for a cyclopentadienyl methyl is missing, likely due to

coincidental overlap. Attempts to get favorable elemental analysis were unsuccessful. CV (NCMe): $E_{1/2} = -0.29$ V Fe(III/II).

Kinetic Study as a Function of P(OCH₂)₃CEt Concentration. A stock solution of **1** (0.080 g, 0.14 mmol) and 2-butyne (22 μ L, 0.28 mmol) was made in 2.0 mL of C₆D₆. CH₃NO₂ (8.0 μ L, 0.15 mmol) was added to the solution as an internal standard. To each of four medium-walled J. Young NMR tubes was added 350 μ L of stock solution and 0 (0.0 g, 0.0 mmol), 0.5 (0.002 g, 0.012 mmol), 1 (0.004 g, 0.024 mmol), and 2 equiv (0.008 g, 0.048 mmol) of P(OCH₂)₃CEt (relative to **1**). The NMR samples were photolyzed for 30 min intervals (a lamp warmup time of 15 min is included within each 30 min) and monitored by ¹H NMR spectroscopy through 3 half-lives using a pulse delay time of 10 s.

Kinetic Study as a Function of 2-Butyne Concentration. A stock solution of **1** (0.081 g, 0.14 mmol) was made in 2.0 mL of C₆D₆. CH₃NO₂ (8.0 μ L, 0.15 mmol) was added to the solution as an internal standard. To each of four medium-walled J. Young NMR tubes was added 350 μ L of stock solution and 10 (19 μ L, 0.24 mmol), 15 (28 μ L, 0.36 mmol), 20 (38 μ L, 0.48 mmol), and 25 equiv (47 μ L, 0.60 mmol) of 2-butyne (relative to **1**). The NMR samples were photolyzed for 30 min intervals (a lamp warm up time of 15 min is included within each 30 min) and monitored by ¹H NMR spectroscopy through 3 half-lives using a pulse delay time of 10 s.

Kinetic Study as a Function of 2-Butyne Concentration in the Presence of P(OCH₂)₃CEt. A stock solution of **1** (0.080 g, 0.14 mmol) and P(OCH₂)₃CEt (0.011 g, 0.068 mmol) was made in 2.0 mL of C₆D₆. CH₃NO₂ (8.0 μ L, 0.15 mmol) was added to the solution as an internal standard. To each of three medium-walled J. Young NMR tubes was added 350 μ L of stock solution and 10 (20 μ L, 0.26 mmol), 20 (40 μ L, 0.52 mmol), and 30 equiv (60 μ L, 0.78 mmol) of 2-butyne. The NMR samples were photolyzed for 30 min intervals (a lamp warm up time of 15 min is included within each 30 min) and monitored by ¹H NMR spectroscopy through the course of the reaction using a pulse delay time of 10 s.

General Procedure for Alkyne Substrate Scope Study. A 10 equiv amount of alkyne was added to a 0.069 M solution of **1** in C_6D_6 and photolyzed. The reaction progress was monitored by 1H NMR spectroscopy. Percent yield was calculated using integrations of **1** and respective furyl ring-opening products, on the basis of CH_3NO_2 as an internal standard. In situ NMR spectral data for selected resonances of the respective furyl ring-opened products $Cp^*Fe[\eta^5-C_5(CH_2CH_3)_4(CH=CHCHO)]$, $Cp^*Fe[\eta^5-C_5(Ph)_2(Me)_2(CH=CHCHO)]$, and $Cp^*Fe[\eta^5-C_5(Ph)_4(CH=CHCHO)]$ are as follows:

$Cp^*Fe[\eta^5-C_5(CH_2CH_3)_4(CH=CHCHO)]$. 1H NMR (500 MHz, C_6D_6): δ 9.74 (d, $^3J_{HH} = 8$ Hz, 1H, $-CHO$), 7.11 (d, $^3J_{HH} = 16.5$ Hz, 1H, $-CH=CH$), 6.63 (dd, $^3J_{HH} = 16, 8$ Hz, 1H, $CH=CH$), 1.41 (s, Cp^*) 1.11 (t) and 0.93 (q) (Et's on C_5Et_4). ^{13}C NMR (201 MHz, C_6D_6): δ 192.9 (CHO), 154.6 (CH=CH), 125.7 (CH=CH), 89.9 (2 C of C_5Et_4 β to olefin), 88.3 (2 C of C_5Et_4 γ to olefin) 80.4 (C_5Me_5), 73.7 (C_5Et_4 α to olefin).

$Cp^*Fe[\eta^5-C_5(Ph)_2(Me)_2(CH=CHCHO)]$. 1H NMR (500 MHz, C_6D_6): δ 9.56 (d, $J = 8$ Hz, 1H, CHO), 7.41, 7.28–7.22 (phenyl resonances), 6.61 (dd, $^3J_{HH} = 16, 8$ Hz, 1H, $CH=CH$), 1.83 (s, 3H, $C_5(Ph)_2(Me)_2$), 1.47 (s, 3H, $C_5(Ph)_2(Me)_2$), 1.41 (s, Cp^*) (the $CH=CH$ doublet is missing due to coincidental overlap with the C_6D_6 resonance). ^{13}C NMR (201 MHz, C_6D_6): δ 192.7 (CHO), 154.9 (CH=CH), 126.9 (CH=CH), 84.5 (2C $C_5(Ph)_2(Me)_2$ β to olefin), 81.0 (2 C $C_5(Ph)_2(Me)_2$ γ to olefin), 79.1 C_5Me_5), 73.1 ($C_5(Ph)_2(Me)_2$ α to olefin).

$Cp^*Fe[\eta^5-C_5(Ph)_4(CH=CHCHO)]$. 1H NMR (500 MHz, C_6D_6): δ 9.48 (d, $^3J_{HH} = 8$ Hz, 1H, CHO), 6.24 (dd, $^3J_{HH} = 16, 8$ Hz, 1H $CH=CH$), 1.54 (s, C_5Me_5). ^{13}C NMR (201 MHz, C_6D_6): δ 192.4 (CHO), 152.7 (CH=CH), 125.0 (CH=CH).

References

- (1) Sargent, M. V. D., F. M. In *Comprehensive Heterocycle Chemistry: The Structure, Reactions, Synthesis and Uses of Heterocyclic Compounds*; Bird, C. W., Cheeseman, G. W. H., Ed.; Pergamon Press: Oxford, U.K., 1984; Vol. 4, p 599.
- (2) Donnelly, D. M. X. M., M. J. In *Comprehensive Heterocycle Chemistry: The Structure, Reactions, Synthesis and Uses of Heterocyclic Compounds*; Bird, C. W., Cheeseman, G. W. H., Ed.; Pergamon Press: Oxford, U.K., 1984; Vol. 4, p 657.
- (3) Mustafa, A. *The Chemistry of Heterocyclic Compounds: Fuopyrans and Fuopyrones*; Interscience Publishers: London, 1967; Vol. 23.
- (4) *The Chemical Synthesis of Natural Products*; Sheffield Academic Press: Sheffield, U.K., 2000.
- (5) Oblak, E. Z.; VanHeyst, M. D.; Li, J.; Wiemer, A. J.; Wright, D. L. *J. Am. Chem. Soc.* **2014**, *136*, 4309.
- (6) Seçinti, H.; Seçen, H. *Helvetica Chimica Acta* **2015**, *98*, 938.
- (7) Raczko, J. J., J. In *Studies in Natural Products Chemistry: Stereoselective Synthesis*; Rahman, A., Ed.; Elsevier: Amsterdam, 1995; Vol. 16, p 639.
- (8) Shirke, R. P.; Ramasastry, S. S. V. *The Journal of Organic Chemistry* **2015**, *80*, 4893.
- (9) Mahmoud, E.; Yu, J.; Gorte, R. J.; Lobo, R. F. *ACS Catal.* **2015**, *5*, 6946.
- (10) Schurgers, B.; Brigou, B.; Urbanczyk-Lipkowska, Z.; Tourwé, D.; Ballet, S.; De Proft, F.; Van Lommen, G.; Verniest, G. *Organic Letters* **2014**, *16*, 3712.
- (11) Cantrell, T. S.; Allen, A. C.; Ziffer, H. *The Journal of Organic Chemistry* **1989**, *54*, 140.
- (12) LaPorte, M.; Hong, K. B.; Xu, J.; Wipf, P. *The Journal of Organic Chemistry* **2013**, *78*, 167.

- (13) Shieh, P. C.; Ong, C. W. *Tetrahedron* **2001**, *57*, 7303.
- (14) Hahn, N. D.; Nieger, M.; Dötz, K. H. *J. Organomet. Chem.* **2004**, *689*, 2662.
- (15) Wenkert, E.; Guo, M.; Lavilla, R.; Porter, B.; Ramachandran, K.; Sheu, J. H. *The Journal of Organic Chemistry* **1990**, *55*, 6203.
- (16) Sacia, E. R.; Balakrishnan, M.; Bell, A. T. *Journal of Catalysis* **2014**, *313*, 70.
- (17) Caes, B. R.; Teixeira, R. E.; Knapp, K. G.; Raines, R. T. *ACS Sustainable Chemistry & Engineering* **2015**, *3*, 2591.
- (18) Nagpure, A. S.; Lucas, N.; Chilukuri, S. V. *ACS Sustainable Chemistry & Engineering* **2015**, *3*, 2909.
- (19) Sutton, A. D.; Waldie, F. D.; Wu, R.; Schlaf, M.; Pete' Silks, L. A.; Gordon, J. C. *Nature Chemistry* **2013**, *5*, 428.
- (20) Chatterjee, M.; Matsushima, K.; Ikushima, Y.; Sato, M.; Yokoyama, T.; Kawanami, H.; Suzuki, T. *Green Chem.* **2010**, *12*, 779.
- (21) Hartwig, J. F. *Organotransition Metal Chemistry From Bonding to Catalysis*; University Science Books: Mill Valley, CA, 2010.
- (22) Riener, K.; Haslinger, S.; Raba, A.; Högerl, M. P.; Cokoja, M.; Herrmann, W. A.; Kühn, F. E. *Chem. Rev.* **2014**, *114*, 5215.
- (23) Gopalaiah, K. *Chem. Rev.* **2013**, *113*, 3248.
- (24) Zhao, H.; Sun, H.; Li, X. *Organometallics* **2014**, *33*, 3535.
- (25) Mikhailine, A. A.; Maishan, M. I.; Lough, A. J.; Morris, R. H. *J. Am. Chem. Soc.* **2012**, *134*, 12266.
- (26) Hitomi, Y.; Arakawa, K.; Kodera, M. *Chemistry – A European Journal* **2013**, *19*, 14697.
- (27) Xu, X.; Sun, H.; Shi, Y.; Jia, J.; Li, X. *Dalton Trans.* **2011**, *40*, 7866.
- (28) Bouwkamp, M. W.; Lobkovsky, E.; Chirik, P. J. *J. Am. Chem. Soc.* **2005**, *127*, 9660.

- (29) Butler, I. R.; Cullen, W. R.; Lindsell, W. E.; Preston, P. N.; Rettig, S. J. *Journal of the Chemical Society, Chemical Communications* **1987**, 439.
- (30) Mei, J.; Pardue, D. B.; Kalman, S. E.; Gunnoe, T. B.; Cundari, T. R.; Sabat, M. *Organometallics* **2014**, *33*, 5597.
- (31) Kalman, S. E.; Petit, A.; Gunnoe, T. B.; Ess, D. H.; Cundari, T. R.; Sabat, M. *Organometallics* **2013**, *32*, 1797.
- (32) Ohki, Y.; Hatanaka, T.; Tatsumi, K. *J. Am. Chem. Soc.* **2008**, *130*, 17174.
- (33) Hatanaka, T.; Ohki, Y.; Tatsumi, K. *Chemistry – An Asian Journal* **2010**, *5*, 1657.
- (34) Crabtree, R. H. *The Organometallic Chemistry of the Transition Metals*; 4th ed.; John Wiley and Sons: Hoboken, NJ, 2005.
- (35) Jia, F.; Li, Z. P. *Org. Chem. Front.* **2014**, *1*, 194.
- (36) Gunay, A.; Theopold, K. H. *Chem. Rev.* **2010**, *110*, 1060.
- (37) Xia, Q.; Chen, W. *The Journal of Organic Chemistry* **2012**, *77*, 9366.
- (38) Donald, W. A.; McKenzie, C. J.; O'Hair, R. A. J. *Angewandte Chemie International Edition* **2011**, *50*, 8379.
- (39) Jones, W. D.; Foster, G. P.; Putinas, J. M. *J. Am. Chem. Soc.* **1987**, *109*, 5047.
- (40) Shang, R.; Ilies, L.; Matsumoto, A.; Nakamura, E. *J. Am. Chem. Soc.* **2013**, *135*, 6030.
- (41) Baker, M. V.; Field, L. D. *J. Am. Chem. Soc.* **1986**, *108*, 7433.
- (42) Ittel, S. D.; Tolman, C. A.; English, A. D.; Jesson, J. P. *J. Am. Chem. Soc.* **1978**, *100*, 7577.
- (43) Tolman, C. A.; Ittel, S. D.; English, A. D.; Jesson, J. P. *J. Am. Chem. Soc.* **1978**, *100*, 4080.
- (44) Hatanaka, T.; Ohki, Y.; Tatsumi, K. *Angewandte Chemie International Edition* **2014**, *53*, 2727.

- (45) Simmie, J. M.; Curran, H. J. *The Journal of Physical Chemistry A* **2009**, *113*, 5128.
- (46) Luo, Y. *Comprehensive Handbook of Chemical Bond Energies*; CRC Press: Boca Raton, FL, 2007.
- (47) Dawson, D. P.; Yongkulrote, W.; Bramlett, J. M.; Wright, J. B.; Durham, B.; Allison, N. T. *Organometallics* **1994**, *13*, 3873.
- (48) Kalman, S. E.; Gunnoe, T. B.; Sabat, M. *Organometallics* **2014**, *33*, 5457.